Genotypic and phenotypic determinants of immunity across gynecological malignancies

Lubbers-Marsman, Joyce

IMPORTANT NOTE: You are advised to consult the publisher's version (publisher's PDF) if you wish to cite from it. Please check the document version below.

Document Version
Publisher's PDF, also known as Version of record

Publication date:
2022

Genotypic and phenotypic determinants of immunity

across gynecological malignancies

Joyce Mary-Ann Lubbers

Joyce M. Lubbers

Genotypic and phenotypic determinants of immunity across gynecological malignancies

PhD dissertation, University of Groningen, The Netherlands

Cover design: Marieke A. Lubbers and Joyce M. Lubbers

Graphic design: Joyce M. Lubbers

umcg
Graduate School of
Medical Sciences

rijksuniversiteit
groningen

EVIDENCIO
CONNECTING SCIENCE AND MEDICAL PRACTICE

Genotypic and phenotypic determinants of immunity across gynecological malignancies

Proefschrift

ter verkrijging van de graad van doctor aan de
Rijksuniversiteit Groningen
op gezag van de
rector magnificus prof. dr. C. Wijmenga
en volgens besluit van het College voor Promoties.

De openbare verdediging zal plaatsvinden op

woensdag 1 juni 2022 om 12:45 uur

door

Joyce Mary-Ann Lubbers

geboren op 6 mei 1992
te Almelo

Paranimfen:
Drs. A. Plat
Drs. N. van Rooij

Content

Chapter 1

General Introduction

General introduction

Immunotherapy has emerged as successful treatment modality of multiple cancer types, even of certain previously treatment-refractory cancers. The studies described in this dissertation aimed at improving the understanding of the immunological tumor microenvironment in gynecological malignancies. Firstly, several important immunologic signaling and cell components were investigated. Lastly, a novel strategy for improvement of (pre)clinical studies is demonstrated.

Basic principles of cancer immunotherapy

The main focus of cancer immunotherapy is to induce or restore the body's natural defense against cancer cells. Immunotherapy mainly targets adaptive immunity, which is selectively reactive to antigens that can be identified as foreign to the host. Typical adaptive immune cells are CD8+ and CD4+ T cells. Host cells constantly present antigen peptides in Major Histocompatibility Complex class I and II molecules, which are scanned by CD8+ and CD4+ T cells, respectively. During their development in the thymus, T cells with receptors specific for host self-antigens are deleted, establishing tolerance. The remaining T cells have receptors for antigens that were not present in the thymus, such as antigens from pathogens like Human Papilloma Virus (HPV) or antigens derived from mutated host DNA. Contact of antigen-presenting cells, presenting these foreign antigens, with T cells leads to activation of the T cells and subsequently proliferation and execution of effector functions. In that respect, CD4+ T cells are mainly known as T helper cells that help the activity of other immune cells. But the immune cell that has acquired most attention in immunotherapy is the CD8+ cytotoxic T cell, which directly kills infected or cancerous cells. CD8+ T cells effectuate their killing function by releasing cytotoxic proteins, granzymes and perforins.

In so-called cold tumors, there is e.g. lack of tumor antigens or physical exclusion of T cells from the tumor. As a result, immunity in these tumors might be lacking, targeting poorly immunogenic antigens or be non-antigen-specific. The latter T cells are referred to as bystander T cells.[1] In these cold tumors, induction of tumor-reactive immunity is pursued by for example vaccination and adoptive CD8+ T cell transfer. In hot tumors, there is an existing but inadequate immune response, e.g. due to exhaustion of CD8+ T cells caused by inhibitory signals in the tumor microenvironment.[1] For example, persistent antigen stimulation of T cells can lead to compromised functionality. Moreover, T cells can become exhausted by hijacking of immune checkpoints, that normally help control immune responses, by cancer cells. Two particular checkpoint are the binding of PD-L1 on cancer cells with PD-1 on T cells and the induction of CTLA-4 on T cells, both leading to inhibition of anti-tumor activity. Restoring this exhaustion is termed reinvigoration and is achieved by checkpoint inhibition therapy. The key advantage of immunotherapy is that it confers memory to the patient's

immune cells to harness residual or recurrent cancer cells, which is beneficial for long-term survival.

Immunotherapy in the treatment of gynecological malignances
Gynecological malignancies still account for a large part of mortality in women. Therefore, efforts have been made to introduce immunotherapy in the treatment of these patients. The most common gynecological malignances are located in the cervix, endometrium and ovaries.

Cervical cancer is associated with persistent infection of human papilloma virus (HPV). HPV infection can be detected in nearly 99% of cervical cancer patients.[2] As persistent infection with HPV is crucial for carcinogenesis, a prophylactic vaccination program has been introduced in the Netherlands in 2009. In addition, a national screening program on cervical scrapings was launched already in 1996, and adjusted in 2017 by inclusion of high risk HPV testing.[3] Despite these programs, the incidence of cervical cancer has increased from 662 cases in 2013 to 912 in 2019.[4] Over the recent decennia, the 5-year survival rate has only slightly increased from 64% to 67%.[4] Thus, the prognosis of patients has not much improved. Choice of treatment highly depends on FIGO stage. Early stage disease is currently treated with primary surgery; late stage disease with primary radio(chemo) therapy. The main exploited immunotherapeutic strategies are HPV-targeting vaccines, immune checkpoint inhibitors Pembrolizumab and Nivolumab and HPV-targeting tumor-infiltrating T cell transfer.[5] Overall response rates for these therapies range from <20% to maximally 50%.

Endometrial cancer is the most common of the three noted gynecological malignancies, accounting for roughly 2000 diagnoses annually in the Netherlands.[4] The incidence of endometrial cancer was 1200 in 1990.[4] This substantial increase may be dedicated to the aging population, as endometrial cancer is typically diagnosed in women above 45 years of age[4], and increased prevalence of adiposity.[6,7] Endometrial cancers are distinguished based on four molecular profiles: *POLE* ultra-mutation, microsatellite instability, copy number low, and copy number high. These molecular profiles aid in stratifying risk categories and establishing potential therapeutic targets. As it is generally symptomatic at an early stage disease, most patient are diagnosed with stage I disease and have a good prognosis with a 5-year survival of 80%.[4] However, patients that are diagnosed with more advanced stage endometrial cancer remain to have a 5-year survival of only 20-60%.[8] Low risk patients are treated with surgery; high risk patients additionally receive adjuvant radiotherapy and/or chemotherapy. Immunotherapeutic approaches for endometrial cancer focus on immune checkpoint inhibition.[5] The response rates of Pembrolizumab, alone or in combination with VEGF receptor kinase inhibitor Lenvatinib reached about 50%.

Ovarian cancer is diagnosed between 1000-1250 women in the Netherlands. This means that about 1,2% of all women suffer from and about 1% of all women die due to ovarian carcinoma.[4] About 75% of patients are diagnosed with an advanced stage of disease (FIGO IIB or higher) due to the often aspecific nature of symptoms, reducing chance of survival.[4] Although most patients initially respond to therapy, patients only have a 5-year survival of about 38% and a 10-year survival of around 30% due to recurrent disease, making ovarian cancer the most deadly gynecological malignancy. Moreover, prognosis has minimally improved over the years. For example, the 5-year survival was 32% in 1990.[4] At present, ovarian cancer patients are treated with neo-adjuvant chemotherapy, cytoreductive surgery, followed by adjuvant chemotherapy. Recurrent ovarian cancer is generally chemotherapy-resistant. Immunotherapies under investigation are NY-ESO-1 and p53 tumor-associated antigen targeting vaccines, recombinant monoclonal antibodies against VEGF-A and CA-125 and immune checkpoint inhibitors Pembrolizumab and Nivolumab.[5] Overall response rates of these treatments generally did not reach 20%, with the exception of anti-VEGF monoclonal antibody Bevacizumab (20-50%).

Outline of this dissertation

The above numbers highlight the strong need for novel, more effective treatment modalities for gynecological malignancies. To enhance the efficacy of immunotherapy as treatment for gynecological malignancies, whether or not combined with other therapeutic strategies such as chemotherapy and radiotherapy, a better understanding on immunological aspects in these malignancies is required. Therefore, the studies in this dissertation address initiation of immunity, composition of anti-tumor immunity and improvement of preclinical research models to study tumor immunology.

Part I: Initiation of immunity: STimulator of INterferon Genes (STING)

In **Chapters 2 and 3**, the emphasis is on a protein that is crucial for initiation of anti-tumor immunity: STimulator of INterferon Genes (STING). STING is a downstream signaler of cyclic GMP-AMP synthase (cGAS), a detector of cytoplasmic DNA, either derived from pathogens such as HPV upon infection or established upon intrinsic DNA damage. Once activated, STING induces a signaling cascade that ultimately leads to type I interferon signaling. These interferons attract and activate components of the innate immune system such as antigen presenting cells, which in turn initiate an antigen-specific adaptive immune response including CD8+ T cells. Down-regulation and dysfunction of STING was reported in the setting of Human Immunodeficiency Virus (HIV)[9] and in multiple cancer types, in which it associated with poor prognosis.[10,11] Low STING associated with poor CD8+ T cell infiltration and response to immune checkpoint inhibition therapy.[12,13] Altogether, these findings led to increasing interest in direct and indirect STING-induction therapies[14,15], of which several are

currently clinically tested. As STING was not yet investigated extensively in gynecological setting, we assessed the implications of STING in cervical cancer.

In **Chapter 2**, we have investigated the prognostic value of STING in two large cohorts of cervical cancer patients.

The STING-encoding gene *STING1* consists of many single nucleotide polymorphisms, indicated as allelic variants. Importantly, some of these cause defective functionality of the STING protein.[9,16]

In **Chapter 3**, we therefore have genotyped *STING1* in a large cohort of cervical cancer patients and a cohort of healthy controls to assess potential consequences of allelic variety in the gene on disease development, progression and response to therapy. Complementary, we assessed STING mRNA and protein levels and analyzed CD8+ T cell infiltration in the tumors.

Part II: Composition of adaptive anti-tumor immunity

Eradication of cancer cells is mainly performed by CD8+ T cells that are antigen-specific for the cancer cells, either for overexpressed self-antigen, neo-antigens or pathogen-derived antigen. As direct identification of antigen specificity via T cell receptor sequencing and *in vitro* reactivity testing is very costly and impossible without acquirement of tumor material, biomarkers that indirectly identify cancer cell-directed CD8+ T cells have been under investigation. Over the years, several cell surface markers have been reported that delineate these so-called tumor-reactive CD8+ T cells. One of them is CD103, which is expressed on CD8+ T cells upon T cell receptor stimulation and signaling of TGFβ and resides T cells in the tumor epithelium.[17,18] CD103 induces e.g. proliferation and cytolytic activity of CD8+ T cells.[19] In line with this, high infiltration with CD103+ CD8+ T cells, but not CD103- CD8+ T cells, associated with improved prognosis in several types of cancer such as cervical cancer, endometrial cancer, ovarian cancer and lung cancer.[17,18,20,21]

Hence, in **Chapter 4,** mRNA sequencing was performed to investigate the intrinsic differences between CD103+ and CD103- CD8+ T cells. As we found that B cell attracting chemokine *CXCL13* was differentially expressed by CD103+ cells, we furthermore focused on exploring a potential new link between T and B cell immunity by assessment of tertiary lymphoid structures in human tumors.

Two other markers for tumor-reactive CD8+ T cells that have gained strong interest are immune checkpoint PD-1 and activation marker CD39.[21–24] However, it remains largely

unknown how (co-)expression of CD103, CD39 and PD-1 defines T cell reactivity, activation and dysfunction in tumors on the transcriptomic or functional level.

As TGFβ signaling is crucial for induction of CD103 on activated T cells, we hypothesized that it may also have an effect on expression of CD39 and PD-1 on T cells. In **Chapter 5**, we therefore studied the effect of TGFβ signaling in CD8+ T cells derived from healthy volunteers and from tumor digests of endometrial cancer patients.

Part III: Establishment of novel preclinical models for tumor immunology and cancer immunotherapy

Preclinical research studies are currently limited to implementation of cell lines or animal models that do not well-reflect patients regarding tumor characteristics such as heterogeneity, tumor micro environmental factors and immunity. In addition, clinical studies are costly and limited by the number of available participants, both patients and healthy volunteers. These limitations complicate stratification of (gynecological) cancer patients for immunotherapy and the development of novel or existing therapeutic modalities.

In **Chapter 6**, we therefore report on an effort to demonstrate the high potential of induced pluripotent stem cells (iPSC) generated from the urine of ovarian cancer patients to improve preclinical research models of tumor immunology and cancer immunotherapy.

A summary of the studies is presented in **Chapter 7**. Finally, the results and implications of this dissertation for immunotherapy in gynecological malignancies are discussed and put into a broader perspective in **Chapter 8**.

1

References

1. Duan, Q., Zhang, H., Zheng, J. & Zhang, L. Turning Cold into Hot: Firing up the Tumor Microenvironment. Trends in Cancer 1–14 (2020). doi:10.1016/j.trecan.2020.02.022

2. Walboomers, J. et al. Human Papillomavirus Is a Necessary Cause. J. Pathol. 189, 12–19 (1999).

3. Naber, S. K. et al. Baarmoederhalskanker in Nederland naar aanleiding van recente ontwikkelingen. (2016).

4. Nederlandse Kanker Registratie. IKNL. 2016-2019. www.iknl.nl.

5. Matanes, E. & Gotlieb, W. H. Immunotherapy of gynecological cancers. Best Pract. Res. Clin. Obstet. Gynaecol. 60, 97–110 (2019).

6. Dashti, S. G. et al. Adiposity and endometrial cancer risk in postmenopausal women: A sequential causal mediation analysis. Cancer Epidemiol. Biomarkers Prev. 30, 104–113 (2021).

7. Adela Hruby, PhD, M. & Frank B. Hu, MD, PhD, M. The Epidemiology of Obesity: A Big Picture. Pharmacoeconomics. 33, 673–689 (2015).

8. Ferlay, J. et al. Cancer incidence and mortality patterns in Europe: Estimates for 40 countries in 2012. Eur. J. Cancer 49, 1374–1403 (2013).

9. Nissen, S. K. et al. Multiple Homozygous Variants in the STING-Encoding *TMEM173* Gene in HIV Long-Term Nonprogressors. J. Immunol. ji1701284 (2018). doi:10.4049/jimmunol.1701284

10. Song, S. et al. Decreased expression of STING predicts poor prognosis in patients with gastric cancer. Sci. Rep. 7, 1–13 (2017).

11. Xia, T., Konno, H., Ahn, J. & Barber, G. N. Deregulation of STING Signaling in Colorectal Carcinoma Constrains DNA Damage Responses and Correlates With Tumorigenesis. Cell Rep. 14, 282–297 (2016).

12. Harding, S. M. et al. Mitotic progression following DNA damage enables pattern recognition within micronuclei. Nature 548, 466–470 (2017).

13. Chon, H. J. et al. STING signaling is a potential immunotherapeutic target in colorectal cancer. J. Cancer 10, 4932–4938 (2019).

14. Su, T. et al. STING activation in cancer immunotherapy. Theranostics 9, 7759–7771 (2019).

15. Flood, B. A., Higgs, E. F., Li, S., Luke, J. J. & Gajewski, T. F. STING pathway agonism as a cancer therapeutic. Immunol. Rev. 290, 24–38 (2019).

16. Patel S, Blaauboer SM, Tucker HR, et al. . (Baltimore, M. : 1950). ;198(2):776-787. doi:10. 4049/jimmunol. 1601585.The common R71H-G230A-R293Q (HAQ) human *TMEM173* is a null allele. J. Immunol. 198, 776–787 (2017).

17. Komdeur, F. L. et al. CD103+ tumor-infiltrating lymphocytes are tumor-reactive intraepithelial CD8+ T cells associated with prognostic benefit and therapy response in cervical cancer. Oncoimmunology 6, 1–14 (2017).

18. Djenidi, F. et al. CD8 + CD103 + Tumor–Infiltrating Lymphocytes Are Tumor-Specific Tissue-Resident Memory T Cells and a Prognostic Factor for Survival in Lung Cancer Patients . J. Immunol. 194, 3475–3486 (2015).

19. Corgnac, S., Boutet, M., Kfoury, M., Naltet, C. & Mami-Chouaib, F. The emerging role of CD8+ tissue resident memory T (TRM) cells in antitumor immunity: A unique functional contribution of the CD103 integrin. Front. Immunol. 9, (2018).

20. Workel, H. H. et al. A Transcriptionally Distinct CXCL13þCD103þCD8þ T cell Population Is Associated with B cell Recruitment and Neoantigen Load in Human Cancer. Cancer Immunol. Res. 7, 784–796 (2019).

21. Webb, J. R., Milne, K. & Nelson, B. H. PD-1 and CD103 are widely coexpressed on prognostically favorable intraepithelial CD8 T cells in human ovarian cancer. Cancer Immunol. Res. 3, 926–935 (2015).

22. Gupta, P. K. et al. CD39 Expression Identifies Terminally Exhausted CD8+ T Cells. PLoS Pathog. 11, 1–21 (2015).

23. Duhen, T. et al. Co-expression of CD39 and CD103 identifies tumor-reactive CD8 T cells in human solid tumors. Nat. Commun. 9, (2018).

24. Thommen, D. S. et al. A transcriptionally and functionally distinct pd-1 + cd8 + t cell pool with predictive potential in non-small-cell lung cancer treated with pd-1 blockade. Nat. Med. 24, (2018).

Chapter 2

Combined STING levels and CD103+ T cell infiltration
have significant prognostic implications for patients with
cervical cancer

Joyce M. Lubbers[1*], Arjan Kol[1*], Anouk L.J. Terwindt[1], Hagma H. Workel[1], Annechien Plat[1],
G. Bea A. Wisman[1], Joost Bart[2], Hans W. Nijman[1#], Marco De Bruyn[1#]

*contributed equally and are co-first authors
#share senior authorship

[1]University of Groningen, University Medical Center Groningen,
Department of Obstetrics and Gynecology, The Netherlands
[2]University of Groningen, University Medical Center Groningen,
Department of Pathology, The Netherlands

Abstract

Activation of STimulator of INterferon Genes (STING) is important for induction of anti-tumor immunity. A dysfunctional STING pathway is observed in multiple cancer types and associates with poor prognosis and inferior response to immunotherapy. However, the association between STING and prognosis in virally induced cancers such as HPV-positive cervical cancer remains unknown. Here, we investigated the prognostic value of STING protein levels in cervical cancer using tumor tissue microarrays of two patient groups, primarily treated with surgery (n=251) or radio(chemo)therapy (n=255). We also studied CD103, an integrin that marks tumor-reactive cytotoxic T cells that reside in tumor epithelium and that is reported to associate with improved prognosis. Notably, we found that a high level of STING protein was an independent prognostic factor for improved survival in both the surgery and radio(chemo)therapy group. High infiltration of CD103+ T cells was associated with improved survival in the radio(chemo) therapy group. The combination of STING levels and CD103+ T cell infiltration is strongly associated with improved prognosis. We conclude that combining the prognostic values of STING and CD103 may improve the risk stratification of cervical cancer patients, independent from established clinical prognostic parameters.

Introduction

Cervical cancer is the most common gynecological cancer worldwide and the fourth leading cause of cancer-related death in women. The development of cervical cancer is largely caused by persistent infection with human papilloma virus (HPV), with type 16 and 18 accounting for approximately 70% of all cervical cancers.[1,2] Some studies have estimated the overall prevalence of HPV in cervical cancer as high as 99%[3], demonstrating that persistent infection with HPV is pivotal in the development of cervical cancer. However, not all HPV infections result in malignant transformation. The immune system is usually effective in eradicating the virus as a large majority of 90% of infections is cleared within 2 years.[4] Apart from preventing carcinogenesis by eradicating the HPV infection, the immune system also plays a protective role in early/developing malignancies by recognizing and destroying transformed cells and hence functioning as an important defense against cancer.[5]

Recent evidence shows that during infection or cancer, STimulator of INterferon type 1 Genes (STING; also known as Transmembrane Protein 173 (encoded by *STING1*) is critical for activation of innate immunity. STING acts after binding to cyclic dinucleotides, which can be derived exogenously from bacteria or can be generated upon detection of foreign (e.g. viral) or host nucleic acids in the cytosol by Cyclic-GMP-AMP (cGAMP) Synthase (cGAS). STING ultimately controls the transcription of numerous host defense genes, including type 1 interferons (IFNs) and several cytokines via downstream signaling, including phosphorylation of interferon regulatory factor 3 (IRF3). Production of IFNs is essential for further activation of both the innate and adaptive immune response.[6] Recent studies using tumor mouse models underline the pivotal role of STING in anti-tumor immunity. Several of these studies showed that STING-deficient mice were more susceptible to developing cancer. These mice show an inadequate anti-tumor immune response and lost control of tumor growth.[7–10] Vice versa, high STING expression led to higher levels of IFN production and numbers of CD8+ tumor-infiltrating lymphocytes (TILs).[11,12] Furthermore, STING plays an essential role in dendritic cell recognition of dying tumor cells and priming of anti-tumor cytotoxic T cell (CTL) responses.[8,11,13] Loss or decreased expression of STING associates with poor prognosis in several human cancer types such as gastric cancer, hepatocellular carcinoma, head and neck squamous cell carcinoma (HNSCC), breast cancer and colorectal cancer.[14–19]

Previously, STING protein expression was evalustated in high grade cervical intraepithelial neoplasia (CIN3).[20] Here, we evaluated STING protein expression and sought to investigate the prognostic value of STING in established cervical cancer. Moreover, we investigated how the prognostic value of STING relates to the prognostic value of CD103,

an integrin that marks anti-tumor tissue-resident memory T cells and has high prognostic value in multiple cancer types, including cervical cancer.[21–24] We included two cervical cancer patient groups and studied pre-treatment STING and CD103 protein levels in relation to clinical characteristics. The first group consisted of patients primarily treated with surgery, the first choice of treatment in early stage of disease. The second group consisted of patients that received (chemo)radiation as the first modality of treatment, which is given as a first choice of treatment to patients with locally advanced cervical cancer. Additionally, we investigated the association between *STING1* (encoding STING) mRNA and survival in cervical cancer patients using RNA sequencing data from The Cancer Genome Atlas (TCGA) cervical carcinoma datasets.

Materials and methods

Patient selection

In the University Medical Center Groningen (UMCG) clinicopathologic and follow-up data are prospectively obtained during standard treatment and follow-up and stored in a computerized registration database. For the present study, cervical cancer patients (n=679) treated between 1986 and 2004 in the UMCG were included in a separate anonymous database, in which patient identity was protected by study-specific, unique patient codes. Codes were only known by two dedicated data managers. Patients were treated with surgery or radio(chemo)therapy (RT/RCT), according to standard-of-care at time of treatment. Tumors were graded and classified by a pathologist specialized in gynecologic malignancies. Tumors were staged according to the Federation of Gynecology and Obstetrics (FIGO) guidelines.[25,26] Patients were divided in two groups based on their primary treatment; surgery or RT/RCT. Surgical treatment consisted of a radical hysterectomy combined with pelvic lymph node dissection. All patients that received RT or RCT as first modality of treatment were included in the RT/RCT group (see characteristics in Table 1). No significant differences in STING levels (including medians) and disease-specific survival (DSS) were observed between RT and RCT (Supplementary Figure 1). Patients with disseminated disease were not excluded from analyses. The tissue used for the analyses was obtained from pretreatment biopsies. Using the registration database, all tissue specimens were identified by unique patient numbers and retrieved from the archives of the Department of Pathology. Therefore, according to Dutch law, no further Institutional Review Board approval was needed.

Tissue micro array construction

Material from the patients that met the inclusion criteria was used to construct a tissue micro array (TMA). The TMA was constructed by the pathology department of the UMCG as described previously.[27] One millimeter-sized tumor (center of the tumor) and

tumor/stroma (invasive margin) cores of each tumor block were randomly distributed on the TMA in triplicate.

Immunohistochemical analysis of p16, STING and CD103

TMA slides were stained for p16 as surrogate marker for HPV status. Pretreatment of the TMA slides was performed using ULTRA Cell Conditioning 1 (Roche Ventana, Tucson, AZ, USA). Next, slides were incubated with ready-to-use primary anti-p16 mouse monoclonal antibody, clone E6H4, (Roche Ventana, Tucson, AZ, USA). After incubation, the primary antibody was visualized using the Optiview detection kit (Roche Ventana, Tucson, AZ, USA). The complete staining protocol was performed using the Ventana Benchmark ULTRA instrument (Roche Ventana, Tucson, AZ, USA), according to the instructions of the manufacturer. Appropriate washings were performed in between steps. Upon staining, slides were scanned using a NanoZoomer 2.0-HT multi slide scanner (Hamamatsu Photonics). Cores were independently scored by two researchers and a pathologist, blinded for clinicopathological data. A patient was annotated to be HPV-positive in case at least one tumor core was found to be p16 positive (Supplementary Figure 2).

Immunohistochemical analysis of CD103 and CD8 was performed previously.[23] To assess STING, TMA slides were first dewaxed in xylene and rehydrated using degrading concentrations of ethanol to distilled water. Antigen was retrieved using a pre-heated buffer of 10 mM citrate. To block endogenous peroxidase, slides were incubated in a 0.3% H_2O_2 solution. Subsequently, slides were incubated with 1 μg/mL anti-STING antibody (EPR13130, Abcam) or an isotype control (Rabbit IgG SP137, Abcam) in PBS solution with 1% BSA + 1% AB serum overnight at 4°C. Afterward, slides were incubated with a peroxidase-labeled polymer (Envision+ anti-rabbit, Dako), followed by a 3.3'-diaminobenzidine solution (DAB) to visualize specific signal. Slides were counterstained with hematoxylin and thereafter dehydrated and mounted. Images were obtained using a NanoZoomer 2.0-HT multi slide scanner (Hamamatsu Photonics). Hematoxylin and eosin (H&E) staining was performed using a standard technique.

Per patient, three cores were assessed. Patients that did not have at least two out of three cores with more than 20% tumor epithelium were excluded from the study (n=173), resulting in a remaining total of 506 patients. Positivity of STING was analyzed by estimating the percentage of tumor epithelium at each staining intensity level (0 = negative, 1 = low, 2 = intermediate and 3 = high) and, subsequently, a Histo-score was assigned using the formula: [0× (% tumor epithelium 0+) + 1× (% tumor epithelium 1+) + 2× (% tumor epithelium 2+) + 3× (% tumor epithelium 3+)].[28,29] This score, ranging from 0 to 300, was averaged over the 3 (or 2) cores of one patient. STING positive immune cells were only observed in a small subset of cores and, therefore, not included

in the analysis. All TMA slides were scored by two individuals who were blinded for clinicopathological data. The interobserver agreement (intraclass correlation coefficient (ICC)) was 0.824. Scores were compared and if a difference of more than 50 was found, slides were reassessed.

TCGA

TCGA RSEM normalized mRNAseq and clinical data were downloaded from FireBrowse (http://firebrowse.org) on August 22, 2016. mRNA data were log2 transformed. After removal of normal tissue controls, 306 cervical cancer cases were informative for this study. Rows without gene names ("?") were removed. Histological subtypes were reclassified as follows: "Endocervical adenocarcinoma of the usual type", endocervical type of adenocarcinoma", endometrioid adenocarcinoma of endocervix" and "mucinous adenocarcinoma of endocervical type" were classified as adenocarcinoma (n=47), squamous (n=254) and adenosquamous (n=6) were not reclassified. *STING1* (*TMEM173* in TCGA) levels were extracted per histological subtype. Stage of disease, i.e. early or late, was categorized according to FIGO stage of disease, with stage I – stage IB1 being early stage of disease and stage IB2- stage IVB as late stage. Patients with stage IB not further specified as A or B (n=38) were removed for this part of the analysis, as were patients with no information on FIGO stage (n=7). For survival analysis, patients were dichotomized based on median *TMEM173* or *ITGAE* expression, respectively. Survival analyses were performed with the survminer package in R (version 0.4.6). Heatmaps of STING and immune-related genes were constructed with ComplexHeatmap package (version 2.2.0) and Circlize package (version 0.4.9) in R.

Statistical analyses

Interobserver agreement of STING scoring was analyzed using the ICC based on a single measurement, absolute agreement, two-way mixed models. The differences between i) STING and CD103 levels for the surgery versus RT/RCT group, ii) CD103 based on below and above median STING per group, iii) *STING1* mRNA expression based on non-cancer and cervical cancer samples (TCGA data) and iv) *STING1* mRNA expression based on early and (locally) advanced stage cervical cancer samples (TCGA data) were assessed with Mann–Whitney U tests. The differences between i) STING based on histology per group and ii) *STING1* mRNA expression in cervical cancer samples based on histology (TCGA data) were assessed by Kruskal–Wallis tests with post hoc Dunn's multiple comparison test. Correlation plots were made and analyzed using GraphPad Prism version 8. Differences in clinicopathological characteristics regarding below versus above median STING per group were assessed by crosstab analyses with Chi-Square tests. DSS, disease-free survival (DFS) and survival probability (TCGA data) were plotted by Kaplan–Meier function and statistically assessed by Log Rank testing. Differences

Table 1. Relation of STING level to clinical characteristics

	STING level - surgery cohort			<STING level - RT/RCT cohort		
	<median (208.33)	≥median (208.33)	P value	≤median (186.44)	>median (186.44)	P value
Patients	123	128		128	127	
Age at diagnosis (y), cont.			0.524			0.471
Median	42.95	43.76		54.73	52.18	
Range	24.43 - 84.65	24.40 - 81.94		25.61 - 84.33	20.61 - 91.95	
HPV status (p16)			0.261			1.000
Positive	107	117		115	114	
Negative	11	5		9	9	
Unknown	5	6		4	4	
FIGO stage			0.077			0.747
IA2	-	-		-	-	
IB1	75	84		12	14	
IB2	21	29		16	10	
IIA	27	15		17	18	
IIB	-	-		59	65	
IIIA	-	-		3	2	
IIIB	-	-		19	14	
IVA	-	-		2	4	
Histology			**0.034**			**0.001**
Squamous carcinoma	74	94		95	116	
Adenocarcinoma	43	26		28	9	
Other	6	8		5	2	
Grade of differentiation			0.662			0.448
Good/moderate	70	80		67	74	
Poor/undifferentiated	51	46		53	43	
Other	2	2		8	10	
Lymphangioinvasion			0.467			0.990
No	54	50		72	76	
Yes	69	77		21	23	
Other	-	-		5	5	
Tumor diameter (cm)			0.937			0.901
0-4	88	91		31	33	
≥4	35	37		89	85	
Unknown	-	-		8	9	
Treatment			0.312			0.663
RH	77	71		-	-	
RH + post operative RT	38	51		-	-	
RH + post operative RCT	8	6		-	-	
Primary RT	-	-		58	61	
Primary RCT	-	-		70	66	
Follow-up (y), cont.			0.542			0.381
Median	5.35	5.93		3.68	3.80	
Range	0.31-19.35	0.53-21.31		0.14 - 16.28	0.17 - 18.36	
Result last follow-up			**0.014**			**0.041**
No evidence of disease	93	106		51	62	
Evidence of disease	2	0		2	0	
Death other cause	1	7		10	18	
Death of disease	27	15		65	47	

Abbreviations
FIGO: International Federation of Gynecologists and Obstetricians
Histology other: small cell carcinoma or unknown
RH: Radical hysterectomy
RT: Radiotherapy
RCT: Radio-chemotherapy

between DSS based on clinicopathological characteristics and STING were analyzed using Cox regression testing on DSS. Clinicopathological characteristics were included in multivariate analyses when P value was <0.05 in univariate analysis. For the RT/RCT group, the number of patients with FIGO stage IIIA was too small for this analysis (non-determinable). All tests were performed two-sided and outcomes were considered significant when the P value was <0.05. All statistical analyses were performed using IBM SPSS Statistics software version 23.0, GraphPad Prism version 8 or R version 3.6.2.

Results

Adenocarcinomas and advanced stage disease associate with lower levels of STING

STING expression has been reported to be lost or down-regulated in multiple cancer types, and loss of STING was associated with poor prognosis.[14–18] To investigate the prognostic value of STING in cervical cancer patients, we assessed STING protein levels by immunohistochemistry (IHC) on tissue microarrays (TMA) of pretreatment cervical cancer biopsies. In line with previous work[30], STING expression was detected in the cytoplasm and perinuclear compartments, and present in both tumor cells and in isolated immune cells (Figure 1). Patients were included when at least two out of three cores contained more than 20% tumor epithelium. Based on this criterion, 506 patients were finally included. A high degree of uniformity in staining intensity was observed within and between the individual cores (Figure 1 and Supplementary Figure 3). This indicates that the staining pattern in most tumors appears to be homogeneous and that our TMA sufficiently captures STING protein levels in cervical cancer patients. Comparison of STING values of early stage disease (FIGO 1B1) versus (locally) advanced disease stages (FIGO IB24A) revealed that STING is significantly lower in the latter group (Supplementary Figure 4). As choice of treatment depends on FIGO stage, patients were divided into two groups based on their primary treatment being surgery (n=251) or radio(chemo)therapy (RT/RCT) (n=255). In line, we observed that STING levels were significantly lower in the RT/RCT group (median 186.44) compared to the surgery group (median 208.33) (Figure 2A, P<.0001). In addition to treatment, each group was dichotomized based on low or high STING, defined as below or equal to/above median STING level per group to avoid bias evoked by the relation of STING with FIGO, and analyses of clinical characteristics were performed to assess whether STING was associated with disease progression (Table 1).

Most clinical characteristics such as age at diagnosis, p16 status as surrogate marker for HPV status, grade of differentiation, lymphangioinvasion, tumor diameter and years of follow-up were found to be consistent between low and high STING. Interestingly, the histological subtype distributions were significantly different between patients with

Figure 1
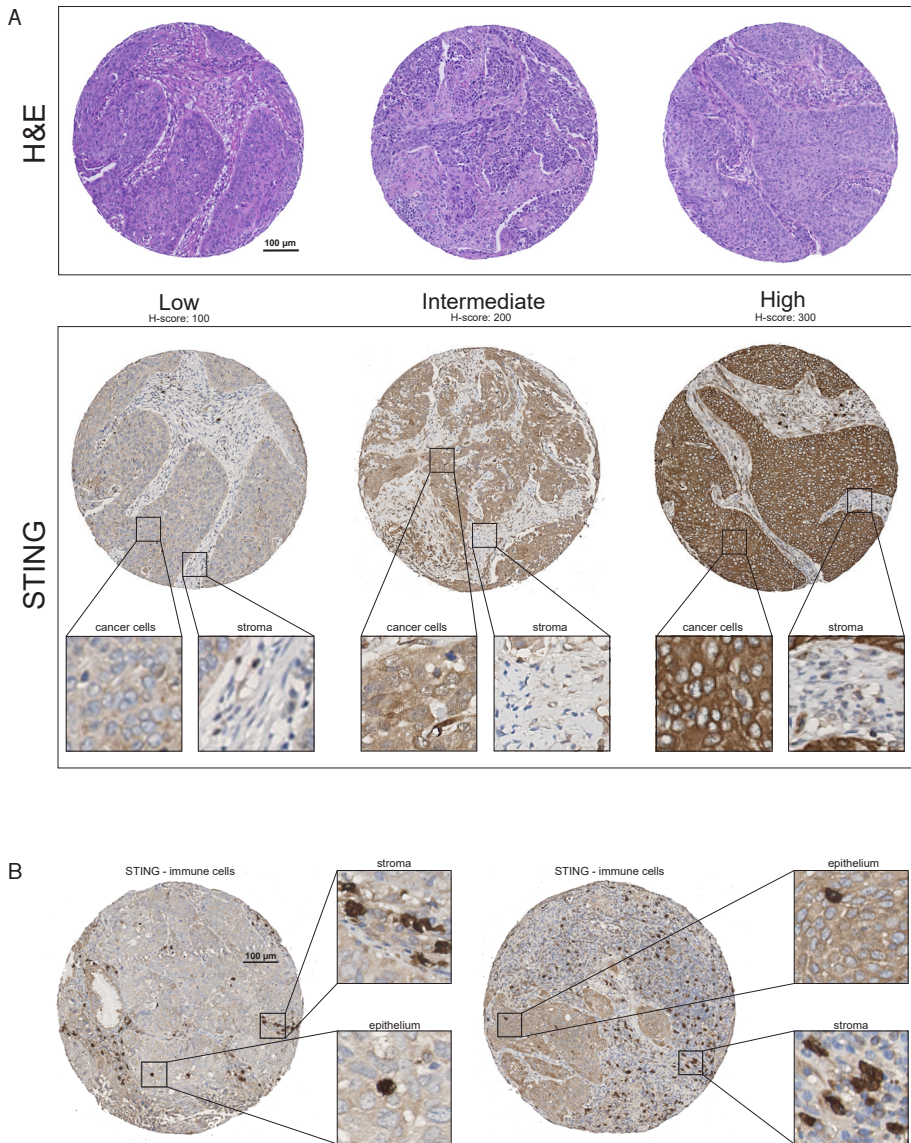
Representative images of H&E stainings and immunohistochemical STING stainings in cervical carcinomas. A) tissue microarray (TMA) cores representing tissue with low (H-score: 100), intermediate (H-score: 200) and high (H-score: 300) STING levels, based on intensity of DAB (brown). For each core magnifications of areas with cancer cells and stroma are depicted. B) TMA cores representing STING protein positivity in tumor infiltrating immune cells. For each core magnifications of areas with epithelium and stroma are depicted. Images were obtained using a NanoZoomer 2.0-HT multi slide scanner (Hamamatsu Photonics).

low and high STING (P=.033 surgery and P<.001 RT/RCT group). Further assessment revealed that STING levels were significantly lower in adenocarcinomas as compared to squamous cell carcinomas in both groups (Figure 2B, P=.0003 surgery and P<.0001 RT/RCT group). We did not observe significant differences in STING levels between cervical adenocarcinoma histological subtypes (Supplementary table S1). Patients with adenocarcinomas tended to have worse outcome than patients with squamous or other tumor types, but these differences did not reach statistical significance (Supplementary Figures 5A, P=.332 surgery and 5B, P=.060 RT/RCT). Previously, it was shown that HPV-cervical carcinomas are more frequently adenocarcinomas and seem to be associated with worse survival.[31,32] In the present study, DSS for patients with p16- adenocarcinomas was indeed worse than for patients with p16+ adenocarcinomas in the RT/RCT cohort (P=.012, Log Rank test), but only regarded two p16- patients. p16 status did not affect STING level in adenocarcinomas (P=.269 surgery and P=.676 RT/RCT, Chi-Square test).

Figure 2
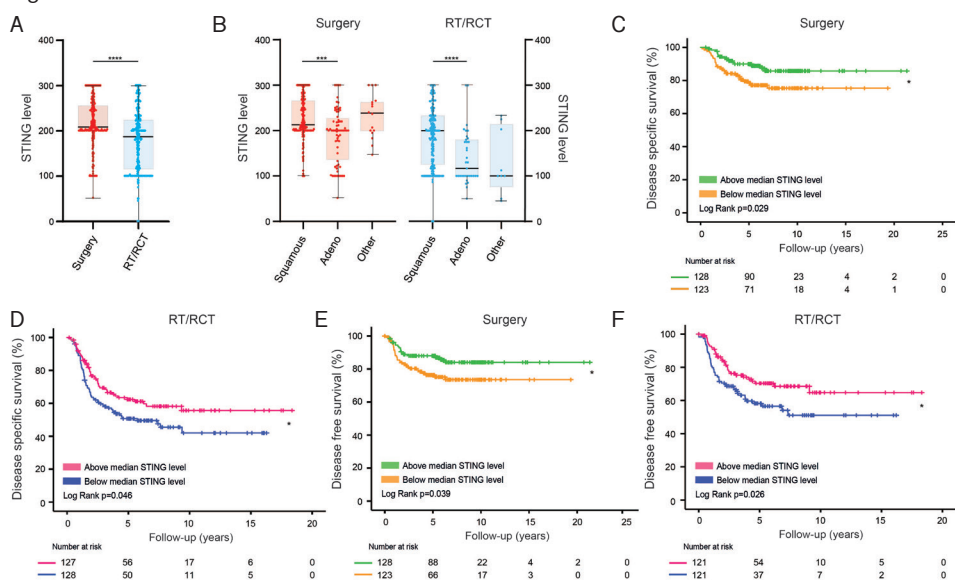
STING is prognostic for survival of cervical cancer patients. *A) STING scores per group, surgery (red) or RT (blue). B) STING scores group, surgery (red) or RT (blue), based on histological subtype. A, B) each dot represents one patient. Median, quartiles and maximal values are depicted by boxplots. Statistical analyses, either by Mann–Whitney U or Kruskal–Wallis with post hoc Dunn testing, were performed using GraphPad Prism version 8. A P value of <.05 was considered statistically significant. C, D) Disease specific survival in years for the C) surgery and D) RT/RCT group. E, F) Disease free survival in years for the E) surgery and F) RT/RCT group. Orange and blue curves represent patients with STING levels below the median level; green and pink curves patients with STING levels above the median. All STING levels were obtained from immunohistochemical STING stainings on TMA. All four statistical analyses were performed by Log Rank testing in SPSS. A P value of <.05 was considered statistically significant. Numbers at risk are depicted below each Kaplan Meier plot and correspond to the years of follow-up at the y-axis.*

STING is prognostic for survival of cervical cancer patients

The status at last follow-up significantly differed between patients with low and high STING in both groups (Table 1, P=.014 surgery and P=.041 RT/RCT group). Here, we observed that patients with low STING showed higher recurrence rates, more residual disease and increased disease-specific mortality compared with that of patients with high STING expression. As expected, having more advanced stage disease, patients included in the RT/RCT group had worse outcomes. Specifically, 112/255 RT/RCT group patients (43.92%) died of disease versus 42/251 (16.73%) in the surgery group. To follow up on these findings, we further explored the relation between STING and survival. As we determined the levels of STING in pretreatment material, we first assessed disease-specific survival (DSS) based on below and above median STING for all 506 patients (adjusted median of 200). High STING strongly associated with improved outcome over patients with low STING levels, irrespective of subsequent therapy (Supplementary Figure 6, P=.000). In line, for both the surgery and the RT/RCT groups, we observed that DSS was significantly worse for patients with low STING (Figures 2C, P=.029 surgery, and 2D P=.046 RT/RCT group). Low STING was also significantly prognostic for worse disease-free survival (DFS) in both groups (Figures 2E P=.039 surgery, and 2F, P=.026 RT/RCT group). We conclude that STING levels associated with prognosis of cervical cancer patients, in both early stage and locally advanced stage disease. Specifically, low levels of STING predicted worse survival outcome.

Multivariate analyses confirms the independent prognostic value of STING in cervical cancer

To examine if the high prognostic value of STING in cervical cancer is independent of other factors, we performed univariate and multivariate Cox regression analyses on both groups (Tables 2 surgery and Tables 3 RT/RCT group). For the surgery group, these analyses revealed that univariate prognostic factors for DSS were age at diagnosis, FIGO stage, lymphangioinvasion, tumor diameter and STING level (based on above and below median level). After multivariate analysis including these factors, only FIGO stage, lymphangioinvasion and STING level were found to be independently prognostic. For the RT/RCT group, FIGO stage, histology, lymphangioinvasion, tumor diameter and STING level were univariate prognostic factors for DSS. Multivariate analysis revealed that FIGO stage and STING level were independently prognostic for survival. Together, the analyses show that STING is an independent prognostic factor for survival in cervical cancer.

High STING levels combined with CD103-positive tumor infiltrating lymphocytes strongly associates with improved prognosis

We have previously reported that CD103-positive tumor-infiltrating lymphocytes are tumor-reactive, intraepithelial CD8-positive T cells that are associated with prognostic

Table 2. Surgery cohort. Cox regression survival analyses

	Univariate analyses				Multivariate analysis			
	HR	95% CI		P value	HR	95% CI		P value
Age at diagnosis (years)								
<54 years	ref	ref	ref	ref				
>54 years	2.098	1.123	3.919	**0.020**				
FIGO stage								
IB1	ref	ref	ref	ref	ref	ref	ref	ref
IB2	2.139	1.010	4.531	**0.047**	1.878	0.864	4.084	0.112
IIA	3.149	1.542	6.430	**0.002**	2.744	1.337	5.632	**0.006**
Histology								
Squamous carcinoma	ref	ref	ref	ref				
Adenocarcinoma	1.694	0.900	3.190	0.103				
Other	0.942	0.223	3.988	0.936				
Differentiation grade								
Good/moderate	ref	ref	ref	ref				
Poor/undifferentiated	1.657	0.898	3.058	0.106				
Other	1.626	0.218	12.122	0.635				
Lymphangioinvasion								
No	ref	ref	ref	ref	ref	ref	ref	ref
Yes	3.830	1.697	8.641	**0.001**	3.831	1.694	8.662	**0.001**
Tumor diameter (cm)								
0-4	ref	ref	ref	ref				
≥ 4	2.303	1.254	4.229	**0.007**				
STING_median								
Low	ref	ref	ref	ref	ref	ref	ref	ref
High	0.501	0.267	0.942	**0.032**	0.456	0.237	0.879	**0.019**

Disease-specific survival, Enter for univariate and Forward Stepwise (LR) for multivariate, n=251
FIGO - International Federation of Gynecology and Obstetrics
Histology other: small cell carcinoma or unknown

benefit and therapy response in cervical cancer.[23] Since STING pathway activation can play a role in the induction of CD8+ T cell responses against tumor-derived antigens *in vivo*[8], we wondered whether CD103+ TIL infiltration associates with STING levels. For this reason, we assessed CD103+ TIL infiltration in cervical cancer patients[23] in combination with STING scores. CD103+ TIL infiltration scores were available for 216 patients in the surgery group and 232 patients in the RT/RCT group. Levels of STING correlated with levels of CD103 (r=0.2323, P<.0001), largely due to patients of the RT/RCT cohort (Supplementary Figures 7A-C). Off note, no correlation between CD8 and STING levels was found (Supplementary Figures 7D-F). Kaplan–Meier plots of DSS and DFS were generated to assess the correlation of STING and CD103+ TIL infiltration with survival. The cut-off was determined based on median STING and median CD103+ TIL infiltration for each group, resulting in four subgroups: STING^{high}/CD103^{high}, STING^{high}/CD103^{low}, STING^{low}/CD103^{high} and STING^{low}/CD103^{low}. Patients in the surgery group appeared to have significantly more CD103 infiltration than patients from the RT/RCT group (Figure 3A, <.0001). When further exploring the difference per group with regard to STING, we observed significantly higher CD103 infiltration in patients with high STING than in patients with low STING in both groups (Figure 3B, P=.0242 surgery and P<.0001 RT/RCT group). In contrast to STING, CD103 was only

Table 3 RT/RCT cohort. Cox regression survival analyses

	Univariate analyses				Multivariate analysis			
	HR	95% CI		P value	HR	95% CI		P value
Age at diagnosis (years)								
<54 years	ref	ref	ref	ref				
>54 years	0.875	0.603	1.270	0.483				
FIGO stage								
IB1	ref	ref	ref	ref	ref	ref	ref	ref
IB2	2.550	0.659	9.864	0.175	1.843	0.439	7.730	0.403
IIA	4.989	1.462	17.025	**0.010**	3.751	1.059	13.295	**0.041**
IIB	4.831	1.515	15.404	**0.008**	4.363	1.357	14.022	**0.013**
IIIA	ND	ND	ND	ND	ND	ND	ND	ND
IIIB	7.590	2.251	25.527	**0.001**	7.952	2.315	27.319	**0.001**
IVA	15.483	3.696	64.849	**<0.0001**	13.227	2.618	66.882	**0.022**
Histology								
Squamous carcinoma	ref	ref	ref	ref				
Adenocarcinoma	1.673	1.025	2.616	**0.039**				
Other	1.701	0.624	4.637	0.300				
Differentiation grade								
Good/moderate	ref	ref	ref	ref				
Poor/undifferentiated	1.353	0.927	1.975	0.117				
Other	0.481	0.175	1.327	0.158				
Lymphangioinvasion								
No	ref	ref	ref	ref				
Yes	1.767	1.115	2.801	**0.015**				
Other	1.108	0.401	3.058	0.844				
Tumor diameter (cm)								
0-4	ref	ref	ref	ref				
≥ 4	1.656	1.035	2.649	**0.035**				
Unknown	0.921	0.373	2.273	0.859				
STING_median								
Low	ref	ref	ref	ref	ref	ref	ref	ref
High	0.684	0.470	0.996	**0.048**	0.597	0.384	0.928	**0.022**

Disease-specific survival, Enter for univariate and Forward Stepwise (LR) for multivariate, n=255
Abbreviations. FIGO - International Federation of Gynecology and Obstetrics. ND- not determinable
Histology other: small cell carcinoma or uknown

prognostic for DSS and DFS of patients in the RT/RCT group, thus with locally advanced disease (Supplementary Figures 8B P=.014 and 8D P=.021, respectively). Combining the factors STING and CD103 revealed significant prognostic value for survival of patients from the RT/RCT group (Figures 3D and 3F, P=.014 and P=.004, respectively). Specifically, patients characterized by a STING^{high}/CD103^{high} pattern had a longer DSS and DFS than patients from the STING^{low}/CD103^{low} group. Similar to the observation that CD103 did not have prognostic value (DSS and DFS) in the surgery group (Supplementary Figures 8A and 8C, P=.280 and P=.690 resp.), the combination of CD103 and STING was also not prognostic in this group (Figures 3C and 3E, P=.154 and P=.148 resp.). The observed effects were independent of HPV infection, as CD103 levels were comparable for p16+ and p16- patients (P=.621 surgery and P=.359 RT/RCT, Chi-Square test).

STING1 expression does not correlate to survival in TCGA samples from patients with cervical cancer

Lastly, we wanted to further explore our observations by investigating mRNA data

Figure 3
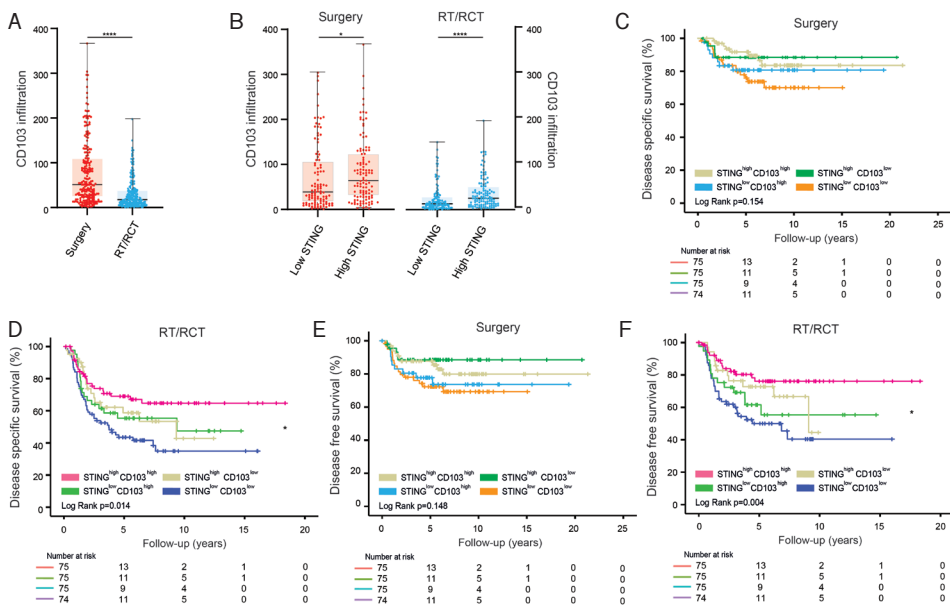
High STING and CD103 is strongly associated with improved prognosis. *A) CD103 scores per group, surgery (red) or RT (blue). B) CD103 scores per group, surgery (red) or RT (blue), stratified for low or high STING levels. A, B) each dot represents one patient. Median, quartiles and maximal values are depicted by boxplots. Mann–Whitney U statistical analyses were performed using GraphPad Prism version 8. A P value of <.05 was considered statistically significant. C, D) disease specific survival in years for the C) surgery and D) RT/RCT group. E, F) disease free survival in years for the E) surgery and F) RT/RCT group. Colors represent specific combinations of STING and CD103 (above and/or below median levels) and are clarified in the legend in each plot. All STING levels were obtained from immunohistochemical STING stainings on TMA, CD103 levels were obtained previously by immunohistochemical TMA staining23. All four statistical analyses were performed by Log Rank testing in SPSS. A P value of <.05 was considered statistically significant. Numbers at risk are depicted below each Kaplan Meier plot and correspond to the years of follow-up at the y-axis.*

of cervical cancer from the TCGA database. *STING1* mRNA expression levels did not differ between non-cancerous tissue (n=3) and cervical cancer tissue (n=306) of patient samples in the TCGA database (Figure 4A, P=.1245). Also, *STING1* expression levels did not differ between non-cancerous tissue (n=3), adenocarcinoma (n=47) and squamous cell carcinoma (n=253) in cervical cancer patients (Figure 4B, P=.2946). Since treatment data was often missing, we separated patient samples from the TCGA database into early (FIGO I–IB1) and (locally) advanced stage disease (FIGO IB2 to IVB). Based on standard-of-care treatment regimens, the early and late stage disease represent our surgery and RT/RCT groups, respectively. In contrast to the observations in our IHC data in these groups, TCGA *STING1* mRNA levels were comparable for cervical cancer patients based on early (n=86) and (locally) advanced stage disease (n=176) (Figure 4C, P=.5609). *STING1* mRNA expression had no prognostic value when looking at overall survival of all cervical cancer patients (Figure 4D, P=.105) and of patients with early stage disease (Figure 4E, P=.4) or (locally) advanced stage disease (Figure 4F, P=.6). In contrast,

Figure 4

2
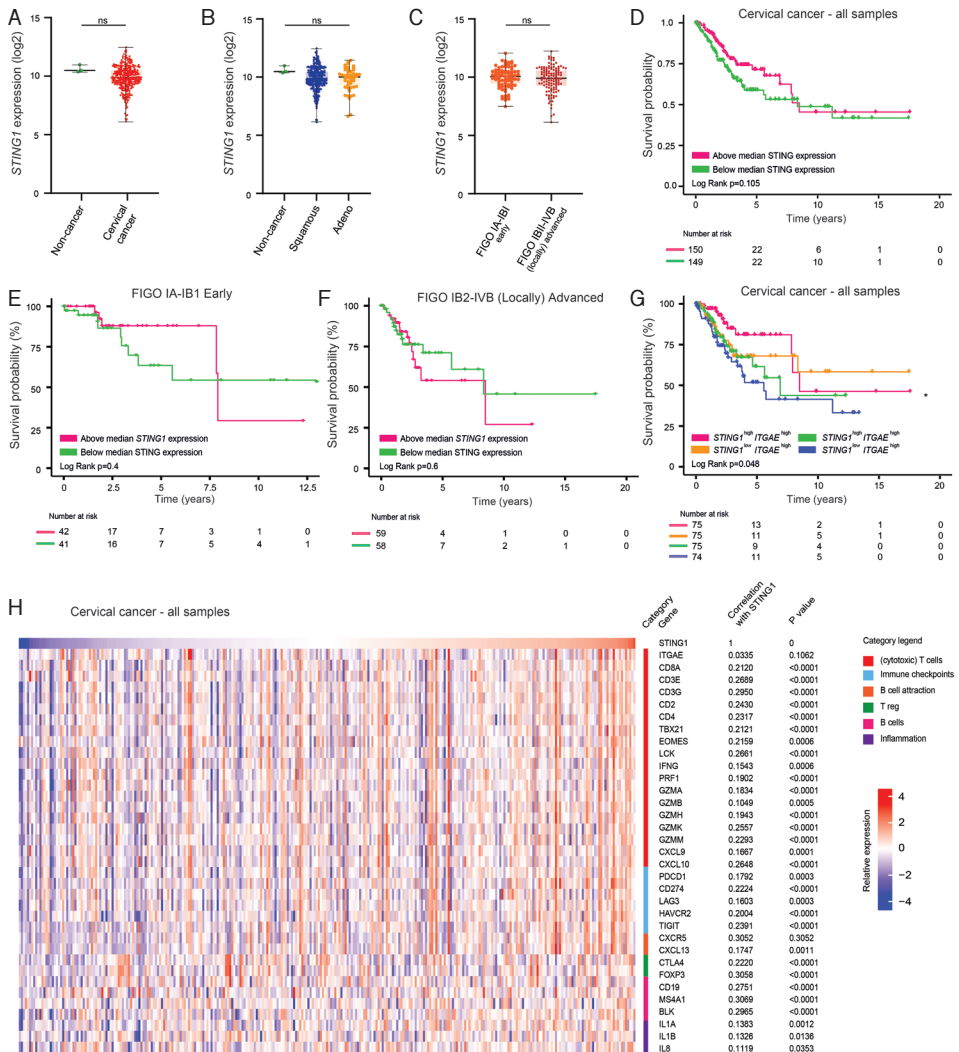
Correlation between STING1 expression and survival in TCGA samples from patients with cervical cancer. All expression and survival data were derived from cervical cancer samples (n=306) in the TCGA database. The mRNA expression data were log2 transformed before analysis. A) STING1 mRNA expression scores in non-cancer samples (green, n=3) and cervical cancer samples (red). B) STING1 mRNA expression scores in non-cancer samples (green) and cervical cancer samples based on histological subtype (squamous cell carcinoma in blue, n=253 and adenocarcinoma in orange, n=47). C) STING1 mRNA expression scores in cervical cancer samples, stratified for early FIGO stage (orange, IA to IB1, n=86) and (locally) advanced FIGO stage (red, IB2-IVB, n=176). A, B, C) each dot represents one patient. median, quartiles and maximal values are depicted by boxplots. Statistical analyses, either by Mann–Whitney U or Kruskal–Wallis with post hoc Dunn testing, was performed using GraphPad Prism version 8. A P value of <0.05 was considered statistically significant. D, E, F) Survival probability plots in years based on above (red) and below (blue) median STING1 expression in D) all cervical cancer samples, E) cervical cancer samples annotated as early FIGO stage and F) cervical cancer samples annotated as (locally) advanced FIGO stage (red, IB2-IVB). G) survival probability based on four above and below median expression combinations of STING1 and ITGAE (encoding CD103), for which color annotations are clarified in the legend. All four statistical survival analyses were performed by Log Rank testing in SPSS. A P value of <0.05 was considered statistically significant. Numbers at risk are depicted below each Kaplan Meier plot and correspond to the years of follow-up at the y-axis. H) Relative gene expression of (cytotoxic) T cells (red),

immune checkpoints (blue), B cell attraction (orange), T regulatory T cells (T reg)(green), B cells (pink) and inflammation (purple) associated genes in TCGA data of cervical cancer. Samples were ranked by STING1 expression. Red indicates high relative expression, and blue indicates low relative expression of the indicated gene. Correlations of gene expression with STING1 expression were determined by Spearman correlation testing using R software.

the combination of *STING1* and *ITGAE* (encoding CD103) expression was prognostic for survival (Figure 4G, P=.048). However, this was likely mainly due to the strong, positive correlation between *ITGAE* expression and survival, as our group previously published.[23] Lastly, we assessed *STING1* expression in cervical cancer patients from the TCGA database in relation to mRNA levels of important immunological markers such as *ITGAE*, *CD8A*, *GZMB*, cytokines and well-known immune checkpoints such as *PDCD1*, *LAG-3* and *TIGIT* (Figure 4H). Notably, *ITGAE* expression did not correlate with *STING1* expression (r=0.0335, P=.1062). On the other hand, expression of *STING1* correlated significantly, although fairly weakly, to expression of many of the other immunological markers, including *CD8A*, effector genes *PRF1* (r=0.1902, P<.0001) and *GMZB* (r=0.1049, P=.0005), immune checkpoints *PDCD1* (r=0.1792, P=.0003) and *TIGIT* (r=0.2391, P<.0001), and B cell attracting chemokine *CXCL13* (r=0.1747, P=.0011). When further exploring this relation by separating the patients based on histology, a similar pattern was only observed for squamous cell carcinomas but not adenocarcinomas (Supplementary Figure 9).

Discussion

In this study we show that high STING protein level is associated with improved survival in cervical cancer patients primarily treated with surgery or with (chemo)radiation therapy (RT/RCT group). Importantly, combining STING levels together with the prognostic factor CD103+TIL infiltration strongly associated with improved survival in the the RT/RCT group.

The prognostic value of pretreatment STING was independent of subsequent therapeutic modality. Nevertheless, patients in the RT/RCT group had significantly lower levels of STING pretreatment than patients in surgery group, the latter having a better prognosis due to more early stage of disease. It was previously reported for gastric cancer and hepatocellular carcinoma patients that STING protein levels were decreased in tumor tissues compared to non-tumor tissues and inversely correlated with tumor stage.[15,33] In line, low STING associated with poor prognosis in multiple cancer types.[14–19] We suggest that STING signaling may be highly deficient in patients with (locally) advanced stage disease, which could lead to poor anti-tumor immunity, immune evasion by the tumor and more progressive disease. In accordance, patients in the RT/RCT group with low STING showed significantly worse outcomes than patients with high STING levels. These findings may also support the hypothesis that STING signaling is important for radiation-mediated anti-tumor immunity in immunogenic tumors[34], in which DNA exonuclease

Trex1 may be an important regulator.[35] The importance of STING is supported by the finding that patients in the surgery group with low STING had significantly worse outcomes than patients with high STING levels. Of note, it would be interesting to investigate the potential role of HPV oncogene E7 protein expression in STING expression in these patients, as E7 is described to act antagonistically in the cGAS-STING pathway and it can promote autophagy-dependent degradation of STING.[19] In both groups, patients with adenocarcinomas appeared to have lower STING levels than patients with squamous cell carcinomas. Moreover, the patients with low STING levels in both groups had significantly worse outcomes than patients with high STING levels. It is reported that cervical cancer patients with adenocarcinomas have worse survival than patients with squamous cell carcinomas.[36,37] We speculated that this may be partially explained by having lower STING levels. In our groups, histology did not significantly associate with survival, although there was a trend toward adenocarcinomas having worse survival compared to other tumor types.

In gastric cancer patients, STING expression was decreased in both low and high stage tumors, indicating that reduced STING expression may already develop in early stages of gastric cancer.[14] STING protein levels have been investigated previously in high grade cervical intraepithelial neoplasia (CIN3).[20] This study showed that STING expression is induced in cervical dysplasia. This finding is in line with our observation that STING is expressed in cervical malignancies. Our data on STING levels is limited to cancerous tissue. Hence, based on our IHC data, no firm conclusions can be drawn regarding down-regulation of STING in cervical cancer. Analysis using mRNA data from the TCGA database indicated that *STING1* expression is similar for non-cancerous tissue and cervical cancer tissue, although the number of non-cancerous samples was limited and mRNA expression may not reflect protein levels as a result of differences in synthesis and turnover.[38] Therefore, it remains to be elucidated whether STING protein is truly down-regulated in cervical cancer as compared to healthy cervix tissue. Based on the function of STING, we speculate that STING expression is not a driver for malignant transformation, but a response to malignant transformation. As activator of innate immune recruitment via interferon induction after sensing of cytoplasmic DNA by cGAS, STING may suppress malignant transformation and low STING protein levels might therefore mark an increased risk for development of premalignant lesions to malignant lesions.

Furthermore, TCGA database analysis showed a correlation between CD103 mRNA, but not STING mRNA, and outcome in cervical cancer. This finding was not reflected on protein level since STING associated with outcome in both our patient groups. The contradiction may indicate a discordance between mRNA levels and protein levels. Of

note, we only included assessment of STING protein and mRNA levels, which might not necessarily reflect STING signaling activity. STING is part of the cGAS-STING pathway, which includes multiple components such as cGAS, IRF3 and TANK-binding kinase 1. In colorectal cancer cell lines for example, it was found that STING-dependent signaling is frequently suppressed through silencing of cGAS.[18] This lead to a reduction in type I IFN production upon DNA-damage, helping tumor cells to escape the immune-surveillance system. Therefore, it may be of interest to study other STING signaling pathway molecules in cervical cancer patients.

STING is reported to be associated with infiltration of CD8+ T cells.[16,39] Previously, we and others have shown that integrin CD103 marks tumor-reactive CD8+ T cells in the tumor epithelium.[22–24,40,41] Interestingly, like STING, CD103 infiltration was significantly higher in patients with early stage disease than patients with more advanced stage disease. High CD103 infiltration, but not CD8, was associated with high levels of STING in both groups. Moreover, analysis of TCGA mRNA data indicated a significant, positive correlation between expression of *STING1* and expression of various T cell related genes, although not for *ITGAE* (encoding CD103). Based on these findings, we speculate that STING signaling may be important for infiltration of tumor-reactive T cells in cervical cancer, without affecting the total CD8 pool. Our findings are in line with previous work that linked STING with immune response.[42]

Although high infiltration of CD103+ cytotoxic T cells is reported to be prognostic for improved outcome of patients with cervical cancer[23] and other cancer types,[40,43] in the current study we did not observe a significant association between CD103 protein and outcome for cervical cancer patients with surgery as first modality of treatment, nor for CD103 individually nor for the combination of CD103 and STING. However, despite statistical insignificance, it appeared that in the surgery group, patients with STING^{high}/CD103^{high} pattern had better outcomes than patients with STING^{low}/CD103^{low} pattern. In addition, outcome for patients in the radiotherapy group was improved when STING expression was combined with CD103 infiltration.

Since cervical cancer patients with low STING have inferior survival and protein STING levels associated with CD103 levels, we speculate that STING agonistic therapy may be beneficial for treatment of cervical cancer patients with defective or reduced STING signaling. Research is being conducted on finding an effective agonist for human STING as a potential new approach in cancer immunotherapy. These agonists include STING agonist formulated cancer vaccines[44], modified cyclic nucleotides for intra-tumoral administration[11], but also a nano-particle incorporated STING agonist for systemic delivery.[45] Thus far, STING agonists alone or in combination with other therapies such

as irradiation, chemotherapy and blockade of immune-system checkpoints, including PD-1[44–49], show promising preclinical results.

In conclusion, our study demonstrated that STING is an independent prognostic factor for favorable survival in cervical cancer. Furthermore, a high STING level combined with high frequencies of CD103+ TIL infiltration strongly associated with improved prognosis in patients with late stage disease. Combining these prognostic factors may improve risk stratification of cervical cancer patients, independent from established clinical prognostic parameters, and aid in identifying patients with defective or reduced STING signaling. Activating the STING pathway in these patients may be therapeutically beneficial and should be considered in the treatment of cervical cancer.

2

References

1. Muñoz N, et al. Epidemiologic classification of human papillomavirus types associated with cervical cancer. N. Engl. J. Med. 2003;348(6):518–527. doi:10.1056/NEJMoa021641.

2. Bosch FX, Lorincz A, Muñoz N, Meijer CJLM, Shah KV. The causal relation between human papillomavirus and cervical cancer. J. Clin. Pathol. 2002;55(4):244–265. doi:10.1136/jcp.55.4.244.

3. Walboomers JMM, et al. Human papillomavirus is a necessary cause of invasive cervical cancer worldwide. J. Pathol. 1999;189 (1):12–19. doi:10.1002/(SICI)1096-9896(199909)189:1<12::AIDPATH431>3.0.CO;2-F.

4. Best SR, Niparko KJ. Biology of HPV Infection and Immune Therapy for HPV-related head and neck cancers. P S. 2013;45:807–822.

5. Litwin TR, Clarke MA, Dean M, Wentzensen N. Somatic host cell alterations in HPV carcinogenesis. Viruses. 2017;9(8):206. doi:10.3390/v9080206.

6. Corrales L, et al. The host STING pathway at the interface of cancer and immunity find the latest version : the host STING pathway at the interface of cancer and immunity. J Clin Invest. 2016;126 (7):2404–2411. doi:10.1172/JCI86892.

7. Ahn J, Konno H, Barber GN. Diverse roles of STING-dependent signaling on the development of cancer. Oncogene. 2015;34 (41):5302–5308. doi:10.1038/onc.2014.457.

8. Woo SR, et al. STING-dependent cytosolic DNA sensing mediates innate immune recognition of immunogenic tumors. Immunity. 2014;41(5):830–842. doi:10.1016/j.immuni.2014.10.017.

9. Klarquist J, et al. STING-mediated DNA sensing promotes antitumor and autoimmune responses to dying cells. J. Immunol. 2014;193(12):6124–6134. doi:10.4049/jimmunol.1401869.

10. Ohkuri T, et al. STING contributes to antiglioma immunity via triggering type I IFN signals in the tumor microenvironment. Cancer Immunol. Res. 2014;2(12):1199–1208. doi:10.1158/2326-6066.CIR-14-0099.

11. Corrales L, et al. Direct activation of STING in the tumor microenvironment leads to potent and systemic tumor regression and immunity. Cell Rep. 2015;11(7):1018–1030. doi:10.1016/j. celrep.2015.04.031.

12. Dunn GP, et al. A critical function for type I interferons in cancer immunoediting. Nat. Immunol. 2005;6(7):722–729. doi:10.1038/ni1213.

13. Woo SR, Corrales L, Gajewski TF. The STING pathway and the T cell-inflamed tumor microenvironment. Trends Immunol. 2015;36 (4):250–256. doi:10.1016/j.it.2015.02.003.

14. Song S, et al. Decreased expression of STING predicts poor prognosis in patients with gastric cancer. Sci. Rep. 2017;7(1):1–13. doi:10.1038/s41598-016-0028-x.

15. Bu Y, Liu F, Jia Q-A, Yu S-N. Decreased expression of TMEM173 predicts poor prognosis in patients with Hepatocellular Carcinoma. PLoS One. 2016;11(e0165681):e0165681. doi:10.1371/journal.pone.0165681.

16. Chon HJ, et al. STING signaling is a potential immunotherapeutic target in colorectal cancer. J Cancer. 2019;10(20):4932–4938. doi:10.7150/jca.32806.

17. Bhatelia K, et al. Antiviral signaling protein MITA acts as a tumor suppressor in breast cancer by regulating NF-κB induced cell death. Biochim. Biophys. Acta - Mol. Basis Dis. 2014;1842 (2):144–153. doi:10.1016/j. bbadis.2013.11.006.

18. Xia T, Konno H, Ahn J, Barber GN. Deregulation of STING Signaling in Colorectal Carcinoma Constrains DNA Damage Responses and Correlates With Tumorigenesis. Cell Rep. 2016;14 (2):282–297. doi:10.1016/j. celrep.2015.12.029.

19. Luo X, et al. HPV16 drives cancer immune escape via NLRX1-mediated degradation of STING. J. Clin. Invest. 2020;130 (4):1635–1652. doi:10.1172/JCI129497.

20. Baird JR, et al. STING expression and response to treatment with STING ligands in premalignant and malignant disease. PLoS One. 2017;12(11):1–16. doi:10.1371/journal.pone.0187532.

21. Komdeur FL, et al. CD103 + intraepithelial T cells in high-grade serous ovarian cancer are phenotypically diverse TCRαβ+ CD8αβ+ T cells that can be targeted for cancer immunotherapy. Oncotarget. 2016;7 (46):75130–75144. doi:10.18632/oncotarget.12077.

22. Workel HH, et al. CD103 defines intraepithelial CD8+ PD1+ tumour-infiltrating lymphocytes of prognostic significance in endometrial adenocarcinoma. Eur J Cancer. 2016;60:1–11. doi:10.1016/j.ejca.2016.02.026.

23. Komdeur FL, et al. CD103+ tumor-infiltrating lymphocytes are tumor-reactive intraepithelial CD8+ T cells associated with prognostic benefit and therapy response in cervical cancer. Oncoimmunology. 2017;6(9):1–14. doi:10.1080/2162402X.2017.1338230.

24. Djenidi F, et al. CD8 + CD103 + Tumor–Infiltrating Lymphocytes Are Tumor-Specific Tissue-Resident Memory T Cells and a Prognostic Factor for Survival in Lung Cancer Patients. J. Immunol. 2015;194 (7):3475–3486. doi:10.4049/jimmunol.1402711.

25. Pecorelli S, Zigliani L, Revised OF. FIGO staging for carcinoma of the cervix. Int. J. Gynecol. Obstet. 2009;105(2):107–108. doi:10.1016/j.ijgo.2009.02.009.

26. Revised PS. FIGO staging for carcinoma of the vulva, cervix, and endometrium. Int. J. Gynaecol. Obstet. 2009;105(2):103–104. doi:10.1016/j.ijgo.2009.02.012.

27. Noordhuis MG, et al. Expression of epidermal growth factor receptor (EGFR) and activated EGFR predict

poor response to (Chemo)radiation and survival in cervical cancer. Clin. Cancer Res. 2009;15 (23):7389–7397. doi:10.1158/1078-0432.CCR-09-1149.

28. Hirsch FR, et al. Epidermal growth factor receptor in non-small- cell lung carcinomas: correlation between gene copy number and protein expression and impact on prognosis. J. Clin. Oncol. 2003;21(20):3798–3807. doi:10.1200/JCO.2003.11.069.

29. John T, Liu G, Tsao MS. Overview of molecular testing in non-small-cell lung cancer: mutational analysis, gene copy number, protein expression and other biomarkers of EGFR for the prediction of response to tyrosine kinase inhibitors. Oncogene. 2009;28(S1):14–23. doi:10.1038/onc.2009.197.

30. Mukai K, et al. Activation of STING requires palmitoylation at the Golgi. Nat. Commun. 2016;7(1). doi:10.1038/ncomms11932.

31. Nicolás I, et al. HPV-negative tumors of the uterine cervix. Mod. Pathol. 2019;32(8):1189–1196. doi:10.1038/s41379-019-0249-1.

32. Rodríguez-Carunchio L, et al. HPV-negative carcinoma of the uterine cervix: a distinct type of cervical cancer with poor prognosis. BJOG An Int. J. Obstet. Gynaecol. 2015;122 (1):119–127. doi:10.1111/1471-0528.13071.

33. Song S, et al. Decreased expression of STING predicts poor prognosis in patients with gastric cancer. Sci. Rep. 2017;7(1):1–13.

34. McLaughlin M, et al. Inflammatory microenvironment remodelling by tumour cells after radiotherapy. Nat Rev Cancer. 2020;20 (4):203–217. doi:10.1038/s41568-020-0246-1.

35. Vanpouille-Box C, et al. DNA exonuclease Trex1 regulates radiotherapy-induced tumour immunogenicity. Nat Commun. 2017;8(15618). doi:10.1038/ncomms15618.

36. Vinh-Hung V, et al. Prognostic value of histopathology and trends in cervical cancer: a SEER population study. BMC Cancer. 2007;7 (1):1–13. doi:10.1186/1471-2407-7-164.

37. Yokoi E, et al. Impact of histological subtype on survival in patients with locally advanced cervical cancer that were treated with definitive radiotherapy. J Gynecol Oncol. 2016;28(e19). doi:10.3802/ jgo.2017.28.e19.

38. Liu Y, Beyer A, Aebersold R. On the Dependency of Cellular Protein Levels on mRNA Abundance. Cell. 2016;165(3):535–550. doi:10.1016/j.cell.2016.03.014.

39. Harding SM, et al. Mitotic progression following DNA damage enables pattern recognition within micronuclei. Nature. 2017;548 (7668):466–470. doi:10.1038/nature23470.

40. Edwards J, et al. CD103+ tumor-resident CD8+ T cells are associated with improved survival in immunotherapy-naïve melanoma patients and expand significantly during anti-PD-1 treatment. Clin. Cancer Res. 2018;24(13):3036–3045. doi:10.1158/1078-0432. CCR-17-2257.

41. Duhen T, et al. Co-expression of CD39 and CD103 identifies tumor-reactive CD8 T cells in human solid tumors. Nat. Commun. 2018;9(1). doi:10.1038/s41467-018-05072-0.

42. Cai H, Yan L, Liu N, Xu M, Cai H. IFI16 promotes cervical cancer progression by upregulating PD-L1 in immunomicroenvironment through STING-TBK1-NF-kB pathway. Biomed Pharmacother. 2020;123:109790. doi:10.1016/j.biopha.2019.109790.

43. Webb JR, Milne K, Nelson BHPD-1. and CD103 are widely coexpressed on prognostically favorable intraepithelial CD8 T cells in human ovarian cancer. Cancer Immunol. Res. 2015;3(8):926–935. doi:10.1158/2326-6066.CIR-14-0239.

44. Fu J, et al. STING agonist formulated cancer vaccines can cure established tumors resistant to PD-1 blockade. Sci. Transl. Med. 2015;7(283):283ra52–283ra52. doi:10.1126/scitranslmed. aaa4306.

45. Cheng N, et al. A nanoparticle-incorporated STING activator enhances antitumor immunity in PD-L1-insensitive models of triple-negative breast cancer. JCI Insight. 2018;3(3). doi:10.1172/ jci.insight.120638.

46. Moore E, et al. Established T cell-inflamed tumors rejected after adaptive resistance was reversed by combination STING activation and PD-1 pathway blockade. Cancer Immunol. Res. 2016;4 (12):1061–1071. doi:10.1158/2326-6066.CIR-16-0104.

47. Deng L, et al. STING-dependent cytosolic DNA sensing promotes radiation-induced type I interferon-dependent antitumor immunity in immunogenic tumors. Immunity. 2014;41(5):843–852. doi:10.1016/j.immuni.2014.10.019..

48. Ramanjulu JM, et al. Design of amidobenzimidazole STING receptor agonists with systemic activity. Nature. 2018;564 (7736):439–443. doi:10.1038/s41586-018-0705-y.

49. Li T, et al. Antitumor Activity of cGAMP via Stimulation of cGAS-cGAMP-STING-IRF3 Mediated Innate Immune Response. Sci. Rep. 2016;6(1):1–14. doi:10.1038/s41598-016-0001-8.

2

Supplementary material

Due to the size, Supplementary Table 1 is not included in this thesis. This table can be found online via https://doi.org/10.1080/2162402X.2021.1936391.

Supplementary Figure 1
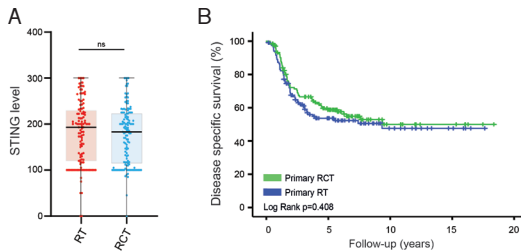
STING scores per RT (red) or RCT (blue) patient group. Each dot represents one patient. Median, quartiles and maximal values are depicted by boxplots. Statistical analysis was performed by Mann Whitney U testing using GraphPad Prism version 8. A P value of <0.05 was considered statistically significant. B) Disease specific survival in years for RT and RCT. Green curve represents patients primarily treated with RCT, and the blue curve with RT. All STING levels were obtained from immunohistochemical STING stainings on TMA. All four statistical analyses were performed by Log Rank testing in SPSS. A P value of <0.05 was considered statistically significant.

Supplementary Figure 2
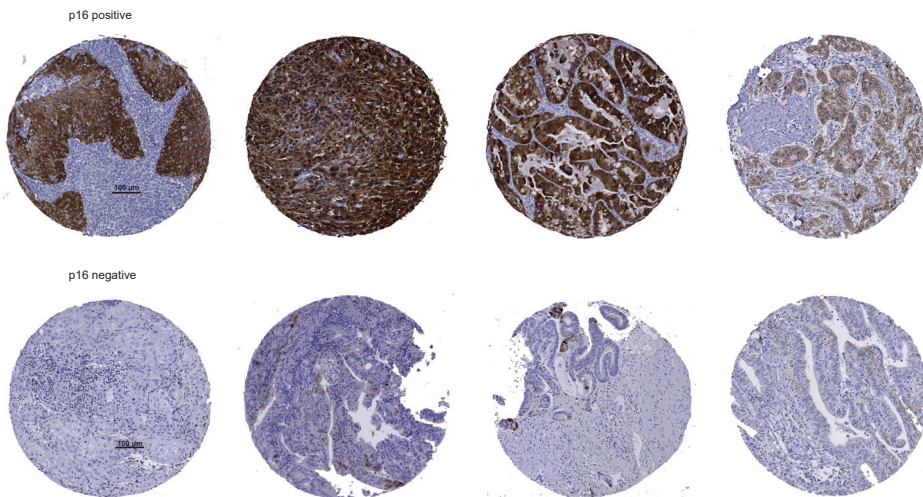
Representative images of immunohistochemical p16 stainings in cervical carcinomas. Tissuemicroarray (TMA) cores representing tissue positive and negative for p16.

Supplementary Figure 3
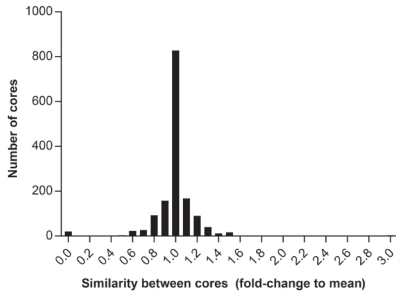
Intratumoral homogeneity of STING protein levels. Per patient the STING score of each TMA core was compared to the mean of 3 (or 2) cores. A value of 1.0 indicates identical STING scores between cores. 78% of all cores showed no more than 0.1-fold difference and 89% of the cores no more than 0.2-fold difference.

Supplementary Figure 4
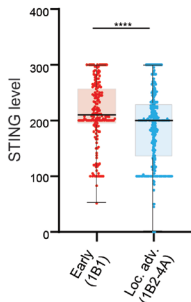
STING scores for early stage disease, FIGO 1B1 (red) and locally advanced stage disease, FIGO 1B2-4A (blue). Each dot represents one patient. Median, quartiles and maximal values are depicted by boxplots. All STING levels were obtained from immunohistochemical STING stainings on TMA. Statistical analysis was performed by Mann Whitney U testing using GraphPad Prism version 8. A P value of <0.05 was considered statistically significant.

Supplementary Figure 5
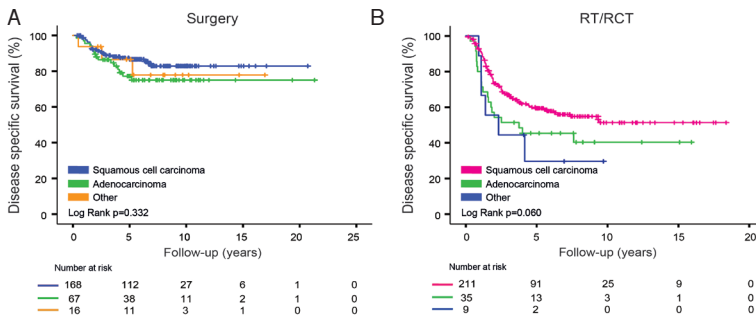
A, B) Disease specific survival in years based on histology for the A) surgery and B) RT/RCT group. Curves represent patients with squamous cell carcinomas (blue in A, pink in B), adenocarcinomas (green in both plots) and other histological subtypes (orange in A, blue in B). Both statistical analyses were performed by Log Rank testing in SPSS. A P value of <0.05 was considered statistically significant. Numbers at risk are depicted below each Kaplan Meier plot and correspond to the years of follow-up at the y-axis.

Supplementary Figure 6
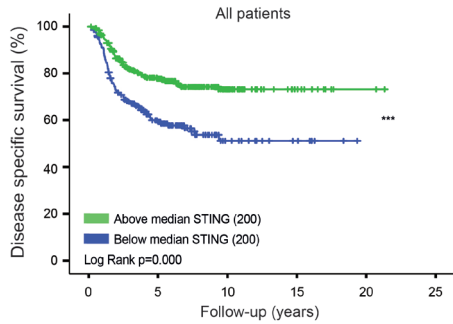
Disease specific survival in years based on above and below median STING levels for all 506 patients. The blue curves represent patients with STING levels below the median level; the green curve patients with STING levels above the median. Statistical analysis was performed by Log Rank testing in SPSS. A P value of <0.05 was considered statistically significant.

Supplementary Figure 7
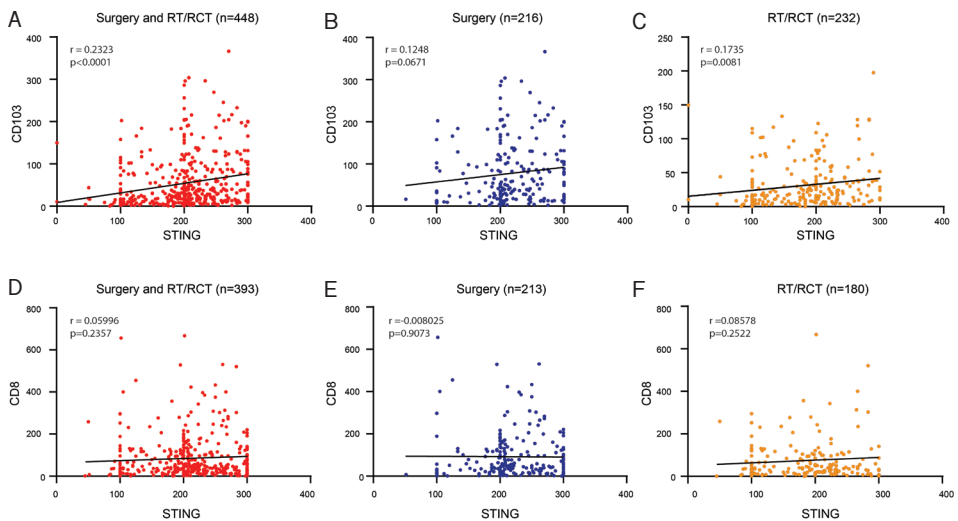
A-D) Correlation plots for CD103 and STING protein levels as assessed by immunohistochemistry for all patients (A), patients from the surgery group (B) and patients from the RT/RCT group (C). D-F) Correlation plots for CD8 and STING protein levels as assessed by immunohistochemistry for all patients (D), patients from the surgery group (E) and patients from the RT/RCT group (F). Plots and statistical analyses were established using GraphPad Prism version 8.

Supplementary Figure 8
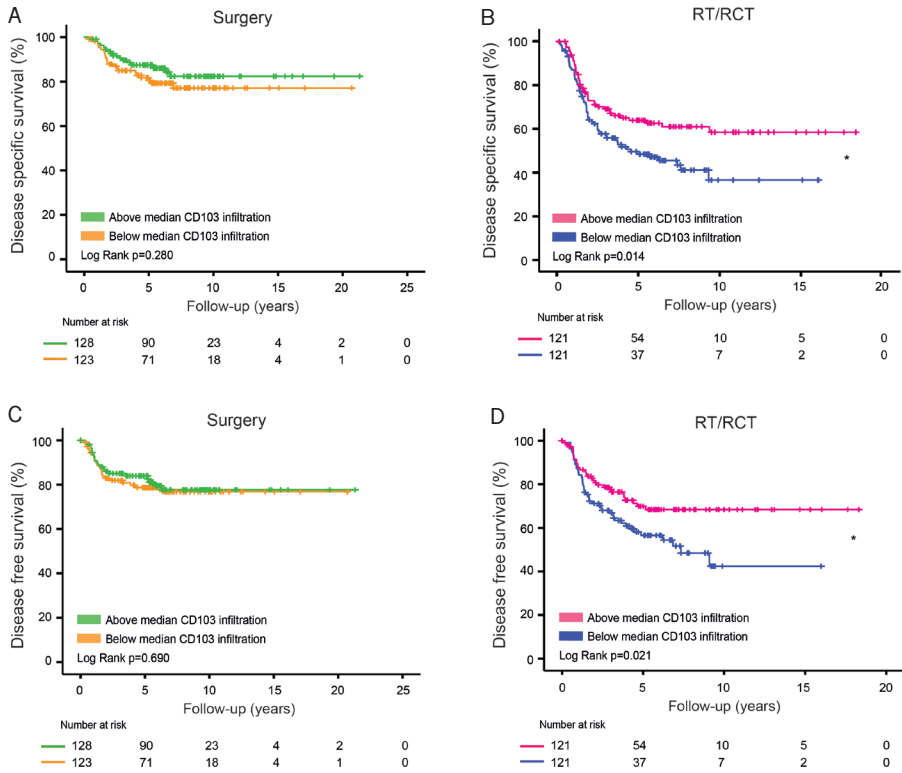
A, B) Disease specific survival in years based on above and below median CD103 infiltration for the A) surgery and B) RT/RCT group. C, D) Disease free survival in years for the C) surgery and D) RT/RCT group. Orange and blue curves represent patients with CD103 levels below the median level; green and pink curves patients with CD103 levels above the median. All CD103 levels were previously obtained from immunohistochemical CD103 stainings on TMA22. All four statistical analyses were performed by Log Rank testing in SPSS. A P value of <0.05 was considered statistically significant. Numbers at risk are depicted below each Kaplan Meier plot and correspond to the years of follow-up at the y-axis.

Supplementary Figure 9

A
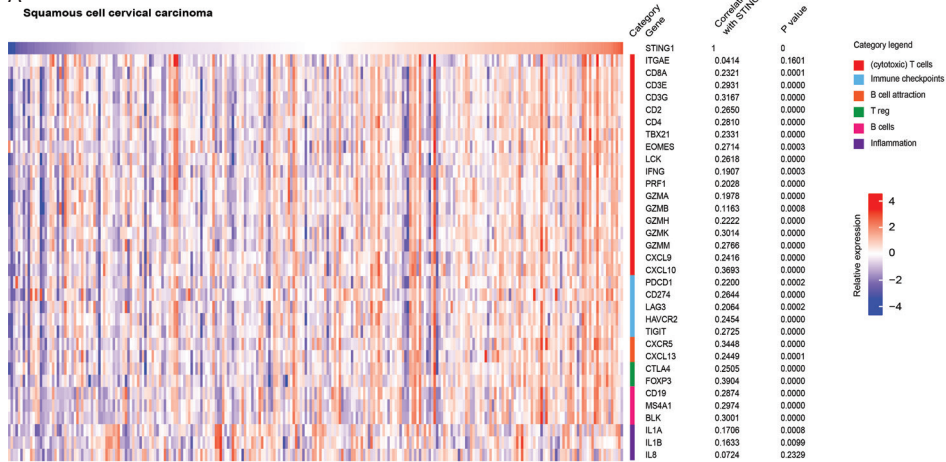
B
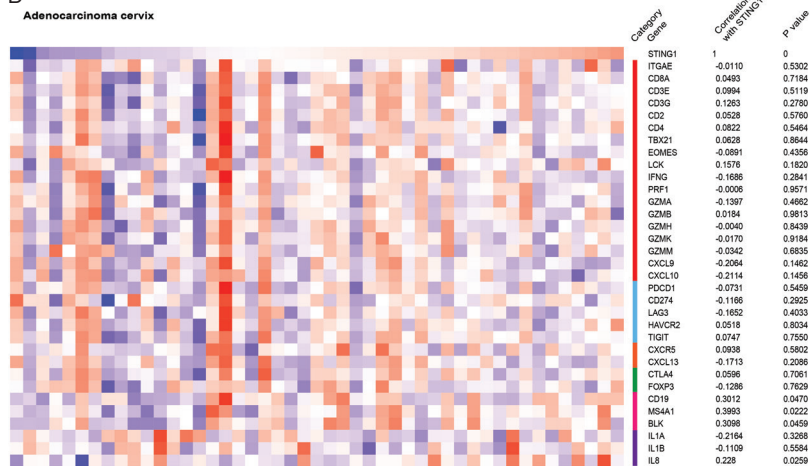
Relative gene expression of (cytotoxic) T cells (red), immune checkpoints (blue), B cell attraction (orange), T regulatory T cells (T reg)(green), B cells (pink) and inflammation (purple) associated genes in TCGA data of cervical cancer samples based on histology: A) squamous cell carcinoma (n=253) and B) adenocarcinoma (n=47). Samples were ranked by STING1 expression. Red indicates high relative expression, and blue indicates low relative expression of the indicated gene. Correlations of gene expression with STING1 expression were determined by Spearman correlation testing using R software.

2

Chapter 3

Association of homozygous variants of *STING1* with outcome in human cervical cancer

Joyce M. Lubbers[1], Bart Koopman[2], Jessica M. de Klerk-Sluis[1], Nienke van Rooij[1], Annechien Plat[1], Harry Pijper,[1] Timco Koopman[3], Bettien M. van Hemel[2], Harry Hollema,[2] Bea Wisman[1], Hans W. Nijman[1#], Marco De Bruyn[1#]

[#]share senior authorship

[1]University of Groningen, University Medical Center Groningen, Department of Obstetrics and Gynecology, The Netherlands
[2]University of Groningen, University Medical Center Groningen, Department of Pathology, The Netherlands
[3]Department of Pathology, Pathologie Friesland, Leeuwarden, The Netherlands

Abstract

DNA-sensing receptor Cyclic GMP–AMP Synthase (cGAS) and its downstream signaling effector STimulator of INterferon Genes (STING) have gained significant interest in the field of tumor immunology, as a dysfunctional cGAS-STING pathway is associated with poor prognosis and worse response to immunotherapy. However, studies so far have not taken into account the polymorphic nature of the STING-encoding *STING1* gene. We hypothesized that the presence of allelic variance in *STING1* would cause variation between individuals as to their susceptibility to cancer development, cancer progression, and potential response to (immuno)therapy. To start to address this, we defined the genetic landscapes of *STING1* in cervical scrapings and investigated their corresponding clinical characteristics across a unique cohort of cervical cancer patients and compared them with independent control cohorts. Although we did not observe an enrichment of particular *STING1* allelic variants in cervical cancer patients, we did find that the occurrence of homozygous variants HAQ/HAQ and R232H/R232H of *STING1* were associated with both younger age of diagnosis and higher recurrence rate. These findings were accompanied by worse survival, despite comparable mRNA and protein levels of STING and numbers of infiltrated CD8+ T cells. Our findings suggest that patients with HAQ/HAQ and R232H/R232H genotypes may have a dysfunctional cGAS-STING pathway that fails to promote efficient anticancer immunity. Interestingly, the occurrence of these genotypes coincided with homozygous presence of the V48V variant, which was found to be individually associated with worse outcome. Therefore, we propose V48V to be further evaluated as a novel prognostic marker for cervical cancer.

Introduction

Cervical cancer is the fourth most common type of cancer in women worldwide and the leading cause of cancer deaths in over 50 countries.[1] A persistent human papillomavirus (HPV) infection underlies the development of cervical cancer.[2] In recent years, several genomewide association studies have led to the discovery of multiple genes influencing the susceptibility to cervical cancer.[3] Allelic variants of these genes together may explain up to 24% of the variance in the risk for developing cervical cancer.[4] One of the genes is *STING1* (also known as *TMEM173* and *MITA*), encoding STimulator of INterferon Genes (STING), which is a downstream signaling effector of the DNA-sensing receptor Cyclic GMP–AMP Synthase (cGAS). During infections, cGAS detects DNA from pathogens in the cytosol of the cell and subsequently elicits STING activation and ultimately induction of interferon type I (IFN-I) signaling, thereby provoking innate and, subsequently, adaptive immunity.[5]

In the context of cancer, the cGAS-STING pathway can identify chromosomal instability in cancerous cells by detecting cytoplasmic DNA[6-8] or identify infection with potentially carcinogenic viruses by detecting viral DNA, such as DNA from HPV.[9] In addition, it is reported to improve the efficacy of (DNA damage–inducing) radiotherapy.[10, 11] Several studies have shown that dysfunction of the cGAS-STING pathway, caused for instance by deficient STING translocation to the Golgi and decreased expression levels of cGAS and STING, leads to poor IFN-I production.[10, 12-16] In multiple cancer types such as breast, gastric, and hepatocellular carcinoma, levels of STING were found to be decreased compared with healthy tissue.[14-16] In another study regarding DNA damage, loss of STING hampered tumor regression upon application of multiple therapeutic strategies such as immune checkpoint blockade.[8] As loss and decreased levels of STING are associated with poor prognosis[15-17], the potential therapeutic benefit of inducing STING is currently under investigation.[18] However, the existence of allelic variants of the STING gene may complicate the efficacy of this treatment modality because some variants cause an inherent defect in STING functionality.[19, 20] A total of 76 biallelic variants are observed in the STING-encoding *STING1* gene. Of these, 26 are located in the coding sequence. Moreover, six represent synonymous substitutions, among which is rs7447927 (V48V, c.144C > G).[21] The most common variants in *STING1* are the non-synonymous rs1131769 (R232H, c.695G > A), rs11554776 (R71H, c.212G > A), rs78233829 (G230A, c.689G > C), and rs7380824 (R293Q, c.878G > A).[21, 22] In combination, the latter three are termed the HAQ genotype, which occurs in 20.4% of the human population.[21] The R232H, G230A, and R293Q substitutions are located in the CDN-binding region of the gene and cause defective response of STING.[23] For instance, a recent study reported on the effect of the homozygous HAQ variant of STING in individuals infected with

human immunodeficiency virus (HIV), stating that it contributes to reduced levels of IFN production and a reduced immune response.[24]

In the context of HPV infection, we hypothesized that allelic variants of *STING1* may increase the susceptibility of patients to persistent infection and thereby risk of cervical cancer development. Furthermore, we hypothesized that the occurrence of particular variants may affect immunity against established cervical cancer. To investigate this, we comprehensively defined the variance in STING by genotyping *STING1* and assessing CD8+T cell infiltration across a large cohort of cervical cancer patients.

Materials and methods

Patient cohort

All patients visiting the outpatient clinic of the University Medical Center Groningen (UMCG, the Netherlands) for diagnostics or treatment of cervical neoplasia or nonmalignant reasons (such as uterovaginal prolapse or uterine myomas) were asked to participate. After informed consent, frozen tissue samples and cervical epithelial scrapings were collected. The cervical scrapings cells were suspended in 250 μL of 4M guanidium isothiocyanate (GT) and frozen at −80°C. Frozen tissue was embedded with Tissue-Tek® OCT™ Compound (Sakura Finetek Europe BV) and stored at −80°C. RNA was isolated using Ambion TRIzol Reagent (Invitrogen) or by chloroform/isopropanol precipitation. cDNA was synthesized using Moloney Murine Leukemia Virus Reverse Transcriptase (M-MLV RT). Data of healthy controls, patient and tumor characteristics, and clinical follow-up data were collected retrospectively in an anonymized database (see also document S1 for detailed experimental procedures). Ethical approval for the study was provided by the Medical Ethics Review committee (METc) of the UMCG (study number 201800288).

Analysis of *STING1* expression and allelic variance

STING1 cDNA was isolated through PCR amplification, followed by gel extraction and Sanger sequencing. The reference sequences of the *STING1* mRNA transcript were obtained online from National Center for Biotechnology Information Gene.[25] To determine prevalence of allelic variants, data from the NCBI 1000 Genomes phase 3 browser[26] were analyzed, containing data from 2504 whole genomes (5008 genotypes), of which 503 (1006 genotypes) were from European donors (107 Spanish, 107 Italian, 99 Finnish, 91 British, and 99 Utah residents with a European background). This population is further referred to as European reference cohort and used as additional reference for the allele and genotype frequencies in the current study population. The following six *STING1* single-nucleotide substitutions were included for analysis: V48V, R71H, G230A,

R232H, R293Q, and A313T. Somatic substitutions such as R284M and R284G were not taken into account, as it was formerly reported that the mutation rate in *STING1* is only 0.11%.[23] Combinations of single-nucleotide substitutions were annotated either as HAQ genotype (V48V, R71H, G230A, and R293Q), R232H genotype (V48V and R232H), or AQ genotype (V48V, G230A, and R293Q); A313T was not observed in the patient cohort. Expression analysis of *STING1* was performed by qRT-PCR (see also Document S1 for detailed experimental procedures).

Immunohistochemistry

Whole tumor tissue sections of 89 and 99 included cervical cancer patients were stained for STING and CD8, respectively. Formalin-fixed, paraffin-embedded (FFPE) slides (obtained from the UMCG Pathology Biobank) were deparaffinized and rehydrated in graded ethanol. Antigen retrieval was instigated by 15 minutes of microwave in preheated 10 mmol/L citrate buffer (pH 6.0). Endogenous peroxidase was blocked by incubating the slides in 0.45% hydrogen peroxide solution for 30 minutes. To stain for STING and CD8, the slides were incubated overnight at 4°C with, respectively, monoclonal rabbit anti-human TMEM173 antibody (EPR13130, ab181125, Abcam) and monoclonal mouse anti-human CD8 antibody (clone C8/144B, Agilent [Dako], M710301), diluted 50X in PBS containing 1% BSA and 1% human AB serum. Next, the slides were incubated for 30 minutes with Envision+/HRP anti-rabbit or anti-mouse antibody (Agilent [Dako]). Signal was visualized with 3.3'-diaminobenzidine (DAB) solution containing hydrogen peroxide, and the slides were counterstained with hematoxylin. In between incubations, the slides were washed with PBS. The sections were dehydrated and embedded in Eukitt quick-hardening mounting medium (Sigma Aldrich), and the slides were scanned using a Hamamatsu digital slide scanner (Hamamatsu Photonics). The numbers of STING + and CD8+ cells in each slide were quantified automatically using QuPath v0.1.2 image analysis software[27] after manual selection of tumor epithelium sections.

Statistical analyses

Genotype counts were compared between patients and controls and the effects of allelic variants on clinical characteristics were assessed using chi-square testing. The effect of allelic variants on the risk of developing cervical cancer was determined by comparing allele frequencies between patients and controls and patients and the European reference cohort using odds ratios and confidence intervals, not adjusted for any external variable. Differences between age of diagnosis, *STING1* expression levels (delta Ct values), STING levels, and CD8 infiltration (number of positive cells per mm^2) between the study groups were analyzed using Kruskal-Wallis testing with post-Dunn tests. Survival was analyzed with Kaplan-Meier curves (log-rank) and univariate and multivariate Cox regression tests. Variables with a P value < .05 in the univariate analyses were included in the multivariate

analyses (Forward Stepwise LR). Significant associations were defined by a P value lower than 0.05. Statistical analyses were performed using SPSS software version 23.0 (IBM SPSS Statistics) or GraphPad Prism 7.02 (GraphPad Software).

Results

Allelic variants in *STING1* are not enriched in cervical cancer

We speculated that allelic variants in the cGAS-STING pathway could predispose to the development of cervical cancer due to the failure of the innate immune system to clear HPV-infected cells. To investigate this hypothesis, we genotyped *STING1* (encoding STING) using cervical scrapings of 150 cervical cancer patients and 20 age-matched healthy controls and compared the results with 503 individuals in the European reference cohort.[26] In the patient cohort, we found the following genotypes: WT/WT (58.0%), WT/HAQ (18.0%), WT/R232H (14.7%), WT/AQ (0.7%), HAQ/HAQ (3.3%), HAQ/R232H (2.0%), R232H/R232H (2.7%), and R232H/AQ (0.7%) (Table 1). Only four of these eight genotypes were found in the healthy controls: WT/WT (55.0%), WT/HAQ (15.0%), WT/R232H (20.0%), and HAQ/R232H (5.0%). In addition, one healthy control had the genotype WT/A313T (5.0%), which was not observed in the patient cohort. Notably, the well-described HAQ variant was not found as homozygous genotype in the healthy control cohort. The genotypes WT/G230A, HAQ/AQ, and AQ/AQ, which have been reported for the European reference cohort[26], were not found in both the patient and healthy control cohorts. However, the overall distribution of *STING1* genotypes within the patient population was comparable to the distribution of the healthy controls and European reference cohort. About half (58.0%) of the patient samples were characterized by two wild-type *STING1* alleles (WT/WT), lacking each of the examined variants, whereas the minority of patients contained a single allele (WT/VAR, 33.4%) or two variant alleles (VAR/VAR, 8.7%), containing at least one of the examined substitutions on one allele or both alleles, respectively. This genotype distribution was comparable to the distribution

Table 1. Distribution genotypes STING1

	Patient cohort n=150	Healthy controls n=20	European reference n=503
WT/WT	87 (58.0)	11 (55.0)	258 (51.3)
WT/HAQ	27 (18.0)	3 (15.0)	97 (19.3)
WT/R232H	22 (14.7)	4 (20.0)	88 (17.5)
WT/AQ	1 (0.7)	-	3 (0.6)
WT/A313T	-	1 (5.0)	4 (0.8)
WT/G230A	-	-	1 (0.2)
HAQ/HAQ	5 (3.3)	-	14 (2.8)
HAQ/R232H	3 (2.0)	1 (5.0)	22 (4.4)
R232H/R232H	4 (2.7)	-	14 (2.8)
R232H/AQ	1 (0.7)	-	-
HAQ/AQ	-	-	1 (0.2)
AQ/AQ	-	-	1 (0.2)

found within the group of healthy controls (55.0%, 40.0%, and 5.0%, respectively) and within the European reference population (51.3%, 38.4%, and 10.4%, respectively).[26] In addition, the prevalence of individual *STING1* alleles in the cohort of cervical cancer patients was similar as well, with no allele showing an (significant) enrichment within the patient cohort (Supplementary Table 1). The synonymous substitution rs7447927 (V48V) had a slightly, but not significantly, higher abundance in the European reference cohort than in the (Dutch) patient and healthy control cohorts (patient vs. European reference cohort P=.074). Altogether, we suggest that allelic variants of *STING1* are not a crucial factor for persistent infection of HPV and that these variants do not predispose to the development of cervical cancer.

Homozygous variants of *STING1* are associated with cervical adenocarcinomas
We next assessed whether the allelic variants could affect disease progression by analyzing the clinical characteristics of the patients (Table 2, Supplementary Table 2). As to tumor typing, 59.8% of the patients with WT/WT genotype had squamous cell carcinomas and 35.6% had adenocarcinomas (Supplementary Figure 1A). In contrast, we found that only 23.1% of patients with VAR/VAR genotype had squamous cell carcinomas, whereas nearly 70% of these patients presented with adenocarcinomas. Patients with WT/VAR genotypes showed histological distribution comparable to patients with a WT/WT genotype. Although allelic variants appear to skew towards adenocarcinoma subtype, the overall difference in histological distribution between the three groups WT/WT, WT/VAR, and VAR/VAR did not reach significance (P=.138). We also noticed that the tumor diameters of patients with WT/WT and WT/VAR genotypes tended to be larger than those of patients with a VAR/VAR genotype (Supplementary Figure 1B). In addition, nearly 70% of patients with VAR/VAR genotypes were diagnosed with early-stage cervical cancer (up to FIGO stage IB1) with a highest FIGO classification of IIB (Supplementary Figure 1C). In contrast, only half of the patients with at least one wild-type allele were diagnosed with early-stage cervical cancer, and the rest was diagnosed with FIGO stage IB2 or higher. Here, the highest FIGO stage found was IVB. Patients with VAR/VAR genotypes tend to receive surgery more often than radiotherapy as their primary treatment (Supplementary Figure 1D), which may be explained by their smaller tumor sizes and lower FIGO stages. However, altogether, our analyses showed no significant difference between any of the discussed clinical factors.

Homozygous variants of *STING1* are prognostic factors in cervical cancer
Previous reports show that the 5-year survival of cervical cancer patients with metastasis is 16.5% compared with 91.5% without metastasis.[28] In addition, in cancer models of chromosomal instability, metastasis was promoted in a STING-dependent manner.[7] Therefore, we assessed whether particular allelic variants of *STING1* were associated

3

Table 2. Characteristics grouped *STING1* genotypes (n=150)

	Bi-allelic wild-type	Monoallelic variant	Bi-allelic variant
Patients	87 (58.0)	50 (33.3)	13 (8.7)
Age at diagnosis (y)			
Median	51.3	48.2	40.1
Range	22.9-83.9	27.3-87.9	25.2-58.3
HPV status			
Negative	3	4	0
Positive	34	9	2
Unknown	50	37	11
FIGO stage			
IA	1 (1.1)	1 (2.0)	0 (0.0)
IB1	39 (44.8)	26 (52.0)	9 (69.2)
IB2	10 (11.5)	3 (6.0)	1 (7.7)
IIA	13 (14.9)	6 (12.0)	1 (7.7)
IIB	15 (17.2)	10 (20.0)	2 (15.4)
IIIA	1 (1.1)	0 (0.0)	0 (0.0)
IIIB	6 (6.9)	2 (4.0)	0 (0.0)
IVA	1 (1.1)	1 (2.0)	0 (0.0)
IVB	1 (1.1)	1 (2.0)	0 (0.0)
Histology			
Squamous cell carcinoma	52 (59.8)	28 (56.0)	3 (23.1)
Adenocarcinoma	31 (35.6)	21 (42.0)	9 (69.2)
Other	4 (4.6)	1 (2.0)	1 (7.7)
Grade of differentiation			
Good/moderate	40 (46.0)	25 (50.0)	7 (53.8)
Poor/undifferentiated	29 (33.3)	16 (32.0)	5 (38.5)
Unknown	18 (20.7)	9 (18.0)	1 (7.7)
Lymphangioinvasion			
No	60 (69.0)	30 (60.0)	8 (61.5)
Yes	26 (29.9)	20 (40.0)	5 (38.5)
Unknown	1 (1.1)	0 (0.0)	0 (0.0)
Tumor diameter (cm)			
0-4	42 (48.3)	21 (42.0)	9 (69.2)
≥ 4	27 (31.0)	17 (34.0)	2 (15.4)
Unknown	18 (20.7)	12 (24.0)	2 (15.4)
Primary treatment			
Wertheim Meigs	46 (52.9)	29 (58.0)	9 (69.2)
Radio-chemotherapy	32 (36.8)	14 (28.0)	2 (15.4)
Other	9 (10.3)	7 (14.0)	2 (15.4)
Follow-up (in years)			
Median	4.63	4.60	3.79
Range	0.08-10.81	0.04-11.72	0.22-7.01
Results last follow-up			
No evidence of disease	63 (72.4)	36 (72.0)	6 (46.2)
Evidence of disease	1 (1.1)	1 (2.0)	0 (0.0)
Death of disease	17 (19.5)	13 (26.0)	7 (53.8)
Death of other disease	6 (6.9)	0 (0.0)	0 (0.0)

Abbreviation. HPV, Human Papilloma Virus

with metastasis. As expected, the occurrence of metastasis was significantly associated with poor outcome (Table 3, univariate cox regression, P<.001). However, we observed that the proportion of patients that presented with distant and lymph node metastasis was comparable for each of the WT/WT, WT/VAR, and VAR/VAR groups (Supplementary Figures 1E and F, respectively), indicating that the occurrence of metastasis is independent of the different *STING1* variants. Although distant metastasis was significantly associated

Table 3. Uni– and multivariate Cox regression survival analyses based on clinical and *STING1* parameters

	Univariate				Multivariate*				Multivariate**			
	HR	95% CI		P value	HR	95% CI		P value	HR	95% CI		P value
Age of diagnosis, cont.	0.977	0.954	1.002	0.070								
Age at diagnosis (y)												
<50.04 median	ref	ref	ref	ref								
>50.04 median	0.657	0.333	1.298	0.227								
Grade												
Good	ref	ref	ref	ref								
Average	0.980	0.358	2.685	0.969								
Bad/not	1.204	0.466	3.109	0.701								
Unknown	1.341	0.456	3.944	0.594								
FIGO stage												
I	ref	ref	ref	ref								
II	3.187	1.445	7.031	**0.004**								
III	6.959	2.374	20.401	**<0.001**								
IV	14.684	4.493	47.988	**<0.001**								
Typing												
Squamous	ref	ref	ref	ref								
Adeno	1.148	0.583	2.260	0.690								
Other	0.872	0.116	6.542	0.894								
Distant met.astasis												
No	ref	ref	ref	ref	ref	ref	ref	ref	ref	ref	ref	ref
Yes	14.952	7.160	31.225	**<0.001**	14.458	6.327	33.041	**<0.001**	14.970	6.410	34.963	**<0.001**
Lymph node metastasis												
No	ref	ref	ref	ref								
Yes	8.637	3.762	19.830	**<0.001**								
Tumor diameter (cm)												
0-4	ref	ref	ref	ref								
≥4	1.655	0.808	3.389	0.168								
Unknown	0.771	0.297	2.002	0.594								
Primary treatment												
WM	ref	ref	ref	ref	ref	ref	ref	ref	ref	ref	ref	ref
RCT	3.753	1.618	8.705	**0.002**	3.005	1.226	7.368	**0.016**	2.860	1.176	6.956	**0.020**
Other	10.413	4.143	26.169	**<0.001**	12.163	4.317	34.269	**<0.001**	11.559	4.152	32.175	**<0.001**
STING1 genotype												
WT/WT	ref	ref	ref	ref	ref	ref	ref	ref				
WT/VAR	1.399	0.672	2.912	0.369	2.169	0.999	4.708	0.050				
VAR/VAR	3.393	1.385	8.310	**0.008**	3.516	1.315	9.397	**0.012**				
V48V/V48V												
WT/WT	ref	ref	ref	ref					ref	ref	ref	ref
WT/VAR	1.271	0.600	2.689	0.531					2.251	1.007	5.032	**0.048**
VAR/VAR	3.564	1.512	8.400	**0.004**					2.930	1.146	7.497	**0.025**
CD8 infiltrate (cont)	1.000	0.999	1.000	0.458								
CD8 infiltrate*												
Low	ref	ref	ref	ref								
High	0.846	0.363	1.972	0.699								

Note: Disease-specific survival, Enter for univariate and Forward Stepwise (LR) for multivariate, n=150
Abbreviations: CI: Confidence Interval; FIGO - International Federation of Gynecology and Obstetrics; HR: Hazard Ratio; RCT: Radiochemotherapy
*when STING1 genotype entered as variable, V48V/V48V not included
**when V48V/V48V entered as variable, STING1 genotype not included
***based on below or above median CD8 count of 392,125 per mm²

with a poor prognosis in the group of patients with at least one wild-type allele (Kaplan-Meier, P<.001, not shown), we observed that occurrence of metastasis did not affect

the outcome of patients with VAR/VAR genotypes of *STING1* (Kaplan-Meier, P=.382, not shown). These patients have a poor prognosis regardless of having metastasis or not, indicating that another factor causes the poor outcome of these patients. To follow up on these findings, we assessed the effect of *STING1* variants on the disease-specific survival (DSS). Interestingly, the DSS of patients with HAQ/HAQ, R232H/R232H, and R232H/AQ genotypes was significantly worse than with WT/WT genotype (P=.049, P=.022, and P=.001, respectively, not shown). As the individual genotype groups were rather small, we next compared the DSS between grouped WT/WT, WT/VAR, and VAR/VAR genotypes and observed a significant difference in outcome, with patients with homozygous allelic variants of *STING1* having a worse DSS than patients with wild-type or heterozygous variants (Figure 1A, P=.019). Although the DSS was slightly worse for the WT/VAR patients than for the WT/WT patients, this difference was not statistically significant (P=.114). Next, we hypothesized that the presence of at least one wild-type allele may result in functional STING and therefore grouped the patients with at least one wild-type allele for additional analysis of DSS. We show that having at least one wild-type allele significantly improves overall survival and DSS (Figure 1B, P=.007). Importantly, multivariate analysis of *STING1* genotype groups and clinicopathological factors revealed an independent association of *STING1* status with DSS (Table 3). Analysis of *STING1* expression levels by qRT-PCR showed that the prognostic value was also independent of *STING1* mRNA levels, as these were statistically comparable for WT/WT, WT/VAR, and VAR/VAR genotypes (Supplementary Figure 2A, P=.207). Moreover, there was no significant difference in DSS (Supplementary Figure 2B, P=.617) or in recurrence-free survival (Suppelementary Figure 2C, P=.226) based on above- and below-median *STING1* mRNA levels. Similar results were found when immunohistochemically assessing STING protein levels in paraffin-embedded tumor tissue (Supplementary Figure 3). We hypothesized that STING variants may affect responsiveness to therapy. Indeed, the DSS was worse for patients with homozygous STING variants, independently of the primary treatment being surgery or radiochemotherapy (RCT) (Figures 1F-1I). These data demonstrate that homozygous mutated variants of *STING1* have independent prognostic value for patients with cervical cancer that cannot be explained by the levels of both STING mRNA and protein.

Homozygous mutated variants of *STING1* appears to be associated with early onset of cervical cancer

To understand the worse survival of VAR/VAR STING patients, we further investigated differences in the clinical data of the patients. We noticed that the age of diagnosis significantly differed between the three genotype groups (Figure 1C, P=.0395). Specifically, the age of diagnosis was significantly lower for patients with VAR/VAR genotypes of *STING1* than for patients with WT/WT (P=.0331). The median ages of diagnosis were

Figure 1
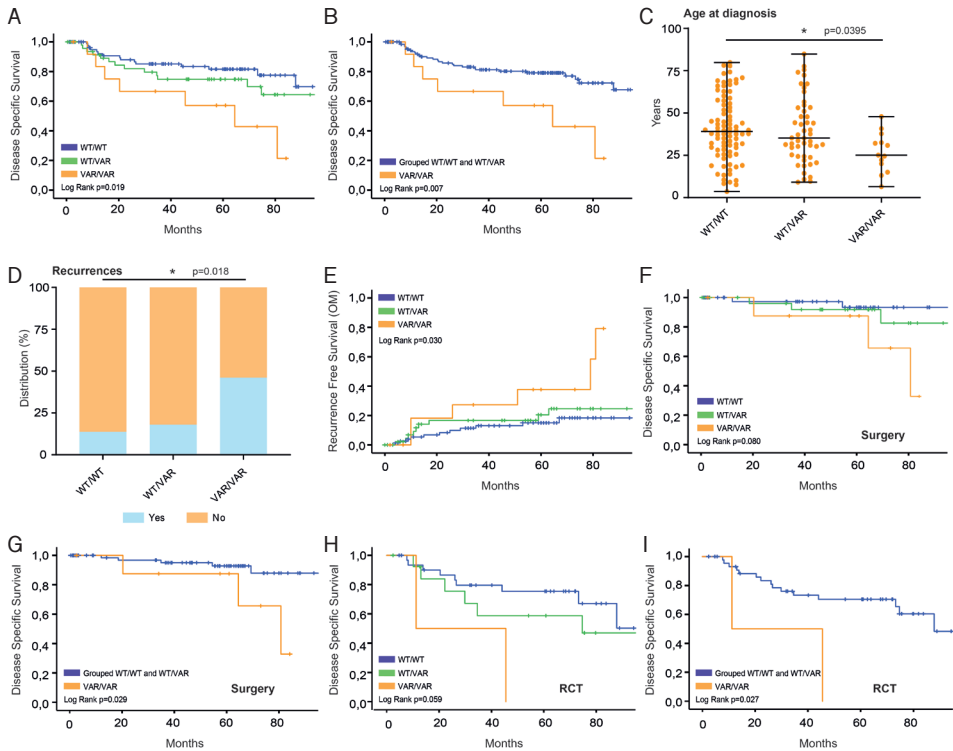
Cervical cancer patients were analyzed regarding disease-specific survival. A, B), based on three groups (A): WT/WT (blue), WT/VAR (green), and VAR/VA (orange) or on two groups (B): WT/WT and WT/VAR combined (blue) and VAR/VAR (orange). C) Age at the time of diagnosis (in years) for the three described groups. Each orange dot represents one patient. Statistical analysis was performed by one-way ANOVA with post-hoc Kruskal-Wallis test. D) Distribution of recurrences (%) among the three described groups: Yes (recurrence, light blue) or No (no recurrence, orange). Statistical analysis was performed by Pearson's chi-square testing. E) Recurrence-free survival (oneminus plot) for WT/WT (blue), WT/VAR (green), and VAR/VAR (orange). F-I,) Disease-specific survival distinguishing cervical cancer patients by primary treatment being surgery (F, G) or RCT (H, I) and by distinguishing three groups (F, H): WT/WT (blue), WT/VAR (green), and VAR/VA (orange) or two groups (G, I): WT/WT and WT/VAR combined (blue) and VAR/VAR (orange). For all survival curves, statistical analyses were performed by log-rank testing. Significance was defined as P<.05. Curves were cut off at 7.5 years.

40.1 vs 51.3 and 48.2 years, respectively (Table 2). Especially the HAQ/HAQ (39.6 years) and R232H/R232H (36.9 years) genotypes contributed to this lower median age. When we subsequently compared the effect of the age at the time of diagnosis on the outcome, we observed that the DSS within the entire cohort of 150 patients was not significantly different between younger and older age of diagnosis (Supplementary Figure 4, based on the median age of the entire cohort of 50.05, P=.224). This was also not the case when first stratifying the cohorts for adenocarcinoma vs squamous cell carcinoma (P=.146 vs P=.822, not shown). Thus, early onset of disease in itself is not a predictor of poor prognosis. Therefore, we suggest an independent negative effect of homozygous variants of *STING1* on the survival of cervical cancer patients.

Homozygous variants of *STING1* are associated with higher frequency of recurrences

In addition to being diagnosed at an earlier age, patients with VAR/VAR variants notably suffered from recurrent disease significantly more often than patients with the WT/WT variant (Figure 1D, P=.018). To confirm whether the occurrence of recurrent disease explains the worse outcome of patients with VAR/VAR *STING1*, we performed additional Kaplan-Meier analyses in which we excluded either all patients with recurrences or only the patients with VAR/VAR genotypes with recurrences. In both cases, there was no difference in survival between the groups (P=.942 and P=.642, respectively, not shown). In accordance, the recurrence-free survival was significantly better for the WT/WT group of patients (Figure 1E, P=.013) and, although insignificantly, for the WT/VAR group (P=.061), compared with the VAR/VAR group of patients. In total, 27 out of 150 patients suffered from a recurrence. From the 21 patients within this group with at least one WT allele, six (28.6%) survived the recurrent disease, whereas the six VAR/VAR patients that recurred all succumbed to the disease (not shown). Altogether, these findings show that although the initial clinical characteristics such as tumor diameter and FIGO stage of patients with VAR/VAR genotypes of *STING1* appear slightly beneficial over patients with WT/WT and WT/VAR, having at least one wild-type allele may protect against (aggressive) recurrent disease and therefore improve outcome.

The prognostic value of mutated *STING1* variants is independent of CD8+ T cell infiltration

High levels of STING protein expression were previously associated with high CD8+ T cell infiltration.[17] In line with this, knock-out of *STING1* led to decreased infiltration of CD8+T cells in animal models.[8] Although we observed no differences in STING expression between the genotypes, we hypothesized that the patients with VAR/VAR genotypes of *STING1* might have lower CD8+T cell infiltration, possibly explaining the poor survival of these patients. To investigate this, we performed immunohistochemistry for CD8+T cells using paraffin-embedded tumor tissue of 99 cervical cancer patients from our cohort. Quantification of CD8+ T cells across the FFPE slides was performed using machine-based quantification (Figure 2A). We found that CD8+ T cell infiltration did not differ between the three *STING1* groups (Figure 2B, P=.687). Patient outcome in this cohort also did not reach statistical significance for outcome based on low and high CD8+ T cell infiltration (Figure 2C and Table 3, P=.699). Lastly, there was no association between CD8+ T cell infiltration and *STING1* expression (P=.295, not shown). Thus, homozygous variants of STING are prognostic factors in cervical cancer, independently of both *STING1* expression and CD8+ T cell infiltration.

Figure 2
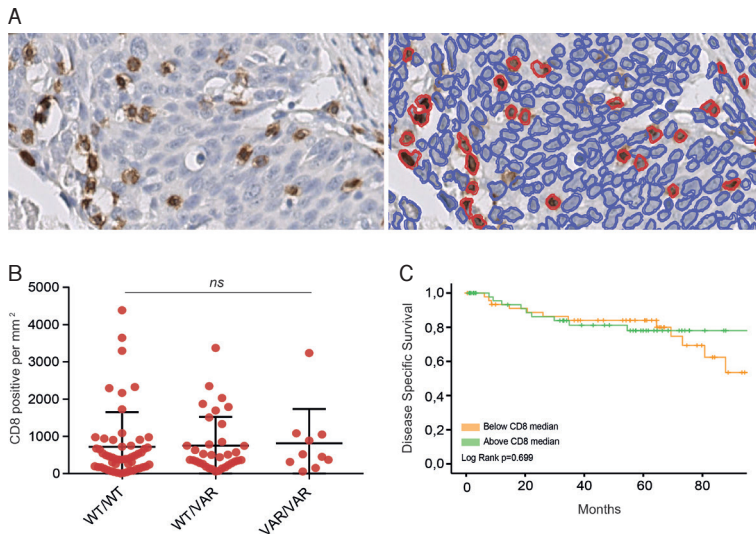
Immunohistochemical staining of CD8 on formalin-fixed, paraffin-embedded (FFPE) slides of tumors obtained from the studied cervical cancer patient cohort. *A, Microscopic image (400X magnification) of CD8 staining (left) and representation of the computerized quantification of membrane 3,3'-diaminobenzidine (DAB)-positive cells (red) and DAB-negative cells (blue) in QuPath image analysis software (right). B, Quantified numbers of DAB/CD8-positive cells per mm^2 tumor tissue for the three groups: WT/WT, WT/VAR, and VAR/VAR. C, Disease-specific survival dividing patients into two groups: below (orange) and above (green) the median number of CD8 infiltrating cells. Statistical analysis was performed by log-rank testing. Significance was defined as P<.05. Curve was cut off at 7.5 years.*

The homozygous V48V variant of *STING1* represents a surrogate genetic marker for *STING1* variations associated with poor outcome in cervical cancer

When assessing the effect of having two wild-type alleles, one wild-type allele, or no wild-type allele of each individual nucleotide substitution on survival, we found that most individual substitutions did not significantly affect DSS (not shown). Only the 14 patients with homozygous V48V presented with significantly worse outcome than patients with homozygous or heterozygous wild-type V48V (Figure 3A, P=.008). In addition, we observed that half of these patients suffered from recurrent disease, in contrast to patients with WT/WT and WT/VAR genotypes (14.0% and 16.0%, respectively) (Figure 3B, P=.005). In accordance, the recurrence-free survival was significantly worse for patients with homozygous mutated V48V when comparing the patients only based on this single-nucleotide substitution (Figure 3C, P=.005). Interestingly, V48V represents a synonymous substitution and therefore likely has no clinical implications in itself. Moreover, we described earlier that V48V variant is not enriched in the patient cohort. However, homozygous presence of V48V almost completely corresponded to the patients with VAR/VAR genotypes of *STING1*, with 13 patients having R232H/R232H, HAQ/HAQ,

Figure 3
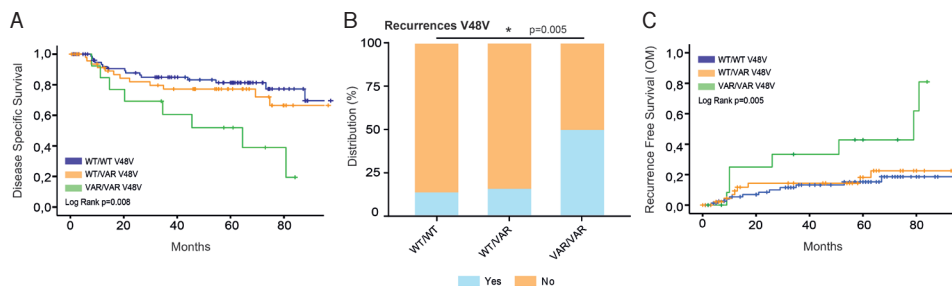
Analysis of the single synonymous substitution rs7447927 V48V. *A, Disease-specific survival dividing patients into three groups: WT/WT (blue), WT/VAR (orange), and VAR/VAR (green) (P=.008). B, Distribution of recurrences (%) among the three described V48V groups: Yes (recurrence, light blue) or No (no recurrence, orange). Statistical analysis was performed by Pearson's chi-square testing. C, Recurrence-free survival (one-minus plot) based on the three described V48V groups. Statistical analyses for survival curves were performed by log-rank testing. Significance was defined as P<.05. Curve was cut off at 7.5 years*

HAQ/R232H, or R232H/AQ (VAR/VAR) genotypes and only one of the 14 patients with homozygous V48V having a WT/AQ (WT/VAR) genotype of *STING1*. Altogether, our findings therefore indicate that homozygous V48V in *STING1* may potentially be used as a surrogate marker for a poor *STING1* genotype–related outcome in cervical cancer.

Discussion

In this study, we genotyped the STING-encoding *STING1* gene across a unique cohort of 150 cervical cancer patients and examined a panel of clinical characteristics. Notably, we found that homozygous variants of *STING1* were significantly associated with worse survival outcome. This association was found to be independent of CD8+ T cell infiltration and *STING1* expression. Thus, specific allelic variants of *STING1* may affect the development and progression of cervical cancer.

STING-encoding *STING1* is one of the genes described to influence the susceptibility of an individual to cervical cancer.[3] We genotyped regions in the STING-encoding *STING1* that can contain key single-nucleotide substitutions using cervical scrapings of 150 cervical cancer patients to investigate whether particular allelic variants in *STING1* are enriched in cervical cancer patients and have a prognostic value. In accordance with the previous conclusion of Xiao *et al.* that no variant of *STING1* is associated with the risk of cervical precancerous lesions[29], we found no allelic variant of *STING1* to be enriched in our cervical cancer patient cohort compared with healthy controls and a European reference population. This suggests that these allelic variants are not a crucial factor for persistent infection with HPV and that they do not predispose to the development of cervical cancer.

Typically, the predominant histological subtype of cervical cancer is squamous cell carcinoma (70%-80% of cases), followed by adenocarcinoma (10%).[2] Interestingly, we found that the nearly 70% of patients in our cohort with VAR/VAR *STING1* genotypes presented with adenocarcinomas. Moreover, we noticed that the tumor diameters of patients with WT/WT and WT/VAR genotypes often were larger, and the FIGO stages at diagnoses were often higher than those of patients with VAR/VAR genotypes, although these differences did not reach statistical significance. In addition, we observed that patients with VAR/VAR genotypes of *STING1* were diagnosed with cervical cancer at a significantly earlier age. The median age at diagnosis of cervical cancer is 48 years.[30] In accordance, we found that the median ages of WT/WT and WT/VAR patients were 51.3 and 48.2, respectively. In contrast, the median age of diagnosis for patients with homozygous variants was 40.1 years. About half of the patients that were diagnosed at an age below the median of the entire cohort presented with adenocarcinomas. These findings are in accordance with previous reports that patients with adenocarcinomas are generally diagnosed at an earlier stage and at a younger age.[31] Together, our findings may indicate again a link between homozygous variants of *STING1*, histology, and age of diagnosis.

Women with locally advanced cervical cancer have a higher rate of local and distant recurrences and worse survival than women that are diagnosed with early-stage disease.[32,33] Interestingly, despite their tendency toward having early-stage disease, patients with VAR/VAR genotypes of *STING1* had significantly worse disease-specific and recurrence-free survival than patients with WT/WT and WT/VAR genotypes. Hence, having at least one wild-type allele may partially protect against (aggressive) recurrent disease and thereby improve outcome. As reported before[30], the outcome of the patients was independent of age at the time of diagnosis. It was previously observed in multiple cancer types and models that decreased levels of STING lead to poor induction of IFN-I.[10, 12-16, 34] To possibly explain the worse survival of patients with homozygous variants of STING, we assessed the mRNA and protein levels of STING. However, we did not observe lower expression of *STING1* and STING in the patients with homozygous variants as compared with patients with at least one wild-type allele. Moreover, survival was comparable for high vs low levels of both. After 60 months of follow-up, patients with *STING1* mRNA expression above median appear to gain a slight survival advantage. We determined mRNA levels using cervical scrapings and lack material to determine potential change in mRNA levels during follow-up time that may explain this advantage. Possibly, a higher mRNA level at baseline may provide a long-term survival advantage. However, based on our data, we cannot draw any conclusions on this.

Despite apparent intact translation, STING variants may be dysfunctional. For example, it was described that the R232H, G230A, and R293Q substitutions are located in the cyclic dinucleotide (CDN)-binding region of the gene and cause defective response of STING.[23] A recent study regarding the effect of the homozygous HAQ variant of STING in individuals infected with HIV showed that this variant contributes to reduced levels of IFN production and a reduced immune response.[24] In accordance, it is reported that this variant is associated with defective functionality of STING due to the occurrence of the rs13181561 substitution upstream of *STING1* in individuals with HAQ/HAQ variants of *STING1*.[19, 20] We did not look into HPV proteins, nor did we assess the presence of the rs13181561 substitution and other substitutions such as the synonymous rs744792735 that has been reported previously with regard to other cancer types. In addition, the limited availability of cDNA did not allow us to study the IFN-I mRNA levels.

As IFN-I signaling ultimately leads to infiltration of CD8+ T cells, we performed immunohistochemistry for CD8 on available tumor tissue. We observed no difference in CD8+ T cell numbers between the patient groups with different *STING1* variants, indicating intact IFN signaling in patients with hetero- and homozygous variants of STING. However, it was formerly reported that HPV+ human head and neck squamous cell carcinomas present with less clonal expansion of cytotoxic T cells and lower levels of antigen-presenting machinery than carcinomas lacking HPV.[36] As cervical cancers are almost exclusively HPV+, it is possible that although patients with homozygous variants of STING have similar numbers of CD8+-infiltrated cells compared with patients with at least one wild-type allele, these CD8+ infiltrates may merely represent irrelevant "bystander" CD8+ cells that do not effectuate actual antitumor immunity. In line, Fu *et al.* showed in mice that activation of dendritic cells was associated with STING-dependent phosphorylation of IRF3, and that antitumor efficacy upon treatment with a CDN-based vaccine depended on STING and CD8+ T cells[37]. Moreover, immune checkpoint inhibition did not induce tumor regression in the context of STING loss[8], suggesting a lack of tumor-reactive CD8+ T cells. Studies are currently ongoing to induce STING-mediated immunity, either directly via eg STING agonists[18] or indirectly through radiotherapy or inhibition of the DNA damage repair pathway.[38] As we speculate that homozygous variants of STING are associated with impaired antitumor immunity and fail to induce the activation of tumor-reactive CD8+ T cells, we hypothesize that STING-inducing therapy may not be effective in patients with these variants. Therefore, we recommend that these studies should include the effect of various *STING1* variants on (immune) therapeutic response against cervical cancer.

Additionally, treatment regimens for cervical cancer are primarily determined based on FIGO stage. Early-stage cancer is usually treated with surgery, whereas for late-stage

disease, patients can be treated with primary or palliative (chemo)radiation therapy or a combination treatment.[32] In accordance with their large proportion of early FIGO stages and small tumors, patients with VAR/VAR genotypes of STING are mainly treated with surgery. However, we demonstrated that these patients have a poor outcome and observed a survival disadvantage even in the group of patients that were primarily treated with RCT. Therefore, we speculate the treatment regimen for patients with homozygous variants of STING may be ineffective and potentially should be reconsidered.

Finally, although V48V was previously associated with esophageal squamous cell carcinoma in Chinese individuals[35], here it appeared to be more abundant in the European reference cohort than in the (Dutch) patient and healthy control cohorts (patient vs European reference cohort P=.074). Interestingly, despite representing a synonymous substitution, V48V was previously reported to be in linkage disequilibrium with both HAQ and R232H and the rs13181561 substitution, making it a surrogate marker for loss of STING function.[35] Here, we showed that the V48V indeed corresponded to homozygous variants of *STING1* and that it was individually prognostic for outcome. As the allelic variants represent germline and not somatic substitutions specific for the cervical tissue, it is possible to identify V48V in the DNA of patients, which may facilitate genotyping for prognostic purposes.

Altogether, our results suggest that patients with homozygous allelic variants of the *STING1* gene have worse DSS and recurrence-free survival and earlier age of diagnosis than patients with at least one wild-type *STING1* allele. Homozygous V48V was found to be individually prognostic and may be investigated as a novel, surrogate prognostic biomarker in cervical cancer.

3

References

1. Global Burden of Disease Cancer Collaboration, Fitzmaurice C, Allen C, Barber RM, Barregard L, Bhutta ZA, et al. Global, Regional, and National Cancer Incidence, Mortality, Years of Life Lost, Years Lived With Disability, and Disability-Adjusted Life-year, 1990 to 2015: A Systematic Analysis for the Global Burden of Disease Study. JAMA Oncol. 2017 Apr 1; 3(4): 524-48. .

2. de Sanjose, S. et al. Human papillomavirus genotype attribution in invasive cervical cancer: a retrospective cross-sectional worldwide study. Lancet Oncol. 11, 1048–1056 (2010).

3. Chen, D. & Gyllensten, U. Lessons and implications from association studies and post-GWAS analyses of cervical cancer. Trends Genet. 31, 41–54 (2015).

4. Chen, D. et al. Analysis of the genetic architecture of susceptibility to cervical cancer indicates that common SNPs explain a large proportion of the heritability. Carcinogenesis 36, 992–998 (2015).

5. Sun, L., Wu, J., Du, F., Chen, X. & Chen, Z. J. Cyclic GMP-AMP Synthase Is a Cytosolic DNA Sensor That Activates the Type I Interferon Pathway. Science (80-.). 339, 786–791 (2013).

6. Chung, K. W. et al. Mitochondrial Damage and Activation of the STING Pathway Lead to Renal Inflammation and Fibrosis. Cell Metab. 30, 784-799.e5 (2019).

7. Bakhoum, S. F. et al. Chromosomal instability drives metastasis through a cytosolic DNA response. Nature 553, 467–472 (2018).

8. Harding, S. M. et al. Mitotic progression following DNA damage enables pattern recognition within micronuclei. Nature 548, 466–470 (2017).

9. Li, T. & Chen, Z. J. The cGAS–cGAMP–STING pathway connects DNA damage to inflammation, senescence, and cancer. J. Exp. Med. jem.20180139 (2018). doi:10.1084/jem.20180139

10. Deng, L. et al. STING-dependent cytosolic DNA sensing promotes radiation-induced type I interferon-dependent antitumor immunity in immunogenic tumors. Immunity 41, 843–852 (2014).

11. McLaughlin, M. et al. Inflammatory microenvironment remodelling by tumour cells after radiotherapy. Nat. Rev. Cancer (2020). doi:10.1038/s41568-020-0246-1

12. Xia, T., Konno, H., Ahn, J. & Barber, G. N. Deregulation of STING Signaling in Colorectal Carcinoma Constrains DNA Damage Responses and Correlates With Tumorigenesis. Cell Rep. 14, 282–297 (2016).

13. Xia, T., Konno, H. & Barber, G. N. Recurrent loss of STING signaling in melanoma correlates with susceptibility to viral oncolysis. Cancer Res. 76, 6747–6759 (2016).

14. Bhatelia, K. et al. Antiviral signaling protein MITA acts as a tumor suppressor in breast cancer by regulating NF-κB induced cell death. Biochim. Biophys. Acta - Mol. Basis Dis. 1842, 144–153 (2014).

15. Song, S. et al. Decreased expression of STING predicts poor prognosis in patients with gastric cancer. Sci. Rep. 7, 1–13 (2017).

16. Bu, Y., Liu, F., Jia, Q.-A. & Yu, S.-N. Decreased Expression of *TMEM173* Predicts Poor Prognosis in Patients with Hepatocellular Carcinoma. PLoS One 11, e0165681 (2016).

17. Chon, H. J. et al. STING signaling is a potential immunotherapeutic target in colorectal cancer. J. Cancer 10, 4932–4938 (2019).

18. Corrales, L. et al. Direct Activation of STING in the Tumor Microenvironment Leads to Potent and Systemic Tumor Regression and Immunity. Cell Rep. 11, 1018–1030 (2015).

19. Patel, S. et al. Response to Comment on "The Common R71H-G230A-R293Q Human *TMEM173* Is a Null Allele". J. Immunol. 198, 4185–4188 (2017).

20. Patel S, Blaauboer SM, Tucker HR, et al. . (Baltimore, M. : 1950). ;198(2):776-787. doi:10. 4049/jimmunol. 1601585. The common R71H-G230A-R293Q (HAQ) human *TMEM173* is a null allele. J. Immunol. 198, 776–787 (2017).

21. Yi, G. et al. Single Nucleotide Polymorphisms of Human STING Can Affect Innate Immune Response to Cyclic Dinucleotides. PLoS One 8, 1–16 (2013).

22. Jin, L. et al. Identification and characterization of a loss-of-function human MPYS variant. Genes Immun. 12, 263–269 (2011).

23. Patel, S. & Jin, L. *TMEM173* variants and potential importance to human biology and disease. Genes Immun. 1–8 (2018). doi:10.1038/s41435-018-0029-9

24. Nissen, S. K. et al. Multiple Homozygous Variants in the STING-Encoding *TMEM173* Gene in HIV Long-Term Nonprogressors. J. Immunol. ji1701284 (2018). doi:10.4049/jimmunol.1701284

25. Gene [Internet]. Gene ID: 340061, Homo sapiens *TMEM173* transmembrane protein 1. Bethesda (MD): National Library of Medicine (US), National Center for Biotechnology Information 1988. Available from: https://www.ncbi.nlm.nih.gov/gene/340061. Cited 2017.

26. The 1000 Genomes Project Consortium. A global reference for human genetic variation. Nature. 2015 Oct 1; 526(7571): 68-74.

27. Bankhead, P. et al. QuPath: Open source software for digital pathology image analysis. Scientific Reports (2017). https://doi.org/10.1038/s41598-017-17204-5.

28. Haoran Li, Xiaohua Wu, X. C. D. Advances in diagnosis and treatment of metastatic cervical cancer. Gynecol. Oncol. 27, (2016).

29. Xiao, D. et al. Interaction between susceptibility loci in cGAS-STING pathway, MHC gene and HPV infection on the risk of cervical precancerous lesions in Chinese population. Oncotarget 7, 84228–84238 (2016).

30. Y., G., J.-L., M., F., G. & L.-P., S. The evaluation of older patients with cervical cancer. Clin. Interv. Aging 8, 783–788 (2013).

31. Anton-Culver, H. et al. Comparison of adenocarcinoma and squamous cell carcinoma of the uterine cervix: A population-based epidemiologic study. Am. J. Obstet. Gynecol. 166, 1507–1514 (1992).

32. Cohen, P. A., Jhingran, A., Oaknin, A. & Denny, L. Cervical cancer. Lancet 393, 169–182 (2019).

33. Manders, D. B. et al. Locally Advanced Cervical Cancer: Outcomes with Variable Adherence to Treatment. Am. J. Clin. Oncol. Cancer Clin. Trials 41, 447–451 (2018).

34. Zhong, B. et al. The Adaptor Protein MITA Links Virus-Sensing Receptors to IRF3 Transcription Factor Activation. Immunity 29, 538–550 (2008).

35. Wu, C. et al. Joint analysis of three genome-wide association studies of esophageal squamous cell carcinoma in Chinese populations. 344, 1173–1178 (2015).

36. Saloura, V. et al. Characterization of the T cell receptor repertoire and immune microenvironment in patients with locoregionally advanced squamous cell carcinoma of the head and neck. Clin. Cancer Res. 23, 4897–4907 (2017).

37. Fu, J. et al. STING agonist formulated cancer vaccines can cure established tumors resistant to PD-1 blockade. Sci. Transl. Med. 7, (2015).

38. Luo, X., Chen, Q. & Lei, Y. L. HPV16 drives cancer immune escape via NLRX1-mediated degradation of STING Graphical abstract Find the latest version : (2019).

3

Supplementary material

Document S1. Supplementary Materials and Methods

Study population

This study included a cohort of histologically confirmed cervical cancer cases diagnosed and treated in the UMCG in Groningen, the Netherlands, between May 30, 2005 and November 12, 2012. To maximize the number of unique cases included, both frozen tumor tissue and cervical scrapings were evaluated for use in RNA isolation. Furthermore, patients were excluded in case of insufficient or absence of material, or when quantitative PCR on cDNA (qRT-PCR) indicated poor RNA quality. Lastly, patients with aberrant clinical characteristics such as inclusion in clinical trials were excluded from the cohort, leaving a total of 150 unique cases to be included in the study (ranging from 22.9 to 87.9 years of age). HPV status was reported for 52 cases, of which 45 (86,5%) tested positive for HPV. HPV typing detected 27 patients HPV-16, 5 with HPV-16 and HPV-18, 9 with HPV-16 and other, 1 with HPV-18 and other, 1 with HPV-16, HPV-18 and other and 1 with other HPV type than HPV-16 or HPV-18.

Patients operated for nonmalignant reasons such as uterovaginal prolapse or uterine myomas between September 30, 2010 and December 11, 2014, were selected as healthy controls. To ensure the controls had healthy cervical epithelial tissue, any individual without a recent Papanicolaou (Pap) smear test result or with a result other than Pap 1 was excluded. Other exclusion criteria were mortality due to any cause, comorbidity with immune-related disorders, comorbidity with other malignancies or lack or insufficient quality of material for RNA isolation. In total, 23 individuals were included in the study cohort of healthy controls (ranging from 35 to 60 years of age). HPV status was reported for six individuals, five were negative and one individual was tested positive for HPV.

RNA isolation from frozen tissue and cervical scrapings and cDNA synthesis

Frozen tissue samples were kept on dry ice. Isolation materials were pre-cooled in liquid nitrogen to minimize breakdown of RNA. Next, 50-100 mg of frozen tissue of each patient was chopped using a clean, sharp scalpel and put into a shaking flask along with a metal ball. Using the Mikro-Dismembrator U (B. Braun Biotech International GmbH), the flask containing the tissue was pulverized at 2000 shakes per minute for 1 minute to grind the tissue. After transferring the tissue into an RNase-free Eppendorf tube, 1 ml of Ambion TRIzol Reagent (Invitrogen) was added for cell lysis. The sample was homogenized and stored at -80°C or directly further processed. RNA extraction was performed according to standard Trizol protocol as provided by the manufacturer.

The cervical scrapings, suspended in GT, were lyzed by adding another 250 µL GT, 500 µL phenol (pH 4.3 ± 0.2 saturated with 0.1 M citrate buffer), 50 µL 3M sodium acetate and 100 µL chloroform/isoamylalcohol (49:1) and vortexing the solution thoroughly. The solution was centrifuged at 12000g for 15 minutes to separate the suspension into two layers, and 400 µL of the upper (aqueous) layer (containing the RNA) transferred into a fresh tube containing 400 µL isopropanol. After addition of 1 µL glycogen and incubation for one hour at -20°C, the samples were centrifuged again (12000g 15 min) to create a pellet, which was resuspended in 150 µL GT. Another 150 µL of isopropanol was added before incubating for one hour at -20°C Following another centrifugation step (12000g 15 min), the pellet was washed with 1 ml of 70% ethanol and spun down again before complete removal of the supernatant and air drying to evaporate residual ethanol. The final pellet, containing isolated total RNA, was resuspended in 50 µL diethyl pyrocarbonate (DEPC)-treated water and incubated at 57°C for 12 minutes to improve solubility.

In addition, part of the cervical scrapings were processed using 1 ml Trizol and standard Trizol protocol as provided by the manufacturer.

Yield and quality (260/280 and 260/230 absorbance ratios) of the isolated RNA were determined using a NanoDrop 1000 spectrophotometer (Thermo Fisher Scientific). Next, up to 10 µg of the isolated RNA was converted to cDNA using 800 U Moloney Murine Leukemia Virus Reverse Transcriptase (M-MLV RT) and provided materials in the supplementary kit (Invitrogen). The samples were stored at 4°C for short term or -20°C for long-term until used for analysis.

RT-PCR and Sanger sequencing

To amplify STING1 for sequencing, PCR was performed using Q5 High-Fidelity polymerase (New England Biolabs, Inc.). Respective forward and reverse primer sequences were 5'-TCCTCGTCATCATCCAGAGCAG-3' and 5'-CTGCTGGACATTCAGCCACTG-3', providing a product of 1267 base pairs. The following program was run on the ProFlex PCR System (applied biosystems by life technologies): 98°C for 30 seconds, then 40 cycles of 98°C for 10 seconds, 70°C for 30 seconds and 72°C for 30 seconds, next 72°C for 2 minutes and finally hold at 4°C. Per patient, two 50 µL reactions were performed to obtain sufficient amount of product using 1 µL of nonpurified cDNA mixture per reaction. The PCR products were extracted by gel electrophoresis using the QIAquick gel extraction kit, eluting the product in 30 µL (Qiagen). Lastly, 20-400 ng of purified STING amplicons was sent for sequencing (GATC Biotech AG, Konstanz, Germany) together with a set of three primers to cover the entire amplicon: 5'-AGCCTGCATCCATCCATC-3', 5'-ACAACAACCTGCTACGG-3' and 5'-ACCTGTGTCCTGGAGTAC-3'.

qRT-PCR

To assess the expression of STING1, qRT-PCR was performed. Per patient, 10 µL of iQ™ SYBR Green supermix (Bio-Rad, 1708886), 0.1 µM primer mix and 5 µL of cDNA template were mixed and added up to a total volume of 20 µL with nuclease-free water. Primers used to amplify STING were TGATCCTGCCAGAGCTCCAG-FW and ACCCCACAGTCCAATGGGAG-REV and to amplify GADPH were CCACCACCCTGTTGCTGTAG-FW and CCCACTCCTCCACCTTTGAC-REV. Next, the following program was run on the CFX Connect™ Real-Time System (Bio-Rad): 50°C for 2 minutes, 95°C for 2 minutes, then 40 cycles of 95°C for 15 seconds, 60°C for 30 seconds and 72°C for 30 seconds and lastly 95°C for 10 seconds. Detection of target template was based on SYBR Green I dye signal. Due to limited availability of cDNA, samples were only measured in mono. Nuclease-free water was used as negative control template to ensure qRT-PCR quality. As the RNA input for cDNA synthesis was not standardized, for analysis, the delta Ct value (Ct GAPDH minus Ct STING1) was used to determine expression levels.

Supplementary Table 1 Frequencies of STING1 allelic variants in cases compared to controls

SNP ID	Allele	Cases n	AF	Ctrls n	AF	Case-ctrl OR (95% CI)	Euro ref. n	AF	Case-Euro OR (95% CI)
rs7447927 (V48V)	C	222	0,740	30	0,750	1.054 (0.493-2.256) P=0.8921	690	0,686	0.767 (0.574-1.026) P=0.074
	G	78	0,260	10	0,250		316	0,314	
rs11554776 (R71H)	G	260	0,867	36	0,900	1.385 (0.468-4.099) P=0.5567	858	0,853	0.892 (0.613-1.299) P=0.551
	A	40	0,133	4	0,100		148	0,147	
rs78233829 (G230A)	G	258	0,860	36	0,900	1.465 (0.496-4.328) P=0.490	851	0,846	0.894 (0.618-1.292) P=0.550
	C	42	0,140	4	0,100		155	0,154	
rs1131769 (R232H)	G	265	0,883	35	0,875	0.925 (0.340-2.516) P=0.8779	857	0,852	0.760 (0.513-1.126) P=0.171
	A	35	0,117	5	0,125		149	0,148	
rs7380824 (R293Q)	G	259	0,863	36	0,900	1.425 (0.482-4.213) P=0.5223	852	0,847	0.876 (0.604-1.270) P=0.484
	A	41	0,137	4	0,100		154	0,153	
rs140837017 (A313T)	G	300	1,000	39	0,975	0.044 (0.002-1.094) P=0.0568	1002	0,996	0.371 (0.020-6.905) P=0.506
	A	0	0,000	1	0,025		4	0,004	

n = number of alleles; AF = allele frequency; OR = Odss Ratio; CI = Confidence Interval; ref. = reference
*Cases = cervical cancer patients; Controls = healthy controls*

Supplementary Table 2. Clinical characteristics per individual STING1 genotype (n=150)

|	WT/ WT	WT/ HAQ	WT/ R232H	WT/ AQ	HAQ/ HAQ	HAQ/ R232H	R232H/ R232H	R232H/ AQ
Patients	87 (58.0)	27 (18.0)	22 (14.7)	1 (0.7)	5 (3.3)	3 (2.0)	4 (2.7)	1 (0.7)
Age at diagnosis (in years)								
Median	51.3	48.2	49.1	27.7	39.6	50.2	36.9	52.6
Range	22.9-83.9	27.3-82.1	28.6-87.9	-	25.2-46.0	45.7-58.3	30.5-40.1	-
HPV status								
Negative	3	2	2	0	0	0	0	0
Positive	34	5	3	1	0	1	1	0
Unknown	50	20	17	0	5	2	3	1
FIGO stage								
IA2	1 (1.1)	1 (3.7)	0 (0.0)	0 (0.0)	0 (0.0)	0 (0.0)	0 (0.0)	0 (0.0)
IB1	39 (44.8)	14 (51.8)	12 (54.5)	0 (0.0)	4 (80.0)	3 (100.0)	2 (50.0)	0 (0.0)
IB2	10 (11.5)	1 (3.7)	2 (9.1)	0 (0.0)	0 (0.0)	0 (0.0)	1 (25.0)	0 (0.0)
IIA	13 (14.9)	3 (11.1)	3 (13.6)	0 (0.0)	1 (20.0)	0 (0.0)	0 (0.0)	0 (0.0)
IIB	15 (17.2)	5 (18.5)	4 (18.2)	0 (0.0)	0 (0.0)	0 (0.0)	1 (25.0)	1 (100.0)
IIIA	1 (1.1)	0 (0.0)	0 (0.0)	0 (0.0)	0 (0.0)	0 (0.0)	0 (0.0)	0 (0.0)
IIIB	6 (6.9)	2 (7.5)	0 (0.0)	0 (0.0)	0 (0.0)	0 (0.0)	0 (0.0)	0 (0.0)
IVA	1 (1.1)	0 (0.0)	1 (4.5)	1 (100.0)	0 (0.0)	0 (0.0)	0 (0.0)	0 (0.0)
IVB	1 (1.1)	1 (3.7)	0 (0.0)	0 (0.0)	0 (0.0)	0 (0.0)	0 (0.0)	0 (0.0)
Histology								
Squamous cell carcinoma	52 (59.8)	16 (59.3)	12 (54.5)	0 (0.0)	1 (20.0)	1 (33.3)	1 (25.0)	0 (0.0)
Adenocarcinoma	31 (35.6)	11 (40.7)	9 (40.9)	1 (100.0)	3 (60.0)	2 (67.6)	3 (75.0)	1 (100.0)
Other	4 (4.6)	0 (0.0)	1 (4.5)	0 (0.0)	1 (20.0)	0 (0.0)	0 (0.0)	0 (0.0)
Grade of differentiation								
Good/moderate	40 (46.0)	14 (51.9)	10 (45.4)	1 (100.0)	3 (60.0)	2 (67.6)	2 (50.0)	0 (0.0)
Poor/undifferentiated	29 (33.3)	8 (29.6)	8 (36.4)	0 (0.0)	2 (40.0)	1 (33.3)	1 (25.0)	1 (100.0)
Unknown	18 (20.7)	5 (18.5)	4 (18.2)	0 (0.0)	0 (0.0)	0 (0.0)	1 (25.0)	0 (0.0)
Lymphangioinvasion								
No	60 (69.0)	16 (59.3)	14 (63.6)	0 (0.0)	4 (80.0)	2 (67.6)	1 (25.0)	1 (100.0)
Yes	26 (29.9)	11 (40.7)	8 (36.4)	1 (100.0)	1 (20.0)	1 (33.3)	3 (75.0)	0 (0.0)
Unknown	1 (1.1)	0 (0.0)	0 (0.0)	0 (0.0)	0 (0.0)	0 (0.0)	0 (0.0)	0 (0.0)
Tumor diameter (cm)								
0-4	42 (48.3)	11 (40.7)	10 (45.5)	0 (0.0)	3 (60.0)	3 (100.0)	3 (75.0)	0 (0.0)
≥ 4	27 (31.0)	10 (37.0)	6 (27.3)	1 (100.0)	1 (20.0)	0 (0.0)	1 (25.0)	0 (0.0)
Unknown	18 (20.7)	6 (22.2)	6 (27.3)	0 (0.0)	1 (20.0)	0 (0.0)	0 (0.0)	1 (100.0)
Primary treatment								
Wertheim Meigs	46 (52.9)	14 (51.9)	15 (68.2)	0 (0.0)	3 (60.0)	3 (100.0)	3 (75.0)	0 (0.0)
Radio-chemotherapy	32 (36.8)	8 (29.6)	5 (22.7)	1 (100.0)	1 (20.0)	0 (0.0)	1 (25.0)	0 (0.0)
Other	9 (10.3)	5 (18.5)	2 (9.1)	0 (0.0)	1 (20.0)	0 (0.0)	0 (0.0)	1 (100.0)
Follow-up (in years)								
Median	4.63	4.56	5.21	2.88	4.79	2.84	3.89	0.66
Range	0.08-10.81	0.04-9.14	0.2-11.72	-	1.22-5.37	0.22-7.01	0.93-6.73	-
Results last follow-up								
No evidence of disease	63 (72.4)	20 (74.1)	16 (72.7)	0 (0.0)	2 (40.0)	3 (100.0)	1 (25.0)	0 (0.0)
Evidence of disease	1 (1.1)	0 (0.0)	1 (4.5)	0 (0.0)	0 (0.0)	0 (0.0)	0 (0.0)	0 (0.0)
Death of disease	17 (19.5)	7 (25.9)	5 (22.7)	1 (100.0)	3 (60.0)	0 (0.0)	3 (75.0)	1 (100.0)
Death of other disease	6 (6.9)	0 (0.0)	0 (0.0)	0 (0.0)	0 (0.0)	0 (0.0)	0 (0.0)	0 (0.0)

Abbreviations. HPV, Human Papilloma Virus. FIGO, Federation of Gynecology and Obstetrics

Supplementary Figure 1
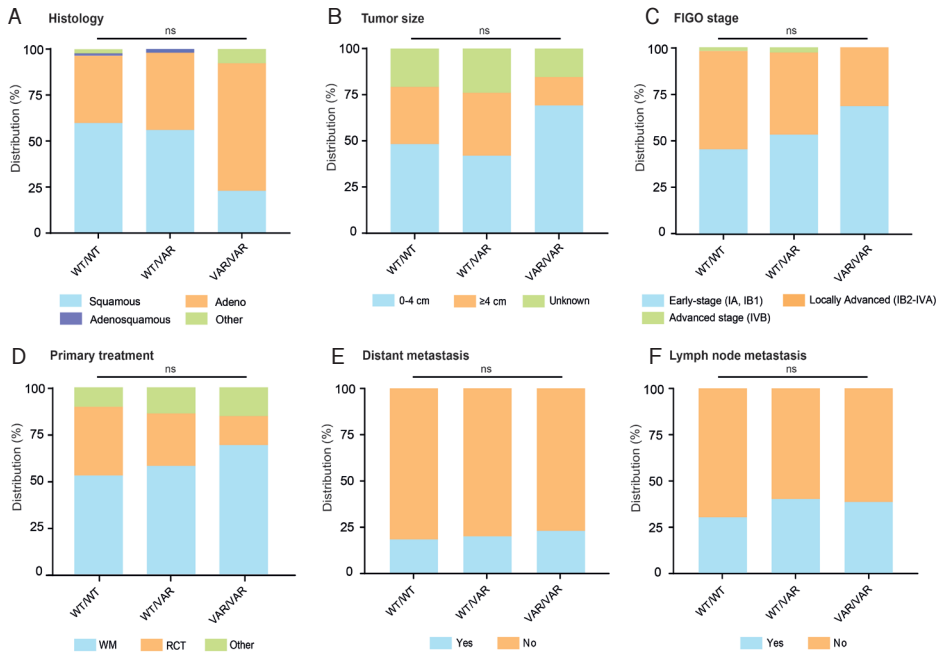
Clinical characteristics of cervical cancer patients divided into three groups: WT/WT, WT/VAT and VAR/VAR and tumors categorized based on A, Histology: Squamous (light blue), Adenosquamous (dark blue), Adeno (orange) and other subtypes of cervix carcinoma (green) B, Tumor size: small tumors of 0-4 cm (light blue), tumors larger than 4 cm (orange) and tumors with unknown size (green) C, FIGO stage: early-stage (IA and IB1, light blue), locally advanced (IB2 until IVA, orange) and advanced stage (IVB, green) cervix carcinoma D, Primary treatment: Wertheim-Meigs surgery (WM, light blue), radiochemotherapy (RCT, orange) and other (such as radiotherapy and lymph node removal, green) E, Distant metastasis: yes (light blue) or no (orange) and F, Lymph node metastasis: yes (light blue) or no (orange). For all characteristics, statistical analyses were performed by Pearson Chi-Square testing. Significance was defined as p<0.05.

Supplementary Figure 2
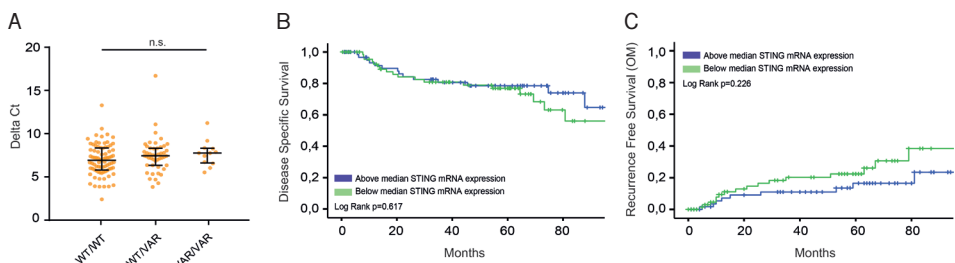
Quantitative PCR on cDNA of cervical cancer patients to analyze STING1 mRNA expression. A, Delta CT values (STING1 Ct values minus GAPDH Ct values). Patients were divided into three groups: :WT/WT, WT/VAT and VAR/VAR. Each orange dot represents one individual patient. Statistical analysis was performed by One-Way ANOVA testing with post-hoc Kruskal-Wallis test. B, Disease-specific survival dividing cervical cancer patients into below (green) and above (blue) median STING1 expression. C, Recurrence free survival (one-minus plot) based on below (green) and above (blue) median STING1 expression. For both survival curves, statistical analyses were performed by Log-Rank testing. Significance was defined as p<0.05. Curves were cut off at 7.5 years.

Supplementary Figure 3

A
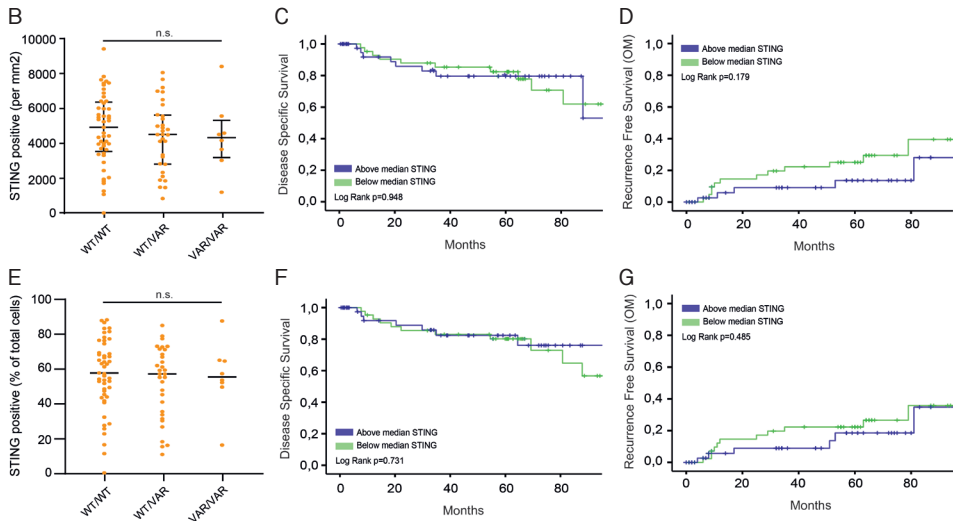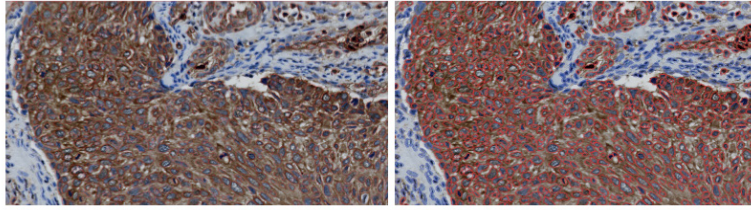
Immunohistochemical staining of STING on FFPE slides of tumors obtained from the studied cervical cancer patient cohort. A, Microscopic image (400X magnification) of STING staining (left) and representation of the computerized quantification of cytoplasmic DAB-positive cells (red) and DAB-negative cells (blue) in uPath image analysis software (right) B and E, Quantified numbers of DAB/STING-positive cells per mm^2 (B) and the percentage of positive cells from the total number of cells (E) in tumor tissue for the three groups: WT/WT, WT/VAR and VAR/VAR. C and F, Disease-specific survival dividing patients into two groups: below (green) and above (blue) median STING positive cells per mm^2 (C) and percentage of positive cells of the total number of cells (F). D and G, Recurrence free survival (one-minus plot) based on below (green) and above (blue) median STING1 positive cells per mm^2 (D) and percentage of positive cells of the total number of cells (G). Statistical analysis was performed by Log-Rank testing. Significance was defined as p<0.05. Curve was cut off at 7.5 years.

Supplementary Figure 4

Disease-specific survival dividing cervical cancer patients into below (green) and above (blue) median age at diagnosis. Statistical analysis was performed by Log-Rank testing. Significance was defined as p<0.05. Curve was cut off at 7.5 years.

3

Chapter 4

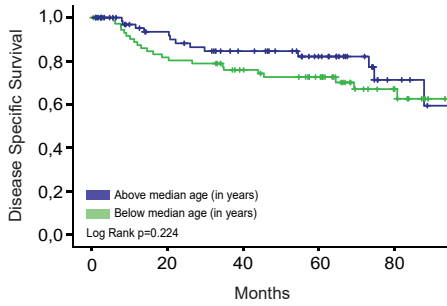A Transcriptionally Distinct CXCL13+CD103+CD8+ T cell Population Is Associated with B cell Recruitment and Neoantigen Load in Human Cancer

Joyce M. Lubbers[1*], Hagma H. Workel[1*], Roland Arnold[2], Thalina M. Prins[1], Pieter van der Vlies[3], Kim de Lange[3], Tjalling Bosse[4], Inge C. van Gool[4], Florine A. Eggink[1], Maartje C.A. Wouters[5], Fenne L. Komdeur[1], Elisabeth C. van der Slikke[1], Carien L. Creutzberg[6], Arjan Kol,[1] Annechien Plat[1], Mark Glaire[7], David N. Church[7,8], Hans W. Nijman[1#], and Marco de Bruyn[1#]

*contributed equally and are co-first authors
#share senior authorship

[1]University of Groningen, University Medical Center Groningen, Department of Obstetrics and Gynecology, The Netherlands
[2]Institute of Cancer and Genomic Sciences, University of Birmingham, Birmingham, United Kingdom
[3]University of Groningen, University Medical Center Groningen, Department of Genetics, The Netherlands
[4]Leiden University, Leiden University Medical Center, Department of Pathology, The Netherlands
[5]Trev and Joyce Deeley Research Centre, BC Cancer, Victoria, British Columbia, Canada
[6]Leiden University, Leiden University Medical Center, Department of Radiation Oncology, The Netherlands
[7]University of Oxford, Molecular and Population Genetics Laboratory, The Wellcome Trust Centre for Human Genetics and Oxford Cancer Centre, United Kingdom
[8] NIHR Oxford Biomedical Research Centre, Oxford University Hospitals NHS Foundation Trust, John Radcliffe Hospital, Oxford OX3 9DU

Abstract

The chemokine CXCL13 mediates recruitment of B cells to tumors and is essential for the formation of tertiary lymphoid structures (TLSs). TLSs are thought to support antitumor immunity and are associated with improved prognosis. However, it remains unknown whether TLSs are formed in response to the general inflammatory character of the tumor microenvironment, or rather, are induced by (neo)antigen-specific adaptive immunity. We here report on the finding that the TGFβ-dependent CD103+CD8+ tumor-infiltrating T cell (TIL) subpopulation expressed and produced CXCL13. Accordingly, CD8+ T cells from peripheral blood activated in the presence of TGFβ up-regulated CD103 and secreted CXCL13. Conversely, inhibition of TGFβ receptor signaling abrogated CXCL13 production. CXCL13+CD103+CD8+ TILs correlated with B cell recruitment, TLSs, and neo-antigen burden in six cohorts of human tumors. Altogether, our findings indicated that TGFβ plays a non-canonical role in coordinating immune responses against human tumors and suggest a potential role for CXCL13+CD103+CD8+ TILs in mediating B cell recruitment and TLS formation in human tumors.

Introduction

Immune checkpoint inhibitors (ICIs) targeting programmed death ligand 1 (PD-L1) or its receptor, programmed death 1 (PD-1), have elicited unprecedented long-term disease remissions in advanced and previously treatment-refractory cancers.[1–3] Unfortunately, only a subset of patients currently benefit from treatment. ICIs are more likely to be effective in patients with a preexisting anticancer immune response, most notably a CD8+ cytotoxic T cell response against tumor neoantigens.[4] Responsive tumors harbor significantly more predicted neoantigens[5,6] and display evidence of a coordinated immune response comprising T cells, dendritic cells (DCs), and B cells.[7] In diseases that parallel tumor development, such as chronic inflammatory conditions, this coordinated infiltration by different immune cell subsets is frequently associated with tertiary lymphoid structures (TLSs)–an ectopic form of lymphoid tissue. TLSs exhibit features of regular lymph nodes, including high endothelial venules, a T cell zone with mature DCs, and a germinal center with follicular DCs and B cells.[8] Several studies have reported the presence of TLSs in tumors, which was generally found to be associated with greater immune control of cancer growth and improved prognosis.[9,10] For several malignancies, the combination of TLS presence and high CD8+ T cell infiltration was found to associate with superior prognosis, whereas high CD8+ T cell infiltration alone associated with poor or moderate prognosis.[11,12] These observations highlight the importance of a coordinated immune response, including TLS formation, in anticancer immunity.

To date, the molecular determinants of tumor TLS formation remain incompletely understood. Current data suggest that TLS formation results from a complex interplay between DCs, T cells, B cells, and supporting stromal cells. Interplay among these cells relies on reciprocal cytokine and chemokine signaling, including chemokine [C-X-C motif] ligand 13 (CXCL13), receptor activator of nuclear factor κ B (ligand)(RANK/RANKL), lymphotoxin αβ (LTαβ), and chemokine (C-C motif) ligand 21 (CCL21).[13] A central role for CXCL13 in this process is suggested by the inability of B cells to home and accumulate into lymphoid aggregates[14] and generate functional lymphoid tissue[15,16] in *Cxcl13*-knockout mice and by the observation that CXCL13 alone is sufficient to generate lymphoid tissues.[17–19] Nevertheless, a key outstanding question remains whether tumor-associated TLSs are formed in response to the general inflammatory character of the tumor microenvironment, or rather, are induced by (neo)antigen-specific adaptive immunity. Two studies suggest that a subset of CXCL13-producing CD8+ tumor-infiltrating lymphocytes (TIL) may link (neo)antigen recognition to TLS formation.[7,20]

Here, we report the finding that TGFβ receptor signaling licensed CD8+ T cells to produce and secrete CXCL13 upon concurrent T cell receptor (TCR) stimulation.

Induction of CXCL13 was paralleled by upregulation of CD103, a marker for tissue-resident TILs. Accordingly, bulk and single-cell RNA sequencing identified exclusive expression of *CXCL13* in human CD103+, but not CD103−, CD8+ TILs. In line with these data, the presence of CD103+ CTLs correlated to B cell recruitment and TLSs in tumors with a high mutational load. This discovery sheds light on how B cells could be recruited to tumors by CTLs, identifying a noncanonical role for TGFβ in the orchestration of a coordinated immune response against human (neo)antigen-rich tumors. Our findings also identify CD103 and B cells as potential biomarkers for ICI in epithelial malignancies.

Materials and methods

Patients

Tumor tissue from four patients with stage IIIC high-grade serous ovarian cancer was collected during primary cytoreductive surgery, prior to chemotherapy, and from one patient with stage IV high-grade serous ovarian cancer during interval debulking upon three cycles of chemotherapy. Written informed consent was obtained from all patients. Selection of patients with uterine cancer was described previously.[21] Briefly, uterine cancer tissue was obtained from patients involved in the PORTEC-1[22] and PORTEC-2[23] studies (n=57), the uterine cancer series (n=67) from Leiden University Medical Center (LUMC, Leiden, the Netherlands), and uterine cancer series (n=26) from the University Medical Center Groningen (UMCG, Groningen, the Netherlands) in accordance with local medical ethical guidelines.[24] Tumor material was fixed in formalin and embedded in paraffin. Tumor material from 119 patients was available for analysis. Mutations in the exonuclease domain of polymerase epsilon (*POLE*-EDM) and microsatellite instability status were known from previous studies.[24] Of the tumors available for this study, 42 tumors were *POLE* wild-type and microsatellite stable (MSS), 38 were *POLE* wild-type with microsatellite instability (MSI), and 39 were *POLE*-EDM. *POLE*-EDM statuses did not co-occur with microsatellite instability. All cases were of endometrioid histology (EEC), and the number of low-grade and high-grade tumors was spread equally over the three molecular groups. Selection of patients with ovarian cancer and CD103 staining was reported previously.[25] Ethical approval for tumor molecular analysis was granted at LUMC, UMCG, and by Oxfordshire Research Ethics Committee B (approval no. 05\Q1605\66).

Analysis of TCGA mRNA sequencing data

RSEM-normalized mRNA-seq data and clinical data from uterine corpus endometrial carcinoma (UCEC), ovarian cancer, breast cancer, and lung adenocarcinoma were downloaded from firebrowse.org on March 13, 2017 (UCEC) and July 14, 2017 (ovarian cancer, breast cancer, lung adenocarcinoma). RSEM mRNA sequencing expression data

were log2+1 transformed, and genes with zero reads in all samples were removed. *POLE*-EDM, MSI, and MSS cases were identified in the endometrial cancer data. The mononucleotide and dinucleotide marker panel analysis status was provided by The Cancer Genome Atlas (TCGA), and mutations in the exonuclease domain of *POLE* were determined previously.[26] Heatmaps were constructed in R (version 3.3.1) with packages gplots and ggplots. The gene set of TLSs was reported previously.[10,27] Gene sets for the CD8+CD103+ and CD8+CD103− signatures were derived from the sequencing data (Supplementary Table S1). Spearman correlations between the TLS signature, the CD8+CD103+ signature, and the CD8+CD103− signature were visualized in correlation plots using the Corrplot package (Version 0.77) in R. CXCL13^{high}CD103^{high} versus CXCL13^{low}CD103^{low} groups in MSS UCEC were based on median expression of *CXCL13* (4.35698) and *ITGAE* (8.086985). Survival curves were constructed with R packages survival (version 2.41-3) and survminer (version 0.4.3). All analyses were performed in R (version 3.4.0), with exception of the construction of the heatmap in Figure 3C, which was made in R version 3.3.1.

Immunohistochemistry

To assess the presence of TLSs in uterine cancer, we stained for the B cell marker CD20 on whole tissue sections. Formalin-fixed, paraffin-embedded (FFPE) slides were deparaffinized and rehydrated in graded ethanol. Antigen retrieval was initiated with a preheated 10 mmol/L citrate buffer (pH=6) and endogenous peroxidase activity was blocked by submerging sections in a 0.45% hydrogen peroxide solution. Slides were blocked in PBS containing 1% human serum and 1% BSA. Slides were incubated overnight with anti-CD20 (0.63 mg/L; clone L26, catalog number M0755, Dako) at 4°C. Subsequently, slides were incubated with a ready-to-use peroxidase-labeled polymer for 30 minutes (Envision+/HRP anti-mouse, 2 drops, catalog number K4001, Dako). Signal was visualized with 3.3′diaminobenzidin (DAB) solution, and slides were counterstained with hematoxylin. Appropriate washing steps with PBS were performed in-between incubation steps. Sections were embedded in Eukitt mounting medium (Sigma Aldrich), and slides were scanned on a Hamamatsu digital slide scanner (Hamamatsu Photonics). The number of CD20+ (dense) follicles in each slide was quantified in NDPview2 software by two independent observers who were blinded to clinicopathologic data.

IHC for CD8 was performed previously in this cohort.[24] To assess the survival effect of CD103 infiltration in mismatch repair–proficient (pMMR) cancers, we used a staining for CD103 on tissue microarray slides of uterine cancer.[28] FFPE slides were prepared as described above and incubated with rabbit-anti human CD103 [1 mg/L; anti-E7-integrin, clone ERPR4166(2), catalog number Ab129202, Abcam), followed by a ready-to-use peroxidase-labeled polymer (Envision+/HRP anti-rabbit, cat.no. K4003, Dako) and Biotin

Tyramide working solution (TSA kit, Perkin Elmer), streptavidin-HRP (TSA kit, Perkin Elmer), and 3.3′-diaminobenzidin/hematoxylin. Positively stained cells were quantified per core and adjusted for core surface. Patients with at least two cores with a minimum of 20% tumor epithelium were included for analysis. All slides were counted manually by two individuals who were blinded for clinicopathologic data.

Multicolor immunofluorescence

FFPE slide preparation and antigen retrieval were performed as described above. Next, slides were incubated overnight at 4°C with primary antibody and subsequently incubated with the appropriate secondary antibody for 45 minutes at room temperature (Supplementary Table S2). Specific signal was amplified using the TSA Cyanine 5 (Cy5) detection kit (Perkin Elmer, NEL705A001KT) or the TSA Cyanine 3 (Cy3) and Fluorescein detection kit (Perkin Elmer, 753001KT), according to the manufacturer's protocols. To allow multiple amplifications on the same slide, primary HRP labels were destroyed between incubations by washing with 0.01 mol/L hydrochloric acid for 10 minutes. Appropriate washing steps with PBS containing 0.05% Tween20 (Sigma-Aldrich) were performed during the procedure. For embedding, Prolong Diamond anti-fade mounting medium with or without DAPI was used (Invitrogen/Thermo Fisher Scientific, P36962 and P36961). Finally, slides were scanned at room temperature using the TissueFAXS acquisition software and microscope (TissueGnostics) with the following specifications: Zeiss EC "Plan-Neofluar" 40×/1.30 Oil, DIC objective, CMOS-color camera PL-B623 Pixelink (3.1 Megapixels), EXFO Excite 120 PC fluorescence illumination and Chroma ET Dapi (49000), Chroma ET CY3 (49004), Chroma ET Cy5 (49006), and Chroma FITC (49011) filter sets. Overlay images were produced using Adobe Photoshop software.

mRNA sequencing

Ovarian tumors from two patients were cut into pieces of <1 mm3 and placed in a T75 culture flask (Nunc EasYFlask Cell Culture Flasks, catalog no. 156499, Thermo Fisher Scientific) with digestion medium, consisting of RPMI (Gibco), 10% FBS (Gibco), collagenase type IV (1 mg/mL; Gibco), and recombinant human DNase (12.6 µg/mL; Pulmozyme, Roche) for overnight digestion at room temperature. After digestion, the suspension was strained through a 70-µm filter and washed with PBS. Cells were centrifuged over a Ficoll-Paque gradient (GE Healthcare Bio-Sciences AB) and lymphocytes were isolated from between the two layers. After a wash with PBS the cells were pelleted. Total cell pellet was suspended in 1 mL FBS with 10% dimethylsulfoxide (Merck) and stored in liquid nitrogen until further use.

Prior to sequencing, tumor digests were thawed on ice, washed with AIM-V medium (Gibco) with 5% pooled human serum (PHS, One Lambda) and centrifuged at 1,000×g.

The total cell pellets were resuspended in AIM-V with 5% PHS, and cells were incubated with CD3-BV421, CD4-PerCP-Cy5.5, CD8α-APCeFluor780, CD8β-PEcy7, TCRαβ-APC, CD103-FITC, and CD56-PE antibodies at 4°C for 45 minutes (Supplementary Table S3). After gating for CD3+CD4−CD8αβ+TCRαβ+CD56− cells, CD103− and CD103+ single cells were sorted on a Beckman Coulter Astrios cytometer directly into 4 μL lysis buffer (2 μL of 0.2% Triton X-100, Sigma-Aldrich, catalog no. T9284) with 5% recombinant RNase inhibitor (Westburg-Clontech, catalog no. 2313A), 1 μL of 10 μmol/L barcoded oligo dT primer, and 1 μL 4×10 mmol/L dNTP mix in 96-well PCR plates. Each well contained a unique indexed Oligo dT primer [custom designed by P. van der Vlies (UMGC, Groningen, the Netherlands); Supplementary Table S4), enabling identification of individual cells after pooled RNA sequencing.

In addition to single-cell wells, small bulk populations of 20 cells were sorted per microplate well. Per patient, 40 single CD8+ T cells (20 wells CD103+, 20 wells CD103−) and 20 small bulk 20-cell populations (10 wells CD103+, 10 wells CD103−) were sorted. After sorting, the plate was vortexed and spun down briefly, and incubated at 72°C for 3 minutes. After this step, the plate was kept cool. The transcriptomes were amplified by a modified SMART-Seq2 protocol using SmartScribe reverse transcriptase (Westburg-Clontech, CL639537), based on a previously published protocol.[29] In brief, custom primers were designed that included a PCR-primer recognition site for pre-PCR, a Unique Molecular Identifier (UMI), a cell barcode (see Supplementary Table S4), and a poly T-stretch. Each cell (or pool) was tagged with an oligo dT primer, including the UMI and cell barcode. A template switching pre-PCR was used to generate cDNA. Pools are made of single cells or pools with unique cell barcodes and 500 pg of the pools was tagmentated and barcoded using a N7xx in-dex and custom P5 hybrid primer: (AAT GATACGGCGACCACCGAGATCTACACGCCTGTC-CGCGGAAGCAGTGGTATC AACGCAGAGT*A*C) according the Illumina Nextera XT DNA Sample Preparation Kit Protocol (Illumina, catalog no. FC-131-1096). The pools were purified using AMPure beads, in a ratio of 0.6:1, to remove primer dimers. Presence and size distribution of the obtained PCR product were checked on a PerkinElmer LabChip GX high-sensitivity DNA chip. A super pool was created by equimolar pooling (1 nmol/L) of the Nextera products, and the samples were sequenced on Illumina NextSeq500 2500 using 50 bp paired-end reads, one read for the mRNA transcript, and the other for the cell-bar-code. The obtained RNA-sequencing data were demultiplexed into individual FASTQ files. The obtained single-end reads were aligned to human reference genome 37 [GRCh37.p13 (GCA_000001405.14), top-level built] using STAR (version 2.5.2).

RNA-SeQC (version 1.1.8) was then used to assess the quality of single cells. Data were visualized and clear low-quality outliers were identified on the basis of number

4

of transcripts, uniquely mapped reads, mapping rate, expression profiling efficiency and exonic rate, and these were removed from further analysis. All cells that did not meet one of the following criteria were removed: <10.000 transcripts detected, <500.000 uniquely mapped reads, <1.000 genes detected, a mapping rate of <0.5, an expression profiling efficiency of <0.4, or an exonic rate of <0.5 (Supplementary Table S5). mRNA expression values for small bulk populations of 20 cells are shown in transcripts per kilobase million (TMP) and for single cells as fragments per kilobase million (FKPM) and log2+1 transformed. Differential expression in the 20-cell populations was analyzed with DESeq2 (version 1.16.1) to obtain insight into the differences between CD103+ and CD103☐ CD8+ T cells. For this analysis, expression values for each sample have been obtained using RSEM (version1.3.0, with Bowtie 2, version 2.2.5, nonstranded and with the single cell prior activated to account for drop-out genes) and have been computed for the Gencode 19 transcriptome annotation for GRCh37 (reference index built with –polyA activated). Genes with a Benjamini–Hochberg FDR <0.01 and log2 fold change >1 were selected for further analysis. Differentially expressed genes were visualized in a Volcano plot (DESeq2, version 1.16.1). The accession number for the sequencing data reported in this study is GSE127888.

ELISA

TILs from three high-grade serous ovarian cancer digests were stained and sorted as described for mRNA sequencing. The numbers of sorted T cells for the three patients were 163×10^3, 216×10^3, and 154×10^3 for CD4+ cells; 82×10^3, 38×10^3, and 83×10^3 for CD8+CD103−; and 207×10^3, 120×10^3, and 146×10^3 for CD8+CD103+ T cells. Sorted T cells remained unstimulated or were activated either with a stimulation cocktail containing phorbol myristate acetate (PMA, 40.5 μmol/L) and ionomycin (670 μmol/L, 500× dilution, Invitrogen, 00-4970-93) or with Dynabeads (2 μL/1×10^5 cells, T-activator CD3/CD28 beads, 11131D, Gibco).

Peripheral blood CD8+ T cells were isolated from blood of four healthy volunteers (Sanquin, written informed consent was obtained) by a Ficoll-Paque gradient followed by magnetic-activated cell sorting with a CD8+ T cell–negative selection kit (purity >90%, MagniSort Human CD8 T cell Enrichment Kit, catalog no. 8804-6812-74; Thermo Fisher Scientific). Peripheral blood CD8+ T cells were incubated in 100 μL AIM-V medium with or without Dynabeads (2 μL/1×10^5 cells) for activation, recombinant TGFβ1 (rTGFβ1, 100 ng/mL, PeproTech), TGFβ1 receptor inhibitor (10 μmol/L, SB431542, Sigma Aldrich/ Merck), or a combination of these. Similar experiments were performed with the addition of IL2 (100 IU/mL, Novartis Pharmaceuticals). For the dose–response curve, peripheral blood CD8+ T cells from three healthy donors were incubated with or without Dynabeads (2 μL/1×10^5 cells) for activation and with recombinant TGFβ1 at

doses ranging from 0 to 100 ng/mL (rTGFβ1, PeproTech). All cells were cultured in AIM-V medium with 5% pooled human serum (catalog no. A25761, One Lambda) in 96-well plates containing 1×10^5 cells per condition. After 7 days, plates were centrifuged and supernatant was collected for ELISA.

CXCL13 sandwich ELISA experiments were performed according to manufacturer's protocol (human CXCL13/BLC/BCA-1 DuoSet ELISA DY801, R&D Systems, Abingdon, United Kingdom). In brief, Nunc MaxiSorp flat-bottom plates (Invitrogen) were coated with a capture antibody, followed by incubation with cell supernatant. Per condition, 70 µL of supernatant was diluted with 40 µL 1% BSA in PBS, after which 100 µL was added to the well. Binding of CXCL13 was detected using secondary antibody, streptavidin-HRP, and TMB 1-Component Microwell Peroxidase Substrate (SureBlue, KPL/SeraCare). Substrate conversion was stopped after 20 minutes with 0.01 mol/L hydrogen chloride. Plates were washed with PBS plus 0.05% Tween20 in-between incubations. Optical density values were obtained using a microplate reader set to 450 nm (Bio-Rad iMark Microplate reader). Finally, the derived CXCL13 concentrations (pg/mL) were multiplied by 1.57 to correct for diluting. AIM-V medium only was used as a negative control.

Chemokine arrays

CD8+ T cells were isolated from blood of three healthy donors as described above in the ELISA section. Per condition, 5×10^5 cells were cultured in AIM-V medium with 5% PHS in a 24-well plate. Cells were either incubated for 7 days in medium alone, with rTGFβ1 (100 ng/mL, PeproTech), with Dynabeads (2 µL/1×10^5 cells, T-activator CD3/CD28 beads, 11131D, Gibco), or with both rTGFβ1 and Dynabeads. Samples were centrifuged, and supernatants were collected to analyze production of chemokines on chemokine arrays, according to manufacturer's instructions (31 chemokines using the Proteome Profiler Human Chemokine Array Kit, ARY017, R&D Systems and 38 chemokines using the Human Chemokine Antibody Array-Membrane, ab169812, Abcam; Supplementary Table S6). In brief, chemokine receptor–coated membranes were incubated with supernatant overnight at 4°C. Per condition, 450 µL of supernatant was diluted with 1,050 µL buffer, provided by the manufacturer, and 1.500 µL was added (R&D Systems), or 1.000 µL was added undiluted (Abcam). Captured proteins were visualized using chemiluminescent detection reagents, provided by the manufacturers. Appropriate washing steps using wash buffers provided by the manufacturers were performed in-between incubation steps. Membranes were imaged on the Bio-Rad ChemiDoc MP Imaging System, and densitometric analysis of chemokine spots was performed using the Protein Array Analyzer plugin for ImageJ.[30]

Statistical analyses

Differentially expressed genes in CD103+CD8+ versus CD103−CD8+ T cells sorted from human ovarian tumors were determined by DESeq2 for 20-cell populations. Genes with a Benjamini–Hochberg FDR <0.01 and log2 fold change >1 were selected for further analysis. Differences in FPKM values of single cells were assessed by a Mann–Whitney U test. Differences in number of CD20+ follicles on FFPE slides of molecular subgroups of endometrial cancer were determined by a nonparametric Kruskal–Wallis test, followed by Dunn post hoc analysis. We analyzed the TCGA mRNA sequencing data and compared differences in gene expression between molecular subgroups of endometrial cancer with a nonparametric Kruskal–Wallis test and a post hoc Dunn test. Differences in survival were determined by a log-rank test. CXCL13 production was analyzed using a Kruskal–Wallis comparison with a post hoc Dunn test, or, for the dose–response curve, with a two-way ANOVA followed by a post hoc Bonferroni test. The chemokine arrays were analyzed using a Kruskal–Wallis test with a post hoc Dunn test. The survival effect of CD103 in pMMR uterine cancer was assessed by Kaplan–Meier analysis and log-rank test by comparing "above median CD103 expression" and "equal to or below median CD103 expression" (cut-off 16.14) patient groups. Uni- and multivariate analyses were performed by disease-specific Cox regression survival analyses [Enter for univariate and Backward and Forward (both LR and conditional) methods for multivariate analyses]. All statistical analyses were performed using R version 3.4.0 or GraphPad Prism (GraphPad Software Inc.). A P value of <0.05 was used as a cut-off for significance.

Results

Epithelial CD8+ T cells associate with an activated and exhausted transcriptional signature

We and others have previously shown that intraepithelial CD103+, but not stromal CD103−, CD8+ TILs are promising targets for ICI therapy.[25,28,30,31] To understand the underlying transcriptional changes in these two cell populations, we performed mRNA sequencing on single- and 20-cell pools of CD8+ T cells isolated from human tumors. We chose ovarian cancer as a model tumor because of its large tumor bulk, availability of pretreatment tissue, and a high number of distinct CD103+ and CD103− infiltrating CD8+ cells. CD8+ TILs were defined on the basis of a CD3+/TCRαβ+/CD8αβ+/CD56−/CD4− phenotype (Figure 1A). Post hoc t-distributed stochastic neighbor embedding (t-SNE) confirmed the presence of unique CD103+ and CD103− CTL populations in these tumors (Supplementary Figures S1A–S1C). The transcriptome of CD103+ CTLs was characterized by an activation and exhaustion signature (Supplementary Table S7) with significant upregulation of *GZMB* (granzyme B), *HAVCR2* (T cell immunoglobulin and mucin domain 3, TIM3), *LAG3* (lymphocyte-activation gene 3), *TNFRSF18* (glucocorticoid-

Figure 1
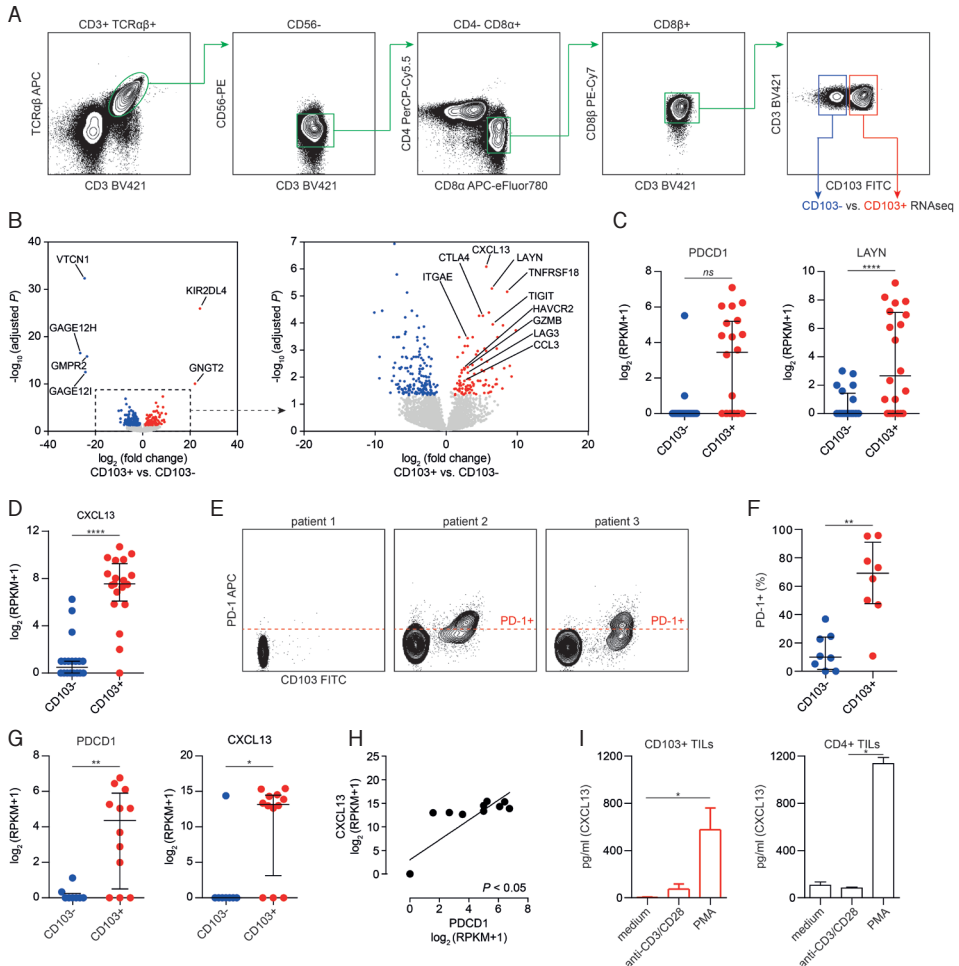
CD103+ CD8+ TILs display a distinct phenotype and gene signature characterized by exhaustion genes and CXCL13 expression. A, Gating strategy of CD103+ and CD103− CD8+ T cells according to TCRαβ, CD3, CD56, CD4, CD8α, CD8β, and CD103 expression. One exemplary ovarian tumor is depicted. B, Volcano plot of up- or downregulated genes in CD103+ and CD103− TILs as determined by RNA sequencing, annotated by a set of exhaustion and chemokine-related genes. Significance was determined as Benjamini–Hochberg FDR <0.01 and log2 fold-change >1. Expression of exhaustion-related genes (C) PDCD1 and LAYN and (D) chemokine CXCL13 in the CD103+ and CD103− subsets (n=20). The lines indicate median Log2 (TPM+1) values ± IQR. E, Cell surface expression of CD103 and PD-1 in gated CD8+ TILs from exemplary ovarian tumor digests (n=3) determined by flow cytometry. The red line represents threshold for PD-1 positivity based on isotype control. F, Cell surface expression of PD-1 on CD103+ and CD103− gated CD8+ TIL subsets determined by flow cytometry (n=8). Graphs indicate median and IQR. G, Expression of PDCD1 and CXCL13 in single CD103− (n=12) and CD103+ TILs (n=12). Lines indicate median Log2 (FPKM+1) ± IQR. Significance in F and G was determined as Mann–Whitney U test (*, P<0.05; **, P<0.01). H, Correlation of PDCD1 and CXCL13 expression in CD103+ TILs (n=24). I, Secretion of CXCL13 by CD103+ TILs and control CD4+ TILs after stimulation overnight at 37°C using anti-CD3/CD28 T cell activation beads (2 µL Dynabeads per 1×10^5 cells) or PMA/ionomycin (500× dilution according to manufacturer's instructions), determined by ELISA Mean plus SEM of TILs from ovarian tumors (n=3) are depicted. Significance was determined by Kruskal–Wallis comparison with a post hoc Dunn test (*, P<0.05; ns, not significant).

induced TNFR-related protein, *GITR*), *KIR2DL4* (killer cell immunoglobulin-like receptor 2DL4), *TIGIT* (T cell immunoreceptor with Ig and ITIM domain), and *CTLA4* (CTL attenuator 4) in the 20-cell pools (Figure 1B). CD103+ CTLs expressed *GNGT2* (G protein subunit gamma transducin 2), encoding a G protein gamma family member expressed in lymph nodes and spleen that is involved in GTPase activity (Figure 1B). The expression of these markers is in-line with our earlier work demonstrating that the intraepithelial CD103+ T cells likely represent CTLs that have undergone activation and/or exhaustion.[25,28] In contrast, CD103− CTLs displayed a more quiescent phenotype with a high differential expression of the V-set domain–containing T cell activation inhibitor 1 (*VTCN1*), a known suppressor of T cell function (Figure 1B). These cells differentially expressed *GAGE12H*, *GAGE12I*, and *GMPR2* (guanosine monophosphate reductase 2), involved in cell energy metabolism (Figure 1B). Finally, CD103+, but not CD103−, cells were characterized by expression of genes previously associated with exhausted CD8+ T cells (Figure 1C).[32]

CD103+ CTLs differentially express the B cell recruiting chemokine CXCL13
In addition to the activated and exhausted gene signature, CD103+ CTLs were also characterized by significantly upregulated expression of the TLS-inducing *CXCL13* (Figures 1B and D; P<0.0001). Although traditionally considered a CD4+ follicular helper T cell (TFH) gene, *CXCL13* is also expressed in subsets of CD8+ TILs from hepatocellular carcinoma, melanoma, breast, and non–small cell lung cancer.[20,33–35] In the latter, *CXCL13* was identified in a transcriptionally unique PD-1–high (PD-1^T) CD8+ T cell population that predicted response to ICI therapy.[20] We, therefore, determined whether ovarian tumor-infiltrating CD103+ and PD-1^T CD8+ populations overlapped phenotypically. *PDCD1* was differentially expressed in CD103+ over CD103− cells on the mRNA level, although this did not reach statistical significance in the 20-cell pools (Figures 1B and C). Nevertheless, at the protein level, PD-1 was expressed almost exclusively on the cell surface of CD103+CD8+ T cells (Figures 1E and F), although considerable heterogeneity existed between patients with regards to PD-1 expression (Figure 1E). Accordingly, analysis of the CD103+ and CD103− CD8+ single-cell mRNA sequencing data revealed that *PDCD1* was heterogeneously expressed in CD103+ cells but absent in CD103− cells (Figure 1G). In contrast, *CXCL13* was homogenously expressed in almost all CD103+CD8+ T cells (Figure 1G). In line with the above, *CXCL13* and *PDCD1* transcripts were significantly, although poorly, correlated (Figure 1H). Finally, we assessed whether CD103+ TILs secreted CXCL13 protein, using CD4+ TILs obtained by flow cytometry–based sorting as controls. CD103+CD8+ TILs and CD4+ TILs readily secreted CXCL13 upon *ex vivo* activation with anti-CD3/anti-CD28-conjugated beads or PMA/ionomycin (Figure 1I).

TGFβ primes cytotoxic CD8+ T cells to secrete CXCL13 *in vitro*

We next sought to define the molecular mechanism underlying production of CXCL13 by CD103+CD8+ TILs. Previously, we and others have demonstrated that induction of CD103 on CD8+ T cells is dependent on concurrent T cell receptor (TCR) and TGFβ receptor 1 (TGFβR1) signaling.[25,36] TGFβ is a reported inducer of exhaustion-related genes such as PD-1 in T cells[37], which is also in-line with the transcriptional and phenotypical profile that we obtained for CD103+CD8+ TILs. Therefore, we hypothesized that TGFβ might stimulate CD8+ T cells to secrete CXCL13. To investigate this, we activated peripheral blood CD8+ T cells from healthy donors with anti-CD3/anti-CD28–conjugated beads in the presence or absence of recombinant TGFβ1 (rTGFβ1) and measured secretion of CXCL13. Resting CD8+ T cells did not produce or secrete CXCL13 (Figure 2A), nor did they express CD103 at the cell surface. Activation using anti-CD3/anti-CD28–conjugated beads induced minimal secretion of CXCL13 (Figure 2A) and a minor upregulation of CD103 (Figure 2B). Secretion of CXCL13 and expression of CD103 was inhibited by coincubation with a TGFβR1 inhibitor, suggesting autocrine TGFβ signaling was required for this induction of CXCL13 (Figures 2A and B). Accordingly, activation of CD8+ T cells in the presence of rTGFβ1 induced significant CXCL13 secretion (Figure 2A) and expression of CD103 on the CD8+ T cell surface (Figure 2B). Again, induction of CXCL13 and CD103 were inhibited by coincubation with a TGFβR1 inhibitor (Figures 2A and B). Induction of CXCL13 by TGFβ was dose-dependent and induced CXCL13 secretion at 0.1 ng/mL rTGFβ1 with a peak at 10 ng/mL rTGFβ1 (Figure 2C). Because IL2 inhibits the secretion of CXCL13 in follicular helper CD4+ T cells[38], we also examined whether IL2 impacted CXCL13 secretion by CD8+ T cells. In contrast to CD4+ T cells, induction of CXCL13 in CD8+ T cells was not inhibited by IL2 (Figure 2D), suggesting underlying differences in *CXCL13* gene regulation and/or IL2 signaling between CD8+ and CD4+ cells. On the basis of our findings, we concluded that TGFβ was sufficient for *CXCL13* induction in activated CD8+ T cells.

Next, we determined whether TGFβ also modulates secretion of other chemokines. Analysis of chemokine mRNA expression in CD103+ versus CD103− TILs revealed a significant upregulation of *CCL3*, *CCL5*, and *CXCL13* and a trend toward overexpression of *CCL3L1*, *CCL4L2*, *CCL20*, and *CXCL9* in CD103+ TILs (Figure 2E). Subsequent analysis of 47 chemokines secreted from peripheral blood CD8+ T cells revealed activation-dependent production of CCL4, CCL5, CXCL9, and CXCL10 (Figures 2F and G; Supplementary Figures S2A–S2C). As before, significantly higher CXCL13 was secreted upon activation of T cells in the presence of rTGFβ1 (Figures 2H and I). In contrast, rTGFβ1 did not affect the induction of other chemokines (Figure 2I). Taken together, our data indicated that TGFβ was a specific inducer of *CXCL13* in CD8+ T cells and identified a hallmark chemokine pattern for CD103+CD8+ TILs.

4

Figure 2
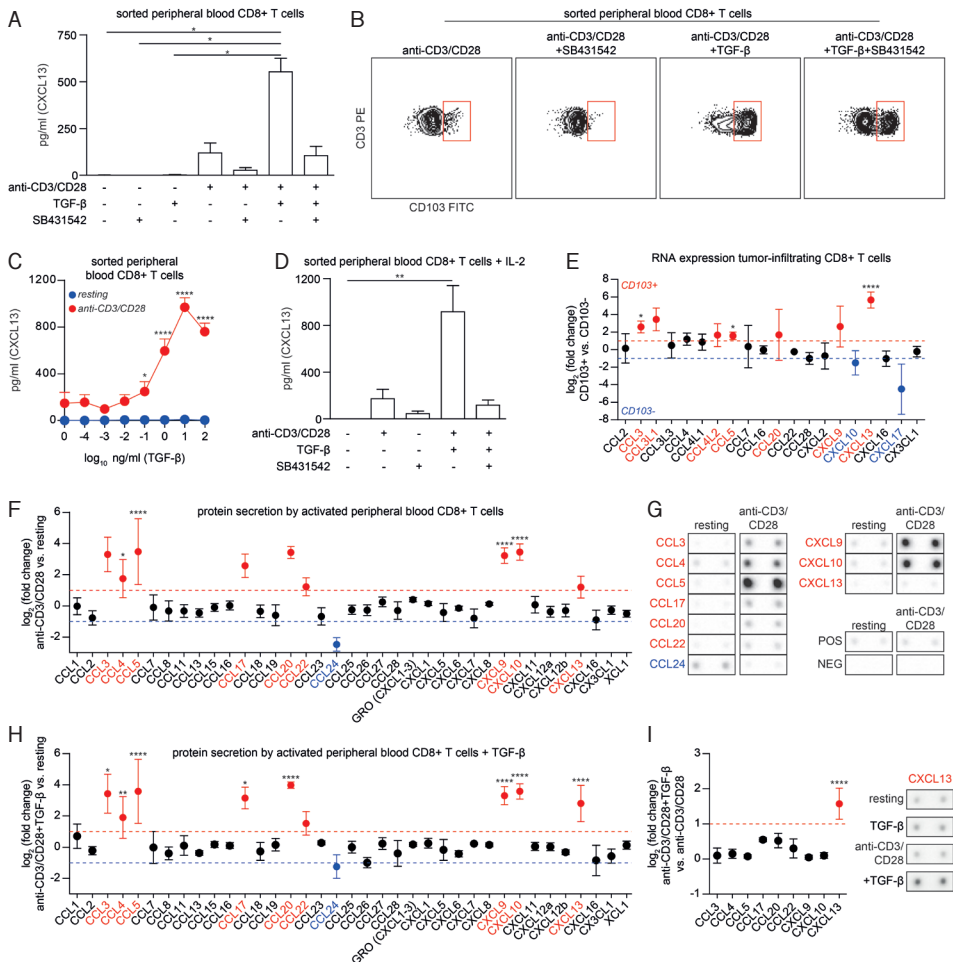
TGFβ-dependent induction of CXCL13 in CD8+ T cells and CD103+ TIL chemokine profile.
A, Secretion of CXCL13 by sorted peripheral blood CD8+ T cells after stimulation for 7 days using anti-CD3/CD28 T cell activation beads (2 µL per 1×10⁵ cells), recombinant TGFβ1 (100 ng/mL), and/or TGFβ1 receptor inhibitor SB431542 (10 µmol/L), determined by ELISA. Depicted are mean plus SEM of CD8+ T cells from 4 donors. Significance was determined using Kruskal–Wallis comparison with a post hoc Dunn test (*, P<0.05). B, Cell surface expression of CD103 on sorted CD8+ T cells after stimulation using anti-CD3/CD28 T cell activation beads, recombinant TGFβ1, and/or TGFβ1 receptor inhibitor SB431542 as described for A. One exemplary donor is depicted. C, Secretion of CXCL13 as determined by ELISA of CD8+ T cells after stimulation using anti-CD3/CD28 T cell activation beads as described for A and/or varying concentrations of recombinant TGFβ1 as depicted on the x-axis. Mean plus SD from 3 donors is depicted. Significance was determined by a two-way ANOVA followed by a post hoc Bonferroni test (*, P<0.05; ****, P<0.0001). D, Secretion of CXCL13 by sorted peripheral blood CD8+ T cells after stimulation using anti-CD3/CD28 T cell activation beads, recombinant TGFβ1, and/or TGFβ1 receptor inhibitor SB431542 (as described for A) in the presence of IL2 (100 IU/mL), determined by ELISA. Depicted are mean plus SEM of CD8+ T cells from 4 donors. Significance was determined using Kruskal–Wallis comparison with a post hoc Dunn test (*, P<0.05). E, Up- or downregulated chemokines between CD103+ and CD103− TILs determined by differential expression of RNA sequencing of 20-cell pools (n=20). Dashed red line indicates ≥2-fold change; dashed blue line indicates ≤0.5-fold change. Error bars indicate fold change SE. Significance was determined using Benjamini–Hochberg FDR. F, Secretion of chemokines by CD8+ T cells after 7 days stimulation using anti-CD3/CD28 T cell activation beads (2 µL per 1×10⁵ cells) determined by a chemokine array kit. n=3. Shown are log2 fold changes of the mean compared with resting unstimulated

CD8+ T cells. Dashed red line indicates ≥2-fold change; dashed blue line indicates ≤ 0.5-fold change. Error bars indicate SEM. G, Exemplary chemokine array data from anti-CD3/CD28-activated CD8+ T cells of one donor depicting chemokines with ≥2-fold and ≤0.5-fold change compared with resting CD8+ T cells from F. H and I, Secretion of chemokines by CD8+ T cells after stimulation using anti-CD3/CD28 T cell activation beads and recombinant TGFβ1 (n=4). Shown are log2 fold changes of the mean compared with resting unstimulated CD8+ T cells (H) or to anti-CD3/CD28–activated CD8+ T cells (I). Dashed red line indicates ≥2-fold change; dashed blue line indicates ≤0.5-fold change. Error bars indicate SEM. Significance in F–I was determine using Kruskal–Wallis comparison with a post hoc Dunn test (*, P<0.05; **, P<0.01; ****, P<0.0001).

CXCL13+CD103+ CTLs associated with a high mutation load, B cell infiltration, and TLSs

CXCL13 is a key driver of B cell recruitment and TLS formation in cancer and autoimmune diseases.[16,35,39–41] As such, we speculated the CXCL13+CD103+ TIL population would be involved in recruitment of B cells and TLS formation across human tumors. We retrospectively analyzed a cohort of 125 (high-grade serous) ovarian tumors for CD103+ cells and CD20+ B cells using a tissue microarray. CD103+ and CD20+ cells were detected in most patients, with some CD20+ cells forming aggregates in close proximity to CD103+ cells in the tumor epithelium (Figure 3A). Indeed, division of patients by high (>26.3), intermediate (8.6-26.3), or low (<8.6) CD103+ cell infiltration revealed a significant association with the number of B cells (Figure 3B). Next, we assessed whether CD103+CD8+ T cells might also link neoantigen-specific T cell responses to B cell–driven immune responses. To address this, we determined whether tumors with a high neoantigen load and concomitantly high CD103+ TIL infiltrate were enriched for B cell– and TLS-associated genes in mRNA sequencing data from The Cancer Genome Atlas (TCGA). Specifically, we analyzed uterine cancer samples stratified by neoantigen load. In brief, four distinct molecular subtypes can be distinguished in uterine cancer: microsatellite stable (MSS), microsatellite unstable (MSI), polymerase epsilon exonuclease domain mutated (*POLE*-EDM) tumors, and p53-mutant tumors. We have previously demonstrated an increased number of mutations, predicted neoantigens, and (CD103+) T cells in *POLE*-EDM and MSI tumors compared with MSS tumors.[24] In-line with the above, MSS tumors mostly lacked B cell– and TLS-related genes, whereas MSI and *POLE*-EDM tumors were enriched for these genes (Figure 3C). To confirm these findings, we further analyzed an independent cohort of MSS, MSI, and *POLE*-EDM tumors from patients with uterine cancer for the presence of CD20+ B cells by IHC. B cells were predominantly observed in large aggregations in the tumor and surrounding stroma (Figures 3D and E). In-line with the TCGA data, only 48% (20/42) of MSS tumors were found to have B cell aggregates, whereas 74% (28/38) of MSI and 92% (33/36) of *POLE*-EDM tumors contained B cell aggregates (Figure 3D). Quantification per tumor revealed a significant increase in the number of B cell aggregates when comparing MSS to *POLE*-EDM and MSI to *POLE*-EDM tumors (Figure 3D, P<0.001 and P<0.01, respectively). To confirm that the observed B cell aggregates were phenotypically similar to TLSs, we performed multicolor immunofluorescence. Indeed, B cell aggregates showed the typical

characteristics of lymphoid tissues, as determined by the presence of high endothelial venules (HEV), germinal B cell centers, and DCs surrounded by a rim of T cells (Figure 3F).

Figure 3
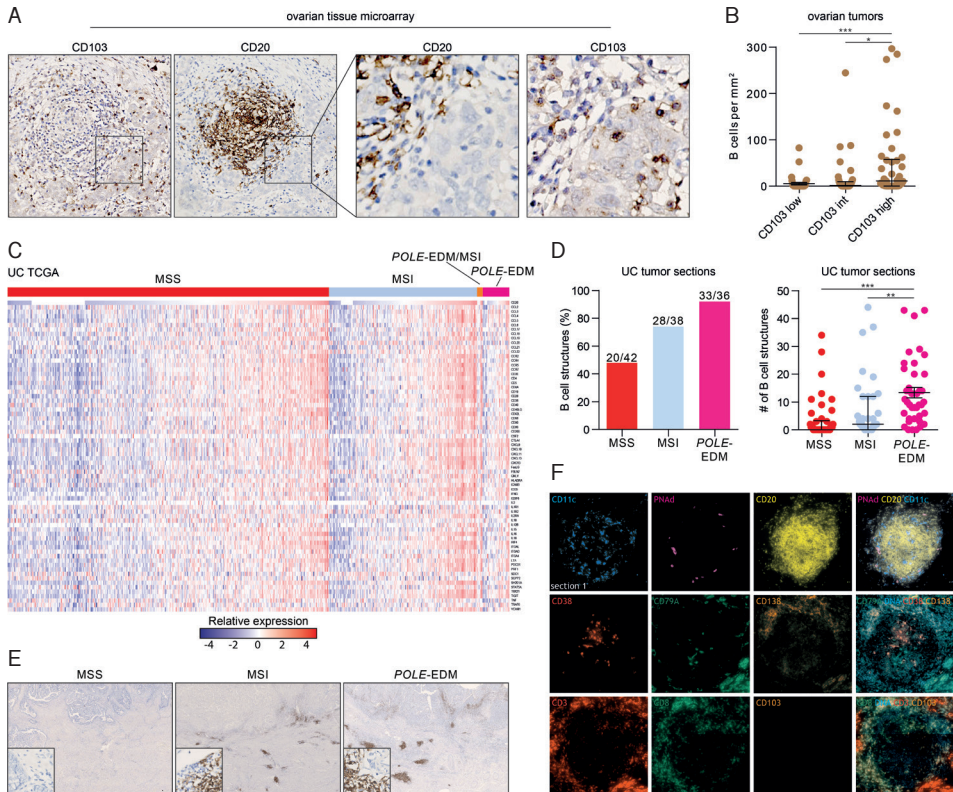
B cells, tertiary lymphoid structures, and correlation to CD103+CD8+ T cells in human tumors. *A,B) IHC analysis of CD103+ and CD20+ cells in ovarian cancer. Exemplary image of a CD20+ aggregate in close proximity to CD103+ cells in the tumor epithelium (A) and B cell infiltration in CD103-low, CD103-intermediate, and CD103-high tumors stratified by tertile (n=125; B). Significance was determined using Kruskal–Wallis comparison with a post hoc Dunn test (*, P<0.05; ***, P<0.001). C) Gene expression of B cell, tertiary lymphoid structure, cytotoxic T cell, CD8+ T cell, and CD4+ follicular helper T cell–associated genes in TCGA data of uterine cancer (UCEC, n=546). Tumors were ranked according to molecular subtype and then by CD20 expression. D, E) Prevalence and number of B cell aggregates (D) in MSS, MSI, and POLE-EDM uterine cancers. E) One exemplary image of each subtype is depicted. Significance was determine using Kruskal–Wallis comparison with a post hoc Dunn test (**, P<0.01; ***, P<0.001). F) Immunofluorescent analysis of CD20 aggregates in uterine cancer. CD20 aggregate expression of characteristic TLS markers CD11c, PNAD, CD20, CD38, CD79A, CD138, CD3, and CD8, one exemplary image is depicted.*

On the basis of the above findings, we speculated that CXCL13+CD103+ CTL genes would associate with TLS genes across human epithelial tumors. To assess this, we analyzed TCGA mRNA expression data of ovarian, uterine, lung, and breast cancer using

the differentially expressed genes from CXCL13+CD103+ and CXCL13−CD103− CTL cells identified by our mRNA sequencing. TLS genes correlated with CXCL13+CD103+, but not CXCL13−CD103−, CTL genes across all four tumor types (Figure 4). Taken together, our data suggested that CXCL13+CD103+ CTLs promote migration of B cells to tumors and the formation of TLSs across tumor types.

Figure 4
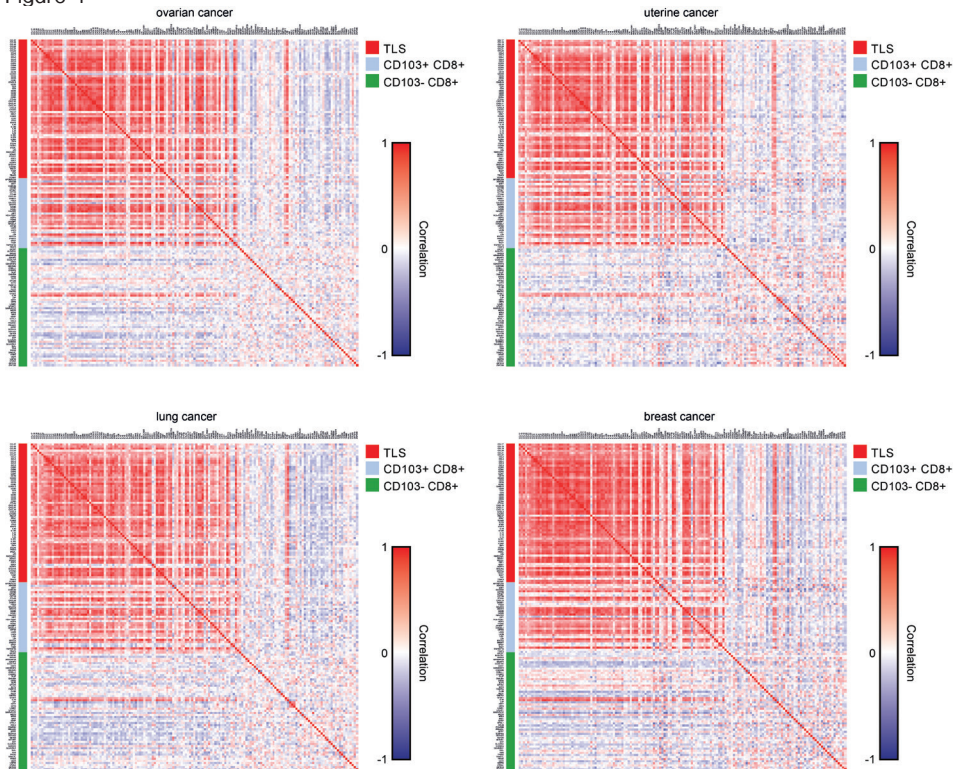
CXCL13+CD103+ TIL genes correlate with TLS-associated genes across cancer types.
Spearman correlation of genes associated with TLS, CD103+CD8+ cells, and CD103−CD8+ cells in ovarian (n=307), uterine (n=546), lung (n=517), and breast (n=1,100) cancer. Correlation plots depict relative correlation of log2+1 transformed mRNA sequencing data from TCGA.

CXCL13+CD103+CD8+ cells correlate to improved survival irrespective of neo-antigen burden

To assess whether CXCL13+CD103+ CTLs were also correlated with improved survival, we analyzed clinical outcomes in two cohorts of patients with uterine cancer. We focused on tumors with a low neoantigen burden because a high neoantigen load is associated with better survival. First, we analyzed TCGA endometrial cancers of the MSS subtype and correlated high *CXCL13* and CD103 (*ITGAE*) gene expression to survival. CXCL13^{high}ITGAE[high] MSS tumors had a significantly improved survival as compared

with CXCL13^{low}ITGAE[low] MSS tumors from TCGA (Supplementary Figure S3A). To confirm this survival benefit for CXCL13+CD103+ CTLs in neoantigen low tumors, we analyzed FFPE tumor tissue of an independent cohort of pMMR uterine cancers by IHC (Supplementary Table S8). We were unable to detect CXCL13 protein expression in CD103+ CTLs, consistent with our previous finding that almost all CD103+ cells express *CXCL13* on the mRNA level (Figures 1B, D, and G), but express and secrete the protein only after reactivation (Figure 1I). Therefore, we analyzed the effect of CXCL13+CD103+ CTL infiltration on clinical outcome in this cohort by proxy, using CD103 staining. We observed a significant survival benefit for patients with mismatch repair–proficient tumors infiltrated by a high number of CD103+ cells over tumors infiltrated by a low number of CD103+ cells (Supplementary Figure S3B). This effect was independent of other clinical variables, as demonstrated by multivariate analysis (Table 1). As such, our data demonstrated that (*CXCL13*+) CD103+ CTLs are associated with improved clinical outcome, independent of neoantigen burden.

Table 1. Cox regression survival analysis

	Univariate				\Multivariate			
	HR	95% CI		P value	HR	95% CI		P value
Age of diagnosis, cont.	1.022	0.989	1.056	0.197				
Grade of differentiation								
Good/moderate	ref	ref	ref	ref	ref	ref	ref	ref
Poor/undifferentiated	4.934	2.307	10.550	**<0.0001**	2.694	1.192	6.091	**0.017**
FIGO stage								
I	ref	ref	ref	ref	ref	ref	ref	ref
II	1.425	0.261	7.780	0.683	1.016	0.184	5.617	0.985
III	8.117	2.646	24.906	**<0.0001**	4.403	1.349	14.371	**0.014**
IV	22.707	7.218	71.432	**<0.0001**	15.697	4.762	51.735	**<0.0001**
Myometrial invasion								
No	ref	ref	ref	ref				
Yes	3.425	1.568	7.480	**0.002**				
LVSI								
No	ref	ref	ref	ref				
Yes	5.617	2.650	11.907	**<0.0001**				
Lymph node metastasis								
No	ref	ref	ref	ref				
Yes	4.620	1.911	11.171	**0.001**				
No sampling	0.775	0.299	2.011	0.601				
CD103								
Low	ref	ref	ref	ref	ref	ref	ref	ref
High	0.249	0.107	0.581	**0.001**	0.273	0.114	0.652	**0.003**

Disease-specific survival - n=189
Abbreviations. FIGO - International Federation of Gynecology and Obstetrics. LVSI - Lymfo-Vasculair Space Invasion.
CD103 - low is lower than or equal to median expression; high is higher than median expression

Discussion

In this study, we reported on the finding that TGFβ stimulates activated CD8+ T cells to produce CXCL13, a known inducer of TLSs.[17–19] This production of CXCL13

was paralleled by the induction of CD103 on the cell surface of CD8+ cells *in vitro*. CD103+CD8+ T cells isolated directly from human tumors expressed *CXCL13* mRNA and secreted CXCL13 protein upon *ex vivo* reactivation. The presence of B cell and TLS genes was increased in mutated, CXCL13+CD103+CD8+ T cell–enriched human tumors from TCGA, and the absolute number of B cells associated with a high load of predicted neoantigens in an independent cohort of uterine cancers and a cohort of high-grade serous ovarian cancers. Our findings shed light on the link between CD8+ T cell activation and the migration of B cells into the tumor. Our data also identified CD103 and B cells as potential biomarkers of interest for cancer immunotherapy.

CXCL13 is generally associated with DCs and TFH.[38,42,43] Nevertheless, single-cell sequencing of exhausted, tumor-infiltrating T cells of liver cancer, breast cancer, lung cancer, and melanoma does support expression of *CXCL13* in TILs.[2.0,33,34] We found that TGFβ1, a cytokine mostly associated with immune suppression[38,44–46], was essential for the induction of CXCL13. Under homeostatic conditions, TGFβ1is abundantly present in epithelial tissue and controls the epithelial localization of resident memory immune subsets, such as the intraepithelial lymphocytes in the colon.[47] In epithelial cancers, we suggest that TGFβ1 has a similar role in promoting not only recruitment, signaling, and retention of CD8+ T cells via CD103 expression[48], but also stimulating immunity via attraction of C-X-C chemokine receptor type 5 (CXCR5)+ immune cells through CXCL13 signaling.

CXCL13 is the key molecular determinant of TLS formation[17–19], ectopic lymphoid structures that are thought to enable efficient local priming of T cells by DCs.[9] Hereby, the time-consuming migration of DCs and T cells to and from lymph nodes may be circumvented, augmenting local antitumor immunity. In-line with this, characteristic components of TLSs, such as HEVs and B cells, are found to be generally associated with an improved prognosis[10], and plasma B cells in the TLSs are thought to enhance antitumor responses by production and subsequent accumulation of antitumor antibodies, potentially leading to antibody-dependent cytotoxicity and opsonization.[12] Thus, TLSs may orchestrate a joint T- and B cell response to improve antitumor immunity. Because TLSs were more abundant in tumors with a high mutational load, we postulated that activated CD103+ CTLs were involved in the migration of B cells to tumors via production of CXCL13. This is supported by our observations that mutated, CD8+ T cell–rich tumors showed higher expression of *CXCL13* and *ITGAE* (CD103) and that they presented with significantly higher numbers of B cells. In accordance, a higher degree of TCR clonality within CD8+ T cells correlates with a higher number of TLSs in non–small cell lung cancer.[49] These TLSs may represent an ongoing immune response that is insufficient to halt tumor progression at an early time point. It would, therefore, be of

4

great interest to study the induction and formation of TLSs in developing cancer lesions and to determine whether CD8+ T cell infiltration precedes TLS formation.

In-line with previous work[25,28,50], CD103+ CTLs from human tumors were also characterized by an activation- and exhaustion-related gene expression signature, with differential expression of granzymes and well-known immune checkpoint molecules, such as *CTLA4*. CD103+ CTLs expressed several additional immune checkpoint genes currently under clinical investigation, such as *TIM3*, *LAG3*, and *TIGIT*. This observed phenotype is concordant with a reported subset of PD-1–high (PD-1[T]) CD8+ T cells in lung cancer.[20] The PD-1[T] subset was transcriptionally distinct and characterized by expression of *CXCL13*. This subset also expressed higher *ITGAE*, although cell surface expression CD103 was not examined. Nevertheless, our analysis of the gene expression profile reported for PD-1[T] CD8+ cells revealed overlapping overexpression of approximately 200 genes with CD103+CD8+ cells, suggesting these populations might represent the same T cell subset. Importantly, CXCL13+PD-1[T] CD8+ cells are associated with response to ICI.[20]

The association between CXCL13+PD-1[T] CD8+ cells and response to ICI is in line with the observation that CD103+ CTLs significantly expand upon treatment with nivolumab or pembrolizumab (anti–PD-1) in tumor specimens of patients with advanced-stage metastatic melanoma.[51] Accordingly, an article by Riaz and colleagues demonstrates that tumors from patients who responded to nivolumab treatment differentially expressed genes such as *CXCL13, CTLA4, TIM3, LAG3, PDCD1, GZMB,* and TNF receptor superfamily member 9 (*TNFRSF9*), all genes overexpressed in CD103+ versus CD103− CTLs.[7] Pretreatment, but not on-treatment, *CXCL13* was differentially expressed in responders versus nonresponders in this study.[7] This may be explained by the low basal CXCL13 secretion we observed in the exhausted, CD103+ CTLs freshly isolated from untreated human tumors. In their exhausted state, CTLs might accumulate mRNA encoding several key effector molecules that is translated only upon reactivation (e.g., by ICI). Consistent with this, Riaz and colleagues observed an increase in the number of B cell–related genes on-treatment in responding patients[7], perhaps hinting at B cell recruitment and the formation of TLSs in these patients upon ICI-mediated release of CXCL13. This hypothesis is supported by the observed increases in serum CXCL13 and concomitant depletion of CXCR5+ B cells from the circulation in patients treated with anti–CTLA-4 and/or anti–PD-1.[52] Our data, therefore, suggest that ICIs are of particular interest for patients with a high CXCL13+CD103+ CTL infiltration pretreatment across malignancies.

Several combination immunotherapy regimes that promote CD8+ T cell infiltration and TLS formation may also function via CD8+ T cell–dependent production of CXCL13. For instance, combined therapy with antiangiogenic and immunotherapeutic agents in mice stimulated the transformation of tumor blood vessels into intratumoral HEVs,

which subsequently enhanced the infiltration and activation of CD8+ T cells and the destruction of tumor cells.[53,54] These T cells formed structures around HEVs that closely resembled TLSs.[53,54] One of these studies found that induction of TLSs was dependent on both CD8+ T cells and macrophages.[53] However, the exact intratumoral mechanism of action remains unclarified. Because macrophages produce TGFβ in a chronically inflamed environment[38], we hypothesize that the macrophages in these studies may have generated a TGFβ-enriched environment, thus, leading to the production of CXCL13 chemokine by activated T cells and subsequently to the formation of lymphoid structures. TLSs may, therefore, reflect an ongoing CD8+ T cell response in cancer. As such, TLSs may be used as a biomarker to predict response to ICI, and these structures may be used as a general biomarker for response to immunotherapy because TLS were found to identify patients with pancreatic cancer who responded to therapeutic vaccination.[55]

Taken together, we demonstrated that TGFβ1 induces coexpression of CXCL13 and CD103 in CD8+ T cells, potentially linking CD8+ T cell activation to B cell migration and TLS formation. Our findings provide a perspective on how (neo)antigens could promote the formation of TLSs in human tumors. Accordingly, CD103+ cells and B cells should be considered as a potential predictive or response biomarker for ICI therapy.

4

References

1. Ansell, S. M. et al. PD-1 blockade with nivolumab in relapsed or refractory Hodgkin's lymphoma. N. Engl. J. Med. 372, 311–319 (2015).

2. Hamid, O. et al. Safety and tumor responses with lambrolizumab (anti-PD-1) in melanoma. N. Engl. J. Med. 369, 134–144 (2013).

3. Borghaei, H. et al. Nivolumab versus docetaxel in advanced nonsquamous non-small-cell lung cancer. N. Engl. J. Med. 373, 1627–1639 (2015).

4. Pardoll, D. M. The blockade of immune checkpoints in cancer immunotherapy. Nat. Rev. Cancer 12, 252–264 (2012).

5. Snyder, A. et al. Genetic Basis for Clinical Response to CTLA-4 Blockade in Melanoma. N. Engl. J. Med. 371, 2189–2199 (2014).

6. Rizvi NA, Hellmann MD, Snyder A, Kvistborg P, Makarov V, Havel JJ, et al. Mutational landscape determines sensitivity to PD-1 blockade in non-small cell lung cancer. Science (80-.). 80-, (2015).

7. Riaz, N. et al. Tumor and Microenvironment Evolution during Immunotherapy with Nivolumab. Cell 171, 934-949.e15 (2017).

8. Dieu-Nosjean, M. C., Goc, J., Giraldo, N. A., Saut??s-Fridman, C. & Fridman, W. H. Tertiary lymphoid structures in cancer and beyond. Trends Immunol. 35, 571–580 (2014).

9. Dieu-Nosjean, M. C. et al. Tertiary lymphoid structures, drivers of the anti-tumor responses in human cancers. Immunol. Rev. 271, 260–275 (2016).

10. Sautès-Fridman, C. et al. Tertiary lymphoid structures in cancers: Prognostic value, regulation, and manipulation for therapeutic intervention. Front. Immunol. 7, 1–11 (2016).

11. Giraldo, N. A. et al. Orchestration and prognostic significance of immune checkpoints in the microenvironment of primary and metastatic renal cell cancer. Clin. Cancer Res. 21, 3031–3040 (2015).

12. Kroeger, D. R., Milne, K. & Nelson, B. H. Tumor-infiltrating plasma cells are associated with tertiary lymphoid structures, cytolytic T cell responses, and superior prognosis in ovarian cancer. Clin. Cancer Res. 22, 3005–3015 (2016).

13. Pimenta, E. M. & Barnes, B. J. Role of tertiary lymphoid structures (TLS) in anti-tumor immunity: Potential tumor-induced cytokines/chemokines that regulate TLS formation in epithelial-derived cancers. Cancers (Basel). 6, 969–997 (2014).

14. Ansel KM, Harris RBS, C. J. CXCL13 Is Required for B1 Cell Homing, Natural Antibody Production, and Body Cavity Immunity. Immunity (2002).

15. Van De Pavert, S. A. et al. Chemokine cxcl13 is essential for lymph node initiation and is induced by retinoic acid and neuronal stimulation. Nat. Immunol. 10, 1193–1199 (2009).

16. Ansel, K. M. et al. A chemokine-driven positive feedback loop organizes lymphoid follicles. Nature 406, 309–314 (2000).

17. Luther, S. A., Ansel, K. M. & Cyster, J. G. Overlapping roles of CXCL13, interleukin 7 receptor α, and CCR7 ligands in lymph node development. J. Exp. Med. 197, 1191–1198 (2003).

18. Luther SA, Lopez T, Bai W, Hanahan D, C. J. BLC Expression in Pancreatic Islets Causes B Cell Recruitment and Lymphotoxin-Dependent Lymphoid Neogenesis. Immunity (2000).

19. Gräbner, R. et al. Lymphotoxin β receptor signaling promotes tertiary lymphoid organogenesis in the aorta adventitia of aged ApoE −/− mice. J. Exp. Med. 206, 233–248 (2009).

20. Thommen, D. S. et al. A transcriptionally and functionally distinct pd-1 + cd8 + t cell pool with predictive potential in non-small-cell lung cancer treated with pd-1 blockade. Nat. Med. 24, (2018).

21. Eggink, F. A. et al. Immunological profiling of molecularly classified high-risk endometrial cancers identifies POLE-mutant and microsatellite unstable carcinomas as candidates for checkpoint inhibition. Oncoimmunology 6, (2017).

22. Nout RA, Bosse T, Creutzberg CL, Jürgenliemk-Schulz IM, Jobsen JJ, Lutgens LCHW, et al. Improved risk assessment of endometrial cancer by combined analysis of MSI, PI3K–AKT, Wnt/β-catenin and P53 pathway activation. Gynecol. Oncol. 466–73 (2021).

23. Creutzberg CL, van Putten WL, Koper PC, Lybeert ML, Jobsen JJ, Wárlám-Rodenhuis CC, et al. Surgery and postoperative radiotherapy versus surgery alone for patients with stage-1 endometrial carcinoma: multicentre randomised trial. PORTEC Study Group. Post Operative Radiation Therapy in Endometrial Carcinoma. Lancet 355, 1404–11 (2000).

24. Van Gool, I. C. et al. POLE proofreading mutations elicit an antitumor immune response in endometrial cancer. Clin. Cancer Res. 21, 3347–3355 (2015).

25. Komdeur, F. L. et al. CD103 + intraepithelial T cells in high-grade serous ovarian cancer are phenotypically diverse TCRαβ + CD8αβ + T cells that can be targeted for cancer immunotherapy. Oncotarget 7, (2016).

26. Rayner, E. et al. A panoply of errors: polymerase proofreading domain mutations in cancer. Nat. Rev. Cancer 16, 71–81 (2016).

27. Bindea G, Mlecnik B, Tosolini M, Kirilovsky A, Waldner M, Obenauf AC, et al. Spatiotemporal Dynamics of

Intratumoral Immune Cells Reveal the Immune Landscape in Human Cancer. Immunity (2013).

28. Workel, H. H. et al. CD103 defines intraepithelial CD8+ PD1+ tumour-infiltrating lymphocytes of prognostic significance in endometrial adenocarcinoma. Eur. J. Cancer 60, 1–11 (2016).

29. Picelli, S. et al. Full-length RNA-seq from single cells using Smart-seq2. Nat. Protoc. 9, 171–181 (2014).

30. Komdeur, F. L. et al. CD103+ tumor-infiltrating lymphocytes are tumor-reactive intraepithelial CD8+ T cells associated with prognostic benefit and therapy response in cervical cancer. Oncoimmunology 6, 1–14 (2017).

31. Djenidi, F. et al. CD8 + CD103 + Tumor–Infiltrating Lymphocytes Are Tumor-Specific Tissue-Resident Memory T Cells and a Prognostic Factor for Survival in Lung Cancer Patients . J. Immunol. 194, 3475–3486 (2015).

32. Guo, X. et al. Global characterization of T cells in non-small-cell lung cancer by single-cell sequencing. Nat. Med. 24, 978–985 (2018).

33. Zheng, C. et al. Landscape of Infiltrating T Cells in Liver Cancer Revealed by Single-Cell Sequencing. Cell 169, 1342-1356.e16 (2017).

34. Tirosh, I. et al. Dissecting the multicellular exosystem of metastatic melanoma by single-cell RNA-seq. Science (80-.). 352, 189–196 (2016).

35. Gu-Trantien, C. et al. CXCL13-producing T FH cells link immune suppression and adaptive memory in human breast cancer. JCI Insight 2, 1–17 (2017).

36. Mokrani, M., Klibi, J., Bluteau, D., Bismuth, G. & Mami-Chouaib, F. Smad and NFAT Pathways Cooperate To Induce CD103 Expression in Human CD8 T Lymphocytes. J. Immunol. 192, 2471–2479 (2014).

37. Park, B. V. et al. TGFβ1-mediated SMAD3 enhances PD-1 expression on antigen-specific T cells in cancer. Cancer Discov. 6, 1366–1381 (2016).

38. Kobayashi, S. et al. TGFβ induces the differentiation of human CXCL13-producing CD4+ T cells. Eur. J. Immunol. 46, 360–371 (2016).

39. Amft N, Curnow SJ, Scheel-Toellner D, Devadas A, Oates J, Crocker J, et al. Ectopic expression of the B cell-attracting chemokine BCA-1 (CXCL13) on endothelial cells and within lymphoid follicles contributes to the establishment of germinal center-like structures in Sjögren's syndrome. Arthritis Rheum. 44, 2633–41 (2001).

40. Steinmetz OM, Panzer U, Kneissler U, Harendza S, Lipp M, Helmchen U, et al. BCA-1/CXCL13 expression is associated with CXCR5-positive B cell cluster formation in acute renal transplant rejection. Kidney Int. 67, 1616–21 (2005).

41. Henry, R. A. & Kendall, P. L. CXCL13 Blockade Disrupts B Lymphocyte Organization in Tertiary Lymphoid Structures without Altering B Cell Receptor Bias or Preventing Diabetes in Nonobese Diabetic Mice. J. Immunol. 185, 1460–1465 (2010).

42. Rasheed, A. U., Rahn, H. P., Sallusto, F., Lipp, M. & Müller, G. Follicular B helper T cell activity is confined to CXCR5hiICOShi CD4 T cells and is independent of CD57 expression. Eur. J. Immunol. 36, 1892–1903 (2006).

43. Vissers, J. L. M., Hartgers, F. C., Lindhout, E., Figdor, C. G. & Adema, G. J. BLC (CXCL13) is expressed by different dendritic cell subsets in vitro and in vivo. Eur. J. Immunol. 31, 1544–1549 (2001).

44. Wrzesinski, S. H., Wan, Y. Y. & Flavell, R. A. Transforming growth factor-β and the immune response: Implications for anticancer therapy. Clin. Cancer Res. 13, 5262–5270 (2007).

45. Blobe, G., Schiemann, W. P. & Lodish, H. F. Role of transforming growth factor beta in human disease. N. Engl. J. Med. 342, 1350–1358 (2000).

46. Johnston, C. J. C., Smyth, D. J., Dresser, D. W. & Maizels, R. M. TGFβ in tolerance, development and regulation of immunity. Cell. Immunol. 299, 14–22 (2015).

47. Konkel, J. E. et al. Control of the development of CD8αα+ intestinal intraepithelial lymphocytes by TGFβ. Nat. Immunol. 12, 312–320 (2011).

48. Boutet, M. et al. TGFβ signaling intersects with CD103 integrin signaling to promote T-Lymphocyte accumulation and antitumor activity in the lung tumor microenvironment. Cancer Res. 76, 1757–1769 (2016).

49. Zhu, W. et al. A high density of tertiary lymphoid structure B cells in lung tumors is associated with increased CD4 + T cell receptor repertoire clonality. Oncoimmunology 4, e1051922 (2015).

50. Ganesan, A.-P. et al. Tissue-resident memory features are linked to the magnitude of cytotoxic T cell responses in human lung cancer. Nat. Immunol. 18, 940–950 (2017).

51. Edwards, J. et al. CD103+ tumor-resident CD8+ T cells are associated with improved survival in immunotherapy-naïve melanoma patients and expand significantly during anti-PD-1 treatment. Clin. Cancer Res. 24, 3036–3045 (2018).

52. Das, R. et al. Early B cell changes predict autoimmunity following combination immune checkpoint blockade. J. Clin. Invest. 128, 2–7 (2018).

53. Johansson-Percival, A. et al. De novo induction of intratumoral lymphoid structures and vessel normalization enhances immunotherapy in resistant tumors. Nat. Immunol. 18, 1207–1217 (2017).

54. Allen, E. et al. Combined antiangiogenic and anti-PD-L1 therapy stimulates tumor immunity through HEV formation. Sci. Transl. Med. 9, (2017).

55. Lutz, E. R. et al. Immunotherapy converts nonimmunogenic pancreatic tumors into immunogenic foci of immune regulation. Cancer Immunol. Res. 2, 616–631 (2014).

4

Supplementary material

Due to the size, Supplementary Table 7 is not included in this thesis. This table can be found online via https://cancerimmunolres.aacrjournals.org/content/7/5/784.long.

Supplementary Table 1. Gene signatures for CD103+CD8+ and CD103-CD8+ T cells

CD103+CD8+	CD103-CD8+
AC002331.1	ABCB7
AP003419.16	AC027612.6
APOBEC3G	ALDH7A1
ATAD2B	ANXA3
BATF	ARHGAP29
CCDC82	BAIAP2
CD79B	CCDC104
CPNE7	CCP110
CPT1B	CDH1
CTLA4	CDK5RAP2
CXCL13	CDKN2D
DNMT1	COBLL1
FGD3	CTC-459F4.3
GALNT2	CYB5R2
GNGT2	DLAT
GZMB	DNAJB4
GZMH	DSG2
HAVCR2	ELF3
HIP1	EPHA4
HLA-DQA1	EXT2
HOPX	FAM210B
ITGAE	FAM21A
JAKMIP1	FLNB
KIR2DL4	GAGE12H
KRT86	GAGE12I
LAG3	GLO1
LAIR2	GMPR2
LAYN	GTSF1
LIG1	IL7R
LTA	JUP
MYO7A	KRT7
PRMT7	KRT8
RP11-222K16.2	LAMB1
SPG7	LPGAT1
TIGIT	MARVELD2
TNFRSF18	MEG3
TRAF5	MTA3
TRAV12-1	MXI1
TTN-AS1	NKRF
	NTHL1
	OCLN
	POLR3H
	PRKAG1
	QPRT
	RP11-14N7.2
	SCNN1A
	SEPHS2
	SETD5
	SETDB1
	SHF
	SLC25A4
	SORBS3
	SUV420H1
	SVIL
	TDG
	THAP9-AS1
	TPD52
	TPRG1L
	TRIM2
	ULK4
	USP53
	VTCN1
	WRAP73
	ZBTB10
	ZNF33B

Supplementary Table 2. Antibody panels used to stain TLS in full slides of endometrial tumors

	Antigen	Animal/label	Clone	Company	Catalog no.	Concentration	Dilution	Secondary	Amplification
Panel 1									
	1. PNAD	HRP-labeled	MECA-79	Biolegend	120803	0.5 mg/mL	1:50	streptavidin-HRP	TSA® Cyanine 5 (Cy5)
	2. CD20	Mouse	L26	Dako	M0755	126 mg/L	1:200	Envision-anti-mouse HRP	TSA® Cyanine 3 (Cy3)
	3. CD11c	Rabbit	EP1347Y	Abcam	Ab52632	0.175 mg/mL	1:25	Envision-anti-rabbit HRP	TSA fluorescein
Panel 2									
	1. CD138	Rabbit	EPR6454	Abcam	128936	1.123 mg/mL	1:100	Envision-anti-rabbit HRP	TSA® Cyanine 5 (Cy5)
	2. CD79a	Mouse	HM47	Biolegend	333502	0.5 mg/mL	1:100	Envision-anti-mouse HRP	TSA® Cyanine 3 (Cy3)
	3. CD38	Biotin-labeled	EPR4106	Abcam	Ab201498	0.5 mg/mL	1:100	streptavidin-HRP	TSA® fluorescein
Panel 3									
	1. CD103	Rabbit	EPR4166(2)	Abcam	Ab129202	0.894 mg/mL	1:200	Envision-anti-rabbit HRP	TSA® Cyanine 5
	2. CD3	Rat	CD3-12	Abcam	11089	1 mg/mL	1:50	rabbit anti-rat HRP	TSA® Cyanine 3 (Cy3)
	3. CD8	Mouse	C8/144B	Dako	M7103	157 mg/L	1:100	Envision-anti-mouse HRP	TSA® fluorescein

Secondary	Company	Catalog no.	Concentration	Dilution
Rabbit anti Rat	Dako	P0450	1.3 g/L	1:100
Envision anti Rabbit	Dako	K4002		2 drops
Envision anti Mouse	Dako	K4000		2 drops
Streptavidin HRP	Dako	P0397	0.78 g/L	1:00

4

Supplementary Table 3. Flow cytometry antibodies used to sort CD103+/- CD8+ T cells from human ovarian tumor digests

Antigen	Clone	Fluorophore	Company	Catalog no.	Amount
CD3	UCHT1	BV421	BD Biosciences	562427	7.5 µl
CD4	OKT4	PerCP-Cy5.5	Thermo Fisher Scientific (eBioscience)	45-0048-42	7.5 µl
CD8α	RPA-T8	APC-eFluor780	Thermo Fisher Scientific (eBioscience)	47-0088-42	7.5 µl
CD8β	SIDI8BEE	PE-cy7	Thermo Fisher Scientific (eBioscience)	25-5273-41	7.5 µl
TCRαβ	IP26	APC	Thermo Fisher Scientific (eBioscience)	17-9986-41	7.5 µl
CD103	Ber-ACT8	FITC	BD Biosciences	33315	30 µl
CD56	CMSSB	PE	Thermo Fisher Scientific (eBioscience)	12-0567-41	7.5 µl

Supplementary Table 4.

BC-TSO	AAGCAGTGGTATCAACGCAGAGTGAATrGrG+G
BC-PCR	AAGCAGTGGTATCAACGCAGAGT
P5-TSO-hybrid	AATGATACGGCGACCACCGAGATCTACACGCCTGTCCGCGGAAGCAGTGGTATCAACGCAGAGT*A*C
BC-Read1Primer	GCCTGTCCGCGGAAGCAGTGGTATCAACGCAGAGTAC
BC-Oligo-dT-1	AAGCAGTGGTATCAACGCAGAGTACNNNNNNNNCTGAATATTTNTTTTTTTTTTTTTTTTTTTTTTTTTTTTTTTVN
BC-Oligo-dT-2	AAGCAGTGGTATCAACGCAGAGTACNNNNNNNNGACAGAGGGCNTTTTTTTTTTTTTTTTTTTTTTTTTTTTTTTVN
BC-Oligo-dT-3	AAGCAGTGGTATCAACGCAGAGTACNNNNNNNATCACTATATNTTTTTTTTTTTTTTTTTTTTTTTTTTTTTTTVN
BC-Oligo-dT-4	AAGCAGTGGTATCAACGCAGAGTACNNNNNNNNACTTCACTAANTTTTTTTTTTTTTTTTTTTTTTTTTTTTTTVN
BC-Oligo-dT-5	AAGCAGTGGTATCAACGCAGAGTACNNNNNNNTTCCGAAACANTTTTTTTTTTTTTTTTTTTTTTTTTTTTTTTVN
BC-Oligo-dT-6	AAGCAGTGGTATCAACGCAGAGTACNNNNNNNATGTACATTANTTTTTTTTTTTTTTTTTTTTTTTTTTTTTTTVN
BC-Oligo-dT-7	AAGCAGTGGTATCAACGCAGAGTACNNNNNNNGAAATAACGANTTTTTTTTTTTTTTTTTTTTTTTTTTTTTTTVN
BC-Oligo-dT-8	AAGCAGTGGTATCAACGCAGAGTACNNNNNNNTTTAGTAAGTNTTTTTTTTTTTTTTTTTTTTTTTTTTTTTTTVN
BC-Oligo-dT-9	AAGCAGTGGTATCAACGCAGAGTACNNNNNNNAAGCATCGAGNTTTTTTTTTTTTTTTTTTTTTTTTTTTTTTTVN
BC-Oligo-dT-10	AAGCAGTGGTATCAACGCAGAGTACNNNNNNNGAAGGGACATNTTTTTTTTTTTTTTTTTTTTTTTTTTTTTTTVN
BC-Oligo-dT-11	AAGCAGTGGTATCAACGCAGAGTACNNNNNNNGACCGCAACANTTTTTTTTTTTTTTTTTTTTTTTTTTTTTTTVN
BC-Oligo-dT-12	AAGCAGTGGTATCAACGCAGAGTACNNNNNNNTGCTTGAGCGNTTTTTTTTTTTTTTTTTTTTTTTTTTTTTTTVN
BC-Oligo-dT-13	AAGCAGTGGTATCAACGCAGAGTACNNNNNNNACGCCCTTACNTTTTTTTTTTTTTTTTTTTTTTTTTTTTTTTVN
BC-Oligo-dT-14	AAGCAGTGGTATCAACGCAGAGTACNNNNNNNGGGTGATGGNTTTTTTTTTTTTTTTTTTTTTTTTTTTTTTTVN
BC-Oligo-dT-15	AAGCAGTGGTATCAACGCAGAGTACNNNNNNNGTAGTCTTTANTTTTTTTTTTTTTTTTTTTTTTTTTTTTTTTVN
BC-Oligo-dT-16	AAGCAGTGGTATCAACGCAGAGTACNNNNNNNATTGACAACCNTTTTTTTTTTTTTTTTTTTTTTTTTTTTTTTVN
BC-Oligo-dT-17	AAGCAGTGGTATCAACGCAGAGTACNNNNNNNCATAACTAGCNTTTTTTTTTTTTTTTTTTTTTTTTTTTTTTTVN
BC-Oligo-dT-18	AAGCAGTGGTATCAACGCAGAGTACNNNNNNNACTGAACCTCNTTTTTTTTTTTTTTTTTTTTTTTTTTTTTTTVN
BC-Oligo-dT-19	AAGCAGTGGTATCAACGCAGAGTACNNNNNNNCACTCTGCTTNTTTTTTTTTTTTTTTTTTTTTTTTTTTTTTTVN
BC-Oligo-dT-20	AAGCAGTGGTATCAACGCAGAGTACNNNNNNNACTCATTCCTNTTTTTTTTTTTTTTTTTTTTTTTTTTTTTTTVN
BC-Oligo-dT-21	AAGCAGTGGTATCAACGCAGAGTACNNNNNNNTTAAGACGGANTTTTTTTTTTTTTTTTTTTTTTTTTTTTTTTVN
BC-Oligo-dT-22	AAGCAGTGGTATCAACGCAGAGTACNNNNNNNTACCTTTCATNTTTTTTTTTTTTTTTTTTTTTTTTTTTTTTTVN
BC-Oligo-dT-23	AAGCAGTGGTATCAACGCAGAGTACNNNNNNNTAGATTATTGNTTTTTTTTTTTTTTTTTTTTTTTTTTTTTTTVN
BC-Oligo-dT-24	AAGCAGTGGTATCAACGCAGAGTACNNNNNNNTTATTTCGTGNTTTTTTTTTTTTTTTTTTTTTTTTTTTTTTTVN

Supplementary Table 5. Quality control data of single cells

Cell	included or excluded	transcripts	*reason for exclusion* genes. detected	mapping. rate	expression efficiency	exonic.rate
CD103n1_702_AAGCATCGAG	Included					
CD103n1_702_ACACCGTCAG	Included					
CD103n1_702_ACTCATTCCT	Included					
CD103n1_702_ACTGAACCTC	Excluded	Exclusion	Exclusion	Exclusion	Exclusion	
CD103n1_702_AGTACATTAC	Excluded	Exclusion	Exclusion	Exclusion	Exclusion	
CD103n1_702_ATACATCCCG	Excluded	Exclusion	Exclusion	Exclusion	Exclusion	
CD103n1_702_ATTGACAACC	Included					
CD103n1_702_CAGGAGACCT	Excluded	Exclusion	Exclusion	Exclusion	Exclusion	
CD103n1_702_CAGGCCAGAA	Excluded	Exclusion	Exclusion	Exclusion	Exclusion	
CD103n1_702_CAGTCTAAAT	Excluded	Exclusion	Exclusion	Exclusion	Exclusion	
CD103n1_702_CATAACTAGC	Included					
CD103n1_702_CTGACTTTCG	Excluded	Exclusion	Exclusion	Exclusion	Exclusion	Exclusion
CD103n1_702_GAACGGTAAT	Excluded	Exclusion	Exclusion	Exclusion	Exclusion	
CD103n1_702_GAAGGGACAT	Included					
CD103n1_702_GACCGCAACA	Included					
CD103n1_702_GTCTGTCAAT	Excluded	Exclusion	Exclusion	Exclusion	Exclusion	
CD103n1_702_TAGTGGAGTT	Excluded	Exclusion	Exclusion	Exclusion	Exclusion	
CD103n1_702_TCACTAACCA	Excluded	Exclusion	Exclusion	Exclusion	Exclusion	
CD103n1_702_TTTAGTAAGT	Included					
CD103p1_702_ACGCCCTTAC	Included					
CD103p1_702_CTATAACCAA	Excluded	Exclusion	Exclusion	Exclusion	Exclusion	Exclusion
CD103p1_702_CTGAATATTT	Included					
CD103p1_702_GAAATAACGA	Included					
CD103p1_702_GACAGAGGGC	Included					
CD103p1_702_GAGAGCTACA	Excluded	Exclusion	Exclusion	Exclusion	Exclusion	
CD103p1_702_GAGATCAGGA	Included					
CD103p1_702_GAGCGTGGCG	Excluded	Exclusion	Exclusion	Exclusion	Exclusion	
CD103p1_702_GTAGTCTTTA	Included					
CD103p1_702_GTCATCAGTA	Excluded	Exclusion	Exclusion	Exclusion	Exclusion	Exclusion
CD103p1_702_GTGAGCATGA	Excluded	Exclusion	Exclusion	Exclusion	Exclusion	
CD103p1_702_GTTGTCATAC	Excluded	Exclusion	Exclusion	Exclusion	Exclusion	
CD103p1_702_TAACGTTGCT	Excluded	Exclusion	Exclusion	Exclusion	Exclusion	Exclusion
CD103p1_702_TACCTTTCAT	Included					
CD103p1_702_TGCTTGAGCG	Included					
CD103p1_702_TGGGTGATGG	Included					
CD103p1_702_TTAAGACGGA	Included					
CD103p1_702_TTATTTCGTG	Included					
CD103p1_702_TTCCGAAACA	Included					

Supplementary Table 6. Chemokines per Array

| Shared chemokines	Array 1 only (Abcam)	Array 2 only (R&D)
CCL1	CCL3	CCL3/CCL4 (both chemokines as one)
CCL2	CCL4	CCL14
CCL5	CCL8	CCL21
CCL7	CCL11	CXCL4
CCL15	CCL13	CXCL12 (SDF1α and SDF1β isoforms)
CCL17	CCL16	CXCL17
CCL18	Ckβ8-1 (CCL23)	RARRES2
CCL19	CCL24	IL-16
CCL20	CCL25	Midkine
CCL22	CCL26	
CCL26	CCL27	
CCL28	GRO (CXCL1-3)	
CX3CL1	CXCL6	
CXCL1	SDF1α (CXCL12)	
CXCL5	SDF1β (CXCL12)	
CXCL7	CXCL13	
CXCL8		
CXCL9		
CXCL10		
CXCL11		
CXCL16		
CXCL1		

Supplementary Table 8. Characteristics mismatch repair proficient endometrial cancers

	All patients	CD103 high	CD103 low
Patients	189 (100.0)	94 (49.7)	95 (50.3)
Age at diagnosis (in years)			
Median	64.0	62.0	68.0
Range	31.0-86.0	31.0-86.0	32.0-84.0
Endometrioid			
Endometrioid	161 (85.2)	84 (89.4)	77 (81.1)
Non-endometrioid	28 (14.8)	10 (10.6)	18 (18.9)
Type			
Adenocarcinoma	154 (81.5)	82 (87.2)	72 (75.8)
Adenocanthoma	1 (0.5)	1 (1.1)	0 (0.0)
Adenosquamous	6 (3.2)	1 (1.1)	5 (5.3)
Clear-cell	13 (6.9)	6 (6.4)	7 (7.4)
Serous/papillary	10 (5.3)	3 (3.2)	7 (7.4)
Undifferentiated	2 (1.1)	0 (0.0)	2 (2.2)
Mixed	3 (1.6)	1 (1.1)	2 (2.2)
FIGO stage			
I	96 (50.8)	53 (56.4)	43 (45.3)
II	35 (18.5)	15 (16.0)	20 (21.1)
III	42 (22.2)	19 (20.2)	23 (24.2)
IV	16 (8.5)	7 (7.4)	9 (9.5)
Grade of differentiation			
Good/moderate	126 (66.7)	66 (70.2)	60 (63.2)
Poor/undifferentiated	63 (33.3)	28 (29.8)	35 (36.8)
Recurrence			
No	144 (76.2)	81 (86.2)	63 (66.3)
Yes	45 (23.8)	13 (13.8)	32 (33.7)
Surgery			
Abd.ut.ext. with adnexa	92 (48.7)	44 (46.8)	48 (50.5)
Abd.ut.ext.adnþpelv þ aort	40 (21.2)	19 (20.2)	21 (22.1)
Abd.ut.ext.adn þ pelv	49 (25.9)	26 (27.7)	23 (24.2)
Otherwise	8 (4.2)	5 (5.3)	3 (3.2)
Radiotherapy			
No	79 (41.8)	40 (42.6)	39 (41.1)
Yes	110 (58.2)	54 (57.4)	56 (58.9)
Chemotherapy			
No	182 (96.3)	91 (96.8)	91 (95.8)
Yes	7 (3.7)	3 (3.2)	4 (4.2)
Follow-up (in years)			
Median	5.1	5.7	3.8
Range	0-21.4	0.2-21.4	0-16.7
Last follow-up			
No evidence of disease	121 (64.0)	73 (77.7)	48 (50.5)
Evidence of disease	11 (5.8)	6 (6.4)	5 (5.3)
Death, not of disease	2 (1.1)	2 (2.1)	0 (0.0)
Death of disease	30 (15.9)	7 (7.4)	23 (24.2)
Death of other disease	25 (13.2)	6 (6.4)	19 (20.0)

Abbreviation. FIGO - International Federation of Gynecology and Obstetrics. ut.ext - uterus extirpation with adnexa
CD103 high: above median CD103 expression (>16.14)
CD103 low: equal or lower than median CD103 expression (≤16.14)

Supplementary Figure 1
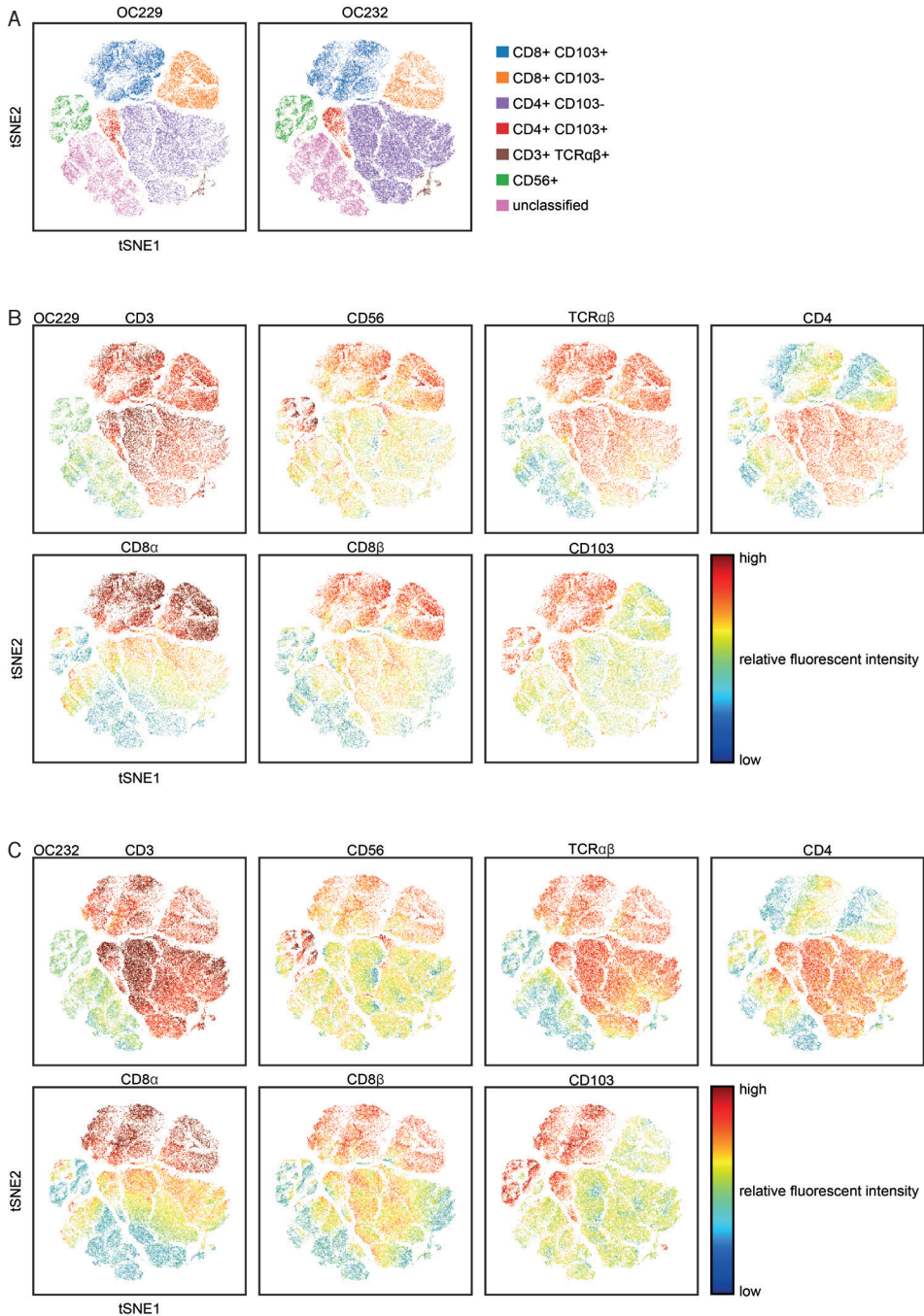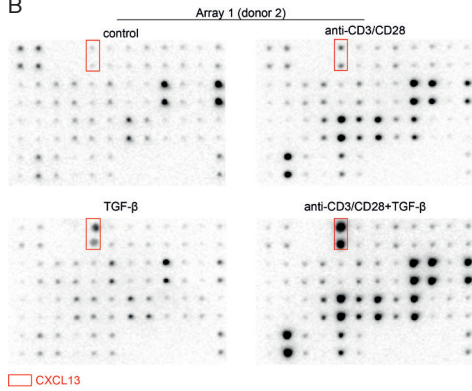

A, t-Distributed Stochastic Neighbour Embedding (tSNE) of flow cytometry data of ovarian tumors used for mRNA sequencing. B,C, Relative fluorescent intensity on tSNE per flow cytometry marker shown for ovarian cancer 229 (B) and ovarian cancer 232 (C) used in mRNA sequencing.
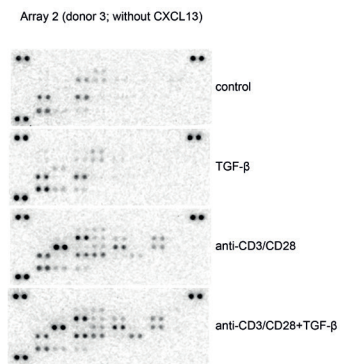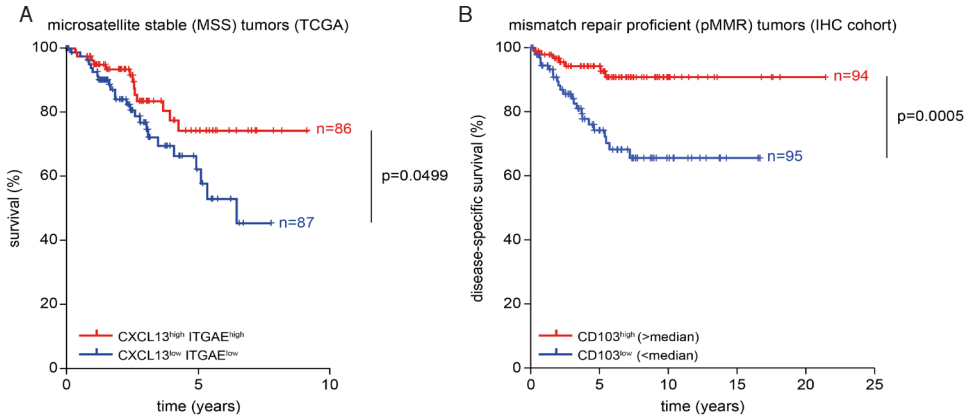
Supplementary Figure 2

A

CXCL13

B

C
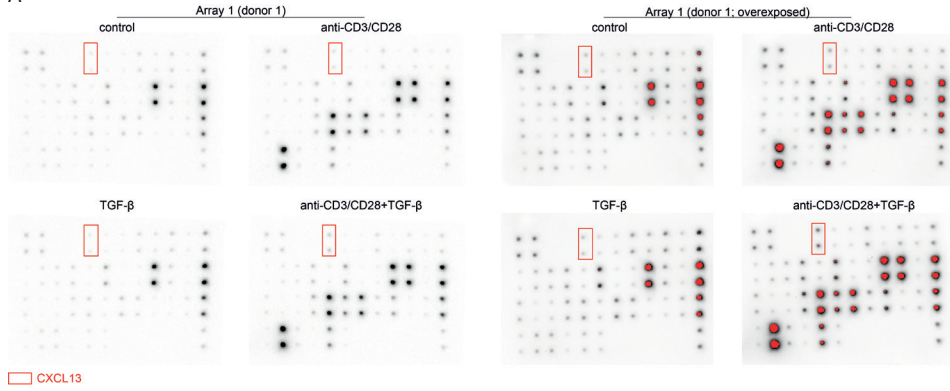
CXCL13

A,B,C Chemokine arrays for donor 1 using normal exposure (A) and overexposure (B) and for donor 8 2 (C) and donor 3 (D).

Supplementary Figure 3

A, B Survival analyses for tumors with low neo-antigen load, comparing CXCL13highITGAEhigh 11 versus CXCL13lowITGAElow microsatellite stable uterine cancers using TCGA data (A) and CD103high 12 versus CD103 13 low mismatch repair proficient uterine cancers using immunohistochemical staining (B).

4

Chapter 5

CD39 Defines Activated Intratumoral CD8+ T Cells
Primed for Tissue Residence

Joyce M. Lubbers[1,*], Marta A. Ważyńska[1,*], Nienke van Rooij[1], Arjan Kol[1], Hagma H. Workel[1], Annechien Plat[1], Sterre T. Paijens[1], Martijn R. Vlaming[2], Diana C.J. Spierings[3], Philip H. Elsinga[4], Edwin Bremer[2], Hans W. Nijman[1,#] and Marco de Bruyn[1,#]

*contributed equally and are co-first authors
#share senior authorship

[1]University of Groningen, University Medical Center Groningen, Department of Obstetrics and Gynecology, The Netherlands
[2]University of Groningen, University Medical Center Groningen, Department of Hematology, The Netherlands
[3]European Research Institute for the Biology of Ageing, University of Groningen, University Medical Center Groningen, Groningen, the Netherlands
[4]University of Groningen, University Medical Center Groningen, Department of Nuclear Medicine and Molecular Imaging, The Netherlands

Abstract

Identification of human cancer-reactive CD8+ T cells is crucial for stratification of patients for immunotherapy and determination of immune-therapeutic effects. To date, these T cells have been identified mainly based on cell surface expression of programmed cell death protein 1 (PD-1) or co-expression of CD103 and CD39. A small subset of CD103- CD39+ CD8+ T cells is also present in tumors, but little is known about these T cells. We here report that CD103- CD39+ CD8+ T cells from mismatch repair deficient endometrial tumors are activated and characterized predominantly by expression of *TNFRSF9*. *In vitro*, transforming growth factor beta (TGFβ) drives the disappearance of this subset, likely through conversion of CD103- CD39+ cells to a CD103+ phenotype. On the transcriptomic level, T cell activation and induction of CD39 was associated with a number of tissue residence and TGFβ responsive transcription factors. Altogether, our data suggest CD39+ CD103- CD8+ tumor-infiltrating T cells are recently activated and likely rapidly differentiate towards tissue residence upon exposure to TGFβ in the tumor micro-environment, explaining their relative paucity in human tumors.

Introduction

Immune checkpoint inhibitors (ICIs) targeting programmed cell death protein 1 (PD-1) or its ligand (PD-L1), have elicited unprecedented long-term disease remissions in advanced and previously treatment-refractory cancers.[1-3] Unfortunately, only a subset of patients currently benefits from treatment. ICIs are more likely to be effective in patients with a pre-existing anti-cancer immune response, most notably a CD8+ cytotoxic T cell response against tumor (neo)antigens.[4] Such CD8+ T cell responses are heterogeneous, comprising multiple CD8+ T cell subsets, including cancer antigen-specific and bystander CD8+ T cells. A number of cell surface markers have been proposed for the identification of cancer antigen-specific T cells from human tumors, with subsequent analysis showing a remarkable transcriptomic and functional overlap.[5-7] However, it remains unclear whether these individual markers enrich for the same subset, or distinct subsets with similar function.

In line with the mode-of-action of ICIs, cell surface expression of PD-1 was reported to enrich for cancer antigen-specific T cells across malignancies.[8-10] High expression of PD-1 was associated with co-expression of other inhibitory receptors, metabolic alterations and the acquisition of novel effector functions in the form of CXCL13 expression and secretion.[5] Moreover, cells with high PD-1 expression physically associated with so-called tertiary lymphoid structures (TLSs) – an ectopic form of lymphoid tissue associated with improved survival.[11,12] As cells with high PD-1 expression were also found to secrete CXCL13, this suggests that these cells may be involved in TLS formation.[5] Importantly, the presence of PD-1-high cells was associated with a better response to ICIs.[5] On the transcriptomic level, high expression of PD-1 was also associated with expression of *TNFRSF9* (CD137), *MKI67* (Ki67), *ENTPD1* (CD39) and *ITGAE* (CD103).[5] Cell surface analysis revealed ~80% of cells with high PD-1 expression also co-expressed CD39.[5]

CD39 is an ectonucleotidase expressed on the cell surface of several immune cell subsets, including regulatory T cells and activated CD4+ and CD8+ T cells. CD39 – in conjunction with CD73 – results in the local production of adenosine. Adenosine promotes the formation of an immunosuppressive micro-environment via adenosine receptor signaling. During chronic viral infection, expression of CD39 has been reported to define antigen-specific exhausted CD8+ T cells.[13] More recently, co-expression of CD39 and cluster of differentiation 103 (CD103) was found to define the cancer-reactive subpopulation of CD8+ T cells in a broad panel of malignancies.[6]

CD103, also known as integrin αE, is induced by combined T cell receptor (TCR) and transforming growth factor beta (TGFβ) receptor signaling on a subset of T cells in

peripheral tissues, where it mediates adhesion to epithelial cell-expressed E-cadherin.[14] On the transcriptomic level, cell surface expression of CD39 and CD103 was defined by co-expression of *PDCD1* (PD-1), *TNFRSF9*, *MKI67*, *CXCL13* as well as host of other genes enriched in the CD8+ T cell subset with high PD-1 expression.[5] Furthermore, co-expression of PD-1 and CD103 was previously described as a prognostic marker for human ovarian cancer.[7]

Despite this wealth of insight into the association of CD103, CD39 and PD-1, one subpopulation that has remained underexplored is the CD103- CD39+ CD8+ T cell subset. These cells are relatively scarce in human tumors, and may represent an intermediate development stage of tumor-reactive T cells. Here, we show that CD103- CD39+ CD8+ T cells in tumors are activated with more naïve-like cell features than their CD103+ CD39+ counterparts. CD103- CD39+ CD8+ T cells appear sensitive for differentiation towards CD103+ CD39+ more exhausted-like cells upon exposure to TGFβ in the tumor micro-environment.

Materials and Methods

Tumor tissue
Tumor tissue from endometrial carcinoma patients was collected during primary surgery. Written informed consent was obtained from all patients. Tumor molecular analysis on mismatch repair (MMR) protein expression was performed as part of stand-ard-of-care. Tumors were minced into small pieces and enzymatically digested using 1 mg/μL collagenase type IV (Gibco Life Technologies, Grand Island, USA) and 12.6 μg/mL recombinant human DNase (Pulmozyme, Roche, Woerden, the Netherlands) in RPMI medium (Gibco, Paisley, UK). Digestion was either done overnight at room temperature or for 30 minutes at 37°C. Digests were filtered using 70 μm cell strainers (Falcon) and enriched for mononuclear cells using Ficoll-Paque PLUS (GE Healthcare Life Sciences, Marlborough, MA, USA). After washing, cells were cryopreserved in fetal bovine serum (FBS, Gibco, Paisley, UK), with 10% dimethylsulfoxide until used for experiments.

Isolation of peripheral blood mononuclear cells
Human PBMCs were isolated via Ficoll-Paque density gradient centrifugation (Fi-coll-Paque PLUS, GE Healthcare Life Sciences, Marlborough, MA, USA) from buffy coats of healthy volunteers after informed consent (Blood bank, Groningen, the Netherlands) and cryopreserved in FBS with 10% dimethylsulfoxide.

In vitro CD8+ T cell stimulation
Human peripheral blood CD8+ T cells were isolated from PBMCs of healthy volunteers by

negative selection using FACS and the following panel of antibodies: CD56-FITC, CD16-FITC, CD19-FITC, CD14-APC and CD4-PE (Supplementary Table 1). In brief, PBMCs were thawed in FBS, washed with PBS and incubated with antibodies diluted in PBS + 2% FBS for 30-60 minutes at 4°C. Upon washing with PBS + 2% FBS, CD8+ T cells were sorted into AIM-V medium (Gibco, Paisley, UK) + 5% pooled human serum (PHS, One Lambda, USA) + 50 U/mL penicillin-streptomycin using a Beckman Coulter MoFlo Astrios sorter. Sorted CD8+ T cells were subsequently incubated with or without Dynabeads® Human T-Activator CD3/CD28 (2.5 µL/5x10^4 cells, Thermo Fisher Scientific, USA) for activation, recombinant TGFβ1 (rTGFβ1, 10 ng/mL, Peprotech, USA), TGFβ1 receptor inhibitor (10 µM, SB431542, Sigma Aldrich/Merck, Saint Louis, USA) or a combination of these. All cells were cultured in AIM-V medium with 5% PHS supplemented with 50 U/mL penicillin-streptomycin in 96-well plates containing 5x10^4 T cells per well. After four days, cells were collected for mRNA sequencing and flow cytometry.

Fluorescence activated cell sorting
Mononuclear cells from tumor digests or PBMCs were thawed in FBS, washed with PBS and stained with Zombie NIR Fixable Viability Kit (BioLegend, #423101) for dead cells, according to manufacturer's instructions. To isolate CD8+ TILs, samples were incubated for 60 minutes at 4°C with the following antibodies: CD279 (PD-1)-PE, CD103-FITC, CD39-APC, CD3-PerCP-Cyanine5.5 and CD8-BV421 (details can be found in Supplementary Table 1). After washing with PBS 2% FBS, cells were filtered using a 35 µm strainer (Falcon) and sorted using a Beckman Coulter MoFlo Astrios cytometer. UltraComp eBeads (Thermo Fisher Scientific) were used as compensation controls. Live, CD3+ CD8+ cells were sorted to obtain CD39, CD103 and PD-1 single-, double- and triple-positive populations. For each population, 20 cells were sorted.

Peripheral blood CD8+ T cells were collected after four days of *in vitro* stimulation and were stained with Zombie Aqua Fixable Viability Kit (Biolegend, #423101) according to manufacturer's instructions, followed by staining with CD3-PerCP-Cyanine5.5 and CD8a-APC-eFluor780 antibodies (Supplementary Table 1) for 60 minutes at 4°C. After washing, cells were filtered through a 35 µm strainer (Falcon) and sorted using a Beckman Coulter MoFlo Astrios cytometer. UltraComp eBeads (Thermo Fisher Scientific) were used as compensation controls. For each of the different treatment conditions 1000 live, CD3+ CD8+ cells were sorted.

mRNA sequencing
TILs and peripheral CD8+ T cells were sorted directly into 4 µL lysis buffer supplemented with 1 µL 10 µM oligo-dT primer and 1 µL 10 mM dNTP mix (Thermo Scientific), in a 96-well plate. Lysis buffer consisted of 0,2% Triton X-100 (Sigma-Aldrich) and 2 U RNAse

inhibitor (Takara). After sorting, the plate was spun down briefly and incubated for 3 minutes at 72 °C after which the plate was kept on ice. A modified SMARTseq2 protocol with custom made primers was followed.[15,16] In brief, SmartScribe reverse transcriptase (Westburg-Clontech) and a template switching oligo (BC-TSO), was used to generate cDNA. This was followed by a PCR preamplification step using the KAPA HiFi HotStart Ready Mix and a custom made PCR primer. Next, cDNA samples were purified using Ampure XP beads (Beckman Coulter MoFlo Astrios) in a ratio of 0.6 : 1 (Ampure : cDNA). Presence and size distribution of the samples was analyzed on a 2100 Bioanalyzer with a PerkinElmer LabChip GX high-sensitivity DNA chip (Agilent). 500 pg of each sample was tagmented and barcoded using N7xx- and S5xx index adapters according to the Illumina Nextera XT DNA sample preparation Kit protocol (Illumina). After purification with Ampure XP beads (ratio 0.6 Ampure : 1 cDNA) and analysis on a 2100 Bioanalyzer, sam-ples were equimolar pooled (4 nM). This superpool was sequenced on an Illumina Nextseq500 2500 using 75 bp single-end reads. The obtained mRNA sequencing data was demultiplexed into individual FASTQ files. Next, single-end reads were aligned to the human reference genome hg38 using STAR (version 2.5.2). Details can be found in Supplementary Table 2.

Analysis of mRNA sequencing data

Differential expression was analyzed with DESeq2 (version 1.26). For peripheral CD8+ T cells, a likelihood ratio test was used to determine differences between the 5 experimental groups from 3 replicates of independent donors. For tumor-infiltrating CD8+ T cells, a multilevel model was used stratifying samples based on patient, CD103, CD39 and PD-1 expression. Differential expression was determined by comparing CD103+ vs. CD103-, CD39+ vs. CD39- and PD-1+ vs. PD-1- samples. Differences between T cell subsets and/ or peripheral blood were performed by pair-wise comparison using the default DESeq2 workflow. Differentially expressed genes were visualized using GraphPad Prism (version 7.2).

Artificial anti-CD3 scFv-presenting cancer cell lines

The artificial anti-CD3 single chain variable fragment (scFv)-presenting cell lines are based on the Lentiviral synNotch receptor construct pHR_PGK_anti-CD19_ synNotch_Gal4VP64 (11397 bp), which was a gift from Wendell Lim[17] (Addgene plasmid #79125). The anti-CD19 scFv in this construct was replaced for anti-CD3 antibody fragment UCHT-1v9 to create pHR_PGK_scFvCD3_synNotch_Gal4VP64 using Gibson assembly. In brief, the scFv-CD3 fragment (775 bp) was amplified by PCR (Q5 Polymerase) from the previously established construct pEE14-anti-CD3:TRAIL (11213 bp)[18] using primers atggccgaggttcagctggt (65.6°C) and TGTCGCGCCCAGCG CCACCTGTGAAGCTGTAGTCCAGGAT ccgttt-gatctccaccttgg (83.9°C). In addition,

two backbone fragments (5375 and 5376 bp) were amplified by PCR (Q5 polymerase) from construct pHR_PGK_anti-CD19_synNotch_Gal4VP64 using the two following primer sets: atcctg-gactacagcttcac (58.2°C) with CGGGGAGAGGCGGTTTGCG-TATTGGGCGCTCTTCCGCTTCctcgctcactgactcgctgc (85.7°C) and gaagcggaagagcgcccaat (65°C) with CCAGGCCACCGCCAGACTCCACCAGCTGAAC-CTCGGCCATgaggtcctcttcagagataa (83.4°C). The three resulting fragments were assembled by Gibson assembly to establish pHR_PGK_scFvCD3_synNotch_Gal4VP64 (11406 bp) according to published protocol[19]. Lentivirus was produced by transient transfection of HEK293T cells with a pCMV and VSV-G packing system using FuGENE (Promega). Viral supernatants were collected and filtered using a 0.2-µm filter (Eppendorf). Transduction of A549 and MDA-MB 231 cells was performed by adding 1.5 mL viral supernatant to 1.5 mL of RPMI medium (Lonza) containing 2.50×10^5 pre-seeded cells in a 6-well tissue culture plate (Corning) in the presence of 4 µg/mL polybrene (Sigma-Aldrich). Transduced cells were sorted for expression of a Myc-tag (fused to the extracellular anti-CD3 scFv) using anti-Myc mAb Alexa Fluor 647 (clone 9B11, Cell Signaling) with a Sony cell sorter sh800s. (Sorted) MDA-MB.231 cells were cultivated in DMEM-L (Gibco) + 10% FBS and A549 cells were cultured in RPMI (Gibco, Paisley, UK) + 10% FBS.

T cell:cancer cell co-cultures

Peripheral blood CD8+ T cells were isolated from PBMCs of healthy volunteers by negative selection by FACS using a panel of four antibodies: CD56-FITC, CD19-FITC, CD14-APC and CD4-PE (Supplementary Table 1). In brief, cryopreserved PBMCs were thawed in FBS on the day of experiment. Next, cells were washed with PBS and incubated with antibodies for 30-60 minutes at 4°C. Upon washing with PBS + 2% FBS, CD8+ T cells were sorted into appropriate cell medium containing 200 U/mL of penicillin-streptomycin, depending on the particular cancer cell line, using a Beckman Coulter MoFlo Astrios sorter. Next, 5×10^4 sorted CD8+ T cells were plated per well of a 96-well plate, which were pre-seeded with 1.25, 2.5, 5.0 or 10×10^3 artificial anti-CD3 scFv-presenting cancer cells (either modified MDA-MB.231 cells with DMEM-L (Gibco) + 10% FBS or modified A549 cells with RPMI (Gibco) + 10% FBS) and incubated with or without recombinant TFGβ1 (rTGFβ1, 200 ng/mL, Peprotech, USA) and TGFβ1 receptor inhibitor (20µM, SB431542, Sigma Aldrich/Merck, Saint Louis, USA) or a combination of these. After 24 and 96 hours, T cell co-cultures were imaged by optical light microscopy (EVOS FL imaging system, ThermoFisher) In addition, after four days, cells were collected for flow cytometry analysis of CD39, CD103 and PD-1 cell surface expression (Supplementary Table 1).

CellTrace Violet

CD8+ T cell proliferation was measured using CellTrace Violet Proliferation Kit

(ThermoFisher) staining using modified manufacturer protocol. In brief, PBMCs were thawed in FBS, washed in PBS and incubated with 10 µM CellTrace dye solution in 2 mL PBS for 8 minutes at 37°C. Next, cells were washed with 8 mL culture medium for 5 minutes at 37°C, washed in PBS, resuspended in 200 µL PBS + 2% FBS and stained using a panel of antibodies: CD56-FITC, CD19-FITC, CD14-APC, CD4-PE and CD45RO-PE-Cy7 (Supplementary Table 1). After incubation for 30-60 minutes at 4°, cells were washed with PBS + 2% FBS and sorted into RPMI + 10% FBS or DMEM-L + 10% FBS medium containing 200 U/mL of penicillin-streptomycin using a Beckman Coulter MoFlo Astrios sorter. Per 96-well, negatively 5×10^4 sorted CD8+ T cells were co-cultured with 1.25, 2.5, 5.0 or 10×10^3 pre-seeded artificial anti-CD3 scFv-presenting cancer cells (either modified MDA-MB.231 cells or modified A549 cells) and incubated with or without rTGFβ1 (200 ng/mL, Pepro-tech, USA) and TGFβ1 receptor inhibitor (20µM, SB431542, Sigma Aldrich/Merck, Saint Louis, USA) or a combination of these. After four days, cells were collected for flow cytometry analysis of CD39, CD103 and PD-1 and proliferation profiling using BD FACSVerse flow cytometer (BD Biosciences). Proliferation profiling was performed by recording BV421 channel and plotting against FSC as histogram chart. Number of cell divisions was quantified and presented in subsets with CD103, CD39 and PD-1 positivity or negativity.

Flow cytometry

To assess CD8+ T cells upon *in vitro* stimulation, CD8+ T cells were collected and resuspended in PBS for staining with Zombie-Aqua (Biolegend, #423101) for 15 minutes at room temperature in the dark. To assess CellTrace Violet stained CD8+ T cells, cells were collected in medium. Next, for both experiments, CD8+ T cells were washed with PBS + 5% FBS and incubated in the dark with CD4-PerCP-Cy5.5, CD8α-APCeFluor780, PD-1-PE, CD103-FITC and/or CD39-APC antibodies (Supplementary Table 1) at 4°C for 30 minutes. Upon additional washing steps with PBS + 2% FBS, cell surface expression of the various markers was measured using the BD FACSVerse flow cytometer (BD Biosciences). Data analysis was performed with the use of Cytobank (www.cytobank. org).

Statistical analyses

Differentially expressed genes were determined by DESeq2. Genes with a Benjamini-Hochberg FDR <0.1 were selected as significantly changed. Differential induction of cell surface markers and cell proliferation was analyzed using two-way ANOVA followed by a post-hoc Bonferroni test. All statistical analyses were performed using DESeq2 (ver-sion 1.22.2) or GraphPad Prism (GraphPad Software Inc., CA, USA). A P value of <0.05 was used in all cases as a cut-off for significance.

Results

Cell surface expression of CD39 is independently associated with CD8+ T cell activation in MSI-H endometrial cancer

The gene expression signature and activation status of CD103- CD39+ CD8+ TILs has so far not been analyzed. Thus, we first addressed this issue by using lymphocytes isolated from tumors of 3 patients with microsatellite unstable (MSI-H) endometrial cancer. In line with previous reports, we found CD8+ TIL were typically CD103+, with or without co-expression of CD39 and/or PD-1 (Figure 1A and 1B). The CD103- CD39+ population was minimal, in line with previous reports (Figure 1A). CD4 TIL were largely negative for CD103, but (co-)expressed PD-1 and CD39 (Figure 1A). Using a multi-level differential expression model we determined that, out of all three cell surface markers, only CD39 independently associated with activation marker *TNFRSF9* (Figure 1B and 1C). In line with its role in tissue residence, CD103 expression was strongly and negatively associated with expression of *P2RY8*, a purinergic receptor involved in germinal center migration, where-as PD-1 independently and positively associated with exhaustion-related methyltransfer-ase *DNMT3A*.

Figure 1
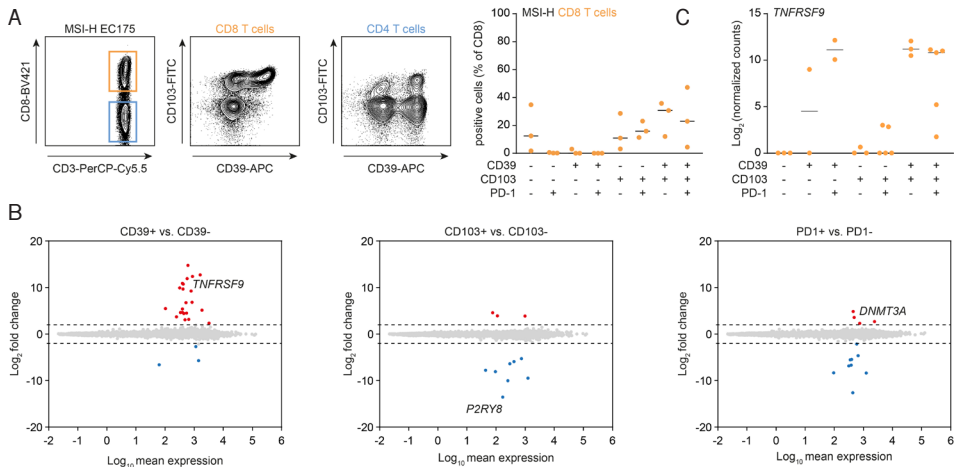
Gene expression independently associated with CD103, CD39 or PD-1 expression. *A) Representative and quantified cell surface expression of CD103 and CD39 on CD8 T cells, as determined by flow cytometry for tumor-infiltrating T cells from 3 independent MSI-H endometrial cancer patients. B) Differential gene expression between positive and negative CD39 (left), CD103 (middle) and PD-1 (right) tumor infiltrating CD8+ T cells as determined by mRNA sequencing. Genes with a Benjamini-Hochberg FDR <0.05 were selected as significantly changed. (C) Log2-normalized gene expression counts for TNFRSF9 in the indicated cell subsets as determined by mRNA sequencing (n=3 patients; >2 technical replicates per population).*

CD103- CD39+ CD8+ T cells in MSI-H endometrial tumors are a recently activated, naïve-like subset

We next analyzed the different CD8+ T cell subsets in greater detail. Differential gene expression analysis of CD103+ CD39+ vs. CD103+ CD39- cells confirmed that, as previously reported for other cancer types, CD103+ CD39+ CD8+ T cells from MSI-H endometrial tumors comprise a recently-activated/exhausted subset expressing a.o. *TNFRSF9* and *HAVCR2* (encoding for TIM3) (Figure 2A). Cytokine and cytotoxicity profiles between these two populations were similar (Figure 2B), again in line with previous reports on the intermediate activation status of the CD103+ CD39- population. Compared to CD103+ CD39+ cells, CD103- CD39+ cells were characterized by more abundant expression of transcripts associated with naïve T cells (such as *SELL*) and germinal center migration (e.g. *P2RY8*) (Figure 2C), again with no overt differences in cytokine/cytotoxicity profiles (Figure 2D).

Figure 2
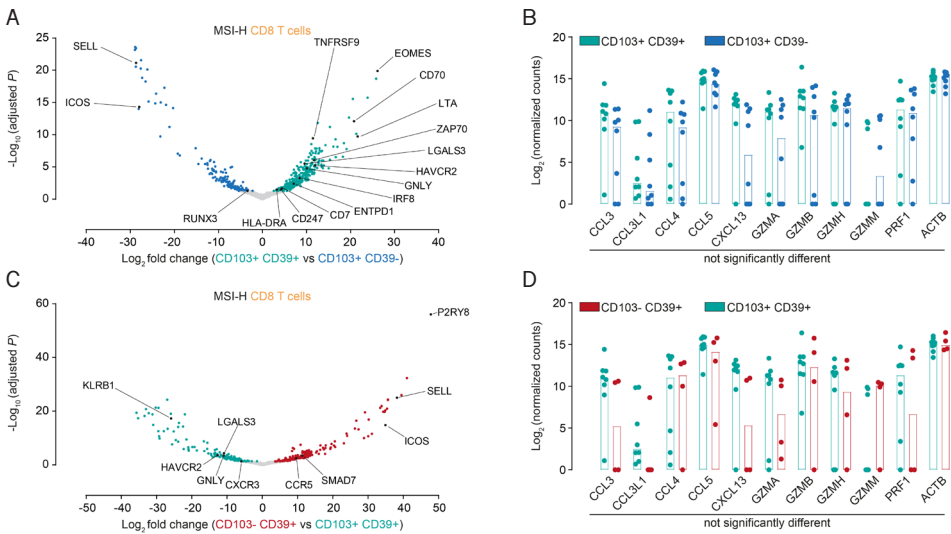
Differentially expressed genes between *A) CD103+ CD39+ and CD103+ CD39-, and (C) CD103-CD39+ and CD103+ CD39+ cells. Genes with a Benjamini-Hochberg FDR <0.05 were selected as significantly changed. B, D) Log2-normalized gene expression counts for the indicated genes in the CD8 T cell subsets as determined by mRNA sequencing (n=3 patients; >2 technical replicates per population).*

Based on these differences, we therefore speculated that CD103- CD39+ CD8+ T cells may represent a recently activated, but more naïve-like subset when compared to CD103+ CD39+ CD8+ T cells. To assess this, we analyzed gene expression differences between these populations and peripheral blood CD8+ T cells. Both CD103- CD39+ and CD103+ CD39+ cells significantly upregulated a consensus activation signature

when compared to peripheral CD8+ cells, including *ENTPD1* (CD39) *TNFRSF9*, *IL2RA* (CD25) and *CXCL13* (Figure 3A). Notably, CD103+ CD39+ cells upregulated a series of exhaustion-related markers when compared to peripheral CD8+ T cells, such as *TOX2*, *NR4A1* and *LAYN* and down-regulated naïve-like genes including *SELL*, *LEF1* and *CCR7* (Figure 3B). By contrast, these genes were not differentially expressed between CD103- CD39+ CD8+ T cells when compared to their peripheral counterparts (Figure 3B).

Figure 3
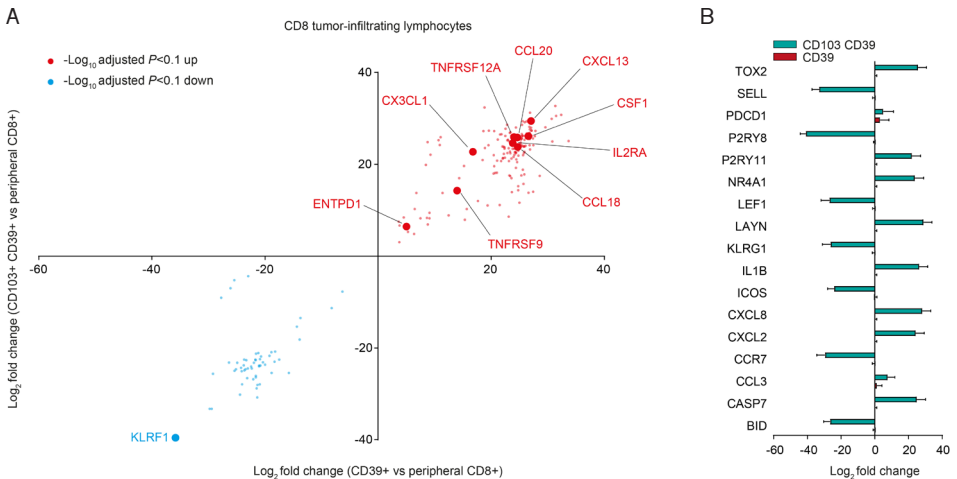
CD103+ CD39+ versus CD103- CD39+. *A) Differentially expressed genes between CD103+ CD39+ and CD103- CD39+ TIL compared to peripheral blood CD8+ T cells. B) Log2 fold change for the indicated genes in CD103+ CD39+ and CD103- CD39+ cells as compared to peripheral blood CD8+ T cells.*

Effect of TGFβ on CD103- CD39+ CD8+ T cell formation

The activated phenotype of CD103- CD39+ cells, and their relative scarceness when compared to CD103+ CD39+ cells, suggested CD103- CD39+ might rapidly differentiate towards tissue-resident CD103+ CD39+ cells when exposed to the tumor micro-environment. We investigated this hypothesis using two engineered artificial anti-CD3 scFv presenting cancer cell (aAPCC) lines. aAPCC-driven activation induced CD103+ CD39-, CD103- CD39+ and CD103+ CD39+ subsets from peripheral CD8+ T cells (Figure 4A). Inhibition of autocrine TGFβ signaling by TGFβ receptor 1 inhibitor SB-431542 abrogated CD103 expression on both CD39- and CD39+ T cells (Figure 4A). Conversely, addition of exogenous rTGFβ increased the induction of CD103 and was associated with a reduction of CD103- CD39+ T cells in the co-culture. Importantly, these effects were observed for both aAPCCs and across a range of cancer cell to CD8+ T cell ratios (Figure 4B and 4C). Thus, TGFβ is associated with the loss of CD103- CD39+ CD8+ T cells in the vicinity of cancer cells, and the formation of both CD103+ CD39+ and CD103+ CD39- CD8+ T cell subsets.

Figure 4
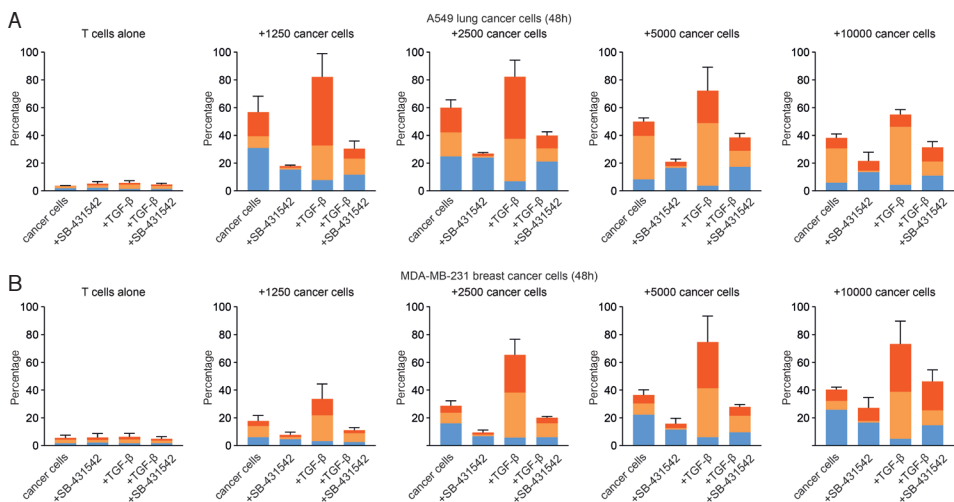
***Quantification of CD103- CD39+, CD103+ CD39- and CD103+ CD39+ CD8 T cells across the various treatment conditions during co-culture with** (A) A549 and (B) MDA-MB-231 aAPCC. aAPCC were seesed at the indicated concentration in a 96-well, allowed to adhere for 24h and 10.000 T cells were added to each well for co-culture. CD103-CD39+ (blue), CD103+CD39- (orange) and CD103+CD39+ (dark orange).*

TGFβ-induced loss of CD103- CD39+ CD8+ T cells is independent of proliferation

We determined whether the loss of CD103- CD39+ T cells induced by TGFβ was a consequence of changes in subset proliferation. Hereto, we co-cultured aAPCCs with freshly isolated naïve CD8+ T cells labeled with CellTrace Violet. Globally, we observed proliferation upon T cell activation that slightly increased upon increasing numbers of aAPCCs (Figure 5A). No significant differences in proliferation were observed when comparing SB-431542 or rTGFβ treatment with control conditions (Figure 5A).

When analyzing CD39 and CD103 expression in relationship to cell proliferation, we observed that even cells that had not divided acquired cell surface expression of either CD39, CD103, PD-1, or all three proteins (Figure 5B), and the number of cell divisions for each population was not significantly different (Figure 5B). As expected, autocrine TGFβ production, particularly at higher aAPCC:CD8 ratios, induced a dominant expression of CD103 on most CD8+ T cells, as did exogenous addition of rTGFβ (Supplementary Figure 1). This effect appeared largely independent of the number of cell cycles the individual CD8+ T cell had underwent (Supplementary Figure 1). With regards to CD39 expression, there was a trend towards increased expression of CD39 on cells that had undergone multiple cycles of cell division, and at lower aAPCC:CD8 T cell ratios, although this did not reach statistical significance (Supplementary Figure 1). As

before, TGFβ receptor 1 inhibitor SB-431542 largely abrogated CD103, but not CD39, expression across all conditions (Supplementary Figure 1). Thus, the loss of CD103-CD39+ CD8+ T cells upon TGFβ signaling in tumor co-cultures was independent of changes in T cell proliferation.

Figure 5
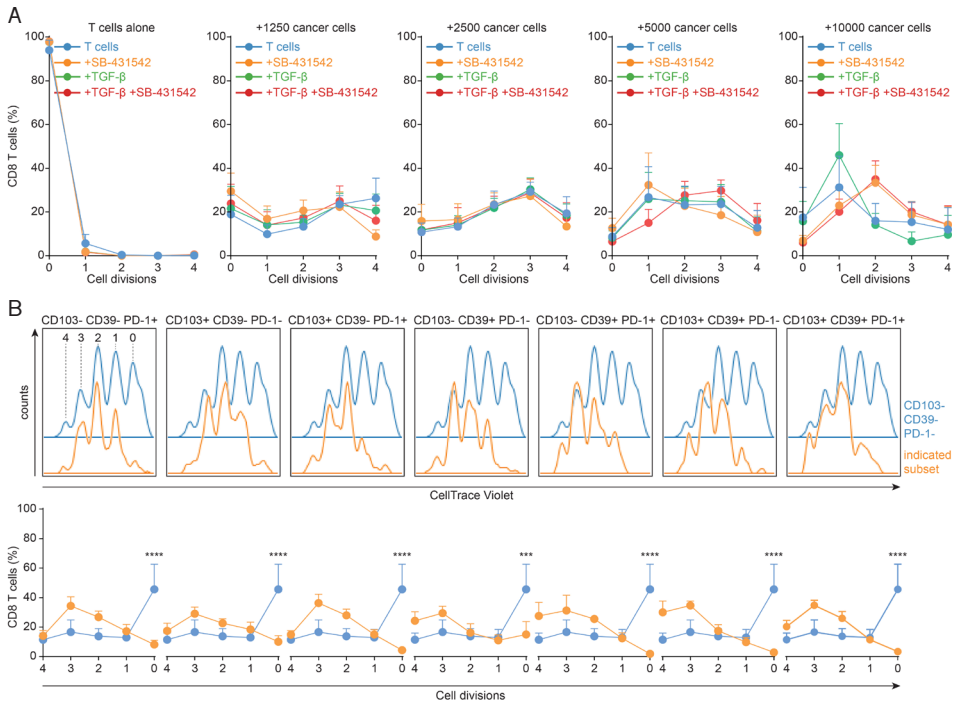
Proliferation assay. *A) Relative number of cell divisions across the indicated culture conditions and ratio of aAPCC:T cell. B) Representative CellTrace Violet traces for the indicated CD8 T cell subsets (top) and the relative number of cell divisions for the indicated CD8 T cell subsets (bottom). aAPCC were seesed at the indicated concentration in a 96-well, allowed to adhere for 24h and 10.000 T cells were added to each well for co-culture.*

Induction of CD39 is associated with upregulation of TGFβ signal regulating transcription factors

Our data suggested CD103- CD39+ CD8+ T cells are early activated naïve-like cells, sensitized to the upregulation of CD103 upon exposure to TGFβ, through a proliferation-independent mechanism. We therefore performed RNAseq of activated T cells in the presence or absence of SB-431542. To exclude tumor-induced transcriptomic changes, we used anti-CD3/CD28-bead based activation in the presence of abscence of SB-431542 or rTGFβ (Supplementary Figure 2). By comparing genes consistently upregulated between anti-CD3/CD28 and anti-CD3/CD28+SB-431542, we identified a consensus TGFβ-independent transcriptome including *ENTPD1* (Figure 6A). As observed

for TILs in human MSI-H tumors, upregulation of *ENTPD1* was strongly correlated with the upregulation of *TNFRSF9* (Figure 6A). Comparison of anti-CD3/CD28+rTGFβ with anti-CD3/CD28+SB-431542 identified a consensus set of TGFβ-driven genes, including *ITGAE*, encoding CD103 (Figure 6B). CD39-associated genes included a series of transcription factors known to promote tissue residence and CD103 expression, such as *BHLHE40*, but also transcription factors previously linked to TGFβ signaling in other cell and tissue types, such as *ZNF165*, *ZBED2*, *FOSL2* and *EGR1* (Figure 6C). The upregulation of these transcription factors was independent of TGFβ signaling (Figure 6C), suggesting an activation-driven effect in CD8+ T cells associated with CD39 upregulation.

Figure 6
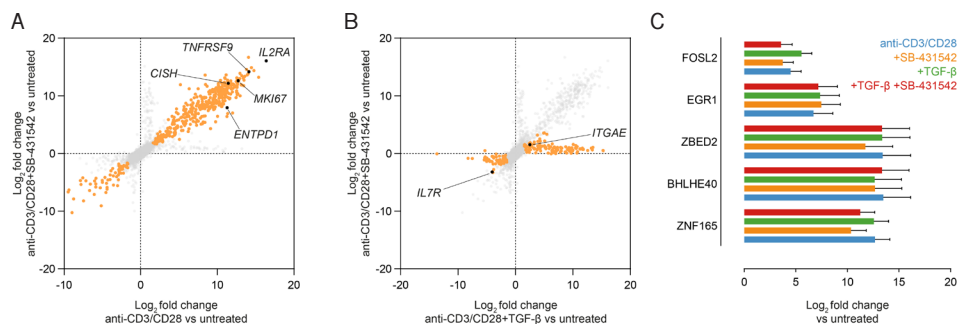
Quantification of CD103- CD39+, CD103+ CD39- and CD103+ CD39+ CD8 T cells across the various treatment conditions during co-culture with (A) A549 and (B) MDA-MB-231 aAPCC. *aAPCC were seesed at the indicated concentration in a 96-well, allowed to adhere for 24h and 1x10^4 T cells were added to each well for co-culture.*

Discussion

Human tumor-reactive T cells have been defined by expression of PD-1 or co-expression of CD103 and CD39.[5-7] However, the phenotype and function of CD103- CD39+ CD8 T cells in tumors has not been determined. Here, we show that CD103- CD39+ CD8 T cells in tumors are recently activated and characterized predominantly by expression of *TNFRSF9*. *In vitro,* CD103- CD39+ cells are lost from CD8 T cell: tumor cell co-cultures when exposed to TGFβ, likely through differentiation towards a CD103+ CD39+ phenotype. The latter is consistent with the observed upregulation of a number of tissue residence and TGFβ responsive transcription factors that strongly correlate with induction of CD39 upon *in vitro* CD8 T cell activation.

Cell surface expression of CD39 was strongly associated with expression of *TNFRSF9* mRNA (encoding CD137) in both CD103+ CD39+ and CD103- CD39+ CD8 T cells. Accordingly, *in vitro* activation of CD8+ T cells with anti-CD3/CD28 beads induced concurrent cell surface expression of CD39 and upregulation of *ENTPD1* and *TNFRSF9* mRNA. Although expression of *TNFRSF9* was previously associated with expression of *PDCD1*[5,8], we did not observe *TNFRSF9* expression in CD103- and/or CD39- PD-1+ cells, nor was cell surface expression of PD-1 associated with *TNFRSF9* after correcting for concurrent CD39/CD103 expression. Indeed, cell surface CD39 was the strongest independent predictor of *TNFRSF9* expression in TILs from human MSI-H endometrial

cancer tumors. *In vitro*, we observed a similar effect with PD-1 upregulation observed in both CD39- and CD39+ CD8 T cells. Our findings are in line with a recent study showing a dissociated expression of CD39 and PD-1 where prolonged TCR stimulation gradually increases the percentage of CD39+ cells over time, and PD-1 expression peaked at 48 hours of TCR stimulation and subsequently decreased upon prolonged stimulation.[6] Interestingly, while expression of CD39 was not directly associated with T cell proliferation, we also observed concomitant upregulation of the proliferation-associated receptor CD25 (*IL2RA*). This discrepancy might be explained by the different expression kinetics of CD39 vs. CD25 on the cell surface (PMID: 1396972).

Our *in vitro* analysis expands these earlier observations and suggests CD39 is induced largely independently of CD8 T cell proliferation. This suggests that either TCR signaling strength and or differential formation of transcription factor complexes may skew the balance of T cell proliferation versus CD39 immune checkpoint expression. As little is known on the transcription factors controlling *ENTPD1* expression, it will be interesting to determine how these factor complexes differ from transcription factors controlling TCR-driven proliferation. Nevertheless, and in contrast to what has been reported for immune checkpoint *PDCD1*, the induction of *ENTPD1* gene expression and cell surface upregulation of CD39 occurs independently of TGFβ receptor, and thereby SMAD2/3 complex, signaling. These data also suggest care should be taken when exploring TGFβ inhibitors, as immune checkpoint inhibitor expression may remain unaffected while CD103 expression is attenuated, preventing T cell retention and cytolytic activity in the tumor micro-environment.

Most notably, our work provides a mechanistic explanation of the paucity of CD103-CD39+ CD8 T cells within the tumor micro-environment, as we demonstrate these cells are likely to rapidly differentiate towards CD103+ tumor tissue resident memory cells when exposed to TGFβ. Similarly, in human tumors, CD103- CD39+ CD8 T cells were activated and likely in the process of differentiating towards CD39+ CD103+ cells. The gene expression profile associated with CD39 (*ENTPD1*) supports this hypothesis with, among others, *BHLHE40* strongly associated with *ENTPD1* expression. BHLHE40 promotes tissue residence by maintaining mitochondrial fitness and promoting an active chromatin state for CD8 T cell residency and functionality. Accordingly, loss of BHLHE40 in T cells abrogated the anti-tumor effects of immune checkpoint inhibitors. In addition to *BHLHE40*, we observed CD39-associated upregulation of series of TGFβ-responsive transcription factors not previously implicated in CD8 T cell biology. A deeper understanding of how these transcription factors function in T cell biology may help further define the mechanisms underlying TGFβ-driven formation of tumor tissue resident memory cells, as well as novel targets to attenuate deleterious TGFβ signaling while maintaining beneficial effects such as the upregulation of CD103.

Finally, we also noted the formation of CD39- CD103+ CD8 T cells upon TGFβ receptor signaling, at similar frequencies as those observed *ex vivo* in human tumors. The induction of CD39- CD103+ T cells occurred largely independently of the formation of CD39+ T cells and was also observed in CD8 T cells that had not undergone any proliferation. The largely independent formation of CD39- CD103+ T cells is consistent with previous

5

work on *ex vivo* human TILs showing minimal clonal overlap when comparing CD103+ CD39+ with CD103+ CD39- CD8 T cells.[6] Although we cannot formally exclude that the formation of CD103+ CD39- T cells required a degree of TCR signaling, the prevailing theory that CD103+ CD39- T cells represent bystander CD8 T cells in tumors not directly involved with tumor control are consistent with our data.

Conclusion

Our data suggest CD103- CD39+ CD8 T cells in endometrial cancer are recently activated and likely differentiate towards tissue residence upon exposure to TGFβ, potentially explaining their paucity in the tumor micro-environment.

5

References

1. Ansell, S.M.; Lesokhin, A.M.; Borrello, I.; Halwani, A.; Scott, E.C.; Gutierrez, M.; Schuster, S.J.; Millenson, M.M.; Cattry, D.; Freeman, G.J.; et al. PD-1 blockade with nivolumab in relapsed or refractory Hodgkin's lymphoma. N. Engl. J. Med. 2015, 372, 311–319, doi:10.1056/NEJMoa1411087.

2. Hamid, O.; Robert, C.; Daud, A.; Hodi, F.S.; Hwu, W.J.; Kefford, R.; Wolchok, J.D.; Hersey, P.; Joseph, R.W.; Weber, J.S.; et al. Safety and tumor responses with lambrolizumab (anti-PD-1) in melanoma. N. Engl. J. Med. 2013, 369, 134–144, doi:10.1056/NEJMoa1305133.

3. Borghaei, H.; Paz-Ares, L.; Horn, L.; Spigel, D.R.; Steins, M.; Ready, N.E.; Chow, L.Q.; Vokes, E.E.; Felip, E.; Holgado, E.; et al. Nivolumab versus docetaxel in advanced nonsquamous non-small-cell lung cancer. N. Engl. J. Med. 2015, 373, 1627–1639, doi:10.1056/NEJMoa1507643.

4. Pardoll, D.M. The blockade of immune checkpoints in cancer immunotherapy. Nat. Rev. Cancer 2012, 12, 252–264, doi:10.1038/nrc3239.

5. Thommen, D.S.; Koelzer, V.H.; Herzig, P.; Roller, A.; Trefny, M.; Dimeloe, S.; Kiialainen, A.; Hanhart, J.; Schill, C.; Hess, C.; et al. A transcriptionally and functionally distinct pd-1 + cd8 + t cell pool with predictive potential in non-small-cell lung cancer treated with pd-1 blockade. Nat. Med. 2018, 24, doi:10.1038/s41591-018-0057-z.

6. Duhen, T.; Duhen, R.; Montler, R.; Moses, J.; Moudgil, T.; De Miranda, N.F.; Goodall, C.P.; Blair, T.C.; Fox, B.A.; McDermott, J.E.; et al. Co-expression of CD39 and CD103 identifies tumor-reactive CD8 T cells in human solid tumors. Nat. Commun. 2018, 9, doi:10.1038/s41467-018-05072-0.

7. Webb, J.R.; Milne, K.; Nelson, B.H. PD-1 and CD103 are widely coexpressed on prognostically favorable intraepithelial CD8 T cells in human ovarian cancer. Cancer Immunol. Res. 2015, 3, 926–935, doi:10.1158/2326-6066.CIR-14-0239.

8. Gros, A.; Yang, J.C.; Rosenberg, S.A.; Gros, A.; Robbins, P.F.; Yao, X.; Li, Y.F.; Turcotte, S.; Tran, E.; Wunderlich, J.R.; et al. PD-1 identifies the patient-specific CD8+ tumor-reactive repertoire infiltrating human tumors. 2014, 124, 2246–2259, doi:10.1172/JCI73639.2246.

9. Inozume, T.; Hanada, K.I.; Wang, Q.J.; Ahmadzadeh, M.; Wunderlich, J.R.; Rosenberg, S.A.; Yang, J.C. Selection of CD8+PD-1+ lymphocytes in fresh human melanomas enriches for tumor-reactive T cells. J. Immunother. 2010, 33, 956–964, doi:10.1097/CJI.0b013e3181fad2b0.

10. Ahmadzadeh, M.; Johnson, L.A.; Heemskerk, B.; Wunderlich, J.R.; Dudley, M.E.; White, D.E.; Rosenberg, S.A. Tumor antigen-specific CD8 T cells infiltrating the tumor express high levels of PD-1 and are functionally impaired. Blood 2009, 114, 1537–1544, doi:10.1182/blood-2008-12-195792.

11. Dieu-Nosjean, M.C.; Giraldo, N.A.; Kaplon, H.; Germain, C.; Fridman, W.H.; Sautès-Fridman, C. Tertiary lymphoid structures, drivers of the anti-tumor responses in human cancers. Immunol. Rev. 2016, 271, 260–275, doi:10.1111/imr.12405.

12. Sautès-Fridman, C.; Lawand, M.; Giraldo, N.A.; Kaplon, H.; Germain, C.; Fridman, W.H.; Dieu-Nosjean, M.C. Tertiary lymphoid structures in cancers: Prognostic value, regulation, and manipulation for therapeutic intervention. Front. Immunol. 2016, 7, 1–11, doi:10.3389/fimmu.2016.00407.

13. Gupta, P.K.; Godec, J.; Wolski, D.; Adland, E.; Yates, K.; Pauken, K.E.; Cosgrove, C.; Ledderose, C.; Junger, W.G.; Robson, S.C.; et al. CD39 Expression Identifies Terminally Exhausted CD8+ T Cells. PLoS Pathog. 2015, 11, 1–21, doi:10.1371/journal.ppat.1005177.

14. Djenidi, F.; Adam, J.; Goubar, A.; Durgeau, A.; Meurice, G.; de Montpréville, V.; Validire, P.; Besse, B.; Mami-Chouaib, F. CD8 + CD103 + Tumor–Infiltrating Lymphocytes Are Tumor-Specific Tissue-Resident Memory T Cells and a Prognostic Factor for Survival in Lung Cancer Patients . J. Immunol. 2015, 194, 3475–3486, doi:10.4049/jimmunol.1402711.

15. Picelli, S.; Faridani, O.R.; Björklund, Å.K.; Winberg, G.; Sagasser, S.; Sandberg, R. Full-length RNA-seq from single cells using Smart-seq2. Nat. Protoc. 2014, 9, 171–181, doi:10.1038/nprot.2014.006.

16. Workel, H.H.; Lubbers, J.M.; Arnold, R.; Prins, T.M.; van der Vlies, P.; de Lange, K.; Bosse, T.; van Gool, I.C.; Eggink, F.A.; Wouters, M.C.A.; et al. A Transcriptionally Distinct CXCL13þCD103þCD8þ T cell Population Is Associated with B cell Recruitment and Neoantigen Load in Human Cancer. Cancer Immunol. Res. 2019, 7, 784–796, doi:10.1158/2326-6066.CIR-18-0517.

17. Morsut, L.; Roybal, K.T.; Xiong, X.; Gordley, R.M.; Coyle, S.M.; Thomson, M.; Lim, W.A. Engineering Customized Cell Sensing and Response Behaviors Using Synthetic Notch Receptors. Cell 2016, 164, 780–791, doi:10.1016/j.cell.2016.01.012.

18. De Bruyn, M.; Wei, Y.; Wiersma, V.R.; Samplonius, D.F.; Klip, H.G.; Van Der Zee, A.G.J.; Yang, B.; Helfrich, W.; Bremer, E. Cell surface delivery of TRAIL strongly augments the tumoricidal activity of T cells. Clin. Cancer Res. 2011, 17, 5626–5637, doi:10.1158/1078-0432.CCR-11-0303.

19. Gibson, D., Young, L., Chuang, R. et al. Enzymatic assembly of DNA molecules up to several hundred kilobases. Nat Methods 6, 343–345 (2009) doi:10.1038/nmeth.1318.

5

Supplementary material

Supplementary Table 1. Flow cytometry and FACS antibodies

Antigen	Clone	Fluorophore	Company	Catalog no.	Amount flow cytometry	Amount FACS
CD56	NCAM16.2	FITC	BD Biosciences	W345811		1 uL per 1x10^6 cells
CD16	NKP15	FITC	BD Biosciences	335035		1 uL per 1x10^6 cells
CD19	4G7	FITC	BD Biosciences	345776		1 uL per 1x10^6 cells
CD14	61D3	APC	eBioscience	17-0149-42		0,33 uL per 1x10^6 cells
CD4	OKT4	PE	eBioscience	12-0048-42		0,33 uL per 1x10^6 cells
CD279 (PD-1)	MIH4	PE	eBioscience	12-9969-41	2 uL per 5x10^4 cells	5 uL per digest
CD103	Ber-ACT8	FITC	BD Biosciences	561677	10 uL per 5x10^4 cells	20 uL per digest
CD39	eBioA1	APC	eBioscience	17-0399-42	2 uL per 5x10^4 cells	5 uL per digest
CD3	OKT3	PerCP-Cyanine5.5	eBioscience	45-0037-42	2 uL per 5x10^4 cells	2 uL per 1x10^5 cells or 5 uL per digest
CD8a	RPA-T8	BV421	BD Biosciences	562428		5 uL per digest
CD8a	RPA-T8	APC-eFluor780	eBioscience	47-0088-42	2 uL per 5x10^4 cells	2 uL per 1x10^5 cells
CD4	OKT4	PerCP-Cyanine5	eBioscience	45-0048-42	2 uL per 5x10^4 cells	
CD45RO	UCHL1	Pe-Cyanine7	eBioscience	25-0457-42		0,33 uL per 1x10^6 cells

Supplementary Table 2. mRNA sequencing materials and methods

Primer	sequence
BC-Oligo-dT	5'- AAG CAG TGG TAT CAA CGC AGA GTA CTT TTT TTT TTT TTT TTT TTT TTT TTT TTT TCA-3'
BC-TSO	5'- AAG CAG TGG TAT CAA CGC AGA GTG AAT RGR G+G-3'
BC-PCR	5'- AAG CAG TGG TAT CAA CGC AGA GT-3'

Nextera index 1 (i7) adapters (N7)

index name	i7 bases in adapter
N701	TCGCCTTA
N702	CTAGTACG
N703	TTCTGCCT
N704	GCTCAGGA
N705	AGGAGTCC
N706	CATGCCTA

Nextera index 2 (i5) adapters (S5)

index name	i5 bases in adapter
S502	CTCTCTAT
S503	TATCCTCT
S504	AGAGTAGA
S517	GCGTAAGA

RNA solution (lysis buffer sorting):

	Volume
Cell lysis buffer (0,2% Triton and 2U/uL RNAse inhibitor)	2
10 uM oligo dT primer	1
4x 10 mM dNTP mix	1
	up to 4 uL

Reverse transcription mix:

	Volume	Final concentration
Smart scribe reverse transcription (100 U/ul)	0,5	5U / uL
Rnase inhibitor (40 U/ul)	0,25	1U / uL
Smart scribe first strand buffer (5x)	2	1x
DTT (100 mM)	0,2	2 mM
Betaine (5M)	2	1 M
BC-TSO (10 uM)	0,1	1 uM
Nuclease free water	0,95	
	up to 6 uL (end volume = 10 uL)	

Reverse transcription program:

Cycle	Temperature (C°)	Time
1	42	90 min
2-11	50	2 min
	42	2 min
12	70	15 min
13	4	hold

PCR preamplification mix:

	Volume	Final concentration
KAPA HiFi HotStart ReadyMix (2x)	12,5	1x
BC-PCR primer (10 uM)	0,25	100 nM
nuclease free water	2,25	
	up to 15 uL (end volume = 25 uL)	

PCR preamplification program:

Cycle	Temperature (C°)	Time
1	98	3 min
2-24	98	20 sec
	67	15 sec
	72	6 min
25	72	5 min
26	4	hold

5

Supplementary Figure 1
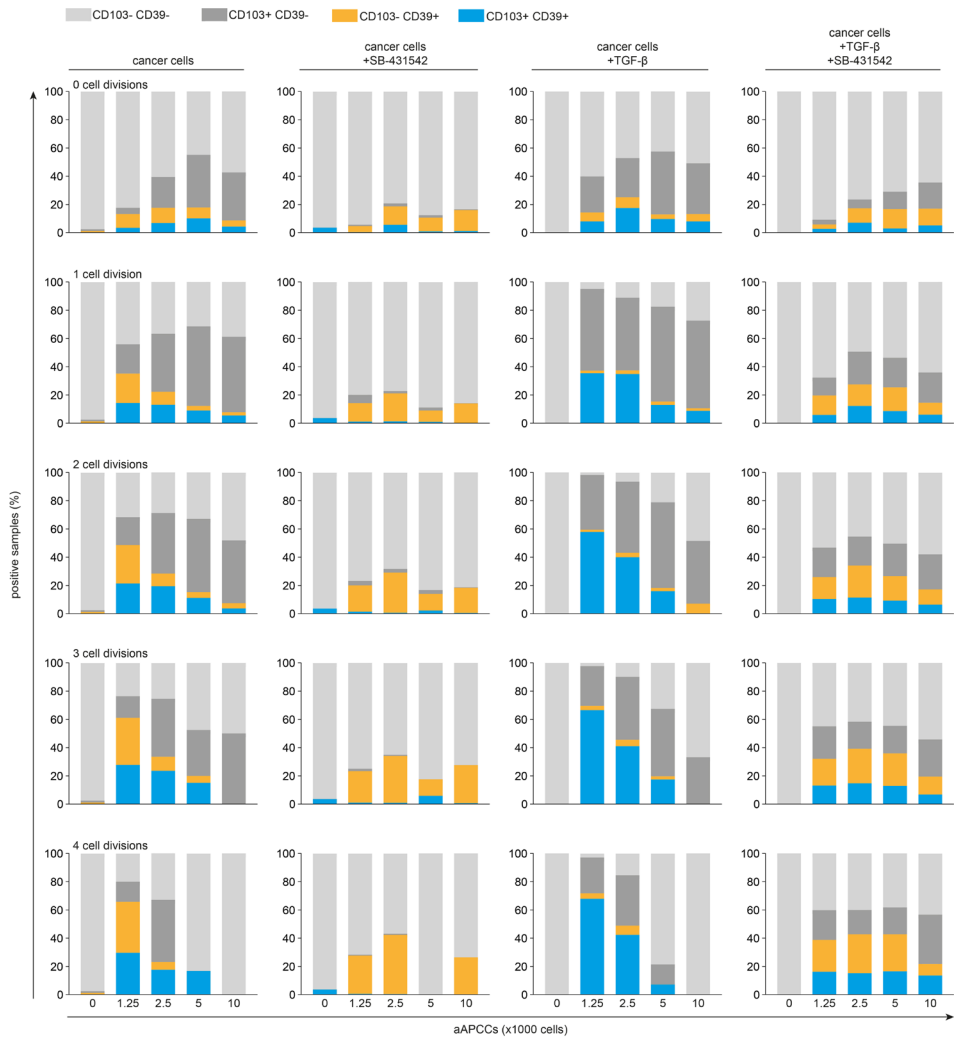
Relative frequencies for indicated CD8 T cell subsets per cell division and ratio of aAPCC:T cell. aAPCC were seeded at the indicated concentration (x1000 cells) in a 96-well, allowed to adhere for 24h and 10.000 T cells were added to each well for co-culture.

Supplementary Figure 2
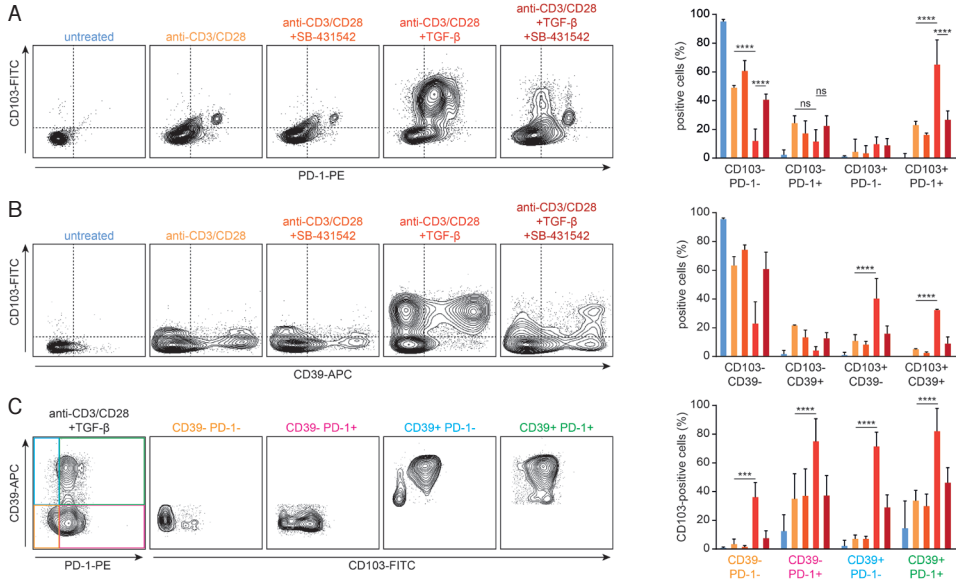
Combined TCR and TGFβ receptor signaling in CD8+ T cells induces robust cell surface expression of PD-1, CD39 and CD103. *Exemplary (left) and quantified (right) expression of A, PD-1 and CD103, B, CD39 and CD103 and C, PD-1, CD103 and CD39 on CD8+ T cells from healthy donors treated in vitro for four days with (a combination of) anti-CD3/CD28 beads, TGFβ and SB-431542.*

5

Chapter 6

Urine-derived ovarian cancer patient iPSC as novel tool to study cancer immunotherapy

Joyce M. Lubbers[1], Nienke van Rooij[1], Mathilde J.C. Broekhuis[2,3], Eslie G.C. Huizinga[2,3], Daniël O. Warmerdam,[2,3] Floris Foijer[2,3], Hans W. Nijman[1#], Marco de Bruyn[1#]

[#]share senior authorship

[1]University of Groningen, University Medical Center Groningen, Department of Obstetrics and Gynecology, The Netherlands
[2]Department of Ageing Biology/ERIBA, University of Groningen, University Medical Center Groningen, Groningen, the Netherlands
[3]iPSC/CRISPR facility, Department of Ageing Biology/ERIBA, University of Groningen, University Medical Center Groningen, Groningen, the Netherlands

Work in progress

Abstract

Immunotherapy has emerged as a promising anti-cancer strategy, with curative treatment even in previously treatment-refractory diseases. However, patient-to-patient variation in response complicates patient stratification for specific immunotherapeutic modalities. A present, no preclinical model exists that accurately resembles patients with regards to both the cancer and the immune system. To address this issue, we propose the use of patient urine-derived induced pluripotent stem cells (iPSC) to establish novel preclinical models. Here, we demonstrate the high potential of these cells in cancer immunotherapy research by showing i) *in vitro* reprogramming of fibroblasts from the urine of ovarian cancer patients to generate iPSC and ii) *in vitro* re-differentiating of these cells into progenitor thymus cells by directed differentiation that mimics embryonic thymus organogenesis. The high success rates of both the reprogramming and re-differentiation support implementation of iPSC in cancer immunotherapy research.

Introduction

Immunotherapeutic strategies have gained ground in the treatment of cancer patients. These strategies mostly target escape mechanisms that are exploited by the tumor to prevent their killing by cytotoxic T cells (CTLs).[1] At present the most promising strategies are immune checkpoint inhibitors Nivolumab and Ipilimumab, targeting Programmed Cell Death Protein 1 (PD-1) on activated T cells and CTLA-4 on regulatory T cells, respectively. However, the investigation of the therapeutic efficacy of these and other therapies can be challenging since the number of participants available for clinical trials is limited, and preclinical models are not well-suited.

Traditionally, immortalized cancer cell lines are used either *in vivo* or *in vitro* to study the effect of therapeutic modalities. However, these cancer cell lines are of limited value as they do not reflect the heterogeneity and complexity of human cancers. Therefore, patient derived xenograft (PDX) models have been developed in which surgically derived tumor tissue from patients is implanted into mice. With the implantation of tumor tissue with an intact tumor architecture comprising of stromal and cancer cells, a preclinical model has been created that more closely resembles human cancer.[2] Notably, these models are generated in immunodeficient mice to avoid immune rejection of the xenograft tissue, limiting the value of these models in exploring the role of the immune system in tumor progression, as well as evaluation of novel immunotherapies. Therefore, efforts are currently made to unite the PDX implantation with immune humanization of mice. For example, selected immune components such as patient-derived tumor infiltrating lymphocytes or peripheral blood mononuclear cells are introduced into mice. Here, the disadvantage is that these cell resources are highly limited. A more sustainable solution may lie in the use of stem cells. These cells have limitless self-renewal and pluripotent potential. Hence, they offer numerous possibilities to create novel models for preclinical cancer research. We here focus on the use of stem cells to introduce immunity to immunodeficient mice.

A commonly used immunodeficient mouse is the *Foxn1* nu/nu nude mouse. These *Foxn1* null mice fail to develop the thymus: an organ essential for development of adaptive immunity. In the thymus, progenitor T cells mature and undergo a selection process based on antigen presentation to exclude auto-reactive cells from the T cell pool.[3] The resulting mature T cells are single CD8+ or CD4+ T cells that migrate to the peripheral blood to exert their functionalities, including the killing of cancerous cells.[4] Recently, studies have assessed the possibility of introducing de novo generated thymus tissue into nude mice to establish an immune-competent mouse model. To this end, progenitor thymus tissue was generated *in vitro* by simulation of thymus organogenesis, thus directing differentiation of

6

embryonic stem cells (ESC) by specifically timed addition of Wnt3a, activin A, FGF, retinoic acid, BMP-4, SB-431542 and cyclopamine-KAAD3.[5–7] This regulated differentiation results in the sequential induction of *HOXA3* and *FOXN1*, both known to be early and essential regulators of thymus development.[6] The resulting thymic epithelial progenitor cells (TEPC) were subsequently implanted in the kidney capsules of nude mice. Herein, they further differentiated to become thymic epithelial cells (TEC) by being in contact with thymocytes. These TEC expressed MHC class II and AIRE[8], both involved in the antigen presentation and selection process within the thymus. Indeed, upon implantation of the generated thymus tissue, the nude mice presented with measurable CD4+ and CD8+ T cells in the blood[5,7,9], indicative of functional thymus tissue.

Although this study was highly successful, the use of ESC lines is not immune-compatible with usage of patient tumor material. Thus, uniting this de novo thymus mouse model with PDX or other patient tissue is not possible. Therefore, we suggest the use of induced Pluripotent Stem Cells (iPSC) that are autologous to the patient. Like ESC, iPSC are characterized by pluripotency and limitless self-renewal, potentiating their infinite usage. Thus far, iPSC are generally generated by reprogramming of blood or skin cells. However, these sources have limited availability and collecting them requires invasive measures. To eliminate these limitations, we propose to generate iPSC from renal epithelial cells present in urine. Here, we demonstrate reprogramming cells from the urine of ovarian cancer patients into iPSC and *in vitro* generation of progenitor thymus tissue by directed differentiation of the iPSC that mimics embryonic thymus organogenesis.

Materials and Methods

Collection of patient urine
Urine of ovarian cancer patients treated with chemotherapy at the University Medical Center Groningen (UMCG), the Netherlands, in 2017 was collected as surgical waste after informed consent was provided. To this end, urine was collected via a catheter into sterile cups (Sarstedt). Collected urine was directly kept on ice to prevent bacterial contamination and immediately anonymously processed for iPSC reprogramming. Patients receiving chemotherapy or with reported mutations in the Breast Cancer 1 or 2 gene were also included in the study.

Animals
Female Crl:NU-Foxn1nu (*Foxn1* nu/nu nude mouse) were obtained from Charles River Laboratories and housed in individually ventilated cages in groups of 6 mice. Surgeries were performed under general anesthesia (2-5% isoflurane) and analgesia (4-5 mg/kg carprofen); Progenitor thymus tissue was implanted under the kidney capsule. Blood

was isolated every six weeks by orbita punctures and collected in heparin tubes. Exactly 30 weeks after implantation, mice were euthanized under general anesthesia by cervical dislocation. Blood was collected via heart puncture in heparin tubes. Spleens were collected in PBS+5% Fetal Calf Serum (FCS, Gibco) on ice. Kidneys were placed immediately in cassettes with formaline. Wellbeing of animals was monitored regularly. Animal study approval was given under CCD license number AVD105002017883 by the Central Animal Facility (CDP, UMCG).

Reprogramming of renal epithelial cells into iPSC

Isolation and expansion of renal epithelial cells from urine to generate iPSC was performed as previously reported by Zhou *et al.*[10] For reprogramming, urine-derived renal epithelial cells were grown on Geltrex-coated 6-well plates and transduced with the lentiviral vector pRRL.PPT.SF.hOct34.hKlf4.hSox2.hmyc.i2dTomato.pre[11] in REGM renal epithelial proliferation medium (Lonza CC-3190) containing 8 μg/ml polybrene (Sigma, 107689-10G). After transduction, cells were cultured for in REGM medium until confluent before changing to Essential 6 medium (Thermo Scientific) plus 10ng/ml FGF-2 (Peprotech, AF-100-18B) until first iPSC colonies appeared. Culture medium was changed to Essential 8 medium (Thermo Scientific) and arising iPSC colonies were transferred mechanically to Geltrex-coated 12-well plates and further cultivated in Essential 8 medium for 10 passages before characterization and cryopreservation. Maintenance of iPSC culture was performed by passaging every three or four days (maximum of 70% confluence) using ReLeSR (Stemcell Technologies) for 30 seconds. Washing steps were performed with dPBS w/o Ca&Mg (Thermo Scientific) and transferring of cells was done with E8 Essential medium or DMEM/F12 medium (Gibco). E8 Essential medium was replaced each 24 hours. Long term cultures were seeded in Essential 8 Flex medium (Thermo Scientific), triple the normal medium volume. Single cell seeding was accomplished using Accutase (Thermo Scientific). Cell cultures were incubated at 37°C.

Assessment of pluripotency status

For embryoid body (EB) formation, iPSC were dissociated using ReLeSR and seeded into low-adherent cell culture flasks in Essential 8 medium. After one day, medium was changed to SRM medium (KnockOut DMEM (Gibco), 15% KnockOut Serum Replacement, 1X GlutaMAX, 1X MEM NEAA, 50 U/ml penicillin/streptomycin) and cells were cultured in SRM medium for 1 to 2 weeks with medium changes every other day. Emerging EBs were then plated onto Geltrex-coated coverslips for immunofluorescence staining or harvested for RNA extraction followed by RT-qPCR or ddPCR analysis.

For immunofluorescence, iPSCs or EBs were grown on Geltrex-coated coverslips for 5 to 14 days, fixed in 4% paraformaldehyde for 20 min and permeabilized in 0.5% Triton-X-100

6

for 5 min before blocking in 2% BSA for 1 h. Samples were probed with primary antibodies (Table 1) at 4 °C overnight and incubated with Alexa Fluor 488- and Alexa Fluor 568-labelled secondary antibodies for 1h at room temperature in the dark before mounting in ProLong Diamond Antifade Mountant with DAPI (Thermo Scientific). Imaging was performed using a Olympus BX43 fluorescent microscope with 10x, 20x and 40x objectives.

Table 1. Antibodies used for immunofluorescence

Primary antibodies

Target	Source	Species raised	Dilution
Sox2	Cell Signaling, 4900	mouse, monoclonal, IgG	1:250
Oct4	kind gift of Veronique Smits	rabbit, polyclonal	1:1000
Nanog	kind gift of Veronique Smits	rabbit, polyclonal	1:250
SSEA4 (PE labelled)	Stem Cell Technologies, 60062PE.1	mouse, monoclonal, IgG	1:100
Tra-1-60	Millipore, MAB4360	mouse, monoclonal, IgM	1:250
Tra-1-81	Santa Cruz, SC-21706	mouse, monoclonal, IgM	1:250
Beta-III Tubulin	Abcam, ab7751	mouse, monoclonal, IgG	1:250
Gata4	Santa Cruz, SC-25310	mouse, monoclonal, IgG	1:100
Desmin	Agilent, M076029-2	mouse, monoclonal, IgG	1:100
FOXN1	Invitrogen, 720152	rabbit, polyclonal, IgG	1:100
K5	Invitrogen, MA 17057	mouse, monoclocal, IgG1	1:100

Secondary antibodies

Target, label	Source	Species raised	Dilution
Mouse IgG, AF488	Thermo Scientific, A21202	donkey, polyclonal	1:1000
Mouse IgM, AF488	Thermo Scientific, A21042	goat, polyclonal	1:1000
Rabbit IgG, AF568	Thermo Scientific, A10042	donkey, polyclonal	1:1000
Rabbit IgG, AF568	Thermo Scientific, A11011	goat, polyclonal	1:300
Mouse IgG, AF568	Thermo Scientific, A11004	goat, polyclonal	1:300

For RT-qPCR and ddPCR, RNA was isolated using the RNeasy mini kit (Qiagen) and cDNA generated using the SuperScript® III First-Strand Synthesis System (Thermo Scientific) using random hexamer primers according to the manufacturer's instructions. Real-time PCR was performed in duplicate on a LightCycler480 (Roche) using the SsoAdvanced™ Universal Probes Supermix (BioRad) and PrimePCR™ ddPCR™ Expression Probe Assays (BioRad)(Table 2). Relative expression levels were calculated using the ddCT method with *GAPDH* or *ACTB* as reference genes and normalized as indicated in the figures.

Table 2. Primers for RT-qPCR and ddPCR

Target	Probe	Source
GAPDH	human, PrimePCR™ ddPCR™ Expression Probe Assay	BioRad, dHsaCPE5031596
ACTB	human, PrimePCR™ ddPCR™ Expression Probe Assay	BioRad, dHsaCPE5190199
SOX2	human, PrimePCR™ ddPCR™ Expression Probe Assay	BioRad, dHsaCPE5030244
NANOG	human, PrimePCR™ ddPCR™ Expression Probe Assay	BioRad, dHsaCPE5191855
OCT4 (POU5F1)	human, PrimePCR™ ddPCR™ Expression Probe Assay	BioRad, dHsaCPE5191335
KLF4	human, PrimePCR™ ddPCR™ Expression Probe Assay	BioRad, dHsaCPE5037000
MYC	human, PrimePCR™ ddPCR™ Expression Probe Assay	BioRad, dHsaCPE5051056
PAX6	human, PrimePCR™ ddPCR™ Expression Probe Assay	BioRad, dHsaCPE5050536
GATA2	human, PrimePCR™ ddPCR™ Expression Probe Assay	BioRad, dHsaCPE5049282
GATA4	human, PrimePCR™ ddPCR™ Expression Probe Assay	BioRad, dHsaCPE5050488

ddPCR was performed with the QX200 Droplet Digital PCR System (BioRad) using the ddPCR Supermix for Probes (No dUTP) (BioRad) and PrimePCR™ ddPCR™ Expression Probe Assays (BioRad)(Table 2) according to the manufacturer's instructions. Relative expression levels were calculated with *GAPDH* as reference gene and normalized as indicated in the figures.

Directed differentiation of iPSC to progenitor thymus tissue

Patient-derived iPSC were re-differentiated to progenitor thymus tissue by directed differentiation mimicking thymus organogenesis (Supplementary Figure 1). First, iPSC were pushed towards SOX17+, CXCR4+ definitive endoderm (DE) by addition of activin A, FGF-basic and Wnt3a using the StemXVivo Endoderm Kit (R&D Systems). Next, DE cells differentiated towards HOXA3+, TBX1+, PAX9+, EYA1+, SIX1+, PBX1+ third pharyngeal pouch endoderm (PPE) by addition of 0.25 µM retinoic acid, 50 ng/mL BMP-4 (R&D Systems) and 10 µM SB-431252 (Sigma Aldrich/Merck) in DMEM F12 medium (Thermo Scientific) + 0.5% B27. Lastly, PPE cells further differentiated to become K5+, FOXN1+ thymic epithelial progenitor cells (TEPC) by addition of 50 ng/mL Wnt3a (R&D Systems), 50 ng/mL FGF8β, 0.5 µM cyclopamine-KAAD (Merck Milipore), 50 ng/mL BMP-4 and 0.1 µM retinoic acid DMEM in F12 medium + 0.5% B27. Medium was changed daily. Cells were incubated at 37°C and harvested or fixated in the plate at day 11 for analysis of lineage markers.

RT-PCR

Expression of lineage markers was analyzed by RT-PCR. To this end, cells were harvested by ReLeSR treatment. The cell pellet was directly homogenized in Ambion TRIzol Reagent (Invitrogen) for RNA isolation and stored at -80°C or directly further processed according to manufacturer protocol. Yield and quality (260/280 and 260/230 absorbance ratios) of the isolated RNA were determined using a NanoDrop 1000 spectrophotometer (Thermo Fisher Scientific). Next, 4 µg of the isolated RNA was converted to cDNA using 800 U Moloney Murine Leukemia Virus Reverse Transcriptase (M-MLV RT) and provided materials in the supplementary kit (Invitrogen). The samples were stored at 4°C for short term or -20°C for long-term until used for analysis. Next, 25 µL reactions with Q5 polymerase (NEB) were used to perform PCR analyses on relevant lineage markers, of which expression was visualized using TBE gel electrophoresis. Primers were obtained from Sun *et al.*[5] and are listed in Table 3. We combined *CXCR4*, *HOXA3*, *EYA1* and *K8* at 53.5°C, *SOX17*, *TBX1*, *PBX1* and *K5* at 57°C and *PAX9*, *SIX1* and *FOXN1* at Tm 58.5°C.

Fluorescent microscopy

To assess thymic differentiation, we stained for lineage markers K5 and FOXN1, using in-plate fluorescent microscopy at the end of the thymus differentiation protocol. To this

6

Table 3. Primers for RT–PCR

Target	Forward primer (5'-3')	Reverse primer (5'-3')	Tm (°C)	Product size (bp)
SOX17	CAGTGACGACCAGAGCCAGACC	CCACGACTTGCCCAGCATCTT	57	292
CXRC4	AAAATCTTCCTGCCCACC	ATCCAGACGCCAACATAG	55	374
HOXA3	ACGCCTTCCACAGCTCCT	CGCTATCTTTGCGTGGGTC	55	352
TBX1	ATGCCAGCAACAACCCTACC	TTGTACTTCATGCGGCGATT	57	242
PAX9	GACTCATACAAGCAGCACCA	TGTCCAGCAACATAACCAG	59	479
EYA1	TTGAAGCCCTGACCGACTC	TTGCTCCTTGTTCTTCTTCTAC	52	282
SIX1	CGCACAATCCCTACCC	CAGCAGAAGGACCGAGT	59	272
PBX1	ATGAAGCCTGCCTTGTTT	CTGTAATCTGAATGCTCCACT	57	236
FOXN1	GTGCTGGGATGTTCTGCTAC	AAGGAAAGTGCTCCGTCATA	58	291
K5	CGATGACCTCCGCAACAC	GACTGGTCCAACTCCTTCTC	57	340
K8	AGGCATCACCGCAGTTAC	CATGTAAGCTTCATCCAC	54	433

end, cells were first washed twice with PBS. Next, 500 μL of 3.7% formaldehyde in PBS was added per well and incubated for 10-15 minutes at 20°C. Subsequently, cells were permeabilized using 500 μL 0.1% Triton in PBS for 5 minutes. Cells were incubated with primary antibodies 1:100 in PBS + 2.5% BSA + 0.05% Tween20 for 2 hours at an RT shaker and with secondary antibody 1:300 in PBS + 2.5% BSA + 0.05% Tween20 for 20-30 minutes covered in aluminum foil at 4°C (Table 1). Visualization of signal was obtained using the EVOS FL microscope (Invitrogen, 10X objective). Appropriate washing steps with PBS or PBS + 0.05% Tween20 were taken in between steps.

Flow cytometry

To assess cell surface expression of markers EPCAM, E-Cadherin and CXCR4, iPSC and cells at day 5 of the differentiation protocol (single cell seeded and clump seeded) were assessed by flow cytometry. Cells were harvested by ReLeSR treatment, collected by centrifugation and incubated with 2μL per tube anti-EPCAM-APC (Miltenyi Biotec, 130-091-254), anti-CD324-PerCP-eFluor 710 (Thermo Fisher Scientific, 46-3249-82) and anti-CXCR4-PE (R&D Systems, FAB173P) for 90 minutes at 4°C in the dark. Appropriate washings with PBS were performed in between steps and twice after incubation with primary antibodies. Analysis was performed using BD Accuri C6 Flow Cytometer (BD Biosciences).

To assess CD8+ cell development in mice, Erylysis treatment (Invitrogen) was performed on fresh blood for 10-15 min at RT and cells were collected by centrifugation. Next, cells were first stained with Zombie Aqua 1:100 in PBS for 15-30 min at RT in the dark and then with 5 μg/mL anti-CD8a-PE-Cy7 (Thermo Fisher, 25-0081-82) in PBS+2% FCS for 50 minutes at 4°C in the dark. Appropriate washings with PBS, PBS+2% FCS or PBS+5% FCS were taken in between steps. Analysis was done using a BD FACSVerse flow cytometer (BD Biosciences).

To assess CD8+ cell presence in the spleens of the mice, harvested spleens were crushed through a 70 μm cell strainer with PBS into a 50 ml tube using a rubber syringe plunger for homogenization. Cells were treated with red blood cell lysis buffer (Invitrogen)

for 5 min at RT and collected by centrifugation. Washings were performed with PBS. Flow cytometry analysis was subsequently performed as described for the blood.

Haematoxylin & Eosin staining

To assess the presence of xenograft tissue in the kidneys, formalin fixed kidneys were processed into 4 mu full slide coupes. To stain for H&E, coupes were first treated with a series of xylene, alcohol dilutions and demiwater. Next, coupes were incubated in haemotoxylin for 10 min, washed with tap water and incubated in eosin for 2 min. After a series of washings in alcohol, coupes were dried for 20 minutes and mounted. Coupes were scanned using a Hamamatsu scanner.

Results

Stem cells can be successfully generated from urine of ovarian cancer patients

Stem cells are of interest due to their unique features of self-renewal and pluripotency. These features offer numerous possibilities for use in medical research. Originally, embryonic stem cells (ESC) were mostly exploited for this purpose. However, as these cells are not readily available or non-autologous in the case of stem cell lines, protocols have been developed to induce stem cells by dedifferentiation of skin[12] and blood[13,14] cells by introduction of Yamanaka factors, key proteins involved in pluripotency. Moreover, successful efforts have been made to generate stem cells from the urine of healthy volunteers.[10] Compared to blood, urine provides an non-invasive manner to collect somatic cells. Here, we aimed to generate stem cells from the urine of cancer patients. To this end, epithelial renal cells were isolated from the urine of ovarian cancer patients and transduced with Yamanaka factors. After several passages, dedifferentiation of urine cells to induced pluripotent stem cells (iPSC) was observed to be highly effective. Altogether, cells could be obtained from ~90% of urine samples and iPSC could be generated from ~75% of the cells. This was confirmed by abundant expression of Yamanaka factors Sox2 and Oct4 (Figure 1, Supplementary Figure 2). Moreover, we observed induction of pluripotent stem cell-specific proteins Nanog, Tra-1-60, Tra-1-81 and SSEA-4 (Supplementary Figures 2 and 3).

iPSC generated from the urine of cancer patients have pluripotent lineage potential

True stem cells have the pluripotent capacity to form each of the three germ layers: i) the ectoderm that will form the skin and nerve system, ii) the mesoderm that will form the heart, blood, skeleton, muscles, reproductive system, connective tissue and urogenital system and iii) the endoderm that will form the digestive tract and internal organs. To demonstrate this multi-lineage potential for the generated iPSC, embryoid bodies

6

(EB) were formed. Fluorescent microscopy showed successful neuronal differentiation by expression of Beta III Tubulin (Figure 2), muscular differentiation by expression Desmin in 2/4 clones (Supplementary Figure 4) and liver differentiation by expression of Gata4 (Supplementary Figure 5).
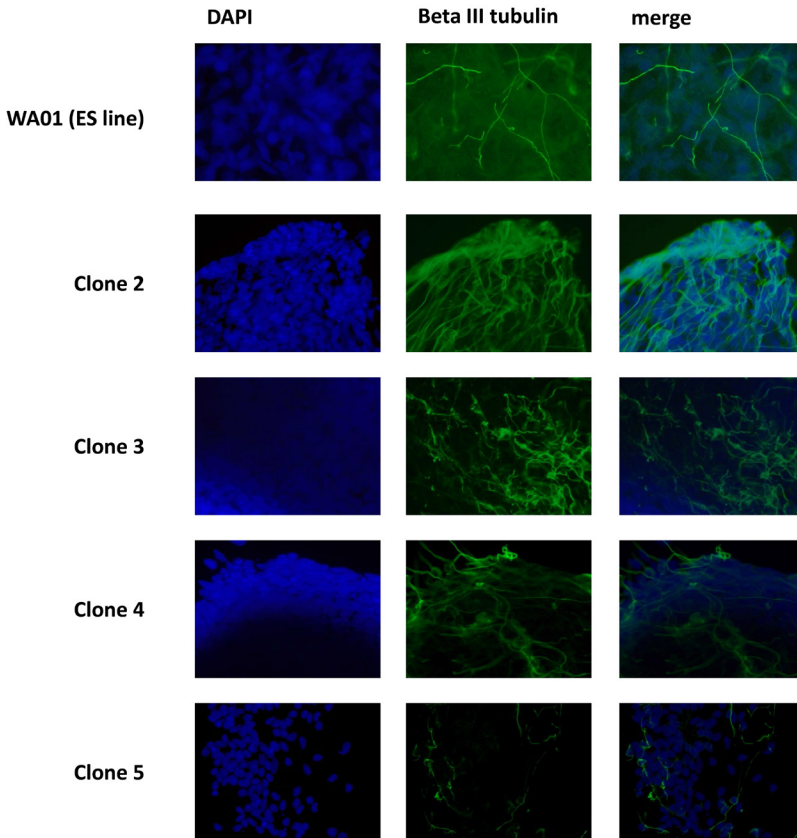
Figure 1
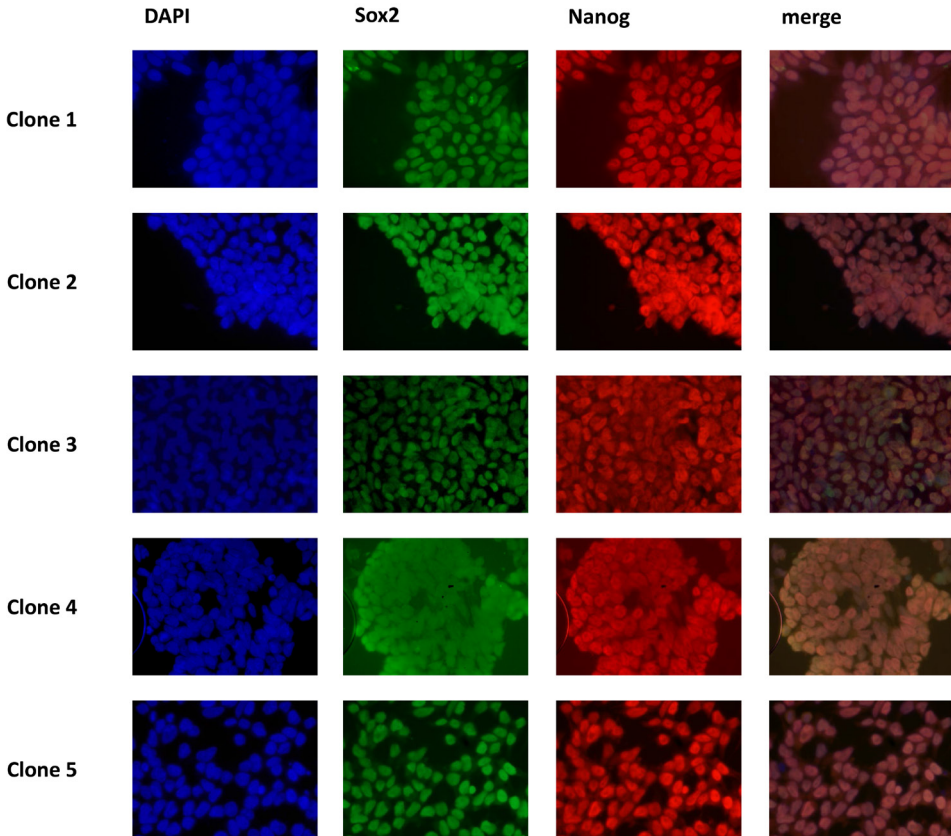
Characterization of established iPSC. *Immunofluorescent staining for DNA with DAPI (blue) and Yamanaka factors Sox2 (green) and Nanog (red). Merge shows overlay of stainings.*

iPSC from urine resemble the transcriptional profile of embryonic stem cells

To compare the generated cells to ESC and confirm their stem cell status, iPSC and ESC were examined at the transcriptional level by digital droplet PCR (ddPCR) and quantitative PCR (qPCR). We observed that expression of Yamanaka Factors *SOX2*, *OCT4*, *KLF4* and *MYC* was highly comparable for iPSC and ESC (Figure 3A and 3C). Moreover, *NANOG* was expressed to similar extent, whereas small deviations in expression were observed for *PAX6*, *GATA2* and *GATA4*. Notably, expression of *GATA2* and *GATA4* appeared to be lower in iPSC than ESC when examined by ddPCR but higher when examined with

Figure 2

Characterization of embryoid bodies generated from the established iPSC to demonstrate multilineage potential. *Immunofluorescent staining for DNA with DAPI (blue) and neural differentiation marker Beta III tubulin (green). Merge shows overlay of stainings.*

6

qPCR. For most of the genes, mRNA expression in EB deviated from the expression pattern in iPSC (Figure 3B and 3D). According to literature[15], expression of pluripotency genes declines during the generation of embryoid bodies. Indeed, *NANOG* and *OCT4*, and to lesser extent *SOX2*, were strongly down-regulated in EB. In contrast, germ layer-specific genes such as ectoderm marker *PAX6* and mesoderm marker *GATA2* showed strikingly higher expression in EB as compared to iPSC. These results suggest that iPSC transcriptionally resemble ESC that can form germ layers.

iPSC of cancer patients show differentiation potential into the thymic lineage
The established iPSC were redifferentiated into progenitor thymus tissue by directed differentiation of the iPSC, mimicking embryonic thymus organogenesis. Clear morphological changes were visible during the differentiation protocol of iPSC to Thymic Epithelial Progenitor Cells (TEPC)(Figure 4A). Before differentiation, iPSC were seeded

Figure 3
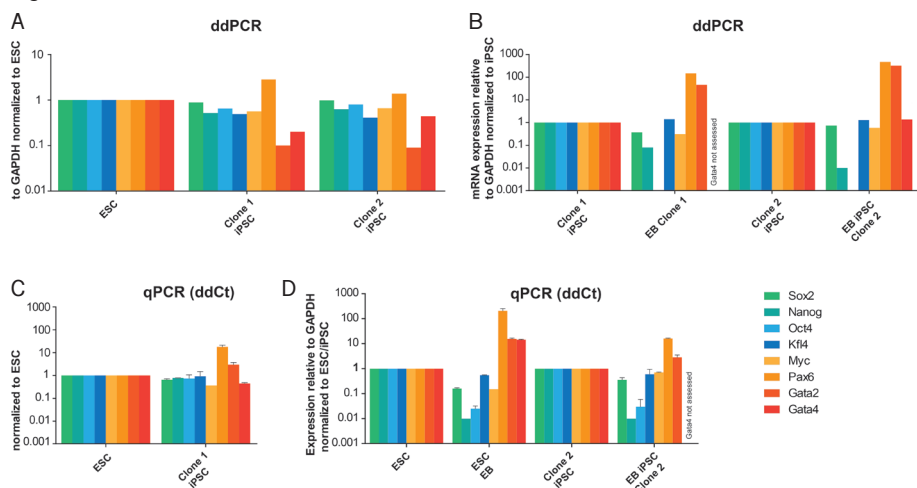
Characterization of established iPSC. *A, B) Digital droplet PCR (ddPCR) and C,D) quantitative PCR (qPCR) for several stem cell related genes (see legend) in iPSC, ESC and EB.*

in clumps and formed dense islands. Upon differentiation, cells stretched and obtained a polygonal shape that is characteristic for epithelial cells.[8] We observed large heterogeneity in microscopic analyses. Therefore, we repeated the differentiation by also seeding the iPSC as single cells. We observed that the change in morphology during differentiation was accompanied by reduction in expression of E-cadherin, important for stem cell pluripotency. Moreover, we observed induction of definitive endoderm marker CXCR4 expression on day 5 of the differentiation protocol (Figure 4B). As expected, more single cell seeded iPSC expressed CXCR4 than traditionally clump-seeded iPSC (75% versus 50%, respectively). Interestingly, redifferentiation of cells that were seeded the regular way, in clumps, led to formation of bridge-like structures (Figure 4C), which were not visible when cells were seeded as single cells. To determine whether the differentiation protocol was effective in generating TEPC, we next assessed markers that specify cell fates DE (*SOX17* and *CXCR4*), PPE (*HOXA3*, *TBX1*, *PAX9*, *EYA1*, *SIX1*, *PBX1*) and TEPC (*FOXN1* and *K5*) by RT-PCR. Whereas iPSC lacked expression of most markers (Figure 5A), clear induction of these markers was observed for cells undergoing differentiation. Although *HOXA3* was expressed on day 5 of the differentiation in clump seeded cells (Figure 5B), *HOXA3* expression lacked in single cell seeded cells (Figure 5C). As *HOXA3* expression at this stage is essential for induction of *FOXN1*, no *FOXN1* was observed in these cells at day 12 (Figure 5D). In another attempt to improve homogeneity of *FOXN1+* cells, we harvested clump-seeded cells at day 5 of differentiation after *HOXA3* induction and reseeded them as single cells before continuing the differentiation protocol. As compared to cells that were single cell seeded from day 1 (Figure 5D), reseeded cells expressed *TBX1* and *PAX9* (Figure 5E). Although *K5* is also slightly expressed in these cells at day

Figure 4
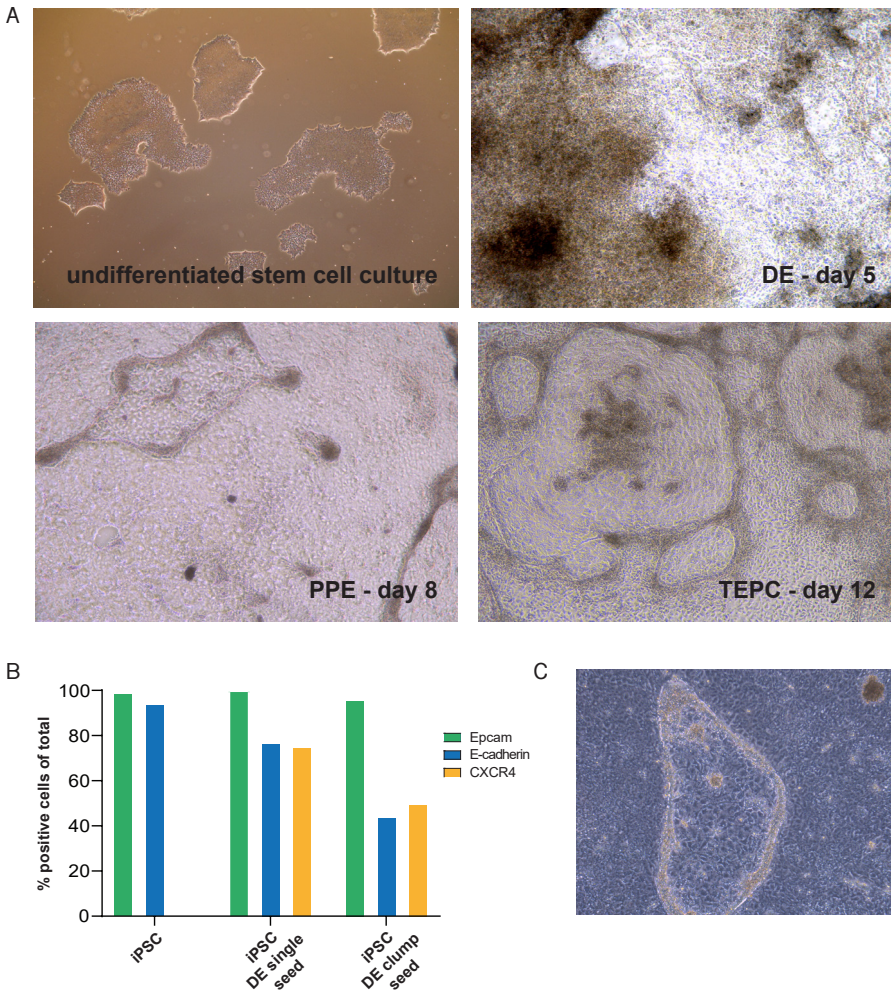
Differentiation of iPSC towards TEPC. *A). Microscope images on day 0, 5, 8 and 12 of differentiation. B). Flow cytometry analyses of iPSC and iPSC differentiated towards DE in single cell and clump mode. C). Microscopic detail image of structures observed at TEPC stage day 12.*

12, expression of *FOXN1* was very minimal. In contrast, clump-seeded iPSC showed clear expression of both *FONX1* and *K5* on day 12 (Figure 5F). Accordingly, clump-seeded cells that were at the end of the differentiation protocol expressed thymic lineage markers FOXN1 and K5 (Figure 6). Expression of these markers was typically observed in the cells located in the bridge-like structures, possibly explaining why single cell seeded iPSC that lacked these structures failed to induce *FOXN1* and *K5* expression. Altogether, iPSC derived from cancer patients show potential to differentiate into the thymic lineage. Yet, homogeneous differentiation is challenging.

Figure 5
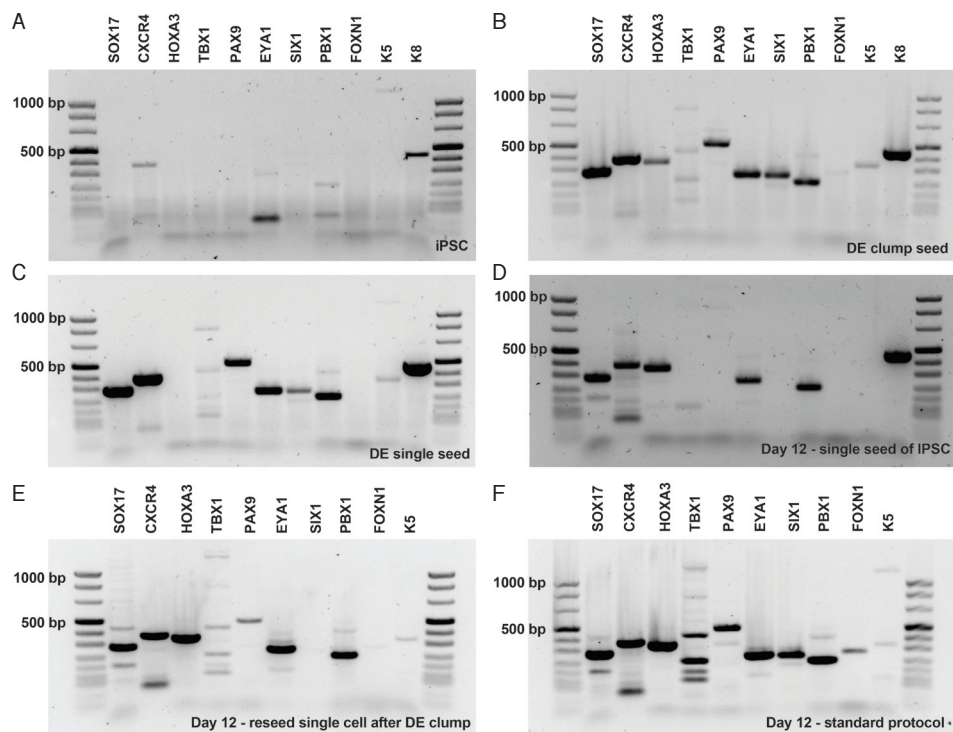
Validation of iPSC differentiation towards TEPC fate. *RT-PCR results for various cell stage markers for A). iPSC, B). clump seeded cells at DE stage, C). single cell seeded cells at DE stage, D). single cell seeded cells at day 12, E). cells reseeded single cell after differentiation of clump iPSC towards DE at day 12, F). profile of cells differentiated by the standard protocol at day 12.*

Implantation of TEPC in nude mice

To further evaluate the potential of the generated TEPC to develop into Thymic Epithelial Cells (TEC) *in vivo*, cells were implanted under the kidney capsule of *Foxn1* null mice and development of CD8+ T cells from progenitor T cells was monitored every six weeks by flow cytometry (Figure 7A). First, analysis of CD3+ cells within the lymphocyte population revealed increases in all mice, including sham-operated mice (figure 7B). No difference between percentages of CD3+ cells of sham-operated and TEPC implanted mice was observed 30 weeks after surgery. Similar results were obtained for CD8 (Figure 7C). Specifically, the increases in CD8+ cells coincided with the increases in CD3+ cells in all mice. In contrast, the development of CD335+ cells (Figure 7D) largely deviated from the development of CD8+ cells. This indicates that CD8+ cells were of CD3+ lineage and not representing CD8+ NK cells. Analyses of kidneys revealed absence of implanted tissues, clarifying the lack of differences between TEPC-implanted and sham-operated mice (Figure 7E and H&E in 7F). The lack of tissue may be explained by technical complications during implantation. Thus, *in vivo* experiments should be optimized.

Figure 6

Day 12 differentiation
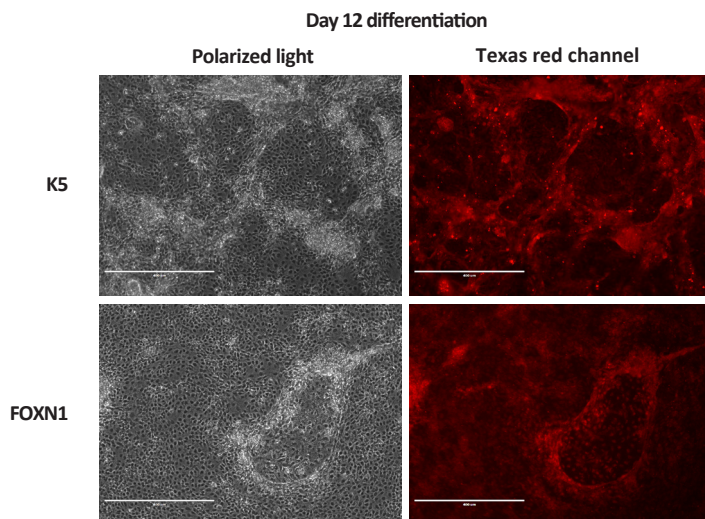
Differentiation of iPSC towards TEPC. *Immunofluorescent staining for TEPC markers K5 (top) and FOXN1 (bottom) in cells at day 12 of differentiation.*

Discussion

In this pilot study, we aimed to establish an immunocompetent preclinical model by implantation of de novo thymus tissue, using induced pluripotent stem cells (iPSC) generated from fibroblasts in the urine of ovarian cancer patients. The *in vitro* reprogramming of these fibroblasts to iPSC and re-differentiation of iPSC to progenitor thymus tissue was highly efficient. Establishment of mature thymus tissue *in vivo* requires optimization.

Sustainable preclinical models that allow to study both cancer xenograft tissue and tumor immunity are lacking. Recent studies show the high potential of stem cells in cancer research and oncology.[16] For example, CD8 T cells than be successfully generated directly from stem cells.[17–19] In addition, functional T cells can be developed indirectly when generating de novo thymic epithelial tissue from stem cells. This was previously achieved by directed differentiation of both human ESC and mouse embryonic fibroblast-derived iPSCs to thymic epithelial progenitor cells, followed by implantation in mice.[5,7,9,20] In the case of ESC-derived thymus tissue, the tissue harbors both mouse and human proteins to which the T cells will be tolerant. This approach thus enables induction of tolerance in T cells towards PDX tissue. However, as ESC are not autologous to the PDX tissue, in this study, we propose to use iPSC generated from same patient as the xenograft tissue. Since acquirement of blood or skin, regular sources for iPSC, is invasive, we propose generation of iPSC from urine. Here, we for the first time applied a combination of the

Figure 7
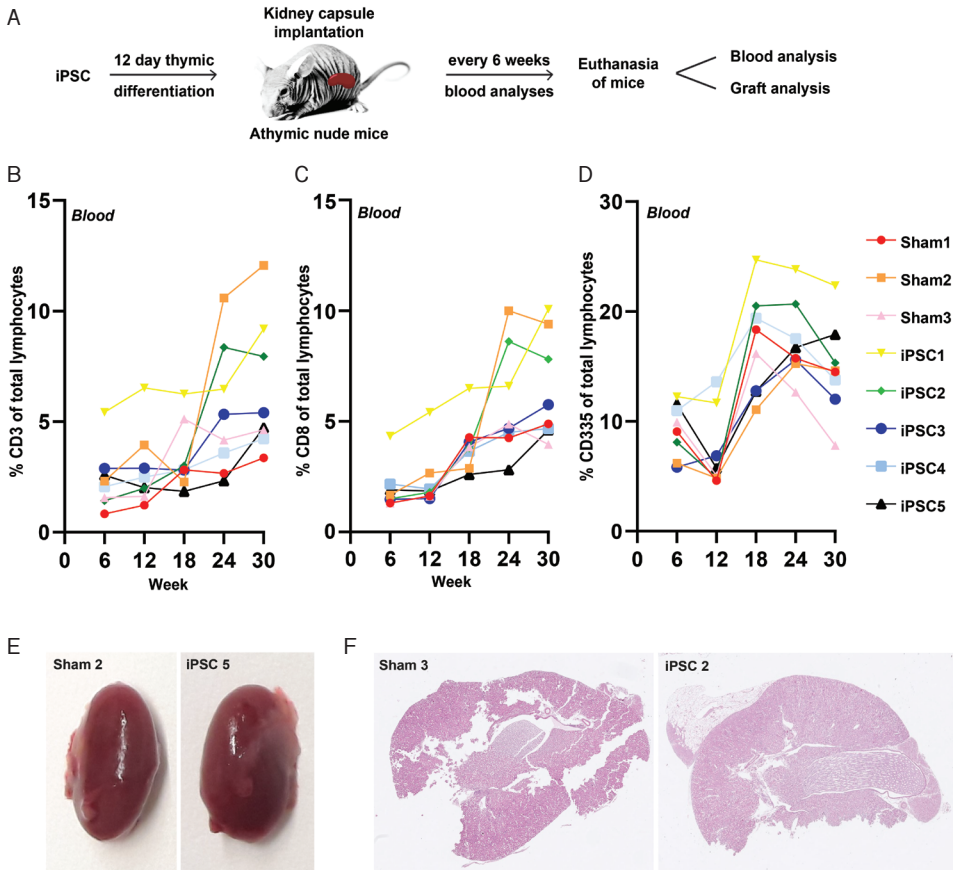
In vivo analyses after TEPC implantation in Foxn1 null mice. *A). Schematic overview of experiment. B-D). blood analyses of CD3, CD8 and CD335 immunomarkers in Sham-operated and TEPC-implanted (iPSC) mice. E). Retrieved kidneys from mice, sham (left) versus TEPC implanted (iPSC)(right). F). H&E staining of retrieved kidneys from mice, sham (left) versus TEPC implanted (iPSC)(right).*

reported thymus differentiation protocols on human iPSC generated from the urine of ovarian cancer patients.

After optimization, we finally established a 12-day protocol to gradually induce TEPC from iPSC. Previous work showed minimal expression of *TBX1*, *EYA1* and *PBX1*, and strong expression of *K8* in human ESC before differentiation.[5] We also observed expression of *EYA1*, *PBX1* and *K8*, but not *TBX1*, in iPSC before differentiation. Moreover, there was already transcript visible for *CXCR4*, although flow cytometry analysis indicated absence of CXCR4 expression in iPSC. Like with differentiation of human ESC[5], we observed additional expression of *SOX17*, *HOXA3*, *TBX1*, *PAX9* and stronger induction of *CXCR4* at DE stage. Moreover, at the end of the differentiation protocol, both *FOXN1* and *K5* were

clearly induced. Although expression of *SOX17*, *CXCR4* and *TBX1* decreased towards the TEPC lineage during differentiation of human ESC[5], we did not see these decreases in the differentiation of iPSC, possibly due to heterogeneity within our cultures. In accordance to previously published fluorescent microscopic images[5], we observed FOXN1 and K5 expression mainly in bridge-like structures. These structures were absent when iPSC were single cell seeded, likely explaining lack of *FOXN1* and *K5* induction in these cells at day 12 of differentiation. These genes were slightly induced when reseeding single cell after cells already reached the DE stage. In accordance, previous work to differentiate human iPSC into lung progenitor cells, that also arise from DE, started by clump seeding using EDTA but reseed and split the cells at DE stage using trypsin.[21] However, single cells reseeded at day 5 of differentiation lacked expression of *SIX1* on day 12, a gene that is crucial for thymus development.[22]

Single cell seeding does not resolve the large heterogeneity that we observed in the TEPC culture tissue. In another attempt to reduce heterogeneity, we also tried to prolong the differentiation phase to establish a more homogeneous monolayer of DE stage cells (not shown), but saw no reduction in heterogeneity. Lastly, we have attempted to enhance differentiation by up-regulating *FOXN1* expression through introduction of a *FOXN1*-overexpression plasmid or a CRISPR/dCas9-VP64 system with *FOXN1*¬ activating guide in DE cells (not shown). Transfection of DE cells was highly efficient. However, overexpression of *FOXN1* was likely lethal as we observed good viability one day post-transfection, but poor viability multiple days after transfection (not shown). Possibly, these cells activated an auto-regulatory mechanism of *FOXN1* expression.[3,8] Further research should look into other methods to enhance the differentiation. For example, thymic epithelial cells have been successfully induced by differentiation of mouse embryonic fibroblast-derived iPSC using a 3D spheroid culture system.[20] Also, the use of decellularized thymus tissue as scaffolds may serve as an option to strengthen natural signaling towards thymus lineage. Moreover, mysenchymal cells may specifically support establishment of TEPC through fibroblast growth factor signaling.[23] In addition, efforts in optimization should be made with regards to unification of TEPC tissue with the mice. Despite implantation trials, we experienced technical difficulties during sub-renal tissue implantation. Indeed, no grafts could be retrieved 30 weeks post-implantation. Thus, the mice experiment was inconclusive and should be optimized and repeated.

It is reported that genetic variation driving molecular heterogeneity in human iPSC causes differences in iPSC functionality, for example with regards to differentiation efficiency.[24] Future experiments should take into account this phenomenon and examine heterogeneity within iPSC lines. Lastly, urine-derived iPSC, when compared to blood- or skin-derived iPSC, provide a large advantage that obtaining urine is non-invasive.

6

However, there exists some uncertainty about the (genomic) quality of urine cells due to selection pressure. It is therefore important to report the cell origin of the iPSC. In this chapter, we did not yet fully genomically characterize the iPSC. To ensure cell quality in the future, we will test for genomic integrity of iPSC, for example by copy number analysis.

In conclusion, we have demonstrated the potential of patient urine-derived iPSC for use in cancer research. Renal epithelial cells could be readily reprogrammed to become pluripotent stem cells, even after treatment with chemotherapy. Moreover, iPSC pluripotent potential was demonstrated by differentiation into the thymic lineage, as shown by successful induction of FOXN1 and K5 on both the transcriptional as well as protein level. A potential application of the iPSC in cancer immunotherapy research is the unification of the immunocompetent mouse model, created using de novo thymus tissue from iPSC, with PDX tissue autologous to these iPSC. This approach creates a sustainable preclinical model for cancer that highly represents the patient. Of course, patient urine-derived iPSC may also be suitable to generate organoids or organ-on-chip models.

6

References

1. Beatty, G. L. & Gladney, W. L. Immune escape mechanisms as a guide for cancer immunotherapy. Clin. Cancer Res. 21, 687–692 (2015).
2. Byrne, A. T. et al. Interrogating open issues in cancer precision medicine with patient-derived xenografts. Nat. Rev. Cancer 17, 254–268 (2017).
3. Sun, L., Li, H., Luo, H. & Zhao, Y. Thymic epithelial cell development and its dysfunction in human diseases. Biomed. Res. Int. 2014, (2014).
4. Klein, L., Kyewski, B., Allen, P. M. & Hogquist, K. A. Positive and negative selection of the T cell repertoire: What thymocytes see (and don't see). Nat. Rev. Immunol. 14, 377–391 (2014).
5. Sun, X. et al. Directed differentiation of human embryonic stem cells into thymic epithelial progenitor-like cells reconstitutes the thymic microenvironment in vivo. Cell Stem Cell 13, 230–236 (2013).
6. Parent, A. V. et al. Generation of functional thymic epithelium from human embryonic stem cells that supports host T cell development. Cell Stem Cell 13, 219–229 (2013).
7. Su, M. et al. Efficient in vitro generation of functional thymic epithelial progenitors from human embryonic stem cells. Sci. Rep. 5, 1–8 (2015).
8. Bredenkamp, N. et al. An organized and functional thymus generated from FOXN1-reprogrammed fibroblasts. Nat. Cell Biol. 16, 902–908 (2014).
9. Parent, A. V. et al. Generation of functional thymic epithelium from human embryonic stem cells that supports host T cell development. Cell Stem Cell 13, 219–229 (2013).
10. Zhou, T. et al. Generation of human induced pluripotent stem cells from urine samples. Nat. Protoc. 7, 2080–2089 (2012).
11. Warlich, E. et al. Lentiviral vector design and imaging approaches to visualize the early stages of cellular reprogramming. Mol. Ther. 19, 782–789 (2011).
12. Takahashi, K. et al. Induction of Pluripotent Stem Cells from Adult Human Fibroblasts by Defined Factors. Cell 131, 861–872 (2007).
13. Agu, C. A. et al. Successful generation of human induced pluripotent stem cell lines from blood samples held at room temperature for up to 48 hr. Stem Cell Reports 5, 660–671 (2015).
14. Sommer, A. G. et al. Generation of human induced pluripotent stem cells from peripheral blood using the STEMCCA lentiviral vector. J. Vis. Exp. 1–5 (2012). doi:10.3791/4327
15. Zeevaert, K., Elsafi Mabrouk, M. H., Wagner, W. & Goetzke, R. Cell Mechanics in Embryoid Bodies. Cells 9, 1–20 (2020).
16. Papapetrou, E. P. Patient-derived induced pluripotent stem cells in cancer research and precision oncology. Nat. Med. 22, 1392–1401 (2016).
17. Maeda, T. et al. Regeneration of CD8αβ T cells from T cell-derived iPSC imparts potent tumor antigen-specific cytotoxicity. Cancer Res. 76, 6839–6850 (2016).
18. Schmitt, T. M. et al. Induction of T cell development and establishment of T cell competence from embryonic stem cells differentiated in vitro. Nat. Immunol. 5, 410–417 (2004).
19. Vizcardo, R. et al. Regeneration of human tumor antigen-specific T cells from iPSCs derived from mature CD8+ T cells. Cell Stem Cell 12, 31–36 (2013).
20. Okabe, M., Ito, S., Nishio, N., Tanaka, Y. & Isobe, K.-I. Thymic Epithelial Cells Induced from Pluripotent Stem Cells by a Three-Dimensional Spheroid Culture System Regenerates Functional T Cells in Nude Mice. Cell. Reprogram. 17, 368–375 (2015).
21. Ghaedi, M. & Niklason, L. E. Human pluripotent stem cells (iPSC) generation, culture, and differentiation to lung progenitor cells. Methods Mol. Biol. 1576, 55–92 (2019).
22. Laclef, C., Souil, E., Demignon, J. & Maire, P. Thymus, kidney and craniofacial abnormalities in Six1 deficient mice. Mech. Dev. 120, 669–679 (2003).
23. Jenkinson, W. E., Jenkinson, E. J. & Anderson, G. Differential requirement for mesenchyme in the proliferation and maturation of thymic epithelial progenitors. J. Exp. Med. 198, 325–332 (2003).
24. Kilpinen, H. et al. Common genetic variation drives molecular heterogeneity in human iPSCs. Nature 546, (2017).
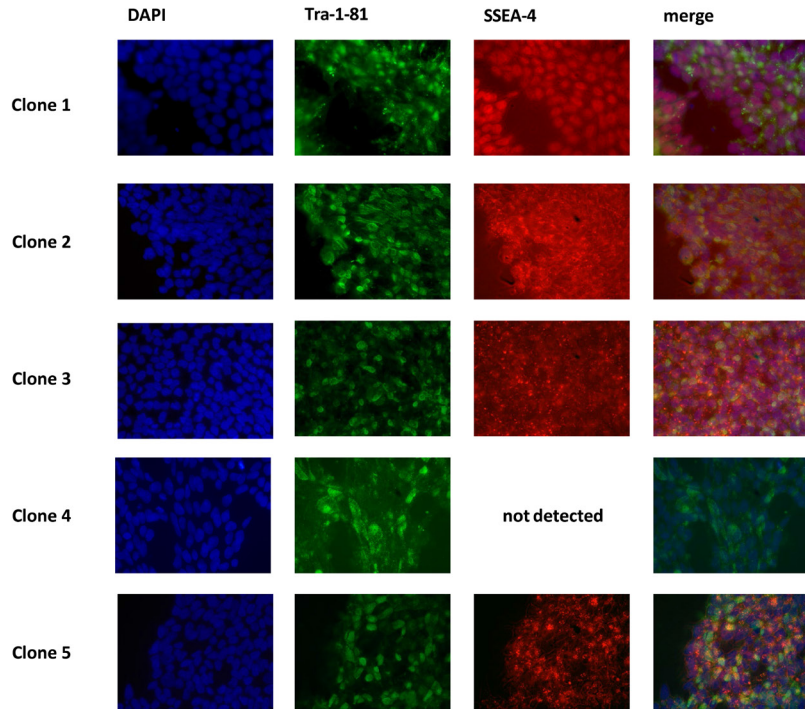
6

Supplementary Figure 1
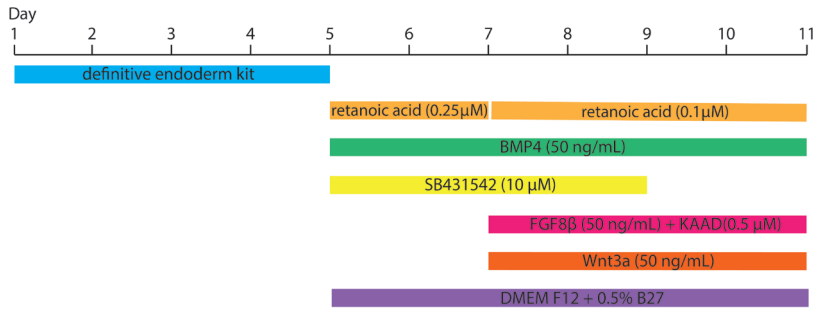
Schematic overview of differentiation protocol.

Supplementary Figure 2
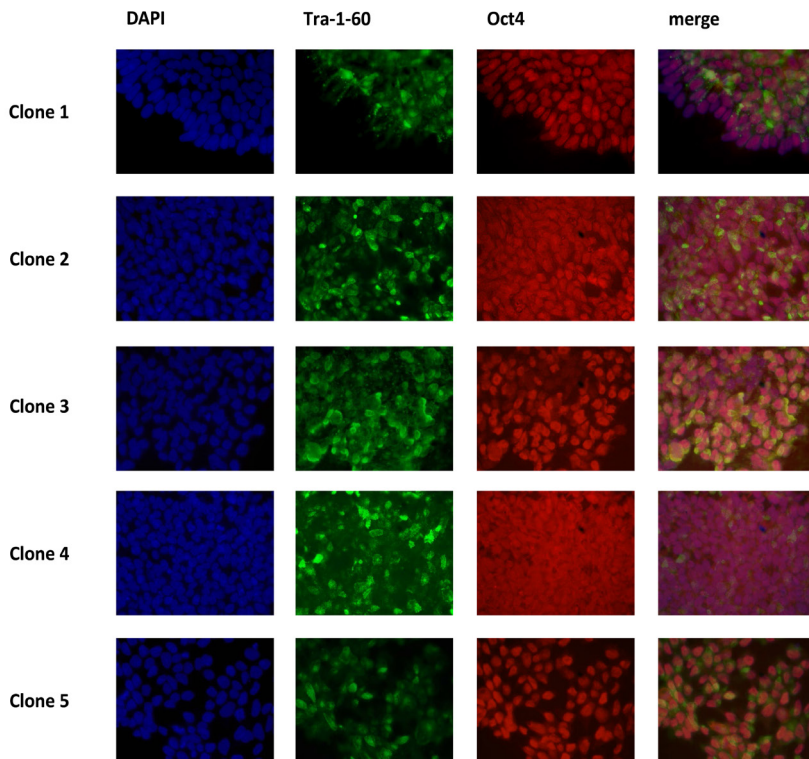
Characterization of established iPSC. Immunofluorescent staining for DNA with DAPI (blue) and for stem cell factors Tra-1-60 (green) and Oct4 (red). Merge shows overlay of stainings.

Supplementary Figure 3

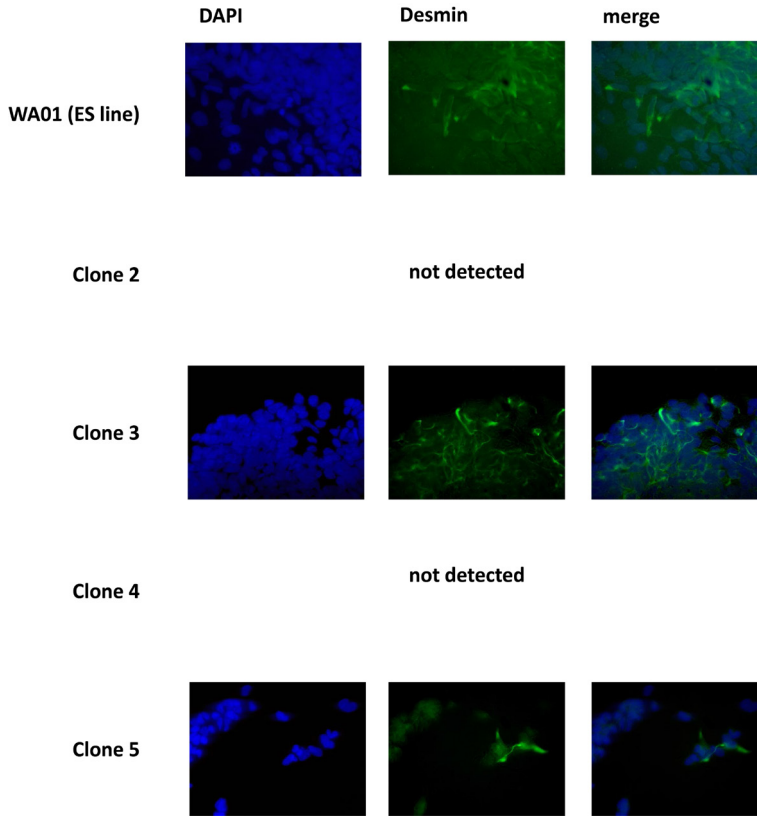|	DAPI	Tra-1-81	SSEA-4	merge
Clone 1				
Clone 2				
Clone 3				
Clone 4		not detected		
Clone 5				

Characterization of established iPSC. *Immunofluorescent staining for DNA with DAPI (blue) and for stem cell factors Tra-1-81 (green) and SSEA-4 (red). Merge shows overlay of stainings.*

6

Supplementary Figure 4

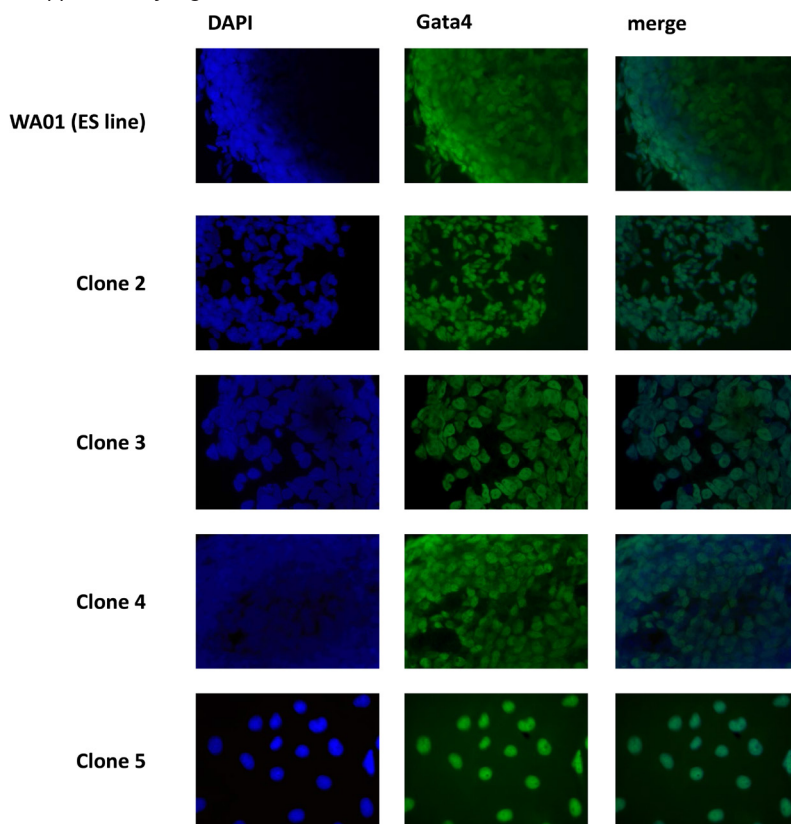**Characterization of embryoid bodies generated from the established iPSC to demonstrate multilineage potential.** *Immunofluorescent staining for DNA with DAPI (blue) and muscular differentiation marker Desmin (green). Merge shows overlay of stainings.*

Supplementary Figure 5

Characterization of embryoid bodies generated from the established iPSC to demonstrate multilineage potential. *Immunofluorescent staining for DNA with DAPI (blue) and liver differentiation marker Gata4 (green). Merge shows overlay of stainings.*

6

Chapter 7

Summary

Summary

Genotypic and phenotypic determinants of immunity across gynecological malignancies

Gynecological malignancies form a major cause of mortality in women. Despite efforts, survival has barely improved over the last decades. In other cancers, implementation of immunotherapeutic approaches has massively improved patient outcomes. However, efficacy in gynecological malignancies is inferior. This thesis contains studies that aimed at enhancing the understanding of tumor-immunological aspects in gynecological malignancies to improve stratification of patients for and development of (novel) immunotherapies.

In **Chapter 1**, an introduction is given on de basic principles of cancer immunotherapy and its current applications in gynecological malignancies. The main explored immunotherapeutic approaches are vaccination, adoptive T cell transfer and immune checkpoint inhibition, aiming either at induction or restoration of a tumor-antigen specific CD8+ T cell response. Choice of strategy largely depends on presence (hot tumor) or absence (cold tumor) of a pre-existing immunity. Success rates of the mentioned therapeutic strategies in cervical, endometrial and ovarian cancer range from no efficacy to, in exceptional cases, approximately 50%. Insights in different components of anti-tumor immunity may help improve these rates.

Initiation of immunity: STimulator of INterferon Genes (STING)

Chapters 2 and 3 comprise studies that examine a crucial inducer of anti-tumor immunity: STimulator of INterferon Genes (STING). As part of the cGAS-STING pathway, STING initiates transcription of Interferon type 1 genes, which, via activation of innate immunity leads to initiation of an antigen-specific adaptive immune response. Consequently, STING positively associates with CD8+ T cell infiltration and prognosis. Down-regulation of STING is observed in multiple cancer types and associated to poor prognosis. Moreover, absence or low levels of STING may affect response to immunotherapy. Therefore, therapeutic induction is currently under (pre)clinical investigation. In the studies described in Chapters 2 and 3, we investigated the association between STING and prognosis in cervical cancer.

In **Chapter 2,** we investigated the influence of STING in cervical cancer by investigating protein expression and prognostic value of STING across two large cohorts of in total 506 patients, 251 primarily treated with surgery (early stage cervical cancer patients) and 255 with radio(chemo)therapy (locally advanced cervical cancer patients). We showed

that the level of STING protein was independently prognostic for outcome of cervical cancer patients in both patient cohorts. We did not analyze non-cancer tissue, but did observe that patients in the radio(chemo)therapy cohort had significantly lower STING protein levels than patients in the surgery cohort, indicating down-regulation of STING during cervical carcinogenesis. As STING mRNA expression did not differ between non-cancerous and cancer tissue according to data obtained from The Cancer Genome Atlas, we suggest that down-regulation is likely established post-transcriptionally. Moreover, STING mRNA expression associated with expression of multiple important immunological markers. Importantly, STING protein level associated with CD103+ T cell infiltration, a marker for tumor-residual T cells that independently predicted improved survival for all patients. Combining STING protein levels and CD103+ T cell infiltration provided strong association with improved prognosis, demonstrating that use of both markers combined may be promising to improve risk stratification in cervical cancer patients.

In **Chapter 3**, we focused on allelic variance in the STING-encoding *STING1* gene. There are 26 reported single nucleotide substitutions located in the coding sequence of the gene, of which 20 represent non-synonymous substitutions that may lead to defective functionality of STING. We investigated whether variance in *STING1* may cause immune failure and facilitate persistent infection with human papilloma virus (HPV), which generally underlies the development of cervical cancer. To this end, we genotyped the *STING1* gene using cervical scrapings of 150 cervical cancer patients and assessed corresponding clinical characteristics compared to independent control cohorts. Allelic variants of *STING1* were not enriched in patients, indicating that they do not predispose for development of cervical cancer. Variants of *STING1* HAQ/HAQ and R232H/R232H did associate with younger age at diagnoses, higher number of recurrences and worse prognosis. These findings were independent of STING mRNA and protein levels and CD8+ T cell infiltration, which was similar for all patients. Thus, likely, these variants in *STING1* cause dysfunction of the cGAS-STING pathway leading to inefficient anticancer immunity. Lastly, we proposed synonymous substitution V48V as surrogate genetic marker for prognosis in cervical cancer, as it independently predicted outcome.

Part II: Composition of adaptive anti-tumor immunity

Chapters 4 and 5 cover in-depth analyses regarding markers that delineate tumor-reactive CD8+ T cells. The most notable markers to date are cell-surface expressed CD103, CD39 and PD-1, which have been described to indicate tumor-reactivity and confer prognostic advantage. Deeper molecular understanding of markers may teach us how to better enforce immunotherapeutic strategies.

7

In **Chapter 4,** we performed mRNA sequencing on ovarian cancer tumor digests to establish transcriptional profiles of CD103+CD8+ versus CD103-CD8+ T cells. As expected, CD103+CD8+ T cells were characterized by several exhaustion markers. Notably, we observed that differential expression of the chemokine *CXCL13* also marked a notable difference between CD103+ and CD103- CD8+ T cells. In addition, the *CXCL13* mRNA was also translated and protein was secreted by CD8+CD103+ T cells. CXCL13 mediates recruitment of B cells to tumors and is essential for formation of tertiary lymphoid structures (TLS), which may serve as local sites for efficient T cell priming in the tumor. Interestingly, tumors that are known for high CD103+CD8+ T cell infiltration presented with significantly higher numbers of TLS. As TGFβ induces CD103 on activated CD8+ T cells, we suggest that TGFβ plays an indirect, non-canonical role in coordinating anti-tumor immunity. CXCL13+CD103+CD8+ tumor infiltrating lymphocytes appear crucial cells for mediation of B cell recruitment and TLS formation in human tumors.

As a follow up study on the role of TGFβ, in **Chapter 5,** we studied the effect of TGFβ signaling in CD8+ T cells derived from healthy volunteers and from tumor digests of endometrial cancer patients by mRNA sequencing. While the focus usually lies on CD103+CD8+ T cells, we observed a small tumor infiltrating CD39+ CD103-CD8+ T cell subset that showed to be activated and therefore likely tumor-reactive. When activating peripheral CD8+ T cells *in vitro* with or without additional TGFβ signaling, it appeared that CD39+ preferably up-regulated cell-surface CD103 in response to TGFβ as compared to CD39-CD8+ T cells. This was accompanied by mRNA expression of several tissue residence and TGFβ responsive transcription markers. These findings suggest that CD39+CD8+ T cells are more sensitive to TGFβ signaling and are primed for tissue resident memory cell formation than CD39- T cells. Moreover, these data could explain why CD39+CD103-CD8+ T cells are relatively scarce in the tumor-microenvironment, as activated CD39+ CD103-CD8+ T cells appear primed for differentiation towards CD103+ tissue residence.

Part III: Establishment of novel preclinical models for tumor immunology and cancer immunotherapy

In order to translate novel insights into tumor immunology from bench to bed, there is a need for good preclinical models. However, at present, a model that represents patients regarding both the tumor and the immune system is lacking. For example, cancer cell lines lack heterogeneity and immune components, while animal models lack immunity. A possible solution may lie in the use of induced pluripotent stem cells (iPSC) to establish immune-competent patient derived xenograft (PDX) animal models by generating de novo thymus tissue and implant this in immune-deficient PDX mice.

In **Chapter 6**, we provide a preliminary study that is directed towards this aim. Firstly, we demonstrated successful *in vitro* reprogramming of fibroblasts from the urine of ovarian cancer patients to generate iPSC. This was supported by expression of important iPSC markers and formation of embryoid bodies to show multi-lineage potential. Secondly, we showed *in vitro* re-differentiation of iPSC into progenitor thymus cells (TEPC) by directed differentiation that mimics embryonic thymus organogenesis. The high success rates of both the reprogramming towards iPSC and re-differentiation towards TEPC supports the high potential of the discussed approach and warrant further *in vivo* studies.

7

Chapter 8

Discussion and future directions

Discussion and future directions

In this dissertation, we aimed to advance our understanding of immune biology in gynecological malignancies. To this end, we studied various aspects involving initiation of anti-tumor immunity, immune-composition of adaptive anti-tumor immunity and establishment of an improved preclinical model for anti-tumor immunity. Summarizing the work described throughout this dissertation, we conclude that

i)   low STING protein levels and homozygous single nucleotide substitutions in *STING1* may hamper efficient induction of tissue-resident anti-tumor immunity,

ii)   expression of CD103 defines tumor-reactive CD8+ tissue-resident T cells after an immune response has been initiated,

iii)   CD103- CD39+ CD8+ T cells in tumors are recently activated, characterized predominantly by expression of *TNFRSF9* and primed for CD103+ tissue residence,

iv)   TGFβ drives this formation of CD103+ tumor tissue-resident memory CD8+ T cells with CD39-associated up-regulation of unique transcription factors,

v)   patients with low intra-tumoral numbers of tertiary lymphoid structures have low numbers of CD103+ CD8+ T cells, possibly due to poor local priming of T cells,

vi)   cancer patient urine derived iPSC may serve well for establishment of novel preclinical models to study tumor immunology and cancer immunotherapy.

Part I: Initiation of immunity: STimulator of INterferon Genes (STING)

STING, as component of the cGAS-STING pathway, is important for initiation of immunity via induction of interferon signaling. Therefore, studies are ongoing to investigate the therapeutic potential of STING induction[1,2], for example in colorectal cancer[3,4], ovarian cancer[5] and breast cancer.[6] In Chapter 2, we studied the levels of STING in cervical cancer. Cervical cancer patients with high levels of STING protein had higher CD103+ T cell infiltration and improved survival upon both surgery and radio(chemo)therapy treatment. Additional studies should establish whether therapeutic STING induction may be beneficial in cervical cancer patients, particularly those with low levels of STING expression.

In accordance with our data, a recent study by Shi *et al.* demonstrates therapeutic potential of STING activation in cervical cancer cell lines with decreased STING signal.[7] Here, activation of STING by ADU-S100 inhibited the viability of these cells, promoted the secretion of IFNβ and IL-6 and activated the TBK1/NK-κβ pathway. Possibly, the cervical cancer patients with improved survival and high STING levels described in Chapter 2 can be characterized with the same patterns, which may be investigated in follow-up studies. Importantly, ADU-S100 suppressed *in vivo* tumor growth and increased

immune infiltration[7], supporting our recommendation to explore STING induction therapy in cervical cancer patients with low STING levels. Interestingly, experiments using a murine model for melanoma revealed that STING induction combined with PD-1 inhibition led to regression of cold tumors that did not respond to mono-treatment with PD-1 inhibitors.[8] This observation is confirmed by recent work from Patel *et al.*, in which low-dose targeted radionuclide therapy dependently of STING sensitized cold melanoma, breast and neuroblastoma tumors to be responsive to anti-CTLA-4 and anti-PD-L1 treatment.[9] Moreover, treatment of murine melanoma derived lung metastasis refractory to anti-PD-1 treatment was overcome upon combined treatment of anti-PD-1 with STING agonist loaded lipid nanoparticles.[10] Of note, the authors show that the observed anti-tumor effect was likely achieved via activation of NK cells.[10] Immune checkpoint inhibition modalities only reach 20-50% response rates in cervical cancer.[11] Hence, combining immune checkpoint inhibition with STING induction may be a promising future direction to enhance treatment outcomes of cervical cancer.

Importantly, data presented in Chapter 3 show that likely not all (cervical) cancer patients are eligible for STING induction therapy. Patients with homozygous single nucleotide variants of STING-encoding *STING1* have significantly worse outcomes. It was previously shown that *Sting1*-/- mice[12,13] and mice with single nucleotide variants that mimic loss-of-function[14–16] fail to induce immunity via interferon signaling. We observed that patients with homozygous variants of *STING1* did have similar CD8+ cell levels as patients with heterozygous and wild-type *STING1*. However, the poor survival of patients with homozygous variants indicates failed induction of anti-tumor immunity and presence of non-specific CD8+ T cells. This hypothesis is supported by data from Chapter 2 demonstrating that low STING levels are associated with lower tumor-reactive CD103+ T cell, but similar CD8+ T cell, infiltration as compared to patients with high STING levels. Patients with homozygous *STING1* variants may readily be identified by DNA sequencing the single nucleotide variant V48V region using e.g. blood or biopsy material, as this variant by itself proved predictive for survival and thus marks patients with defective STING (Chapter 3).

There is a noticeable discrepancy between prognostic value of STING value in Chapter 2 versus Chapter 3. Specifically, STING expression, as assessed by IHC, was prognostic for survival of cervical cancer patients in Chapter 3, but not Chapter 2. First, these may be explained by technical differences: full slide versus TMA and QuPath scoring versus manual scoring, respectively. Likely, scoring full slides using QuPath is more accurate as it largely avoids heterogeneity and researcher subjectivity. Furthermore, the patient numbers, the date ranges of tissue collection (2004-2014 versus 1984-2007) and distributions of clinical characteristics differ greatly. For example, the patients in the cohort in Chapter

2 have greater frequencies of adenocarcinomas (39% versus 20.9%), possibly explaining the lack of prognostic value for STING. When assessing disease-specific survival of only squamous cell carcinomas in the cohort of Chapter 2 (n=46) based on STING IHC, there is a clear trend that a higher STING level gives prognostic benefit. Moreover, when assessing disease-specific survival of only patients with double wild-type *STING1* (n=49), we also clearly observe this trend. Lastly, the STING values of Chapter 2 overall were relatively similar. Thus, distinguishing between above and below median may have been inadequate here. When distinguishing between patients with more deviating values (n=12 low STING and n=22 high STING), again, a clear trend can be observed suggesting that patients with high STING levels have improved survival. Altogether, technical differences and variation between the cohort characteristics may both account for the observed discrepancy.

Ultimately, the chapters discrepancy actually may provide confirmation that both STING protein level and *STING1* variants are prognostic for survival in cervical cancer. Examination of STING protein levels as well as genotyping may both be important to predict responsiveness to STING agonist therapy. In accordance to literature, 61.2% of patients with above median CD8+ cells per mm^2 also had above median STING level, whereas only 31.6% of patients with low CD8 level had high STING level (P=0.006, not shown). Furthermore, we observed discrepancies in conclusions when studying mRNA versus protein of STING, highlighting the necessity to assess both mRNA as protein when investigating a gene of interest. Lastly, our data analysis may be optimized by assessing STING more specifically as to its localization, as Parkes *et al*. describe that perinuclear localization is essential for the good prognosis of STING.[6]

Part II: Composition of adaptive anti-tumor immunity

In order to effectively treat cancer patients with immunotherapy, adequate understanding of tumor immunology is critical. Therefore, efforts are made to elucidate therapy targets and markers for effective and ineffective anti-tumor immunity. Previously, cell surface CD103 was found to define intra-epithelial CD8+ T cells in tumors, which were associated with prognostic benefit.[17,18] In Chapter 4 we demonstrate that CD103+ CD8+ T cells secrete CXCL13, a chemokine essential for induction of tertiary lymphoid structures (TLS)[19–21], which are suggested to facilitate efficient on-site priming of T cells.[22] Furthermore, the number of TLS correlated with the number of CD8+ T cells in the tumor. In line, CXCL13 co-localized with TLS and associated with prolonged survival in high-grade serous ovarian cancer patients, likely due to increased T cell infiltration.[19] Interestingly, this study shows that TLS only associated with prognostic benefit in the presence of CXCL13.[19] This indicates importance for C-X-C chemokine receptor type 5 (CXCR5)+ T cells, as CXCR5 is the signaling target for CXCL13. Interestingly, recent

analyses reveal strong, independent favorable prognostic impact of TLS in endometrial cancer (preprint at Research Square).[23] Here, an association was found between TLS and L1CAM expression in the tumor.

CXCL13 has been increasingly described in the context of cancer.[24,25] For example, a study investigating genomic alterations in tumor cells showed that CXCL13 is expressed at lower levels in patients that exhibit genomic alterations compared to those that do not.[26] Patients with CXCL13 deletion tumors relapsed significantly more often[26], suggesting the importance of CXCL13. In line with Chapter 4, Thommen *et al.* found T cells with high PD-1 expression to differentially express CXCL13 and secrete CXCL13.[27] Moreover, these T cells mostly localized in TLS in and around the tumor.[27] Interestingly, the density of CD103+ CD8+ T cells in naïve lung tumors associated with improved survival, but was also found to increase after anti-PD-(L)1 therapy in most responsive, but not in non-responsive, patients.[28] Moreover, treatment of melanoma patients with anti-CTLA4 and/or anti-PD-1 resulted in increased serum CXCL13 levels and decreased levels of circulating B cells[29], possibly indicating the recruitment of B cells to and establishment of TLS at the tumor site. Although Thommen *et al.* show *in vitro* migration of CXCR5+ cells towards CXCL13[27], a definite causal relation between *in vivo* CXCL13 excretion by CD8+ T cells and TLS formation is not yet established. It therefore remains unknown whether CXCL13 has an active role in anti-tumor immunity or is foremost a highly informative marker. Next to differential expression of CXCL13, CD103+ CD8+ T cells described in Chapter 4 presented with a highly exhausted transcriptional profile indicative of tumor-reactivity. These CD103+ CD8+ T cells differentially expressed various immune checkpoint such as *PDCD1*, encoding immune checkpoint PD-1, previously described to mark tumor-reactive T cells.[30,31] These findings are underlined by various papers describing CD103+ CD8+ T cells either alone or in combination with PD-1.[28,32–34] For example, Webb *et al.* hypothesize that the tumor tissue resident character of CD103+ cells might cause an exhausted phenotype due to chronic antigen exposure.[33]

As CD103 is induced by concomitant T cell receptor activation and TGFβ signaling, we assessed the transcriptional profiles of CD8+ T cells either or not stimulated by TGFβ in Chapter 5 to possibly decipher important features related to efficient anti-tumor immunity. Interestingly, we observed that an infrequent CD103- CD39+ subset of CD8+ T cells showed a transcriptional profile of recent activation, which was predominantly characterized by expression of *TNFRSF9* (encoding CD137). When concomitantly activated and stimulated with TGFβ, these cells start to co-express CD103. Thus, activation by T cell receptor stimulation initially induces a CD39+ population that is primed for CD103+ tissue residence. CD39 was previously described to mark exhausted CD8+ T cells, that also express PD-1.[35] Duhen *et al.* reported that CD39+ CD103+ co-expression marks tumor reactivity and exhaustion on tumor infiltrating CD8+ T

8

lymphocytes in both primary and metastatic tumors.[36] Moreover, these cells were found to be clonally expanded in these tumors and able to kill autologous tumor cells *in vitro*.[36] In line, CD39 and CD103 have together been described to mark poly-functional and reactivation-responsive CD8+ T cells based on their expression profile.[37] Lastly, the association between TGFβ signaling and CD39 expression on regulatory T and myeloid derived suppressor cells strengthens the connection between CD103 and CD39[38,39], as TGFβ induces CD103. Altogether, there appears to be an interaction between CD103, CD39 and PD-1 in the orchestration of anti-tumor immunity. However, despite their active transcriptional and phenotypical profile, the cells investigated in this thesis by RNA sequencing may not be tumor-antigen specific. Therefore, demonstration of actual tumor reactivity of these particular CD8+ T cell subsets requires follow-up studies including T cell receptor sequencing and (*ex vivo*) functional experiments. Survival analyses demonstrate the potential of these proteins for use as biomarkers.

A potential drawback considering sequencing of tumor digest-derived immune cells is that important information is lost during the process. For instance, the original localization of the cells in the tumor is unknown. As a result, data from irrelevant bystander cells may be included in analyses whereas relevant cells may have been lost in the process, and potential associations are speculative when not extensively confirmed in follow-up experiments. To this end, it would be interesting for future studies to focus more on biological context. An idea may be to perform map-directed single cell dissection of tumor tissue preparatory to RNA sequencing or other applications such as single cell western blot and flow cytometry. The approach of spatial transcriptomics is actually already being developed by Nanostring GeoMx and 10X Genomics.

Part III: Establishment of novel preclinical models for tumor immunology and cancer immunotherapy

Good preclinical models to study tumor immunology and cancer immunotherapy are lacking. Although cancer cell lines have greatly aided cancer drug development, a lack of heterogeneity and immune interactions are great drawbacks. Patient derived xenograft models that better capture this tumor heterogeneity can overcome some of these disadvantages of cell lines, but cannot be used in immune competent mice. In Chapter 6, we therefore aimed to establish a novel immune-competent PDX mouse model by implantation of patient-specific de novo generated thymus tissue. Hereto, we chose the use of patient-urine to establish induced pluripotent stem cell (iPSC) lines that could be further differentiated towards the thymic lineage. An advantage of using iPSC is that these have unlimited renewal capacity and could theoretically be differentiated into most cell lineages.

Firstly, the protocol based on work of Zhou *et al.*[40] for reprogramming of renal epithelial cells from urine of ovarian cancer patients towards iPSC appeared to be highly reproducible. Combining protocols from several previous reports[41–43], we achieved successful re-differentiation of these iPSC to tissue with markers characteristics for progenitor thymus tissue. Whereas these other studies showed successful *in vivo* differentiation of this tissue towards mature, functional thymus tissue[41–43], we could not retrieve the grafts and likely require optimization of tissue implantation to overcome this obstacle. In contrast to the 2D culture described here in Chapter 6, it would likely also be beneficial to culture the cells in 3D44. Moreover, it may be optimal to recreate the target tissue niche[45], for example by using decellularized tissue matrix.[46]

As an alternative to animal studies, the use of stem cell organoids has been increasingly explored. Based on previous reports[47–51], we made preliminary efforts to re-differentiate iPSC into T cells *in vitro* and observed distinct potential by the initial differentiation into CD34+ cells, an early marker of T cells (not shown in this thesis). Importantly, iPSC can be genetically edited using CRISPR/Cas9 technology[52–54], which we observed by the successful knock-out of *PDCD1*, encoding PD-1 (not shown in this thesis).

Altogether, we conclude that cancer patient urine provides a non-invasive source for iPSC generation. These iPSC may be exploited for preclinical cancer modeling to study tumor immunology and cancer immunotherapy or in the future, even for therapeutic applications.

Overall conclusion and future perspective

Tumor-immunology is complex but can be characterized by various outstanding markers. Several markers discussed in this dissertation proved to be highly informative for prognoses and (personalized) treatment strategies. Moreover, although not discussed in this dissertation, these markers may be suitable for treatment monitoring. Using combinations of markers will likely allow for even better results. As technology evolves and costs drastically decrease, the field of immunotherapy may move towards mapping a panel of molecular and cell surface markers for each individual patient. Due to this massive technical progress in (cancer) research, the immune landscape in cancer is being deciphered at rapid speed. However, several methodologies such as RNA sequencing also lead to great amount of data, potentially clouding valuable knowledge. It is therefore key to carefully organize these data and keep asking the right questions.

8

References

1. Le Naour, J., Zitvogel, L., Galluzzi, L., Vacchelli, E. & Kroemer, G. Trial watch: STING agonists in cancer therapy. Oncoimmunology 9, (2020).

2. Amouzegar, A., Chelvanambi, M., Filderman, J. N., Storkus, W. J. & Luke, J. J. Sting agonists as cancer therapeutics. Cancers (Basel). 13, (2021).

3. Chon, H. J. et al. STING signaling is a potential immunotherapeutic target in colorectal cancer. J. Cancer 10, 4932–4938 (2019).

4. Shi, J. et al. STING agonist and IDO inhibitor combination therapy inhibits tumor progression in murine models of colorectal cancer. Cell. Immunol. 366, 104384 (2021).

5. Huvila, J. et al. STING pathway expression in low-grade serous carcinoma of the ovary: an unexpected therapeutic opportunity? J. Pathol. Clin. Res. (2021). doi:10.1002/cjp2.230

6. Parkes, E. E. et al. The clinical and molecular significance associated with STING signaling in breast cancer. npj Breast Cancer 7, (2021).

7. Shi, F., Su, J., Wang, J., Liu, Z. & Wang, T. Activation of STING inhibits cervical cancer tumor growth through enhancing the anti-tumor immune response. Mol. Cell. Biochem. 476, 1015–1024 (2021).

8. Fu, J. et al. STING agonist formulated cancer vaccines can cure established tumors resistant to PD-1 blockade. Sci. Transl. Med. 7, (2015).

9. Patel, Ravi; Hernandez, Reinier; Carlson, Peter; Grudzinski, Joseph; Bates, Amber; Jagodinski, Justin; Erbe Amy, Marsh, Ian; Alucio-Sarduy, Eduardo; Rakhmilevich, Alexander; Vail, DAvid; Engle, Jonathan; Kim, KyungMann; Bednarz, Bryan; Sondel, Paul; Weich, J. M. Z. Low-dose targeted radionuclide therapy renders immunologically 'cold' tumors responsive to immune checkpoint blockade. Submitted 1–18 (2020).

10. Nakamura, T. et al. STING agonist loaded lipid nanoparticles overcome anti- resistance in melanoma lung metastasis via NK cell activation. 1–15 (2021). doi:10.1136/jitc-2021-002852

11. Matanes, E. & Gotlieb, W. H. Immunotherapy of gynecological cancers. Best Pract. Res. Clin. Obstet. Gynaecol. 60, 97–110 (2019).

12. Woo, S. R. et al. STING-dependent cytosolic DNA sensing mediates innate immune recognition of immunogenic tumors. Immunity 41, 830–842 (2014).

13. Ohkuri, T. et al. STING contributes to antiglioma immunity via triggering type I IFN signals in the tumor microenvironment. Cancer Immunol. Res. 2, 1199–1208 (2014).

14. Nissen, S. K. et al. Multiple Homozygous Variants in the STING-Encoding TMEM173 Gene in HIV Long-Term Nonprogressors. J. Immunol. ji1701284 (2018). doi:10.4049/jimmunol.1701284

15. Sauer, J. D. et al. The N-ethyl-N-nitrosourea-induced Goldenticket mouse mutant reveals an essential function of sting in the in vivo interferon response to Listeria monocytogenes and cyclic dinucleotides. Infect. Immun. 79, 688–694 (2011).

16. Hansen, K. et al. Listeria monocytogenes induces IFNβ expression through an IFI16-, cGAS- and STING-dependent pathway . EMBO J. 33, 1654–1666 (2014).

17. Komdeur, F. L. et al. CD103 + intraepithelial T cells in high-grade serous ovarian cancer are phenotypically diverse TCRαβ + CD8αβ + T cells that can be targeted for cancer immunotherapy. Oncotarget 7, (2016).

18. Workel, H. H. et al. CD103 defines intraepithelial CD8+ PD1+ tumour-infiltrating lymphocytes of prognostic significance in endometrial adenocarcinoma. Eur. J. Cancer 60, 1–11 (2016).

19. Yang, M. et al. CXCL13 shapes immunoactive tumor microenvironment and enhances the efficacy of PD-1 checkpoint blockade in high-grade serous ovarian cancer. J. Immunother. Cancer 9, (2021).

20. Gräbner, R. et al. Lymphotoxin β receptor signaling promotes tertiary lymphoid organogenesis in the aorta adventitia of aged ApoE -/- mice. J. Exp. Med. 206, 233–248 (2009).

21. Van De Pavert, S. A. et al. Chemokine cxcl13 is essential for lymph node initiation and is induced by retinoic acid and neuronal stimulation. Nat. Immunol. 10, 1193–1199 (2009).

22. Dieu-Nosjean, M. C. et al. Tertiary lymphoid structures, drivers of the anti-tumor response in human cancers. Immunol. Rev. 271, 260–275 (2016).

23. Horeweg, Nanda; Workel, Hagma; Loiero, Dominik; Church, David; Vermij, Lisa; Léon-Castillo, Alicia; Krog, Ricki; de Boer, Stephanie; Nout, Remi; Powel, Melanie; Mileshkin, Linda; MacKay, Helen; Leary, Alexandra; Singh, Naveena; Jürgenliemk-Schulz, Ina; Cr, M. Tertiary lymphoid structures critical for prognosis in endometrial cancer patients - a TransPORTEC study. 1–18 (2021).

24. Hussain, M., Adah, D., Tariq, M., Lu, Y. & Zhang, J. CXCL13 / CXCR5 signaling axis in cancer. Life Sci. 227, 175–186 (2019).

25. Kazanietz, M. G., Durando, M. & Cooke, M. CXCL13 and Its Receptor CXCR5 in Cancer : Inflammation , Immune Response , and Beyond. 10, 1–15 (2019).

26. Bindea, G. et al. Spatiotemporal Dynamics of Intratumoral Immune Cells Reveal the Immune Landscape in Human Cancer. (2008). doi:10.1016/j.immuni.2013.10.003

27. Thommen, D. S. et al. A transcriptionally and functionally distinct PD-1 + CD8 + T cell pool with predictive

potential in non-small cell lung cancer treated with PD-1 blockade. 24, 994–1004 (2018).

28. Corgnac, S. et al. CD103+CD8+ TRM Cells Accumulate in Tumors of Anti-PD-1-Responder Lung Cancer Patients and Are Tumor-Reactive Lymphocytes Enriched with Tc17. Cell Reports Med. 1, (2020).

29. Das, R. et al. Early B cell changes predict autoimmunity following combination immune checkpoint blockade. J. Clin. Invest. 128, 2–7 (2018).

30. Gros, A. et al. PD-1 identifies the patient-specific CD8+ tumor-reactive repertoire infiltrating human tumors. 124, 2246–2259 (2014).

31. Inozume, T. et al. Selection of CD8+PD-1+ lymphocytes in fresh human melanomas enriches for tumor-reactive T cells. J. Immunother. 33, 956–964 (2010).

32. Djenidi, F. et al. CD8 + CD103 + Tumor–Infiltrating Lymphocytes Are Tumor-Specific Tissue-Resident Memory T Cells and a Prognostic Factor for Survival in Lung Cancer Patients . J. Immunol. 194, 3475–3486 (2015).

33. Webb, J. R., Milne, K. & Nelson, B. H. PD-1 and CD103 are widely coexpressed on prognostically favorable intraepithelial CD8 T cells in human ovarian cancer. Cancer Immunol. Res. 3, 926–935 (2015).

34. Edwards, J. et al. CD103+ tumor-resident CD8+ T cells are associated with improved survival in immunotherapy-naïve melanoma patients and expand significantly during anti-PD-1 treatment. Clin. Cancer Res. 24, 3036–3045 (2018).

35. Gupta, P. K. et al. CD39 Expression Identifies Terminally Exhausted CD8+ T Cells. PLoS Pathog. 11, 1–21 (2015).

36. Duhen, T. et al. Co-expression of CD39 and CD103 identifies tumor-reactive CD8 T cells in human solid tumors. Nat. Commun. 9, (2018).

37. Workel, H. H. et al. Transcriptional activity and stability of CD39+CD103+CD8+ T cells in human high-grade endometrial cancer. Int. J. Mol. Sci. 21, 1–18 (2020).

38. Peres, R. S. et al. TGFβ signalling defect is linked to low CD39 expression on regulatory T cells and methotrexate resistance in rheumatoid arthritis. J. Autoimmun. 90, 49–58 (2018).

39. Li, J. et al. CD39/CD73 upregulation on myeloid-derived suppressor cells via TGFβ-mTOR-HIF-1 signaling in patients with non-small cell lung cancer. Oncoimmunology 6, (2017).

40. Zhou, T. et al. Generation of human induced pluripotent stem cells from urine samples. Nat. Protoc. 7, 2080–2089 (2012).

41. Su, M. et al. Efficient in vitro generation of functional thymic epithelial progenitors from human embryonic stem cells. Sci. Rep. 5, 1–8 (2015).

42. Parent, A. V. et al. Generation of functional thymic epithelium from human embryonic stem cells that supports host T cell development. Cell Stem Cell 13, 219–229 (2013).

43. Sun, X. et al. Directed differentiation of human embryonic stem cells into thymic epithelial progenitor-like cells reconstitutes the thymic microenvironment in vivo. Cell Stem Cell 13, 230–236 (2013).

44. Vizcardo, R. et al. Generation of Tumor Antigen-Specific iPSC-Derived Thymic Emigrants Using a 3D Thymic Culture System. Cell Rep. 22, 3175–3190 (2018).

45. Dellatore, S. M., Garcia, A. S. & Miller, W. M. Mimicking stem cell niches to increase stem cell expansion. Curr. Opin. Biotechnol. 19, 534–540 (2008).

46. Song, J. J. & Ott, H. C. Organ engineering based on decellularized matrix scaffolds. Trends Mol. Med. 17, 424–432 (2011).

47. Schmitt, T. M. et al. Induction of T cell development and establishment of T cell competence from embryonic stem cells differentiated in vitro. Nat. Immunol. 5, 410–417 (2004).

48. Timmermans, F. et al. Generation of T Cells from Human Embryonic Stem Cell-Derived Hematopoietic Zones. J. Immunol. 182, 6879–6888 (2009).

49. Vizcardo, R. et al. Regeneration of human tumor antigen-specific T cells from iPSCs derived from mature CD8+ T cells. Cell Stem Cell 12, 31–36 (2013).

50. Maeda, T. et al. Regeneration of CD8αβ T cells from T cell-derived iPSC imparts potent tumor antigen-specific cytotoxicity. Cancer Res. 76, 6839–6850 (2016).

51. Okabe, M., Ito, S., Nishio, N., Tanaka, Y. & Isobe, K.-I. Thymic Epithelial Cells Induced from Pluripotent Stem Cells by a Three-Dimensional Spheroid Culture System Regenerates Functional T Cells in Nude Mice. Cell. Reprogram. 17, 368–375 (2015).

52. Xu, X. et al. Efficient homology-directed gene editing by CRISPR/Cas9 in human stem and primary cells using tube electroporation. Sci. Rep. 8, 1–11 (2018).

53. Geng, B. chuan et al. A simple, quick, and efficient CRISPR/Cas9 genome editing method for human induced pluripotent stem cells. Acta Pharmacol. Sin. 41, 1427–1432 (2020).

54. Jehuda, R. Ben, Shemer, Y. & Binah, O. Genome Editing in Induced Pluripotent Stem Cells using CRISPR/Cas9 Modeling Human Disease in a Dish Using Induced Pluripotent Stem Cells (iPSCs). 323–336 (2015).

8

Appendix 1

Nederlandse samenvatting (Dutch summary)

Nederlandse samenvatting

Genotypische en fenotypische determinanten van immuniteit
in gynaecologische kankers

Ondanks veel onderzoek is de overleving bij gynaecologische kankers de afgelopen decennia nauwelijks verbeterd. Een recente veelbelovende ontwikkeling op het gebied van oncologische behandelingen is immuuntherapie. Immuuntherapie is een vorm van therapie waarbij het immuunsysteem van de patiënt wordt ge(re)activeerd om diens kanker te bestrijden. Deze strategie heeft de laatste jaren bij meerdere kankersoorten goede resultaten geboekt, waaronder bij eerder onbehandelbare kankers. Echter zijn de positieve resultaten nog maar in geringe mate zichtbaar bij gynaecologische kankers. De studies in dit proefschrift hebben als doel om meer kennis te verkrijgen over tumor-immunologische aspecten van gynaecologische kankers. Dat moet er toe leiden dat immuuntherapie in de toekomst effectiever kan worden ingezet bij gynaecologische kankers, onder andere doordat de therapeutische strategie beter kan aansluiten bij het klinische beeld. Ook biedt deze kennis inzichten voor de ontwikkeling van nieuwe vormen van immuuntherapie.

In **hoofdstuk 1** wordt het concept van immuuntherapie uitgelegd. Daarnaast worden de huidige toepassingen van immuuntherapie in gynaecologische kankers besproken. De meest toegepaste immuuntherapieën zijn vaccinatie, adoptieve celtherapie en immuun checkpoint inhibitie. Immuun checkpoint inhibitie richt zich voornamelijk op het herstellen van een al aanwezige anti-kanker immuunreactie. Vaccinatie en adoptieve celtherapie richten zich op het initiëren en / of ondersteunen van een immuunreactie in patiënten waar deze initiatie tijdens de ontwikkeling van de ziekte onvoldoende is geweest. Toepassing van de genoemde therapieën in baarmoederhalskanker, baarmoederkanker en eierstokkanker laat wisselende uitkomsten zien, variërend van geen respons tot, in uitzonderlijke gevallen, bij 50% van de patiënten een respons. Het verkrijgen van meer kennis van de verschillende onderdelen van de anti-kanker immuunreactie zal helpen om de effectiviteit te verbeteren.

Deel 1: Initiatie van anti-kanker immuniteit: STimulator of INterferon Genes (STING)

De **hoofdstukken 2 en 3** bevatten studies die zich richten op een eiwit dat belangrijk is bij het opstarten van anti-kanker immuniteit, namelijk STimulator of INterferon Genes (afgekort STING). STING is onderdeel van een cel-systeem dat geactiveerd wordt als DNA op plekken in de cel komt waar het normaal niet aanwezig is. Dit is bijvoorbeeld het geval in cellen die geïnfecteerd zijn met een virus. Nadat dit cel-systeem geactiveerd

is, worden uiteindelijk zogeheten Interferon type I signaalmoleculen aangemaakt. Deze moleculen activeren het immuunsysteem, waarna de ongewenste cellen geëlimineerd worden. In tumoren met veel STING zijn doorgaans veel immuuncellen aanwezig, wat samenhangt met een verbeterde prognose voor de patiënt. In vele kankersoorten zijn de niveaus van STING echter verlaagd, wat associeert met een slechtere prognose. Mogelijkerwijs hebben volledige afwezigheid of lage niveaus van STING invloed op de effectiviteit van immuuntherapie. Daarom wordt momenteel in verschillende studies onderzocht of het zinvol is om STING middels therapie te activeren. In de hoofdstukken 2 en 3 hebben wij de niveaus van STING en de relatie met prognose onderzocht in baarmoederhalskanker.

In **hoofdstuk 2** onderzochten we de rol van STING in baarmoederhalskanker door de niveaus en prognostische waarde van STING te bepalen in twee grote cohorten van tezamen 506 patiënten. Hiervan waren 251 patiënten behandeld met chirurgie (betreffende de vroeg-stadium patiënten) en 255 met radio(chemo)therapie (betreffende de laat-stadium patiënten). In beide groepen bleek een hoog niveau van STING in de tumor onafhankelijk geassocieerd met verbeterde prognose. STING niveaus waren daarnaast significant lager in patiënten met laat-stadium kanker dan in patiënten met vroeg-stadium kanker. Dit zou kunnen betekenen dat STING niveaus omlaag gaan gedurende kankerontwikkeling. Tot slot was er een sterke associatie tussen STING niveaus en de aanwezigheid van immuuncellen die belangrijk zijn voor de specifieke eliminatie van kankercellen. Een combinatie van STING niveau en aantal immuuncellen zou mogelijk bruikbaar zijn als prognostische parameter. Studies naar de effectiviteit van selectief activeren van STING in patiënten met baarmoederhalskanker kunnen inzicht geven in de therapeutische rol van STING.

In **hoofdstuk 3** hebben we gekeken naar de genetische variatie in het gen dat codeert voor STING, namelijk *STING1*. Een aantal varianten van het gen leidt tot een defecte functie van het STING eiwit. Hierdoor worden de Interferon type I signaalmoleculen, die het immuunsysteem activeren, niet meer aangemaakt. Chronische infectie met HPV is onderliggend aan de ontwikkeling van bijna alle gevallen van baarmoederhalskanker. Wij onderzochten of aanwezigheid van deze varianten van *STING1* wellicht associeert met chronische infectie met het Humaan Papilloma Virus (HPV) en daarmee met ontstaan van baarmoederhalskanker. Hiervoor zijn de genetische variatie in *STING1* tezamen met klinische eigenschappen in kaart gebracht voor een cohort van 150 baarmoederhalskanker patiënten, en zijn vervolgens de resultaten vergeleken met onafhankelijke controlecohorten. Allereerst vonden we dat de *STING1* varianten die defecte STING functionaliteit veroorzaken waarschijnlijk geen rol hebben in het initiëren van kankerontwikkeling, aangezien deze varianten niet vaker voorkwamen in de patiënten

A

dan in de controles. Echter werden patiënten met deze varianten gediagnosticeerd op jongere leeftijd, recidiveerden zij vaker en hadden zij een algeheel een slechtere prognose. Deze bevindingen waren onafhankelijk van de niveaus van STING en de aantallen immuuncellen in de tumor. Concluderend lijken deze *STING1* varianten niet in staat een functionele anti-kanker immuunreactie tot stand te brengen. Deze kennis is van belang voor studies waarbij therapeutische STING activatie onderzocht wordt. Om vast te stellen of een patiënt een *STING1* variant heeft die associeert met slechte prognose, kan V48V gebruikt worden als surrogaat genetische marker. V48V is een heel klein stukje variatie binnen het STING-coderende gen dat aanwezig was bij alle patiënten met de relevante *STING1* varianten. V48V aanwezigheid is een onafhankelijk prognostische factor.

Deel 2: Samenstelling van immuuncellen in de anti-kanker immuunreactie

Het immuunsysteem bestaat uit verschillende typen cellen. De cel die bij tumor immunologisch onderzoek veel aandacht krijgt, is de T cel die het eiwit CD8 tot uiting brengt op het oppervlak (CD8+ T cel). Deze cellen hebben de capaciteit om kankercellen direct te doden. Ook CD8+ T cellen bestaan er weer in een variatie van soorten, waarvan sommige relevanter zijn in de anti-kanker reactie dan anderen. Zo worden CD8+ T cellen die ook de eiwitten CD103, CD39 en PD-1 op het oppervlak van de cel hebben vaak beschreven als zeer kankerreactief en geassocieerd met betere prognose. In de **hoofdstukken 4 en 5** hebben we deze markers verder geanalyseerd. Moleculaire kennis over deze markers helpt mogelijk om immuuntherapie bij (gynaecologische) kankers te verbeteren.

In **hoofdstuk 4** hebben we mRNA sequencing toegepast op T cellen uit eierstokkanker en hierbij gekeken naar het verschil tussen de profielen behorende bij CD103+CD8+ versus CD103-CD8+ T cellen om genen te identificeren die mogelijk een rol spelen bij anti-kanker reactiviteit. CD103+ cellen associeerden met uiting van het PD-1 eiwit. Een belangrijke vinding die we in dit onderzoek deden was dat de CD103+, en niet de CD103- cellen, het gen *CXCL13* tot uiting brachten. CXCL13 is een immunologisch signaalmolecuul dat zogeheten B immuuncellen aantrekt, in dit geval naar de tumor. Vervolgens initiëren deze B cellen de formatie van zogeheten tertiaire lymfoïde structuren (TLS). TLS lijken op lymfeklieren, plaatsen in het lichaam waar immuuncellen samenkomen en waar zij geactiveerd worden als er bijvoorbeeld een bacteriële of virale infectie is. In de lymfeklieren vindt aansturing van het immuunsysteem plaats. Van TLS wordt vermoed dat zij lokale activatie van immuuncellen in de tumor faciliteren. Dit is waarschijnlijk efficiënter dan wanneer de immuuncellen eerst door het lichaam naar de lymfeklieren moeten migreren. Een hoog aantal TLS in de tumor associeert met een betere prognose. In ons onderzoek zagen we vervolgens dat tumoren met veel

CD103+CD8+ T cellen significant hogere aantallen van TLS hadden. Wij concluderen op basis van onze resultaten dat CXCL13+CD103+CD8+ T cellen die zich in de tumor bevinden cruciaal zijn om B cel werving en TLS formatie in de tumor te organiseren. Hiermee dragen zij bij aan effectieve anti-kanker reactiviteit. Tot slot wordt het eiwit CD103 aangezet op geactiveerde CD8+ T cellen wanneer zij ook gestimuleerd worden door het signaalmolecuul TGFβ. Hieruit blijkt dat TGFβ, een molecuul met vele rollen in de tumor, ook een indirecte rol speelt in de organisatie van anti-kanker immuniteit.

Gezien deze rol van TGFβ in anti-kanker immuniteit, wilden we in **hoofdstuk 5** verder bestuderen welke effecten dit molecuul nog meer zou kunnen hebben op CD8+ T cellen. Daarom hebben we CD8+ T cellen geïsoleerd uit endometriumkanker en uit het bloed van gezonde vrijwilligers en na stimulatie van deze T cellen, met of zonder TGFβ, bestudeerd middels mRNA sequencing. In het vorige hoofdstuk lag de focus op CD103+CD8+ T cellen. Echter zagen wij in dit onderzoek ook een kleine subgroep van CD39+CD103-CD8+ T cellen in de tumoren die geactiveerd waren en mogelijk anti-kanker reactief zijn. Wanneer CD8+ T cellen geïsoleerd uit het bloed geactiveerd werden, zonder of met stimulatie van TGFβ, bleken de CD39+CD8+ T cellen gevoeliger voor TGFβ stimulatie en werd bij hen vaker CD103 tot uiting gebracht op het celoppervlak ten opzichte van de CD39-CD8+ T cellen. Dit verklaart mogelijk waarom de subgroep van CD39+CD103-CD8+ T cellen in de tumoren zo klein was. De data in dit hoofdstuk tezamen wijzen erop dat CD39-CD8+ T cellen minder relevant zijn voor anti-kanker immuniteit. TGFβ lijkt met name belangrijk voor het aanzetten van de genen voor CD103 en CXCL13.

Deel 3: Een nieuwe benadering om tumor immunologie en kanker immunotherapie te bestuderen

Om nieuwe inzichten in tumor immunologie goed te kunnen vertalen van het lab naar de patiënt, zijn goede preklinische modellen essentieel. Momenteel ontbreekt een goed model dat de patiënt representeert wat betreft zowel de tumor als het immuunsysteem. Zo ontbreken bij de meeste kanker cel modellen die in het laboratorium worden gekweekt en getest, maar ook bij proefdiermodellen, de heterogeniteit van de tumor en de interactie met immunologische cellen en moleculen. Wij stellen voor om zogeheten geïnduceerde pluripotente stamcellen (iPSC) te gebruiken als oplossing om (dier)modellen met zowel een stukje tumor van de patiënt als een immuunsysteem te ontwikkelen. Stamcellen zijn cellen die nog alle typen cellen van het lichaam kunnen worden en van waaruit alle type cellen in ons lichaam gevormd worden. Bij iPSC maak je van volwassen lichaamscellen uit bijvoorbeeld het bloed of in urine weer stamcellen. Deze stamcellen kun je vervolgens weer omzetten naar elk gewenste type cel. Ons idee is om van iPSC, gegeneerd van cellen uit de urine van kankerpatiënten, thymuscellen

A

te maken op dezelfde manier als dat op natuurlijke wijze gebeurt tijdens embryonale thymusvorming. Deze cellen kunnen vervolgens geïmplanteerd worden in muizen zonder immuunsysteem, waarna het zal door ontwikkelen tot functioneel thymusweefsel. De thymus is een orgaan dat essentieel is in de ontwikkeling van T immuuncellen. Om afstotingreacties van humaan tumorweefsel te voorkomen zijn de muizen die in het lab gebruikt worden als diermodel zodanig genetisch gemodificeerd dat zij geen thymus bevatten en dus immuun gecompromitteerd zijn. De verwachting is dat met onze strategie muis T immuuncellen ontwikkelen die door de geïntroduceerde thymus genetisch afgestemd zijn op het tumorweefsel, waardoor afstoting voorkomen wordt. Uiteindelijk is dan een diermodel gecreëerd met zowel tumorweefsel van de patiënt als immuunsysteem van dezelfde patiënt. In **hoofdstuk 6** hebben wij een eerste stap gezet in dit onderzoek door van cellen uit de urine van eierstokkanker patiënten iPSC te maken. Vervolgens hebben we laten zien dat deze iPSC succesvol omgezet konden worden tot voorloper thymuscellen. De volgende stap die nu gezet moet worden is om de implantatie van deze voorloper thymuscellen in muizen te optimaliseren. In deze muizen zullen de geïmplanteerde cellen zich naar verwachting verder ontwikkelen tot functioneel thymusweefsel waarin de T immuuncellen zich kunnen vormen. Deze kunnen dan gedetecteerd worden in het bloed van de muizen.

Concluderend, met de studies in dit proefschrift hebben we een klein deel van de complexiteit van het immuunsysteem in de context van tumoren ontrafeld. We hebben verschillende genetische en fenotypische markers geïdentificeerd die informatief zijn voor het opstellen van prognoses en behandelingsstrategieën. Mogelijk kunnen ze ook geschikt zijn voor monitoring van behandeling. Doordat technologische ontwikkelingen elkaar snel opvolgen, zullen we op de korte termijn nog veel beter in staat zijn om genetische profielen en cel oppervlakte markers van (individuele) immuuncellen bij patiënten met kanker in kaart te brengen. Alles met de hoop en de verwachting dat we met al deze kennis de uiteindelijke prognose voor patiënten met kanker kunnen verbeteren.

A

Appendix 2

Curriculum vitae
Publicatielijst (List of publications)
Dankwoord (Acknowledgements)

Curriculum Vitae

Joyce Lubbers was born May 6th 1992 in Almelo, the Netherlands. Early on, she developed an interest in oncology and genetics. Following high school graduation in 2010, Joyce studied Biomedical Sciences at the University of Groningen, the Netherlands, from which she graduated with distinction in May, 2016. As a result from her minor studies, Joyce additionally obtained an education degree for biology. Throughout her studies, she was actively involved in various committees and set up her own company offering tutor services to high school students. During a bachelor research project in the lab of Prof. Dr. Toos Daemen in 2013, she gained a strong interest in the field of tumor immunology and cancer immunotherapy. Joyce pursued this interest and joined the group of Gynecological Oncology, led by Prof. Dr. Hans Nijman and Dr. Marco de Bruyn as a PhD student in June, 2016, resulting in this dissertation. Moreover, she joined the PhD council and was awarded two Dutch research grants and a prize for 'Best Poster Presentation' at the Annual PDX meeting in Switzerland. Combining her two passions, research and education, Joyce currently works as a teacher in biomedical research.

Joyce Lubbers werd op 6 mei 1992 geboren in Almelo. Nadat zij slaagde voor haar gymnasiumdiploma in 2010, volgde Joyce haar interesse in oncologie en genetica en ging zij Biomedische Wetenschappen studeren aan de Rijksuniversiteit Groningen. Als resultaat van haar minor in de bachelor behaalde zij een tweedegraads onderwijsbevoegdheid voor biologie. In mei 2016 slaagde Joyce *cum laude* voor haar mastergraad. Gedurende haar studie nam zij deel aan verschillende commissies en zette zij een onderneming op die bijlessen en huiswerkbegeleiding verzorgde aan middelbare scholieren. Tijdens een bachelor onderzoeksstage in het lab van Prof. Dr. Toos Daemen in 2013 ontwikkelde Joyce een sterke interesse in het veld van tumor immunologie en kanker immunotherapie. Naderhand bleef Joyce gericht op dit onderzoeksveld en mocht zij in juni 2016 als promovenda aansluiten bij de Gynecologische Oncologie onderzoeksgroep, geleid door Prof. Dr. Hans Nijman en Dr. Marco de Bruyn. Het daaruit resulterende onderzoek is gebundeld in dit proefschrift. Als promovenda heeft zij ook deel genomen aan de PhD council, kreeg zij twee onderzoeksbeurzen toegekend en ontving zij een prijs voor 'Beste Poster Presentatie' tijdens de jaarlijkse PDX meeting in Zwitserland. Momenteel combineert Joyce haar twee passies onderzoek en onderwijs als docent Biologie en Medisch Laboratoriumonderzoek.

Publicatielijst

Joyce M. Lubbers, Marta A. Ważyńska, Nienke van Rooij, Arjan Kol, Hagma H. Workel, Annechien Plat, Sterre T. Paijens, Martijn Vlaming, Diana C.J. Spierings, Philip H. Elsinga, Edwin Bremer, Hans W. Nijman, Marco de Bruyn. CD39 Defines Activated Intratumoral CD8 T Cells Primed for Tissue Residence. Geaccepteerd door Cancers. Mrt 2022.
Gedeeld eerste auteur

Arjan Kol, Joyce M. Lubbers, Anouk L.J. Terwindt, Hagma H. Workel, Annechien Plat, G. Bea A. Wisman, Joost Bart, Hans W. Nijman, Marco De Bruyn. Combined STING levels and CD103+ T cell infiltration have significant prognostic implications for patients with cervical cancer. Oncoimmunology. 2021 Jun 12;10(1):1936391. DOI: 10.1080/2162402X.2021.1936391.
Gedeeld eerste auteur

Joyce M. Lubbers, Bart Koopman, Jessica M. de Klerk-Sluis, Nienke van Rooij, Annechien Plat, Harry Pijper, Timco Koopman, Bettien M. van Hemel, Harry Hollema, Bea Wisman, Hans W. Nijman, Marco de Bruyn. Association of Homozygous Variants of STING1 with Outcome in Human Cervical Cancer, Cancer Science, 2021 Jan;112(1):61-71. DOI: 10.1111/cas.14680. Epub 2020 Nov 20.

Kim L. Brunekreeft, Sterre T. Paijens, Maartje C.A. Wouters, Fenne L. Komdeur, Florine A. Eggink, Joyce M. Lubbers, Hagma H. Workel, Elisabeth C. van der Slikkde, Noor E.J. Pröpper, Ninke Leffers, Julien Adam, Harry Pijper, Annechien Plat, Arjan Kol, Hans W. Nijman and Marco de Bruyn (2020) Deep immune profiling of ovarian tumors identifies minimal MHC-I expression after neoadjuvant chemotherapy as negatively associated with T cell dependent outcome, Oncoimmunology, 9:1, DOI:10.1080/2162402X.2020.1760705

Hagma H. Workel, Joyce M. Lubbers, Roland Arnold, Thalina M. Prins, Pieter van der Vlies, Kim de Lange, Tjalling Bosse, Inge C. van Gool, Florine A. Eggink, Maartje C.A. Wouters, Fenne L. Komdeur, Elisabeth C. van der Slikke, Carien L. Creutzberg, Arjan Kol, Annechien Plat, Mark Glaire, David N. Church, Hans W. Nijman, and Marco de Bruyn (2019) A Transcriptionally Distinct CXCL13+CD103+CD8+ T cell Population Is Associated with B cell Recruitment and Neoantigen Load in Human Cancer, Cancer Immunol Res (7) (5) 784-796, DOI: 10.1158/2326-6066.CIR-18-0517
Gedeeld eerste auteur

Oana Draghiciu, Joyce M. Lubbers, Hans W. Nijman and Toos Daemen (2015) Myeloid derived suppressor cells—An overview of combat strategies to increase immunotherapy efficacy, OncoImmunology, 4:1, DOI: 10.4161/21624011.2014.954829

A

Dankwoord

Onderzoek doen is geweldig en kent tegelijkertijd haar uitdagingen. Ik wil graag de volgende mensen bedanken voor het plezier dat ik met ze beleefd heb en de ondersteuning die ik van ze heb mogen krijgen gedurende de afgelopen jaren.

Allereerst ben ik grote dank verschuldigd aan mijn copromotor **Dr. Marco de Bruyn**. Marco, ik vergeet nooit meer het leuke gesprek dat wij hadden toen bleek dat ik een positie zocht als PhD-student in het veld van kanker immunotherapie, en jij een kandidaat zocht. Nog dagen heb ik van enthousiasme lopen stuiteren. Ook tijdens mijn traject hebben we nog veel van zulke gesprekken gevoerd waarbij allerlei ideeën de revue passeerden (handig om één kantoor te zitten). Er zijn er waarschijnlijk niet velen die een dergelijk bizar project zoals met de stamcellen ook daadwerkelijk zouden aangaan. Ik vond het een fantastische uitdaging en het was natuurlijk helemaal leuk om ook nog zulke goede resultaten te behalen. Naast je enorme passie voor wetenschap en intrinsieke biologische encyclopedie, zijn je optimisme en nuchtere kijk op zaken ook leerzaam geweest. "Het is pas een probleem als het een probleem is", "gewoon één voor één" en natuurlijk "Als je geen ballen laat vallen, probeer je er niet genoeg in de lucht te houden" (eerlijk geleend van Hans). Wanneer je - zomaar als voorbeeld - door een lab-ongelukje een hersenschudding oploopt, is het erg fijn als je leidinggevende deze houding heeft. Veel dank voor jouw steun in alle opzichten. Ik gun je alle subsidies en publicaties die je maar wenst, en natuurlijk veel geluk met jouw prachtige gezin.

Uiteraard volgt hierna de andere belangrijkste spil in mijn promotie-traject: mijn promotor **Prof. Dr. Hans Nijman**. Toen Marco een afspraak met ons drieën plande, bracht hij dit naar mij onder die noemer "even kennismaken met Hans". Ondanks mijn zenuwachtige, onvoorbereide gebrabbel toen het ineens een officieel sollicitatiegesprek bleek, zag jij kennelijk toch nog enige potentie in mij: ik mocht beginnen in jullie groep. Sinds de gezamenlijke woensdagmeetings die ik tijdens mijn stage al bijwoonde, was ik al onder de indruk van je kennis, kritische vragen en welbespraaktheid. Waar ik hier als beginnend promovenda wat nerveus van kon worden, leerde ik het langzamerhand door groeiend zelfvertrouwen juist meer waarderen. Je was op allerlei vlakken fantastisch om als voorbeeld te hebben. Tel daar bij op je humor en zangkunsten, en het is duidelijk waarom de belangrijke en gewaardeerde rol als afdelingshoofd aan jou is toebedeeld. Bedankt voor de kansen en begeleiding die ik van je heb mogen krijgen.

Hartelijke dank aan de beoordelingscommissie, bestaande uit **Prof. Dr. S. M. Willems**, **Prof. Dr. T. D. de Gruijl** en **Prof. Dr. S. de Jong**, voor het grondig doornemen van mijn proefschrift ter goedkeuring voor promotie.

Alle studies in dit proefschrift waren er niet geweest zonder de medewerking van alle patiënten. Ik en andere onderzoekers zijn jullie veel dank verschuldigd. Door jullie blijft de medische wetenschap grote stappen maken.

De **Gynaecologische Oncologie** betreft een onderzoeksgroep waar, tot mijn grote voldoening, veel wordt samengewerkt aan projecten. Dit geeft niet alleen veel plezier maar ook optimale benutting van ieders kwaliteiten. Wat was het fijn om deel uit te maken van deze club. **Annechien** en **Nienke**, wat moet een onderzoeksgroep zonder analisten? Onze groep heeft met jullie het geluk over de capaciteiten van maar liefst twee toppers van analisten te beschikken. Ik hoop voor de groep dat zij nog lang mogen profiteren van jullie enorme kennis en kunde. Ik wil jullie in ieder geval al graag bedanken voor al jullie wetenschappelijke en persoonlijke bijdragen aan dit proefschrift. Omdat jullie zo belangrijk voor mij waren en zijn voor de groep, heb ik jullie verzocht te shinen als mijn paranimfen. Ere wie ere toekomt. Daarnaast, ook jullie natuurlijk veel geluk gewenst met jullie prachtige gezinnen. **Hagma**, het paper dat ik met jou heb gepubliceerd is een prachtig voorbeeld van hoe onderzoek naar mijn idee idealiter zou moeten gaan. Twee afzonderlijke projecten die samen gebracht werden door een belangrijke – en gelukkig opgemerkte - connectie tussen beide. Het schrijven van ons stuk duurde door onze beider nauwkeurigheid lang, maar wat was het gezellig. Ook van onze samenwerking voor andere projecten en ons contact buiten werk om heb ik enorm genoten. Gedeeld sarcasme is weinig smart. **Arjan** en **Marta**, ook met jullie beide heb ik het genoegen gedeeld eerste-auteur te mogen zijn. Arjan, ik ken niemand met zo'n secuur labjournaal en nette werkhouding zien als jij hebt. Dank voor je behulpzaamheid, met name als koning flow cytometry. Marta, with your passion for science I foresee you and Fransesco running your own chemistry lab with five pipetting children and pets that you train to hold your gear. I wish you the best in loverville and look forward to all the amazing work you will do in the future! **Sterre**, jij held. Ik hou van jouw genietende levenshouding die altijd pret bracht in de werkdag met je goede, slechte grappen. De roadtrip naar het congres in Mainz met jou, Hagma, Marco zal ik niet vergeten. De gesprekken en vooral (niet nader te noemen) grappen hebben wonderbaarlijk genoeg niet verhinderd dat wij veilig door Marco werden afgeleverd in zowel Mainz als terug in Groningen. Als ik nog eens een muis zie, zal ik aan je denken. **Annegé**, **Anneke** en **Marta R**, de nieuwste promovendi in de groep. Ik heb er alle vertrouwen in dat jullie er een groot succes van gaan maken. Veel plezier met jullie projecten! **Fenne** en **Florine** wil ik als mijn voormalige collega-onderzoekers absoluut niet overslaan, daar zij mij warm hebben ontvangen toen ik begon als promovenda. Iets later kwam ook **Kim** er weer bij vanuit de kliniek. Bedankt voor alle herinneringen aan mijn gebrek aan culinaire expertise. Dank aan de hele groep voor de gezelligheid en ontzettend fijne werksfeer!

A

Tijdens mijn promotie-traject heb ik verschillende studenten begeleid en geholpen. Ik wil hen bedanken voor het plezier dat ik heb beleefd aan het geven van dit onderwijs en van de lessen die ik hier bij heb geleerd. Door jullie kon mij passie voor onderwijs als vlammetje blijven branden tijdens het onderzoek. In het bijzonder waardeer ik de grote inzet van **Bart** en **Jessica** bij het STING-werk. Jullie gaan vast ver komen in jullie medische loopbanen.

Niet alleen leden van mijn eigen onderzoeksgroep hebben bijgedragen aan dit proefschrift. Bij deze wil ik alle overige coauteurs bedanken voor hun bijdragen. Speciale dank aan **Diana**, voor jouw hulp bij de sequencing experimenten. **Mathilde**, **Eslie**, en **Prof. Dr. Floris Foijer,** bedankt voor al jullie hulp bij de stamcel experimenten. Floris, dank ook dat jij me het vertrouwen gaf een PhD-traject na te jagen. Ik heb veel geleerd en genoten tijdens mijn masterstage in jouw groep. **Prof. Dr. Harry Hollema** en **Dr. Joost Bart,** dank voor jullie onmisbare bijdragen vanuit de pathologie.

Naast bovengenoemden is er nog de in dit proefschrift meer onzichtbare hulp aan de projecten. Iedereen van de 'woensdagmeeting' met **Prof. Dr. Toos Daemen**, bedankt voor jullie input. Ook dank aan iedereen die via MOL- en TARGON gerelateerde meetings een bijdrage hebben geleverd aan dit werk, waaronder **Dr. Hilde Jalving**, **Prof. Dr. Steven de Jong, Prof. Dr. Marcel van Vugt, Prof. Dr. Frank Kruyt, Dr. Bea Wisman** en **Prof. Dr. Wijnand Helfrich.** Dank aan **Hetty, Coby, Neeltje** en andere personen die het werk op het lab überhaupt mogelijk maken. Dank aan mijn (voormalige) kantoorgenootjes **Aniek, Dorieke, Nienke** en **Simone** die immer klaarstonden voor erg gezellige of ondersteunende gesprekjes. Ook ben ik dank verschuldigd aan het secretariaat van de afdeling Obstetrie en Gynaecologie, **Heidi, Janette, Linda, Jikke,** en in het bijzonder **Diane en Mirjam.**

Zoals gezegd geeft onderzoek doen veel plezier. Echter was het vertier ernaast minstens net zo belangrijk. Om te beginnen de **TGIF** en **Wij(ve)ngenootschap** groepen. Onder andere de borrels, wijnproeverij, zeilmiddag, 'theatervoorstelling' en volleybaltoernooien (inclusief karaoke) waren erg gezellig. **Stijn**, de kebabpizza 's nachts op de stoep blijven favoriet. **Francien**, **Johannes** en **Martijn**, het was leuk met jullie labcommissie F.C. Eppendorf - en tevens een beetje Cupido - te spelen. In dit rijtje wil ik ook de **PhD Council** noemen. Ik heb ervan genoten verschillende PhD days en workshops met jullie te organiseren.

Dank ook aan alle nog niet benoemde personen voor de behulpzaam- en gezelligheid tijdens het labwerk, waaronder ook 'de hemato-kant' van het MOL, werknemers van het **Flow cytometry centrum** en van het **Microscopiecentrum.**

Tot slot zijn er nog allerlei collegae waar ik na mijn onderzoek nog van heb mogen leren en die me ook motiveerden de lange laatste loodjes door te komen. Zo heb ik genoten van de samenwerking met **Bert, Carla, Hilde, Jarnick, Jasper, Myrthe** en met allerlei leuke collegae tijdens mijn werkzaamheden rondom de corona-crisis. Collegae van **Saxion**, teveel om individueel op te noemen: wat kreeg ik een warm welkom waardoor de werkvloer direct goed voelde. Dank ook voor alle inhoudelijke en professionele lessen. Die zullen ongetwijfeld goed van pas komen bij het verdedigen.

Daarnaast ben ik dankbaar om met de volgende mensen slingers op te mogen hangen in mijn privéleven.

Allereerst de 'vriendengroep', vanaf het begin al een warm bad: **Anne, Arden, Bastiaan, Desiree, Emil, Erik, Guus, Joep, Laura, Rick, Sander, Sharyna** en **Tim**. De vele café- en andere borrelavondjes (met allerlei soorten bubbels) als ook de uitstapjes en weekendjes weg zijn altijd erg gezellig. Inmiddels zijn ook allerlei mijlpalen de revue gepasseerd zoals bruiloften en de geboorte van **Sam**. Ongetwijfeld zullen er nog vele mooie gelegenheden volgen, waaronder een mooie bruiloft over een paar maanden. Dank ook voor alle klushulp; ik beloof dat wij (waarschijnlijk) nooit weer zullen verhuizen. **Carin**, ik leerde jou kennen als huisgenote van Nick. Zo fijn hoe je mij regelmatig in Groningen kwam opzoeken voor gezellige etentjes. Hopelijk kun je snel jouw grote droom volgen in Australië. Het is je gegund!

Anneleen. Ik ken jou al sinds de basisschool. Ook al zien we elkaar niet vaak, ik waardeer ons contact en de nu en dan heel gezellige reünies.

Daarnaast heb ik ook al sinds de middelbare school goud in handen met mijn allerliefste vriendinnen **Anne, Lotte, Sylvia** en hun aanhang: **Luuk, Kevin** en **Bjorn**. Bedankt voor de oneindige hoeveelheid herinneringen die ik met jullie heb opgebouwd. Van de ontelbare potjes '30 seconds' en andere spellen, borrels, dagjes weg, weekendjes weg en bijzondere gelegenheden zoals bruiloften en de geboortes van **Nina** en **Yara**, tot de keren waarop we er in mindere tijden voor elkaar zijn. Wat is het heerlijk dat we weer zo dicht bij elkaar wonen. Op naar de wijntjes in het bejaardentehuis.

Met het hebben een partner komt het krijgen een schoonfamilie. **Wim, Anny, Angelique, Roy** en kleine **Jade**, samen zijn met jullie betekent pure chaotische gezelligheid. Het is fijn om schoonfamilieleden te hebben met zulke gouden harten, en natuurlijk een schoonzus met de meest intrigerende verhalen. Dit proefschrift betekent overigens dat ik eindelijk écht klaar ben met 'school', Angelique.

A

Wanneer je zus al vanaf tienertijd dezelfde partner heeft, gaat die partner een beetje als je broer voelen. **Niels**, bedankt voor jouw kinderlijke enthousiasme over de kleinste dingen en je hulp bij allerlei klusjes zoals – belangrijk - vuurtjes aanmaken. Mijn grootste dank voor het 'maken' van mijn twee jongste nichtjes, **Marèll** en **Lisan**. Jullie zijn engeltjes.

Arnica en **Marieke**. Mijn liefste zusjes (oké, zussen). Wat moesten we zonder elkaar beginnen (en wat soms met?), en wat is de zussenband een speciale. Mogen er nog maar veel zussendates volgen waarbij we even fanatiek zijn bij spelletjes en tennis, gezellig samen eten en allerlei leuke uitjes maken zoals naar de musical. Wanneer je twee zussen hebt, heb je automatisch al twee goede vriendinnen door dik en dun. Ik ben blij met jullie.

Pap en **Mam**, zullen er ouders zijn die net zo voor hun kinderen klaar staan als jullie? Altijd doen jullie je uiterste best voor ons. Ondanks dat jullie geen kaas hebben gegeten van de wetenschap en mijn verhalen over mijn onderzoek enigszins (totaal) onbegrijpelijk waren, weet ik en voelt het fijn dat jullie trots op me zijn. Bedankt voor jullie onvoorwaardelijke steun en liefde.

Nick, ons samenzijn dateert al vóór mijn eerste dag als student Life Sciences. Onze eerste jaren als koppel brachten wij dus grotendeels gescheiden door de afstand Groningen-Twente door. Het feit dat we die beproeving zo makkelijk hebben doorstaan, onder andere door heel veel trein- en autoritjes, zegt veel over ons en onze toekomst. Het feit dat jij naar Groningen bent verhuisd voor mij, zegt mij ook veel. Dankjewel voor jouw oneindige liefde en steun, en voor het feit dat je voor alles open staat en aan alles plezier beleeft. Zo heb ik enorm genoten van onze mooie reizen, onze bruiloft en het éindelijk adopteren van onze eigen hond, lieve Zoë. Ik ben blij dat je mijn man bent en kijk uit naar alles wat we samen nog mogen beleven.

Ik sluit graag af met het bedanken van **Groningen**. Wat ben je prachtig en gezellig. Twente riep, maar mis soms toch ook je mooie grachten, de mensen, stadjers, studenten. Dank voor bijna 10 jaar samenzijn.

Liefs,
Joyce

A